DEPARTMENT OF CHEMISTRY
UNIVERSITY OF ABERDEEN
UNITED KINGDOM

'The Influence of Inorganic Chemical Accelerators and Corrosion Inhibitors on the Mineralogy of Hydrated Portland Cement Systems'

by

Magdalena Balonis

MSc in Analytical Chemistry and Quality Control, AGH-University of Science and Technology, Krakow, Poland

A Thesis presented for the degree of Doctor of Philosophy at the University of Aberdeen

Aberdeen, June 2010

Declaration

This thesis is submitted to the University of Aberdeen for the degree of Doctor of Philosophy. It is a record of the research carried out by the author, under supervision of Professor Fredrik P. Glasser. It has not been submitted for any previous degree or award, and is believed to be wholly original, except were due acknowledgement is made.

Magdalena Balonis

Aberdeen, June 2010

Abstract

Thermodynamics provides a powerful tool to characterise the phase constitution of cementitious systems. Geochemical modelling software packages such as GEMS enable calculation of the stable phase assemblage as a function of reactant composition, temperature and pressure. However thermodynamic calculations require a database of thermodynamic properties of cement substances. A key purpose of this research has been (i) to extend the database for cementitious substances with respect to chloride, nitrate and nitrite bearing phases and determine their binding power. And (ii) to apply the data to some long-standing problems.

Calcium nitrate nitrite or chloride are often used as set accelerating admixtures which are added to concrete either to increase the early strength development or counteract slow strength gain in cold conditions. Additionally, nitrites act as corrosion inhibitors for embedded steel. Soluble chlorides, nitrates nitrites may also ingress from the service environment and interact with cement hydrates but the impact of nitrate and nitrite on cement hydrates is largely unknown. Physical chemistry and thermodynamics have been applied to characterise some of these reactions. The thermodynamic properties of chloride, nitrate and nitrite hydrates have been determined. Investigations of solid solutions and calculations on the influence of these anions were performed and compared with focused experimental data.

To calculate volume changes, densities of principal crystalline phases occurring in Portland cement were critically assessed and tabulated, in some cases with addition of new data. Independent laboratory work was undertaken to synthesize major AFm and AFt cement phases, determine their unit cell parameters and compare the results with those recorded in the literature. Parameters were refined from powder diffraction patterns using CELREF 2 software. A reliable and self-consistent density set for crystalline phases was obtained by calculating densities from crystallographic data and unit cell contents. A density value is reported for each phase, showing literature sources, in some cases describing limitations on the data, and the weighting attached to numerical values where an averaging process was used for accepted data.

To understand the impact of chloride on the cement mineralogy a literature review of its impacts has been made and new experimental data obtained. Phase preparations of

Friedel's salt, $Ca_4Al_2(Cl)_{1.95}(OH)_{12.05}\cdot 4H_2O$, and Kuzel's salt, $Ca_4Al_2(Cl)(SO_4)_{0.5}(OH)_{12}\cdot 6H_2O$, were synthesized and their solubilities measured at various temperatures. The solid solutions and interactions of Friedel's salt with other AFm phases were determined at 25˚C experimentally and by calculations. In hydrated cements, anion sites in AFm are potentially occupied by OH, SO_4 and CO_3 ions. Chloride readily displaces hydroxide, sulfate and carbonate in the AFm structures. A comprehensive picture of phase relations of AFm phases and their binding capacity for chloride was provided for pH~12 and 25˚C. The role of chloride in AFt formation and its relevance to corrosion of embedded steel were discussed in terms of calculated aqueous $[Cl^-]/[OH^-]$ molar ratios.

Layered double hydroxides corresponding to $Ca_4Al_2(NO_3)_2(OH)_{12}\cdot 4H_2O$ and $Ca_4Al_2(NO_2)_2(OH)_{12}\cdot 4H_2O$ (nitrate and nitrite AFm phases) were synthesized and characterized. Solubility and regions of stability including thermodynamic data are presented. The water content of nitrate AFm was found to be sensitive to humidity conditions, unlike nitrite AFm, whose water content seems to be independent of the moisture conditions over a wide range of p_{H2O}. Nitrates and nitrites readily displace hydroxide, sulfate and carbonate from the AFm structures. Nitrates and nitrites do not have ability to displace chloride from the Friedel's salt though. The binding power of AFm for nitrite/nitrate was calculated and confirmed experimentally at 25˚C. It was found that presence of nitrate and nitrite alters the AFm/AFt balance and thereby affect the specific volume of paste solids. Implications for the distribution of nitrate and nitrite in cements undergoing alteration were discussed.

Calcium nitrite is commonly used as corrosion inhibitor so the binding of nitrite in the presence of chloride was evaluated. It was found that the success of nitrite as a corrosion inhibitor for protection of embedded steel arises from its "smart" behaviour; AFm normally stores and sequesters nitrite in preference to sulfate, carbonate and hydroxyl ions so that the nitrite concentrations of pore fluid is low. However if chloride ingress occurs in service, the AFm undergoes ion exchange, partially gaining chloride and forming Friedel's salt, while releasing soluble nitrite ions to the pore fluid. As a result, the aqueous ratio of $[NO_2^-]/[Cl^-]$ increases as chloride increases and remains within the passivation range for steel. The exchanges are automatic and rapid, equilibrium being reached within days at ~25ºC.

This Thesis is dedicated to my mother
for all her support and loving care.

Dla Ciebie Mamo…

Acknowledgements

The writing of this Thesis has been one of the most significant academic challenges I have ever had to face. Without of support, patience and guidance of the following people, this study would not have been completed. It is to them that I owe my deepest gratitude:

Professor Fredrik P. Glasser for his excellent supervision during this project. His wisdom, knowledge and commitment to the highest standards inspired and motivated me.

Dr. Barbara Lothenbach (EMPA, Switzerland) for her help and assistance on thermodynamic modelling. Her enthusiasm and patience significantly contributed to completion of this work.

My academic coordinator, Professor Karen Scrivener (EPFL, Switzerland), for her valuable comments and constructive criticism.

My industrial advisor, Dr. Ellis Gartner (Lafarge, France), for providing numerous ideas and useful discussions regarding fate of nitrates and nitrites in cement paste.

Dr. Thomas Matschei (Holcim, Switzerland) for his friendship, patience and introduction to thermodynamic modelling.

Nanocem the European Community under the Marie Curie Research Training Network MRTN-CT-2005-019283 “Fundamental understanding of cementitious materials for improved chemical physical and aesthetic performance” for the full financial support of my project.

Professor Mette Geiker (DTU, Denmark) for stimulating discussions on chloride binding in cementitious systems.

Professor Carmen Andrade (CSIC, Spain) for the guidance on the effect of nitrite corrosion inhibitors.

I also wish to express my appreciation to all Nanocem members for giving me this great opportunity to gain training and expertise in cement field and to Marie Curie students for their support and encouragement.

Special gratitude to Professor Donald MacPhee (University of Aberdeen, UK), Professor André Nonat (Université de Bourgogne, France), Dr. Reiner Haerdtl (Heilderberg Cement, Germany), Dr. Duncan Herfort (Aalborg Portland, Denmark), Dr. Robert Flatt (Sika, Switzerland) and Dr. Silvia Vieira (Holcim, Switzerland) for their useful comments and questions with regard to my presentations and scientific publications.

Dr. Dimitrii Kulik (PSI, Switzerland) for his help with GEMS software.

Gwenn Le Saout (EMPA, Switzerland) for his assistance with an X-ray diffraction and fruitful collaboration on chloride topic.

Dr. Xiaolin Pardal (Lafarge, France) and Dr. Jean Michel Casabonne (Lafarge, France) for being so patient and helpful during my stay in France.

All staff and my colleagues at the Department of Chemistry (University of Aberdeen), Laboratory of Construction Materials (EPFL Switzerland), Laboratory of Concrete and Construction Chemistry (EMPA, Switzerland), Lafarge Research Group (France) for their great technical and intellectual support during my PhD. Special thanks to Mr. Gary Smith and Aberdeen ‘cement group’: Dr. Radim Skapa, Dr. Xinyu Zhang, Dr. Ines Garcia Lodeiro and Guillaume Jauffret.

Marie Alix Dalang Secrétan and Gillian Hewison for their help and assistance with administration throughout this project.

I would like to thank to my examiners, Professor Christopher Hall (University of Edinburgh, UK) and Dr. Jan Skakle (University of Aberdeen) for critical review of this work.

I am very grateful to:

Dr. Marta Mędala and Dr. Marta Kargol for their encouragement and support regarding academic and private life aspects.

My parents and grandparents for never letting me give up and for supporting me every step of the way.

My friends and family especially: Karolina Majka, Dąbrowka Grodź, Patrycja Kaźmierczak, Tadeusz Fronc, Krzysztof Rozmus, Agnieszka Brandys, Katarzyna Morawa Eblagon and Leszek Majewski for believing in me.

Finally, I would like to express special thanks to Dr. Gaurav Sant for his unending love and being beside me in every situation. He helped me to concentrate on completing this dissertation and supported mentally during the course of this work. Without Gaurav's help, academic guidance and encouragement, this study would not have been completed. He always takes my problems as his own, helps me to overcome them, and encourages me to achieve a high level.

Abbreviations

Notation used on graphs/tables/text:

Monosulfoaluminate = SO_4-AFm = Ms

Monocarboaluminate = CO_3-AFm = Mc

Nitrate AFm = NO_3-AFm = N

Nitrite AFm = NO_2-AFm = Ni

Friedel's salt = Cl-AFm = Fs

Hydroxy AFm = OH-AFm

Hemicarboaluminate = Hc

Kuzel's salt = Ks

Hydrogarnet (katoite) = HG

Ettringite = E

Portlandite = CH

ss (subscript) = solid solution

Nomenclature used in cement chemistry:

C = CaO

A = Al_2O_3

S = SiO_2

$\bar{S}$ = s = SO_3

$\bar{C}$ = c = CO_2

H = H_2O

AFm = aluminate ferrite monosubstituent phase

AFt = aluminate ferrite trisubstituent phase

C-S-H = calcium silicate hydrate

C-A-S-H = calcium aluminate silicate hydrate

C_3A = tricalcium aluminate

w/s = water/solid weight-ratio

Other abbreviations:

XRD = X-ray diffraction

DTA = Differential thermal analysis

TG = Thermogravimetry

DTG = Derivative thermogravimetry

FTIR = Fourier transform infrared spectroscopy

SEM = Scanning electron microscopy

EN = European standard

GEMS = Gibbs energy minimisation selector

PSI = Paul Scherrer Institut

MBSSAS = code for the computation of Margules parameters and equilibrium relations in binary solid-solution aqueous-solution systems

CELREF 2 = unit cell refinement software- used to refine cell parameters from the powder diffraction patterns

RH = relative humidity

HDPE = high density polyethylene

Θ = theta

Related publications and conferences

Journal Publications:

Balonis M., Glasser F. P., 'Calcium nitrite corrosion inhibitor: influence of chloride on nitrite binding and mineralogy of Portland cement', Journal of the American Ceramic Society, (under review, submitted in 2010)

Balonis M., Mędala M., Glasser F.P., 'Influence of calcium nitrate and nitrite on the constitution of the AFm and AFt cement hydrates - experiments and thermodynamic modelling', Advances in Cement Research, (accepted for publication in 2010)

Balonis M., Lothenbach B., Le Saout G., and Glasser F.P., 'Impact of chloride on the mineralogy of hydrated Portland cement systems', Cement and Concrete Research, 40, 1009-1022 (2010)

Balonis M., Glasser F.P., "Densities of Cement Phases", Cement and Concrete Research, 39, 733-739, (2009)

Presentations at conferences:

EUROMAT 2009, Glasgow, UK , September 7-10, 2009
Presentation: Impact of cement admixtures: calcium nitrate and nitrite-experiments and thermodynamic modelling.

Marie Curie Actions Final Conference, Villars, Switzerland, September 1-3, 2009
Presentation: Impact of calcium nitrates and nitrites on AFm cement hydrates.

The Fred Glasser Cement Science Symposium, Aberdeen, UK, **June 17-19, 2009**
Poster: Influence of calcium nitrates and nitrites on the constitution of AFm phases-experiments and modelling.

Table of contents

Abstract 3

Acknowledgements 5

Abbreviations 9

Related publications and conferences 11

1. General introduction 16
1.1 Historical development of cement 16
1.2 Portland cement: general 16
1.3 Main cement hydration products 17
1.4 Aims of the project 19

2. Thermodynamic modelling 21
2.1 History and cement hydrates database development 21
2.2 Software and databases 21
2.3 Correction of aqueous activity coefficients, estimation of heat capacity, solubility products and their temperature dependence 22
2.4 Solid solutions 26

3. Analytical methods 29
3.1 General preparation of samples 29
3.2 Solubility determinations 29
3.2 Analysis of cation and anion concentrations in solutions 30
3.2.1 Chloride, nitrate, nitrite, sulfate and carbonate 30
3.2.2 Calcium, sodium and aluminium 30
3.2.3 pH measurements 31
3.3 Analysis of solids 31
3.3.1 Microscopy (SEM) 31
3.3.2 Thermal analysis (TG/DTG/DTA) 32
3.3.3 X-ray diffraction (XRD) 32
3.3.4 Infrared spectroscopy (FTIR) 33

4. The density of cement phases 34
4.1 Introduction and aims of data collection 34
4.2 Synthesis and characterisation of AFm and AFt phases 38
4.2.1 AFm phases 38
4.2.2 AFt phases 39
4.2.3 Data collection 40
4.3 Density values of principal crystalline phases occurring in Portland cement 40
4.4 Discussion on the data compilation and consequences of the water packing on the density changes in AFm and AFt structures 45

5. Impact of chloride on the mineralogy of hydrated Portland cement systems 51
5.1 Introduction 51
5.1.1 Chloride in cement 51
5.1.2 Corrosion of reinforcing steel 52
5.1.3 Chloride salts as an accelerating admixtures 53
5.1.4 Chloride hydrates 53
5.1.5 Chloride binding capacity of cement 55
5.2 Synthesis of chloride-aluminate hydrates 57
5.2.1 Friedel's salt 57
5.2.2 Kuzel's salt 57
5.2.3 Solid solutions amongst AFm phases 57
5.2.4 Cl-ettringite 57
5.3 Results 58
5.3.1 Friedel's salt 58
5.3.2 Kuzel's salt 61
5.3.3 AFm solid solutions 67
5.3.3.1 Friedel's salt and hydroxy AFm 67
5.3.3.2 Friedel's salt and monosulfoaluminate 73
5.3.3.3 Friedel's salt and monocarboaluminate 75
5.4 Ion exchange experiments 77
5.5 Interactions of chloride within cement systems 83
5.5.1 Carbonate- free system 84
5.5.2 Carbonate- containing system 87
5.5.3 Relationships of AFm phases 90

5.5.4 Influence of temperature 92
5.5.4.1 Carbonate free system 93
5.5.4.2 Carbonate containing system 98
5.6 Discussion 102
5.6.1 Structure of the phases: carbonate in Friedel's salt 102
5.6.2 Polymorphism of Friedel's salt 103
5.6.3 Implication for solid solution formation 103
5.6.4 Application to commercial Portland cement: binding capacity for chloride 104

6. Influence of calcium nitrate and nitrite on the constitution of cement hydrates 107
6.1 Nitrates and nitrites in cement 107
6.2 Synthesis of nitrite and nitrate AFm phases and their solid solutions with other AFm phases 108
6.3 Characterisation of nitrate AFm 109
6.4 Characterisation of nitrite AFm 115
6.5 AFm solid solutions 122
6.5.1 Nitrate AFm and hydroxy AFm 122
6.5.2 Nitrate AFm and monosulfoaluminate 126
6.5.3 Nitrate AFm and monocarboaluminate 128
6.5.4 Nitrate AFm and Friedel's salt 133
6.5.5 Nitrite AFm and hydroxy AFm 137
6.5.6 Nitrite AFm and monosulfoaluminate 142
6.5.7 Nitrite AFm and monocarboaluminate 144
6.5.8 Nitrite AFm and Friedel's salt 150
6.5.9 Nitrate AFm and nitrite AFm 152
6.6 Ion exchange experiments 159
6.7 Interactions of nitrate and nitrite within cement systems 166
6.7.1 Carbonate- free systems 166
6.7.2 Carbonate- containing systems 170
6.7.3 Influence of temperature 173
6.7.4 Practical implications 176
6.8 Discussion 176

7 Influence of calcium nitrite corrosion inhibitor on chloride binding in Portland cement 179
7.1 Introduction about corrosion inhibition 179
7.2 Experimental procedure 181
7.2.1 Phase assemblage experiments 181
7.2.2 Thermodynamic modelling 182
7.3 Results 182
7.4 Discussion 194
7.4.1 Influence of chloride on nitrite binding in cement pastes 194
7.4.2 Influence of nitrate on corrosion inhibition 200

8. Summary 201

References 205

Figures and Tables 229

Appendix 243

1. General introduction

1.1 Historical development of cement

Since ancient times civilizations have needed a material that would bind brick and stones into a solid, formed mass. The Assyrians and Babylonians used clay for this purpose, and the Egyptians advanced to the discovery of lime and gypsum mortar as binding agents for building such structures as the Pyramids.

The Greeks made further improvements and the Romans developed cement that produced structures of remarkable durability. The secret of Roman success in making cement was traced to the mixing of slaked lime - chemically, calcium hydroxide - with a pozzolana admixture, an altered volcanic ash widely distributed in the Mediterranean, for example near Mount Vesuvius [1]. This process produced cement capable of hardening under water. The first artificial cement, termed 'Portland cement', was invented in 1824 by Joseph Aspdin and has become one of the dominant construction materials. Since then cement technology has significantly improved. Modern concrete mixtures often contain supplementary cementitious materials (*e.g.* blast furnace slag, silica fume, fly ash). Various admixtures are added to concrete to improve its performance *e.g.* to accelerate or retard setting, decrease the quantity of water needed to obtain a given degree of workability, increase the freeze resistance, etc.

1.2 Portland cement: general

Portland cement is made by heating raw materials with an appropriate chemistry, usually mixtures of limestone and clay, to a temperature of about 1450°C. The main clinker minerals are commonly termed: alite, belite, etc. The name, shorthand designation and idealised formulae of these clinker minerals are:

Alite- C_3S, $3CaO \cdot SiO_2$

Belite- C_2S, $2CaO \cdot SiO_2$

Celite - C_3A, $3CaO \cdot Al_2O_3$

Ferrite - C_4AF, $4CaO \cdot Al_2O_3 \cdot Fe_2O_3$ (but with variable Al/Fe)

Minor oxide components in cement also include - MgO, P_2O_5, Fe_2O_3, Na_2O, K_2O, MnO.

'Clinker' has a composition in the region of: 67% CaO, 22% SiO_2, 3% Fe_2O_3, 5% Al_2O_3 plus smaller proportions of minor oxides. The clinker is calcined and subsequently ground with a few per cent of calcium sulfate (used to delay initial set) to make Portland cement [2]. Some modern cement specifications, EN 197-1, also permit adding up to 5% limestone in the course of clinker grinding.*

Cement clinker particles are multiphase solids. Each phase has a specific reaction with water to produce a range of hydration products. Moreover, solids react with each other, *e.g.* the calcium aluminate with sulphate. The rates of reaction are important. The dissolution rates of the clinker phases can be calculated using the semi-empirical Parrot and Killoh approach [3]. The C_3A reaction is fastest and also generates most heat but gives little contribution to strength. The principal contributors to long-term strength are from the calcium silicates. C_3S is most reactive, giving early strength, but C_2S also has a significant longer term contribution. The C-S-H produced is the principal binding phase in Portland cements and is quantitatively the most important hydration product. The C_4AF reactions have intermediate hydration rates between those of C_3S and C_2S [2].

1.3 Main cement hydration products

The solid phases in hydrated cement systems consist mainly of portlandite and a gel-like phase, a calcium silicate hydrate termed C-S-H. Alumina combines with water, calcium and sulfate to form mainly AFt (ettringite) and AFm phases. Commercial Portland cement pastes contain ~5-15% of (AFm+AFt).

$Ca(OH)_2$ - crystalline phase (conventional cement shorthand notation: CH), natural mineral is known as portlandite. The structure consists of layers containing rows of linked $Ca(OH)_6$ octahedra. Calcium hydroxide dehydrates to calcium oxide at about 400°C.

* *The specification permits adding up to 5% limestone. A subsequent defining clause requires that the limestone contains* $\geq$ *70%* $CaCO_3$.

C-S-H - generic term for calcium silicate hydrate $xCaO \cdot SiO_2 \cdot yH_2O$, a poorly crystalline product of variable composition in terms of its H_2O/SiO_2 ratio and Ca/Si ratio. It forms a gel that is nearly X-ray amorphous and is responsible for the development of strength in Portland cement. In Portland cement its Ca/Si ratio is ~1.8 - 2.0. However it is believed that the range of single phase homogenous gels extends to much lower Ca/Si ratios, in the range to about 0.8. For the systems containing supplementary cementitious materials (blast furnace slag, silica fume, fly ash), some amounts of Al are build into the C-S-H (substitution known to increase with decreasing Ca/Si ratio) [4, 5]. It is reported [6, 7] that when Mg is present, another gel -like phase forms, M-S-H, which could coexist with C-S-H.

AFm is shorthand for a family of hydrated calcium aluminate hydrate phases (aluminate-ferrite-monosubstituent phases). Its crystalline layer structure is derived from that of portlandite, $Ca(OH)_2$, but with one third of the Ca^{2+} ions replaced by a trivalent ion, nominally Al^{3+} or Fe^{3+}. The resulting charge imbalance gives the layers a positive charge which is compensated by intercalated anions (*e.g.* SO_4^{2-}, OH^-, Cl^- etc.); the remaining interlayer space is filled with H_2O. Its general formula is $[Ca_2(Al,Fe)(OH)_6].X.xH_2O$, where X represents a monovalent ion or 0.5 of a divalent interlayer anion and *x* represents the number of water molecules. Studies have shown a multiplicity of AFm hydrate states and limited solid solution formation between various X anions [8-12]. Pöllmann described phase relations and ternary solid solutions between SO_4^{2-}, and CO_3^{2-} and OH^- [8] as well as between Cl^-, OH^- and CO_3^{2-} [12] anions. Except for reported replacement of sulfate by hydroxide, chloride by hydroxide and chloride by carbonate these anions do not form extensive AFm solid solutions and, from the mineralogical point of view, behave as separate phases. Moreover, chloride and sulfate AFm phases form an anion-ordered compound, Kuzel's salt, ideally with the 2:1 molar ratio of $[Cl]/[SO_4]$ [11, 13]. AFm containing Cl^-, OH^- and CO_3^{2-} has been defined by mineralogists as 'hydrocalumite' [14, 15]. SO_4-AFm (monosulfoaluminate) is also known as 'kuzelite' [16, 17] whereas Cl-AFm is termed as 'Friedel's salt' [18, 19].

In commercial cements, the constitution of AFm is historically defined as containing OH^- and SO_4^{2-} in anion positions. But under service conditions or when calcium carbonate is added, the AFm phase may also contain carbonate and form

monocarboaluminate (CO_3-AFm) or at very low carbonate contents hemicarboaluminate (AFm containing OH^- and CO_3^{2-} with the 2:1 molar ratio of $[OH]/[CO_3]$) [9, 20]. Carbonate can be also introduced from unavoidable pre-hydration and carbonation during grinding, transport, and storage. Studies have shown a multiplicity of AFm hydration states [16, 17, 21-23] resulting in variation in their physical densities [24].

AF_t - $[Ca_3Al(OH)_6]_2(SO_4)_3 \cdot (24+2)H_2O$ (conventional cement shorthand notation: $C_6A\bar{S}_3H_{32}$) or ettringite, crystalline - trigonal. Product of hydration of C_3A and gypsum. AFt (aluminate-ferrite-trisubstituted) compound is typically needle-shaped. It is stable at 20°C down to ~4 percent relative humidity. Various analogues (carbonate, iron, hydroxide, etc.) and solid solutions have been reported [25-28].

Hydrogarnet - $Ca_3Al_2(OH)_{12}$ (conventional cement shorthand notation: C_3AH_6), an end-member of the hydrogrossular solid-solution series, having the general formula $Ca_3Al_2(SiO_4)_{3-x}(OH)_{4x}$; x = 1.5-3.0 for katoite. Not normally a product of modern OPC hydration, although reported to occur in older Portland cements, calcium aluminate cements (CAC) [2] and in warm cured Portland cements [29]

Hydrotalcite – blast furnace slag introduces Mg to the system which upon hydration gives a hydrotalcite - like phase characteristic for slag cement blends [2].

Aqueous phase (pore solution) - permeates hardened cement paste *via* the pore system. It is highly alkaline (pH > 13) due to dissolution of Na and K salts from the cement clinker.

1.4 Aims of the project

Accelerating admixtures are added to concrete either to increase the rate of early strength development or to shorten the time of setting (*e.g.* in the case of low temperature conditions which slow concrete hydration). Chemical compositions of accelerators include some inorganic, compounds *e.g.* soluble chlorides, nitrates and nitrites. They are usually added a maximum of around 1-2% by weight. The effects of calcium chloride on concrete properties used to be widely studied and quantified

mostly in terms of chloride ingress and corrosion, but the role of nitrates and nitrites and their coexistence with other cement hydrates is less well known. Calcium nitrite is also used as an effective admixture to inhibit corrosion of reinforcing steel bars in concrete but its interaction, for example with Friedel's salt, is not reported in the literature. Very little has been done to better understand the role of nitrite and nitrate in Portland cements and their impact especially on constitution of AFm and AFt phases.

An aim of this work was to gain experimental data on chloride, nitrite and nitrate cement hydrates, determine their regions of stability, solubilities, solid solutions with other cement phase, integrate collected information into thermodynamic database and predict phase changes in the course of admixing: $CaCl_2$, $Ca(NO_2)_2$ and $Ca(NO_3)_2$.
Calculations simulated potential ion redistribution between cement hydrates and pore solution. A key purpose of the calculation was to determine the binding power of AFm for (Cl, NO_2, NO_3) in competition with hydroxides, sulfates and carbonates in cement.
Relevant experiments on phase assemblages were performed to verify thermodynamic predictions. The implications for retention of chloride, nitrate, nitrite in the cement are discussed.

2. Thermodynamic modelling

2.1 History and cement hydrates database development

Thermodynamic modelling was first developed and applied by geochemists to perform calculations on complex multi-component systems as occur in nature. Routines employing special algorithms for the minimisation of Gibbs free energies have been implemented on a PC and applied since about 1980 (*e.g.* ChemSage [30], MTDATA [31], Thermo-Calc [32], GEMS-PSI [33]). Thermodynamic databases have become available, either free or commercially, for different materials like steels, super-alloys, semiconductor materials, aqueous solutions, slags, cement hydrates etc. To give reliable calculations on phase relations, databases need to be internally consistent and comprehensive. Babushkin et al. [34] was the first who published compiled thermodynamic data for cement substances. Reardon [35, 36], Atkins et al. [37, 38], Stronach [39], Damidot et al. [40-45], Lothenbach et al. [46-49], Kulik and Kersten [50] further contributed to the knowledge about thermodynamic properties of cement hydrates and calculations on phase equilibria in cementitious systems. Matschei et al. [51, 52] provided the most recent self-consistent database for Portland cement phases used for thermodynamic modelling of cement hydration at various temperatures, including solid solution formation [9, 20, 52-56]. The database contains entries for the main hydrate phases of commercial Portland and blended cements, *i.e.* AFm, AFt, hydrogarnet, hydrotalcite and C-S-H (Kulik & Kersten model [50]), and can be used over a range of temperatures, 1-99°C. This represents a major advance over previous databases which, with few exceptions, only contained data for 25°C and moreover, lacked data for several important phases and information about solid solutions.

2.2 Software and databases

All calculations were carried out using the GEMS-PSI software package including GEM solver, a build in NAGRA-PSI 'Kernel' and slop98.dat thermodynamic databases [57-59]. Input data for cement hydrates (cemdata07.1) were taken from Matschei et al. [56] and the title study (Tab. 2.1). GEMS is a broad-purpose geochemical modelling code which uses Gibbs energy minimization (GEM) criterion and computes equilibrium phase assemblage and speciation in a complex chemical system from its total bulk

elemental composition. The total Gibbs energy of the system is minimized at given temperature and pressure. Chemical interactions involving solids, solid solutions, and aqueous electrolyte are considered simultaneously. As mentioned above, GEMS-PSI calculates the chemical speciation (*i.e.* amounts or concentrations of chemical components in all phases present at the equilibrium state) from a given total bulk composition of the system. Thus mass is conserved in the calculations and allows an exact quantification of the modelled phases which are in equilibrium. For aqueous species, the data treatment is based on the HKF (Helgeson-Kirkham-Flowers) set of equations [59, 60] which can correct temperature and pressure in a wide range from 0°C to 1000°C and 1-5 kbar.

2.3 Correction of aqueous activity coefficients, estimation of heat capacity, solubility products and their temperature dependence

2.3.1 Calculation of the heat capacity

The heat capacity was calculated according to Eq. 2.1:

$$C_p^o = a_o + a_1T + a_2T^{-2} + a_3T^{-0.5} \qquad \textit{Eq. 2.1}$$

where a_0, a_1, a_2 and a_3 are empirically derived, temperature independent parameters characteristic for a particular solid.

Heat capacities $C_p°$, where not known, were estimated based on the reference reactions with the structurally similar monosulfoaluminate with known $C_p°$ [61]. If such reference reactions involve only solids and no "free" water, the change in heat capacity and the entropy is approximately zero. As shown in the literature this principle has been successfully applied in the past [51, 62]. Tabs. 2.2 and 2.3 show reactions and equations used to estimate heat capacity data of Friedel's salt, Kuzel's salt, nitrate AFm and nitrite AFm. Heat capacity data for reference phases: $Ca_4Al_2(OH)_{12}(SO_4)\cdot 6H_2O$ (monosulfoaluminate), $CaCl_2$, $Ca(NO_3)_2$ and $Ca(NO_2)_2$, $CaSO_4$, $CaSO_4\cdot 2H_2O$ were taken from [51, 58, 61, 63-65]. Using the same principle, entropy S° can be also estimated using reference reactions.

*Table 2.1: Standard molar thermodynamic properties of cement hydrates at 25°C, 1 bar; t.w.- this work, *- values calculated from the density data in chapter 4 and [24].*

Phase	$\log K_{SO}$	$\Delta_f G^0$ [kJ/mol]	$\Delta_f H^0$ [kJ/mol]	S^0 [J/(mol·K]	a_0 [J/(mol·K)]	a_1 [J/(mol·K²)]	a_2 [J·K/mol]	a_3 [J/(mol·K^0.5)]	V°* [cm³/mol]	Ref
Hydrogarnet (katoite)										
C_3AH_6 (hydrogarnet)	-20.84	-5010.1	-5540	419	292	0.561	0	0	150*	[51]
$C_3AS_{0.8}H_{4.4}$ (siliceous hydrogarnet)	-29.87	-5368.0	-5855	369	109	0.631	-1.95e+06	2560	143	[51]
AFt										
C_6AsH_{32} (ettringite)	-44.90	-15205.9	-17535	1900	1939	0.789	0	0	706*	[51]
C_6AcH_{32} (carbonate ettringite)	-46.50	-14565.7	-16792	1858	2042	0.558	-7.78e+06	0	651*	[51]
AFm										
C_4AsH_{12} (monosulfoaluminate)	-29.26	-7778.5	-8750	821	594	1.168	0	0	309*	[51]
C_4AcH_{11} (monocarboaluminate)	-31.47	-7337.5	-8250	657	618	0.982	-2.59e+06	0	261*	[51]
$C_4Ac_{0.5}H_{12}$ (hemicarboaluminate)	-29.13	-7336.0	-8270	713	664	1.014	-1.30e+06	-800	284*	[51]
$C_4ACl_{1.95}H_{10.025}$ (Friedel's salt)	-27.69	-6814.6	-7609	731	503	0.89	-1.99e+06	1425	271.*	[66], t.w.
$C_4ACl_2H_{10}$ (Friedel's salt- theoretical values for ideal composition)	-27.27	-6810.7	-7604	731	498	0.89	-2.03e+06	1503	271.*	t.w.
$C_4A(NO_3)_2H_{10}$ (nitrate AFm)	-28.67	-6778.0	-7719	821	580	1.02	-2.77e+06	872.2	297	[67], t.w.
$C_4A(NO_2)_2H_{10}$ (nitrite AFm)	-26.24	-6606.0	-7493	799	565	0.99	-2.24e+06	703.3	275	[67], t.w.
C_4AH_{13} (hydroxy AFm)	-25.40	-7326.6	-8300	708	711	1.047	0	-1600	274*	[51]
C-S-H										
jennite-type ($C_{1.67}SH_{2.1}$)	-13.17	-2480.8	-2723	140	210	0.120	-3.07e+06	0	78	[48, 51, 68]
tobermorite -type ($C_{0.83}SH_{1.3}$)	-8.0	-1744.4	-1916	80	85	0.160	0	0	59	[48, 51, 68]
supplementary data										
water (H_2O)		-237.2	-286	70	75	0	0	0	18	[51]
SiO_2 (amorph)		-848.9	-903	41	47	0.034	-1.13e+06	0	29	[51, 58]
gypsum ($CaSO_4{\cdot}2H_2O$)		-1797.8	-2023	194	91	0.318	0	0	74.5*	[50, 51]
anhydrite ($CaSO_4$)		-1322.1	-1435	107	70	0.099	0	0	46*	[51, 58]
portlandite ($Ca(OH)_2$)		-897.0	-985	83	187	-0.022	0	-1600	33*	[51, 58]
lime (CaO)		-604.0	-635	39	49	0.004	-6.53e+05	0	17*	[51, 58]
calcite ($CaCO_3$)		-1129.2	-1207	93	105	0.022	-2.59e+06	0	37*	[51, 58]
gibbsite ($Al(OH)_3$)		-1151.0	-1289	70	36	0.191	0	0	32*	[51, 58]
C_3A (tricalcium aluminate)		-3382.3	-3561	205	261	0.019	-5.06e+06	0	89*	[34, 51]

Table 2.2: Reference reactions used to calculate heat capacities of relevant AFm phases.

Phase	Reference reaction for estimation heat capacity
Friedel's salt	$\mathbf{Ca_4Al_2(OH)_{12.05}(Cl)_{1.95}\cdot 4H_2O}+CaSO_4\cdot 2H_2O=Ca_4Al_2(OH)_{12}(SO_4)\cdot 6H_2O+0.975CaCl_2+0.025Ca(OH)_2$
Kuzel's salt	$\mathbf{Ca_4Al_2(SO_4)_{0.5}(Cl)(OH)_{12}\cdot 6H_2O}+0.5\cdot CaSO_4=Ca_4Al_2(OH)_{12}(SO_4)\cdot 6H_2O+0.5\cdot CaCl_2$
Nitrate AFm	$\mathbf{Ca_4Al_2(OH)_{12}(NO_3)_2\cdot 4H_2O}+CaSO_4\cdot 2H_2O=Ca_4Al_2(OH)_{12}(SO_4)\cdot 6H_2O+Ca(NO_3)_2$
Nitrite AFm	$\mathbf{Ca_4Al_2(OH)_{12}(NO_2)_2\cdot 4H_2O}+CaSO_4\cdot 2H_2O=Ca_4Al_2(OH)_{12}(SO_4)\cdot 6H_2O+Ca(NO_2)_2$

Table 2.3: Equations used to calculate heat capacities of relevant AFm phases.

Phase	Equation used for calculation of the heat capacity
Friedel's salt	$\mathbf{C_p^\circ}\{Ca_4Al_2(OH)_{12.05}(Cl)_{1.95}\cdot 4H_2O\}=\mathbf{C_p^\circ}\{Ca_4Al_2(OH)_{12}(SO_4)\cdot 6H_2O\}+0.975\cdot\mathbf{C_p^\circ}\{CaCl_2\}+0.025\cdot\mathbf{C_p^\circ}\{Ca(OH)_2\}-\mathbf{C_p^\circ}\{CaSO_4\cdot 2H_2O\}$
Kuzel's salt	$\mathbf{C_p^\circ}\{Ca_4Al_2(SO_4)_{0.5}(Cl)(OH)_{12}\cdot 6H_2O\}=\mathbf{C_p^\circ}\{Ca_4Al_2(OH)_{12}(SO_4)\cdot 6H_2O\}+0.5\cdot\mathbf{C_p^\circ}\{CaCl_2\}-0.5\cdot\mathbf{C_p^o}\{CaSO_4\}$
Nitrate AFm	$\mathbf{C_p^\circ}\{Ca_4Al_2(OH)_{12}(NO_3)_2\cdot 4H_2O\}=\mathbf{C_p^\circ}\{Ca_4Al_2(OH)_{12}(SO_4)\cdot 6H_2O\}+\mathbf{C_p^\circ}\{Ca(NO_3)_2\}-\mathbf{C_p^\circ}\{CaSO_4\cdot 2H_2O\}$
Nitrite AFm	$\mathbf{C_p^\circ}\{Ca_4Al_2(OH)_{12}(NO_2)_2\cdot 4H_2O\}=\mathbf{C_p^\circ}\{Ca_4Al_2(OH)_{12}(SO_4)\cdot 6H_2O\}+\mathbf{C_p^\circ}\{Ca(NO_2)_2\}-\mathbf{C_p^\circ}\{CaSO_4\cdot 2H_2O\}$

2.3.2 Calculation of aqueous ion activities and solubility products

Aqueous ion activities of relevant species were calculated using the GEMS database**,** applying the Truesdell-Jones modification of the extended Debye-Hückel equation (Eq. 2.2):

$$\log\gamma_i = \frac{-Az_i^2\sqrt{I}}{1+B\alpha_i\sqrt{I}} + bI \qquad \textit{Eq. 2.2}$$

where γ_i is the activity coefficient of ion 'i', A and B are Debye-Hűckel solvent parameters dependent on the dielectric constant of water and temperature, z_i is the ionic

charge, α_i is a parameter dependent on the size of ion, i (Kielland's parameter for individual ions) [58], 'b' is a semi-empirical parameter (~0.064 at 25˚C) and I is the effective ionic strength.

This equation is be applicable up to ~2 M ionic strength using b = 0.064. Temperature dependent solubility products were calculated according to the reactions presented in Eqs. 5.4, 5.5, 6.1, 6.2 and summarised in Tab. 2.4.

Table 2.4: Dissolution reactions used to calculate solubility products.

Phase	Dissolution reaction
Friedel's salt	$Ca_4Al_2(OH)_{12.05}(Cl)_{1.95}\cdot 4H_2O = 4\ Ca^{2+} + 2\ AlO_2^- + 1.95\ Cl^- + 4.05OH^- + 8H_2O$
Kuzel's salt	$Ca_4Al_2(SO_4)_{0.5}(Cl)(OH)_{12}\cdot 6H_2O = 4\ Ca^{2+} + 2\ AlO_2^- + Cl^- + 0.5SO_4^{2-} + 4OH^- + 10H_2O$
Nitrate AFm	$Ca_4Al_2(OH)_{12}(NO_3)_2\cdot 4H_2O = 4\ Ca^{2+} + 2\ AlO_2^- + 2\ NO_3^- + 4OH^- + 8H_2O$
Nitrite AFm	$Ca_4Al_2(OH)_{12}(NO_2)_2\cdot 4H_2O = 4\ Ca^{2+} + 2\ AlO_2^- + 2\ NO_2^- + 4OH^- + 8H_2O$

Gibbs energy of reaction $\Delta_r G^0_T$ at temperature T was calculated according to

$$\Delta_r G^0_T = - RT \ln K_T \qquad \textit{Eq. 2.3}$$

where R=8.315 J/(mol·K), R is the universal gas constant and K_T is a thermodynamic equilibrium solubility product at the stated temperature.

2.3.3 Correction for the temperature dependence

The solubility of Friedel's salt, Kuzel's salt, nitrate AFm or nitrite AFm was measured between 5 and 85°C and thus data to describe the solubility as a function of temperature could be derived the solubility products calculated at the different temperatures. The thermodynamic properties were calculated using a built-in 3-term temperature extrapolation [52, 69, 70], to obtain the temperature dependent log K_T function (Eqs. 2.4-2.10)

The entropy was adjusted to obtain the best fit between the measured solubility data at different temperatures and the calculated solubility products. As only a few solubility measurements were available, only the entropy was fitted, while the heat capacity of reaction was assumed to be constant over the temperature range 0-100˚C.

$$\log K_T = A_0 + \frac{A_2}{T} + A_3 \ln T \qquad \textit{Eq. 2.4}$$

$$A_o = \frac{0.4343}{R} \cdot [\Delta_r S^0_{To} - \Delta_r C_{p\,To}^0 (1 + \ln T_o)] \qquad \textit{Eq. 2.5}$$

$$A_2 = \frac{0.4343}{R} \cdot (\Delta_r H^0_{To} - \Delta_r C_{p\,To}^0 T_o) \qquad \textit{Eq. 2.6}$$

$$A_3 = \frac{0.4343}{R} \cdot \Delta_r C_{p\,To}^0 \qquad \textit{Eq. 2.7}$$

$$\Delta_r S^0_T = \Delta_r S^0_{To} + \Delta_r C_{p\,To}^0 \ln \frac{T}{T_O} \qquad \textit{Eq. 2.8}$$

$$\Delta_r H^0_T = \Delta_r H^0_{To} + \Delta_r C_{p\,To}^0 (T - T_o) \qquad \textit{Eq. 2.9}$$

$$\Delta_r G^0_T = \Delta_r H^0_T - T\,\Delta_r S^0_T \qquad \textit{Eq. 2.10}$$

2.4 Solid solutions

Solid solutions are frequently encountered in cementitious systems [9, 26, 48, 50, 71, 72] and result from the partial substitution of one or more types of atoms or ions in a single crystalline structure [73]. If the size, shape and charge of the host and substituent ions are similar, solid solution may be ideal but the larger the differences, the stronger is the tendency to non-ideality [73, 74] and the tendency to form miscibility gaps. Solid solution can provide thermodynamic stabilisation for particular compositions or range of compositions and may reflect in a non ideal trend of dissolved ion concentrations. Solid solutions are often more stable than mechanical mixtures of the end members and thus stabilize the formation of the solid solution with respect to other solid phase assemblages.

The molar Gibbs free energy ΔG_{ss} of a solid solution between different end members 'i' can be calculated according to Eq. 2.11 [51, 52]:

$$\Delta G_{ss} = \sum_i X_i \Delta_f G_i^0 + \Delta G_M \qquad \textit{Eq. 2.11}$$

$$\Delta G_M = \Delta G_{id} + \Delta G_{ex} \qquad \textit{Eq. 2.12}$$

$$\Delta G_{id} = RT \sum X_i \ln X_i \qquad \textit{Eq. 2.13}$$

$$\Delta G_{ex} = RT \sum X_i \ln \gamma_i \qquad \textit{Eq. 2.14}$$

where: ΔG_{ss} is a free energy of mechanical mixture of the end members 'i' of the solid solution and is calculated using mole fraction $X_i = n_i/\Sigma n_i$, n_i is mole amount of the end member 'i'; $\Delta_f G_i^o$ is standard molar Gibbs energy of formation of end member 'i', ΔG_M is molar Gibbs energy of mixing for given composition (Eq. 2.12) which is a sum of Gibbs energy of mixing of ideal solid solution ΔG_{id} (Eq. 2.13) and the excess Gibbs energy of solid solution ΔG_{ex} - which is only needed to calculate properties of non ideal solid solution (Eq. 2.14); R=8.315 J/(mol·K) is universal gas constant; T-temperature; γ_i is the activity coefficient of the end member and in the case of ideal solid solution all γ_i equal 1 therefore ΔG_{ex} equals zero.

When we regard non ideal solid solution $\gamma_i \neq 1$ and ΔG_{ex} of a binary solid solution can be calculated as follows (Eq. 2.15) [52]:

$$\Delta G_{ex} = RT(X_1 \ln \gamma_1 + X_2 \ln \gamma_2) \qquad \textit{Eq. 2.15}$$

where: X_1 and X_2 are amounts of end members (X_1 and $X_2 = 1$)

The GEMS code has a built in function for non ideal solid solution [68]. A semi empirical model was used to estimate ΔG_{ex} (Eq. 2.16) [51, 52, 75-77]:

$$\Delta G_{ex} = X_1 X_2 RT(a_o + a_1(X_1 - X_2) + a_2 (X_1 - X_2)^2 + \ldots) \qquad \textit{Eq. 2.16}$$

where: a_0, a_1, … are dimensionless Guggenheim parameters [52].

The software MBSSAS was used to derive the Guggenheim parameters a_0 and a_1 based on experimentally-observed compositional boundaries of the miscibility gap in relevant binary solid solution series. Detailed description of MBSSAS is given in [77].

Activity coefficients γ_i of the end members can be calculated by (Eqs. 2.17, 2.18) [51, 52]:

$$\ln \gamma_1 = X_2^{\,2}\left[a_0 + a_1(3X_1 - X_2)\right] \qquad \textit{Eq. 2.17}$$

$$\ln \gamma_2 = X_1^{\,2}\left[a_0 - a_1(3X_2 - X_1)\right] \qquad \textit{Eq. 2.18}$$

3. Analytical methods

3.1 General preparation of samples

Preparations were made using reagents of analytical purity and de-ionised double distilled CO_2-free water. Cement hydrates are sensitive, therefore to minimise atmospheric carbonation all the experiments were performed under N_2. For this purpose an either 'Atmosbag' or glovebox was used. Where agitation was required, it was done on a magnetic stirrer using a Teflon-coated magnetic follower.

Synthesized samples were stored and aged in inert HDPE or PTFE bottles and later on vacuum-filtered under N_2 atmosphere using Whatman # 4 filter paper. Solids were dried over saturated $CaCl_2$ solution at around 35% relative humidity (RH) for 2 weeks. Detailed description of synthesis of particular cement phases is provided in the further chapters.

3.2 Solubility determinations

Dried samples were dispersed in double distilled water and equilibrated at 5, 25, 55 and 85˚C. After equilibration at a w/s ratio ~30, ion concentrations were measured using AAS and ion chromatography. Solutions for analysis were obtained by filtering 15 ml of liquid phase through a syringe 'Millex' filter unit equipped with 0.22 μm 'MF-milipore' membrane. For alumimium and calcium analysis, part of the solution was acidified with 0.1 ml of 37% HCl per 10 ml of sample. Solutions were stored in alkali-resistant polypropylene tubes. Measured concentrations of calcium, aluminium, chloride, nitrate, nitrite or sulfate were used as input to calculate the solubility products. Aqueous ion activities and speciation were calculated using the GEMS database, by applying the Truesdell-Jones modification of the extended Debye-Hückel equation to correct for activities [46, 47, 51, 67].

3.2 Analysis of cation and anion concentrations in solutions

3.2.1 Chloride, nitrate, nitrite, sulfate and carbonate

Aqueous, chloride, nitrate, nitrite and sulfate concentrations were analysed using a DX-120 IC ion chromatograph equipped with a 4 mm ion exchange analytical column, IonPac AS 4A. A small volume of analyte (1 ml) was injected into a loop, carried through the system by an eluent and into the analytical column where separation took place. Applied pressure was set between 1000-1100 psi (67-74 bars). The eluent used was a mixture of 1.8 mM Na_2CO_3/l.7 mM $NaHCO_3$ and its flow rate was set at 1.8 ml/min. Eluent conductivity was suppressed by an ASRS self-regenerating suppressor with an ultra pure water (> 18 M Ω cm) regenerator.
The chromatograph was calibrated in the range 1-15 ppm. Standards were prepared from 1000 mg/L 'Spectrosol' solutions (analytical reagent purity, VWR chemicals). The background conductivity was approximately 14 μS. Due to high chloride/nitrite/nitrate concentrations all the measurements were performed on diluted samples, therefore low sulfate concentrations were below limit of detection (< 0.5 mg/l). Thus values outside the limit of detection were estimated assuming saturation with respect to phase of known thermodynamic properties *e.g.* monosulfoaluminate [51, 67].

The carbonate content was measured by total inorganic carbon (TIC) analysis. Total inorganic carbon is measured by carbon analyser in which the carbon (bicarbonate, carbonate anions etc.) contained in the sample are transformed into CO_2 (by the acidification of the sample). This gas is then sparged from solution, trapped, and the quantity trapped is analysed by infrared spectroscopy. The detection limit for a reliable TIC measurement using this method is ~1 mg/l. In most cases the concentrations of carbon in solution were lower than the detection limit therefore values were estimated assuming saturation with respect to calcite [51].

3.2.2 Calcium, sodium and aluminium

Aqueous calcium, sodium and aluminium were analysed by atomic absorption spectrometry (AAS) using a Varian SpectrAA 10 flame AAS. A nitrous oxide/

acetylene flame was used for aluminium and air /acetylene flame for calcium. In the determination of calcium and aluminium a solution of $LaCl_3$ (of final concentration~10000 ppm) was employed as a releasing agent. In the case of aluminium, additionally a KCl at a 2500 ppm K^+ was added to suppress ionisation.
Calcium was measured at wavelength 422.7 nm sodium at 589 nm and aluminium at 309.3 nm. Standards were prepared from 1000 mg/L 'Spectrosol' solutions (analytical reagent purity, VWR chemicals) were used for calibration. A linear calibration curve for calcium was obtained in the range 0-5 ppm for calcium, 0-3 ppm for sodium and 1-100 ppm for aluminium. To minimise analytical error the mean value of 3 replicates was taken for each sample.

3.2.3 pH measurements

The pH was determined by a Mettler Toledo ion selective electrode INLAB 413, which simultaneously measures aqueous pH and temperature. The pH-meter was calibrated at 25˚C using 3-point calibration with certified commercial buffers at pH 9.21, 10.00 and 13.00. For the samples equilibrated at 5, 55 and 85˚C, pH was determined at room temperature and later corrected by the calculation to the measurement temperature (pH buffer solutions were provided with information about the temperature dependence of pH, enabling correction). To avoid atmospheric carbonation, all the measurements were performed immediately after filtration.

3.3 Analysis of solids

3.3.1 Microscopy (SEM)

A scanning electron microscope FEI Quanta 200 equipped with a PGT X-ray analyzer was used for observing sample morphologies. A small quantity of the sample powder was mounted on sample holder equipped with double-sided 'Sellotape'. To reduce charging effects from the electron beam, samples were coated with gold in an argon atmosphere prior to microscopic examinations. Operating voltage was set at 15 kV.

3.3.2 Thermal analysis (TG/DTG/DTA)

A Stanton Redcroft STA-781 was used. This instrument can simultaneously record thermo-gravimetric weight changes (TG) together with the first derivative of TG (DTG) and differential thermal effects (DTA) in the course of heating. DTA gives us information about differences in thermal behaviour between the sample and reference material (corundum). The sample was packed into a platinum crucible, which was placed into the thermal analyser. The observed temperature range was between 25ºC and 1000ºC. The heating rate was set at 10ºC/min. All measurements were done under nitrogen atmosphere. Thermal analysis was used to determine the state of hydration and thermal characteristics of Kuzel's salt, nitrite and nitrate AFm phases. Those monitored weight losses occurring during thermal decomposition can be later used for identification and distinction of the solids in phase mixtures.

3.3.3 X-ray diffraction (XRD)

A Bruker D8 advance powder diffractometer was used for X-ray analysis of solids. To obtain homogenous powders solid samples before the measurement were ground in an agate mortar. Data were collected using CuKα radiation (λ=1.54 Å) at room temperature (23±3°C). Powder samples were side-loaded to the sample holder to reduce preferred orientation effects, occurring for samples with platy crystals, *e.g.* portlandite or AFm phases. EVA graphic software was used for evaluation and presentation of data.

Solid solutions were measured at room temperature (23±3°C) on the PANalytical X'Pert Pro MPD diffractometer using CuKα radiation (λ=1.54 Å) between 5 and 42° (2θ) with an integrated step scan of 0.017° (2θ) using a X'Celerator detector. The total time required for data acquisition of the diffraction pattern was 10 minutes. To process raw data, X'pert HighScore Plus software was used. Powder samples were side loaded to the sample holder to reduce preferred orientation effects in samples with platy crystals, *e.g*. portlandite or AFm. HighScore Plus software package and ICSD CIF files (Inorganic Crystal Structure Database, version 2009/1) were used for Rietveld refinement of Friedel's salt (for the rhombohedral phase ICSD: 88617 [78], 51890 [79]; for the monoclinic phase ICSD: 62363 was used [19, 80]). When attempts to apply the

structure file to refine were unsuccessful (as for the monoclinic phase of Friedel's salt ICSD 62363) a Le Bail simulation fit was used.

3.3.4 Infrared spectroscopy (FTIR)

Infrared spectroscopic analysis was made using Nicolet 205 FR-IR Spectrometer over the frequency range 400 cm^{-1}- 4000 cm^{-1}. About 0.0015 g of sample was mixed with 0.2 g of previously dried spectroscopic quality KBr. The mixture was finely ground and then compressed under 10 tonnes pressure to form a translucent pellet. Because of the hygroscopic nature of KBr special precautions were taken to minimise moisture take up. Raw data were analysed using OMNIC software.

4. The density of cement phases

4.1 Introduction and aims of data collection

The density of cement phases are a fundamental parameter with many uses, for example, calculating space filling in pastes by solid cement substances as well as assessment of the potential for changes in dimension and porosity within hardened pastes undergoing phase changes. Yet it is difficult to access a self-consistent set of density data and values reported in the literature for the same substance can vary widely. The importance of having a self-consistent data set has long been recognized: for example Taylor [81] provided data for crystalline calcium silicate hydrates and, in a later publication, gave density and powder diffraction data for many of the main cement phases [2]. Richardson [82] published updated table of crystal data together with density values for calcium silicate hydrates and related phases, but previous compilations regarding other cement compounds are incomplete and somewhat out of date. Values of densities presented in this section were implemented into the GEMS cement database and in the subsequent chapters, used for volume change calculations.

The substances comprising cement can be divided into two groups: crystalline and amorphous. The distinction is operational: in the present context, “crystalline” refers to substances having sufficiently regular internal structures, in terms of atomic, ionic and molecular arrangement, to enable characterization by classical crystallographic concepts.

Some of the relevant phases occur in nature and some can be obtained as single crystals, natural or synthetic. Classical methods of density measurement can often be applied to single crystals. But many cement substances, while crystalline, do not occur in adequate purity or size to apply classical methods. Therefore for most crystalline substances we rely on crystallochemical data for the calculation of densities, but with the cautions given below.

The principal amorphous substance of Portland cement is C-S-H. It presents particular problems in determining its density as it is insufficiently crystalline for application of conventional crystallographic methods: only experimentally-determined measurements

are useful [2, 83-85]. Moreover uncertainties persist especially with respect to its water content and only arbitrary distinctions between "bound" and "free" water are possible. Other phases may also be intercalated within C-S-H on a nanoscale *e.g.*, portlandite or AFm, thus affecting density. Uncertainty therefore exists over the Ca/Si ratio as well as extent of incorporation of other ions (alkali, alumina, sulfate...), all of which potentially affect the density. Finally, possible errors may arise from classical density measurements where, for example, a liquid used for density measurement by the Archimedes method may react with C-S-H. Thus for C-S-H there is no choice but to accept experimentally-determined data.

Crystalline solids, on the other hand, are amenable to calculation of density from crystallographic constants using the relationship (Eq. 4.1):

$$D = (Z \times M)/(N_A \times V) \qquad \textit{Eq. 4.1}$$

where: D = density in kg/m^3, Z = number of formula units per unit cell, M= formula weight, V the unit cell volume and N_a = Avogadro's number.

Volumes of the unit cells were calculated for relevant crystal systems using standard formulae (Eqs. 4.2-4.7):

Isometric/cubic crystal system: $V = a^3$ *Eq. 4.2*

Tetragonal crystal system: $V = a^2c$ *Eq. 4.3*

Hexagonal/trigonal crystal system: $V = a^2c \sin(60°)$ *Eq. 4.4*

Orthorhombic crystal system: $V = abc$ *Eq. 4.5*

Monoclinic crystal system: $V = abc \sin(\beta)$ *Eq. 4.6*

Triclinic crystal system: $V = abc((1-\cos^2\alpha-\cos^2\beta-\cos^2\gamma) + 2(\cos(\alpha)\cos(\beta)\cos(\gamma))^{½}$ *Eq. 4.7*

where *a, b, c* are the unit cell axial dimensions and α ,β, γ are the relevant angles. In some cases the unit cell contents require elucidation in order to establish the exact chemistry.

The crystallographic approach provides a uniform and consistent basis for calculation but many substances contain defects which result in real densities being slightly lower than calculated (usually the error is less than one part in x 10^4). The occurrence of solid solution in which, for example, substitution of Fe for Al occurs, also affects the mean

atomic mass of ions occupying a particular lattice site or sites and hence the density. Many substances occur in several polytypes, each of which may differ in true unit cell size and symmetry and the possibility exists that preparations may contain mixtures of polytypes. Except where noted, isomorphic substitution is negligible in the selected data. Polytypism was addressed by choosing a single subcell for the calculation. Provided subcell and Z are correctly matched. It was also noted that rhombohedral crystals have generally been treated on the basis of a larger hexagonal cell: again, no error results provided Z is chosen correctly.

Variable site occupancy may occur, with some sites left partially vacant. For example the subcell water (H_2O) content of ettringite attains a maximum of 36 but more commonly water contents lie in the range 30 to 32 H_2O per formula unit, but with little change in cell size occurring in this range. This uncertainty over composition is addressed by stating the formula used for calculation although the author also develops density-composition relationships in selected cases. Where a particular phase is impurity-stabilized, the impurity is deemed to be minor but, although the presence of impurity is noted, the author was often unable to include it in the formula because no analysis of the phase was recorded in the data source.

Temperature and pressure affect densities and the values shown here are nominally reported for 20°-25°C and ambient pressure, unless otherwise noted. The literature is often indefinite about the temperature used for collection of crystallographic data apart from stating that data were collected at “room temperature”. It has been assumed that “room temperature” lies within the range 20-25°C.

Where cell dimensions were determined from single crystal methods by the Weissenberg method [86, 87], or from precession methods using photographic recording, cell dimensions thus obtained are probably only accurate to +/- 1%. Therefore where a choice of methods for determination of cell parameters occurred, priority has been given to those made using calibrated powder X-ray diffraction or automated single-crystal methods with electronic recording.
For syngenite, the values given in [88, 89] are preferred because the coefficients of thermal dilation, necessary to correct data obtained at 154 K [90] to ambient are not available.

In a few cases recalculation of density provided in this chapter does not agree with the calculation presented in the reference. Where such disagreement exceeds the normal limits of arithmetic error, reference value is noted [Tab. 4.2], but the author has generally been unable to resolve the discrepancy between calculations.
This work is not complete because of multiplicity of phases, hydration states, and solid solution possibilities but it does include most of the significant compounds occurring in Portland cement and cement pastes. The order of data presentation divides substances into twelve main groups:

- Simple oxides and hydrated oxides
- Carbonates
- Sulfates and hydrated sulfates
- Tricalcium aluminate
- Tetracalcium aluminoferrite
- Tricalcium silicate
- Dicalcium silicate
- Aluminate-ferrite-trisubstituent phases
- Aluminate-ferrite-monosubstituent phases
- Hydrogarnet
- Selected crystalline calcium silicate hydrates structurally related to C-S-H (data including other calcium silicate hydrates presented by Richardson [82])
- Hydrotalcite and related phases

Experimental work was also undertaken to synthesize major AFm and AFt cement phases, determine their unit cell parameters and compare the results with those recorded in the literature. Results obtained from these preparations are included in the compilation.

4.2 Synthesis and characterisation of AFm and AFt phases

Many of these preparation routes are described in the previous literature [51] and were used here with minor changes. The synthesis of the relevant cement hydrates required several solid precursors. These were made from analytical reagent grade (AR) chemicals. Lime, CaO, was obtained by decarbonation of AR grade $CaCO_3$ at 1000°C for ~24 hours. Anhydrite, $CaSO_4$, was prepared by dehydration of AR gypsum ($CaSO_4 \cdot 2H_2O$) in a muffle furnace at 550°C for 12 hours.

Tricalcium aluminate, C_3A ($Ca_3Al_2O_6$), was prepared from a 3:1 molar ratio of $CaCO_3$ and Al_2O_3, fired in a platinum crucible at 1400°C for 3 days in an electrically heated furnace. Every 12 hours, the sample was cooled, reground in an agate mortar to achieve homogenization, placed back in the platinum crucible and reheated repeating until free lime was no longer present.

4.2.1 AFm phases

Using the above precursors, "hydroxy AFm", $Ca_4Al_2(OH)_{14} \cdot 6\text{-}12H_2O$, was synthesized by mixing CaO and C_3A in a 1:1 molar ratio. The solids were slurried in degassed, ultra pure CO_2-free water (water/solid ratio~10) and reacted at 5°C in a sealed system with stirring for the first 72 hours and thereafter periodically agitated at 5°C for 3 weeks. Finally the solid was vacuum filtered at 5°C under N_2 atmosphere.

"Monosulfoaluminate", $Ca_4Al_2(SO_4)(OH)_{12} \cdot 6H_2O$, becomes more stable at temperatures above 40°C, therefore a 1:1 molar mixture of C_3A and $CaSO_4$ was suspended in ultra pure, CO_2-free water (water/solid ratio ~10), and reacted at 85°C. After 7 days the solid was vacuum filtered under N_2 atmosphere.

"Monocarboaluminate", $Ca_4Al_2(CO_3)(OH)_{12} \cdot 5H_2O$, was prepared by mixing C_3A and $CaCO_3$ in a 1:1 molar ratio with previously degassed ultra-pure water at 25°C (water/solid ratio ~10), and stored for 10 days with periodic agitation.

"Hemicarboaluminate", $Ca_4Al_2(CO_3)_{0.5}(OH)_{13} \cdot 5.5H_2O$, was made by addition of C_3A, $CaCO_3$ and CaO in stoichiometric quantities to previously degassed ultra pure water at

25°C (water/solid ratio ~10) and continuously stirred in plastic (HDPE) bottles for 14 days before filtration .

Strätlingite, $Ca_2Al_2SiO_2(OH)_{10} \cdot 3H_2O$, was synthesized from a stoichiometric mix of CaO, $Na_2Si_2O_5 \cdot 2H_2O$, $NaAlO_2$ and water at 25°C (water/solid ratio ~10). The suspension was stirred for 5-6 weeks at 25°C. After filtration, sodium was washed out by flushing the remaining solid with double distilled water. From previous experience the sodium content of the washed solid is known to be negligible.

'Friedel's salt' $Ca_4Al_2(Cl)_2(OH)_{12} \cdot 4H_2O$ was made by mixing C_3A and $CaCl_2 \cdot 2H_2O$ in a 1:1 molar ratio, which were dispersed in double distilled, CO_2 free water (water/solid ratio ~10), sealed in an airtight polythene bottle and left to age with stirring for 30 days [18]. After ageing the solid was filtered under nitrogen atmosphere.

4.2.2 AFt phases

'Sulfate ettringite', $Ca_6Al_2(SO_4)_3(OH)_{12} \cdot 26H_2O$, was prepared by using method described by Perkins and Palmer [91] where two reactant solutions were initially made, solution (1) by adding 6.65 g $Al_2(SO_4)_3$ $18H_2O$ to 100 ml and solution (2) by dispersing 4.44 g $Ca(OH)_2$ in 250 ml of ultrapure water (>14 MΩ cm) all under CO_2-free conditions. The two reactant solutions were transferred to a N_2-filled glove box, mixed and diluted to 500 ml with additional reagent water to which 0.5 ml of 1 M NaOH had been added. The preparation was sealed in a 500 ml high density polyethylene (HDPE) bottle, removed form the dry box and placed on a hot plate at 60°C, with stirring. After 48 hours, the contents were filtered under N_2 using a ceramic filter funnel and rapidly dried under N_2 using a poor vacuum.

'Carbonate ettringite', $Ca_6Al_2(CO_3)_3(OH)_{12} \cdot 26H_2O$, was prepared by precipitation from a stochiometric mixture of CaO, $NaAlO_2$ and Na_2CO_3 in a 10 wt% sucrose solution [51]. Previously-prepared slurries of sodium aluminate and sodium carbonate were added to the sucrose-portlandite mixture, stirred for 3 days and periodically agitated at 25°C for 2 weeks and thereafter filtered and washed. Experience of this preparation indicated that thorough washing was required to prevent retention of sucrose.

4.2.3 Data collection

The angular range of Bruker D8 powder diffractometer was set between 5-55º 2θ. Unit cell parameters were refined from the powder diffraction patterns using unit cell refinement software- CELREF 2.

The number of selected reflections admitted into the unit cell refinement is shown below:

$Ca_4Al_2(OH)_{14} \cdot 13\ H_2O$ – 22 reflections

$Ca_4Al_2(SO_4)(OH)_{12} \cdot 6H_2O$- 23 reflections

$Ca_4Al_2(CO_3)(OH)_{12} \cdot 5H_2O$ – 27 reflections

$Ca_2Al_2SiO_2(OH)_{10} \cdot 3H_2O$ – 29 reflections

$Ca_4Al_2(CO_3)_{0.5}(OH)_{13} \cdot 5.5H_2O$ – 22 reflections

$Ca_4Al_2(Cl)_2(OH)_{12} \cdot 4H_2O$ – 23 reflections

$Ca_6Al_2(SO_4)_3(OH)_{12} \cdot 26H_2O$ – 71 reflections

$Ca_6Al_2(SO_4)_3(OH)_{12} \cdot 30H_2O$ – 38 reflections

$Ca_6Al_2(CO_3)_3(OH)_{12} \cdot 26H_2O$ – 35 reflections

4.3 Density values of principal crystalline phases occurring in Portland cement

A summary of recommended density values is provided in Table 4.1.

Table 4.1: Density of Selected Cement Phases at 20-25ºC, t.w. – this work.

Mineral or Chemical Name	Formula	Density [kg/m^3]	References
lime	CaO	3341	[92, 93]
periclase	MgO	3584	[93, 94]
corundum	Al_2O_3	3990	[93, 95, 96]
quartz	SiO_2	2641	[14, 97]
gibbsite	$Al(OH)_3$	2421	[98, 99]
brucite	$Mg(OH)_2$	2368	[100, 101]
portlandite	$Ca(OH)_2$	2251	[102, 103]
calcite	$CaCO_3$	2710	[86, 104, 105]
aragonite	$CaCO_3$	2930	[106, 107]
vaterite	μ- $CaCO_3$	2661	[108, 109]
magnesite	$MgCO_3$	3011	[105, 110]
dolomite	$CaMg(CO_3)_2$	2852	[105, 111-113]
anhydrite	$CaSO_4$	2968	[114-116]
‘soluble anhydrite’	$Ca(SO_4)\cdot<0.05\ H_2O$	2958	[117]
hemihydrate	$CaSO_4\cdot 0.5H_2O$	2733	[117]
hemihydrate	$CaSO_4\cdot 0.8H_2O$	2783	[118]

Mineral or Chemical Name	Formula	Density [kg/m^3]	References
gypsum	$CaSO_4 \cdot 2H_2O$	2311	[119, 120]
arcanite	K_2SO_4	2668	[121]
thenardite	Na_2SO_4	2662	[122, 123]
aphthitalite	$K_3Na(SO_4)_2$	2703	[124]
syngenite	$K_2Ca(SO_4)_2 \cdot H_2O$	2575	[88-90]
‘aluminosulfate’	$Ca_4(Al_2O_3)_3(SO_4)$	2607	[125]
‘silicosulfate’	$Ca_5(SiO_2)_2(SO_4)$	2972	[126]
tricalcium aluminate (cubic)	$Ca_3Al_2O_6$	3030	[127-129]
tricalcium aluminate (othorombic)	$Ca_3Al_2O_6$	3023	[129]
tetracalcium aluminoferrite	$Ca_2(Al,Fe)_2O_5$	3708	[130, 131]
R-tricalcium silicate at 1200ºC	R-Ca_3SiO_5	3025	[132]
R-tricalcium silicate- Sr stabilized	R-Ca_3SiO_5	3168	[133]
M3-tricalcium silicate- Mg stabilized	M3-Ca_3SiO_5	3182	[134]
M3-tricalcium silicate- less well ordered	M3-Ca_3SiO_5	3153	[135]
T1-tricalcium silicate	T1-Ca_3SiO_5	3120	[136]
α-dicalcium silicate- Ba stabilized	α-Ca_2SiO_4	2968	[137]
α'_H-dicalcium silicate- P_2O_5 stabilized	α'_H-Ca_2SiO_4	3148	[138]

Mineral or Chemical Name	Formula	Density [kg/m^3]	References
α'_L-dicalcium silicate- Sr stabilized	α'_L-Ca_2SiO_4	3092	[133]
β-dicalcium silicate	β-Ca_2SiO_4	3326	[139, 140]
γ-dicalcium silicate	γ-Ca_2SiO_4	2960	[141]
ettringite with low H_2O content (30 H_2O)	$[Ca_3Al(OH)_6]_2(SO_4)_3 \cdot 24H_2O$	1768	[17]
Ettringite (32 H_2O)	$[Ca_3Al(OH)_6]_2(SO_4)_3 \cdot (24+2)H_2O$	1778	[17, 25, 142, 143], t.w.
ettringite with high H_2O content (36 H_2O)	$[Ca_3Al(OH)_6]_2(SO_4)_3 \cdot (24+6)H_2O$	1863	[17], t.w.
carbonate ettringite	$[Ca_3Al(OH)_6]_2(CO_3)_3 \cdot (24+2)H_2O$	1760	[25], t.w.
iron ettringite	$[Ca_3Fe(OH)_6]_2(SO_4)_3 \cdot (24+2)H_2O$	1830	[25, 144]
thaumasite	$Ca_3(SO_4)(CO_3)[Si(OH)_6] \cdot 12H_2O$	1882	[145, 146]
Hydroxy-AFm	$Ca_4Al_2(OH)_{14} \cdot 6H_2O$	2044	[23], t.w.
Fe-hydroxy AFm	$Ca_4Fe_2(OH)_{14} \cdot 6H_2O$	2162	[147]
α_1-tetracalcium aluminate -19- hydrate	α_1-$Ca_4Al_2(OH)_{14} \cdot 12H_2O$	1804	[22]
α_2-tetracalcium aluminate -19- hydrate	α_2-$Ca_4Al_2(OH)_{14} \cdot 12H_2O$	1802	[22]
monosulfoaluminate (12 H_2O)	$Ca_4Al_2(SO_4)(OH)_{12} \cdot 6H_2O$	2015	[16, 17, 21], t.w.
monosulfoaluminate (14 H_2O)	$Ca_4Al_2(SO_4)(OH)_{12} \cdot 8H_2O$	1998	[17]
monosulfoaluminate (16 H_2O)	$Ca_4Al_2(SO_4)(OH)_{12} \cdot 10H_2O$	1983	[17]
Fe-monosulfoaluminate	$Ca_4Fe_2(SO_4)(OH)_{12} \cdot 6H_2O$	2117	[148, 149]

Mineral or Chemical Name	Formula	Density [kg/m^3]	References
strätlingite	$Ca_2Al_2SiO_7 \cdot 8H_2O$	1937	[150-152], t.w.
monocarboaluminate	$Ca_4Al_2(CO_3)(OH)_{12} \cdot 5H_2O$	2175	[23, 153], t.w.
Fe-monocarboaluminate	$Ca_4Fe_2(CO_3)(OH)_{12} \cdot 6H_2O$	2219	[154]
hemicarboaluminate	$Ca_4Al_2(CO_3)_{0.5}(OH)_{13} \cdot 5.5H_2O$	1985	[23], t.w.
dicalcium aluminate -8-hydrate	$Ca_2Al_2(OH)_{10} \cdot 3H_2O$	1950	[155]
α-Friedel's salt	α-$Ca_4Al_2(Cl)_2(OH)_{12} \cdot 4H_2O$	2064	[80, 156, 157], t.w.
β-Friedel's salt	β-$Ca_4Al_2(Cl)_2(OH)_{12} \cdot 4H_2O$	2094	[78, 148, 156, 157]
β-Fe-Friedel's salt	β-$Ca_4Fe_2(Cl)_2(OH)_{12} \cdot 4H_2O$	2228	[148, 158]
Kuzel's salt	$Ca_4Al_2(SO_4)_{0.5}(Cl)\ (OH)_{12} \cdot 6H_2O$	2114	[148, 154]
Fe- Kuzel's salt	$Ca_4Fe_2(SO_4)_{0.5}(Cl)\ (OH)_{12} \cdot 6H_2O$	2222	[148]
hydrogarnet (katoite)	$Ca_3Al_2(OH)_{12}$	2530	[159-161]
Fe-hydrogarnet	$Ca_3Fe_2(OH)_{12}$	2809	[2, 87]
siliceous hydrogarnet	$Ca_3Al_2\,SiO_4(OH)_8$	2832	[87, 162]
jennite	$9CaO \cdot 6SiO_2 \cdot 11H_2O$	2331	[2, 163, 164]
tobermorite 14 Å	$5CaO \cdot 6SiO_2 \cdot 8H_2O$	2228	[2, 165]
afwillite	$3CaO \cdot 2SiO_2 \cdot 3H_2O$	2645	[166, 167]
hydrotalcite	$Mg_4Al_2(OH)_{12}CO_3 \cdot 3H_2O$	2122	[168-170]

Mineral or Chemical Name	Formula	Density [kg/m^3]	References
Fe-hydrotalcite	$Mg_4Fe_2(OH)_{12}CO_3 \cdot 3H_2O$	2269	[170]
meixnerite	$Mg_6Al_2(OH)_{18} \cdot 4H_2O$	1945	[171, 172]
OH-hydrotalcite	$Mg_4Al_2(OH)_{14} \cdot 3H_2O$	2036	[172]

4.4 Discussion on the data compilation and consequences of the water packing on the density changes in AFm and AFt structures

The classification of cement phases as 'important' (and hence worthy of inclusion) is partly a matter of opinion and partly a matter of the availability of data. For example data on solid solutions at well-spaced intervals are largely absent.

The compilation therefore rests on the values critically extracted from the literature but with a special focus on AFm and AFt phases. Where multiple data were available, and admitted into the compilation, an averaging process was used and density described as 'mean density'. If some methods had relatively poor absolute accuracy [86, 87, 90] and data were rejected or not heavily weighted, the density is expressed as 'recommended density'. For brevity, only the compiled values are given in this chapter with selected key references. A worksheet was generated for each substance showing all references and numerical values, together with comment: the worksheets are attached in Appendix I. Review shows that quality of data reported in the literature varies. One of the principal difficulties of determining the densities of substances experimentally by classical methods is in providing assurance that preparation is phase–pure. This assurance is often given by using single crystals, or handpicking enough smaller crystals, for analysis. With cement phases, this is often not possible: not only are crystals too small to select, but an ever-present inaccuracy arises because bulk preparations may contain significant content of amorphous material which escapes detection by X-ray powder analysis, etc.

Regarding natural samples solid solution has to be taken into consideration as well as possible physical inclusions which may affect density. However by determining unit cell sizes, coupled with the known cell contents, errors arising from physical inclusions, adhering impurities, etc. are eliminated: unit cell sizes as determined by refinement of the powder pattern are also insensitive to the presence of non-crystalline impurities.

The use of crystallographic methods also calls into question the definition of a 'phase'. For example, the cement literature tends to treat 'AFm' as though it were a single phase, but this is an oversimplification. Literature review has disclosed that several AFm or AFt phases may coexist, which form limited solid solutions [8, 9, 12, 28]. Thus the density classification reflects current knowledge and, as data permit, densities are also given for AFm phases differing in water content *e.g.* 13 and 19 H_2O states (hydroxy AFm), for different trivalent substituents in the principle layer e.g. with octahedral Al or Fe (III) and with different anions, *e.g.* sulfate, chloride, carbonate and hydroxide. Data are however available for only a few permutations; indeed not all the permutations may be stable and in at least two known examples, phase development is further complicated by ordering of anionic substituents, as occurs in Kuzel's salt (distinguished by ordering of Cl and SO_4) and in hemicarboaluminate (distinguished by ordering of OH and CO_3). It appears that ordered AFm arrangements require both a mono-and divalent anionic substituent and it is possible that other, as yet undiscovered, anion-ordered AFm phases exist.

Problems of assessing the impact of solid solution on densities have been noted. For example, as expected from the relative formula weights, the density of Al-AFm is much less than the density of corresponding Fe(III)-AFm (Al=27 g/mol, Fe = 55.8 g/mol). Given that the two AFm phases are isostructural, or very nearly isostructural, the density difference is expected. In the absence of data on intermediate compositions, Vegard's law (that density is a linear function of composition) has to be assumed.

However a number of systems are known in which significant departure from Vegard's law occurs: for example in the Al-AFm series with (OH, SO_4) anions, where solid solution is incomplete but no ordered compound occurs, analysis of the thermodynamic data discloses that sulfate has a strong stabilizing action on the OH-AFm phase [9], *i.e.*,

that the solid solutions are non-ideal. It may be that similar non-ideal changes are also reflected in the density function.

Other possibilities occur for non-ideal solid solution. For example, carbonate can replace other anions in AFm. While some anions, *e.g.* chloride and hydroxide appear to behave as simple spherical ions, carbonate can appear either as a spherical ion or as a trigonal planar group. Depending on carbonate orientation, the two possibilities differ in the effective molar volume of the anionic substituent and hence differ in their contribution to density. Fig. 4.1 shows the densities in the series of AFm phases with OH and CO_3. Of course changing composition influences density but the density of hemi- and monocarboaluminate are also affected by the orientation of the trigonal planar carbonate group. It is most efficiently packed in monocarboaluminate, in which it is sub-parallel to the principal layer spacing [2, 173], hence the high density, whereas in hemicarboaluminate, it is perpendicular to the principal layers. Thus the density of hemicarboaluminate falls much below the trend line deduced for its end-members. These differences in carbonate orientation also affect the basal spacings (d_{001}), numerical values of which are shown in the Fig. 4.1.

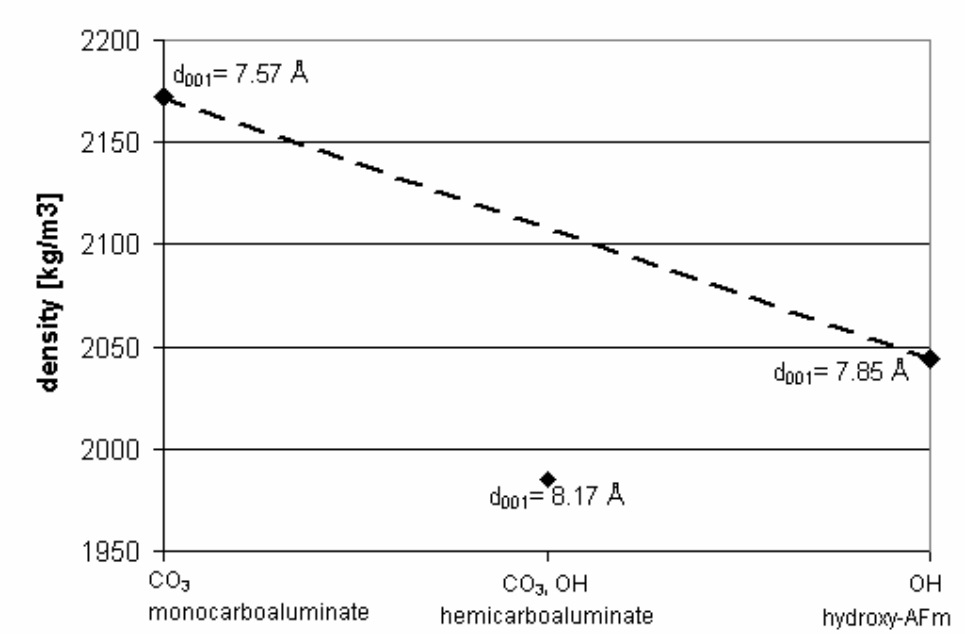

Figure 4.1: Density trends in the (OH, CO_3) AFm phases.

Interesting relations exist between the composition and density relationships in the AFm and AFt families, as shown in Fig. 4.2. The two structures, of AFm and AFt, differ in bonding requirements. The layer spacings in AFm are easily increased to allow

variable water contents, as a result of which the density decreases as the water content increases. This relation appears to be linear (as expected) for OH-AFm but it is also observed to be approximately linear for the SO_4-AFm series. The structural role of water is relatively well-defined: it can be expected for example to have the 13 H_2O state or 19 H_2O state but not, apparently, intermediate water contents, which can only be achieved by having a mixture of discrete AFm phases. For that reason, trend lines are shown as dashed, to emphasize that water contents are not continuously variable within a single AFm phase. Similarly, sulfate AFm at room temperature exhibits three hydrate states: 12 H_2O, 14 H_2O and 16 H_2O, depending on relative humidity. Pöllmann [17] has established three additional lower hydration states, the densities of which are not sufficiently well established to show in Fig. 4.2(b).

However the three examples of sulfate AFm phases show a linear trend of decreasing density with increasing water content, with a much lower slope than observed for OH-AFm.

The actual hydration state achieved by AFm in cement is not always well known: loss of water may occur in the course of specimen preparation unless special precautions are taken in the course of specimen preparation and handling. However it is apparent that potential volume changes can occur in AFm, due to its hydration state change. The greatest potential seems to occur for OH-AFm, where the transition from 13 H_2O to 19 H_2O results in an increase in specific volume of more than 10%. For sulfate AFm, a comparable change occurs but is less marked, only a few %.

The calculated volume change cannot be associated with an actual expansion or contraction: it is best regarded as indicating a *potential for change*. This potential might, for example, be achieved in the course of thermal cycling because, other factors being equal, the highest hydration states are achieved at low temperatures. Nevertheless, the potential for expansion can be minimized by inclusion of sufficient sulfate to convert all AFm to its sulfated form with perhaps a sufficient reserve to stabilize AFt in the cement. Because sufficient sulfate is usually added to Portland cement to achieve this mineralogical state, the problem of dimensional instability resulting from changing AFm hydration states is unlikely to arise in commercial Portland cements. The arguments continue about optimum sulfate content in cement but it can be noted that there are good reasons, more than just control of set times, why cement should not be under-sulfated: in this instance, to avoid potential dimensional instability resulting from the presence of OH-AFm in different hydration states.

The hydration states of AFt show a non- linear density trend in response to changing water content, Fig. 4.2(c). However the density trend shows a slope opposite to that of AFm: intercalation of more water in the AFt structure increases the physical density. This state is believed to arise because AFt is a three dimensional structure [2]; it is not easy to expand or contract its framework so water in excess of 30 H_2O per formula unit has to fit into a relatively unchanged physical space. However between 30 and 32 H_2O the density change per water molecule changes much less than between 32 and 36. Probably water in excess of 32 occupies a different set of sites than between 30 and 32, thus impacting differently on cell dimensions.

Density values gathered in this compilation were implemented into a GEMS cement database [51] and used for further calculations on the volume changes performed in this thesis. Many reactions occurring in cementitious systems are isochemical: that is, the chemistry remains constant but a redistribution of ions occurs amongst coexisting phases. This compilation may serve as a benchmark to enable the precise calculation of volume changes to be made in the course of isochemical mineralogical changes. Reactions between cement and its service environment generally involve exchange of mass: that is, they are not isochemical. In these conditions, the database presented forms the basis of calculation but requires application of more sophisticated calculations, taking into account the impact of mass balance changes.

Table 4.2: Density of Selected Cement Phases given by some authors, where recalculation of density does not agree with the author's own calculation.

Author/ Reference	Formula	Density given by author [kg/m^3]
Gaines, et al. [14]	SiO_2	2660
Abriel [118]	$CaSO_4 \cdot 0.8H_2O$	2630
Okada, et al. [124]	$K_3\,Na(SO_4)_2$	2690
Swanson, et al. [142]	$[Ca_3Al(OH)_6]_2(SO_4)_3 \cdot (24+2)H_2O$	1754
Rinaldi, et al. [152]	$Ca_2Al_2SiO_7 \cdot 8H_2O$	1960
Rinaldi, et al. [162]	$Ca_3Al_2\,SiO_4(OH)_8$	2760

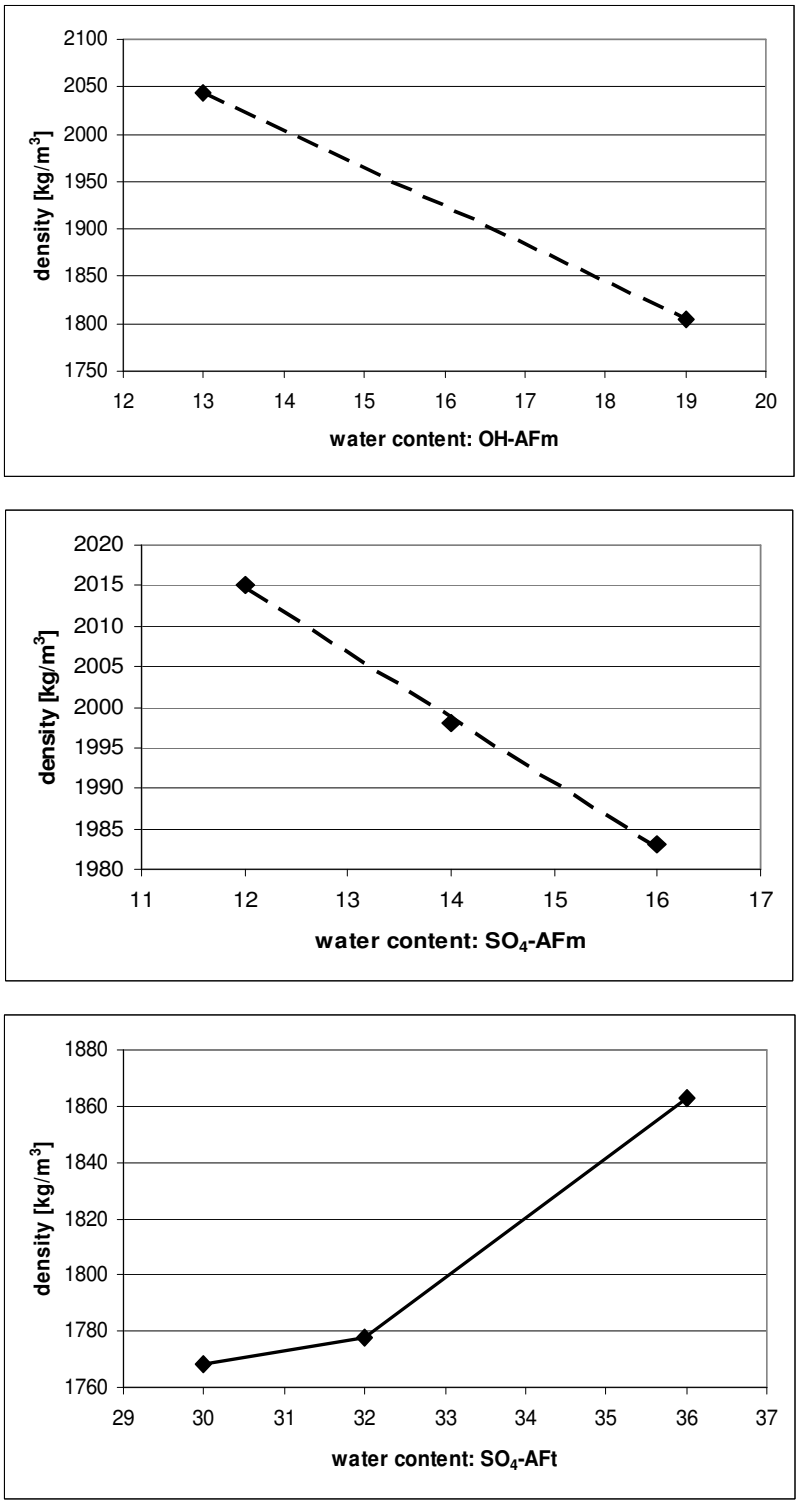

Figure 4.2: Relation between water content and density of: OH-AFm (a, top), SO_4-AFm (b, middle) and SO_4-AFt (c, bottom).

5. Impact of chloride on the mineralogy of hydrated Portland cement systems

5.1 Introduction

5.1.1 Chloride in cement

Chloride may enter cementitious systems in various ways, through the mixing water, chloride-bearing aggregate when calcium chloride is used as set accelerating admixture or from the service environment like sea water, ground water or de-icing salt [174-177]. When chloride diffuses into the system from an external source, the resulting diffusion profile has a shape similar to that predicted from Fick's laws [178]. Although the diffusion process is affected by other factors including ion exchange and chloride binding into the C-S-H and the AFm phase(s), AFm serves as an important "sink" for chloride ions. This process has been studied extensively in the past [10, 179-198] but conditions are not always well related to the environments encountered in commercial cement materials. The underlying mechanisms of chloride binding in cement systems are complex as several different processes act simultaneously. For example, chloride ions may interact with hydrated cement forming chloroaluminate phases, such as Friedel's and/or Kuzel's salt and solid solutions with other AFm phases [10, 11, 18, 199-203] but can also be chemisorbed by C-S-H [176, 184, 197, 202, 204, 205].

Chloride in cement paste has been widely studied because of its impact on the corrosion of steel in reinforced concrete. Two important parameters determining the risk of chloride-induced corrosion are believed to be: (i) the ratio of concentrations of chloride and hydroxyl ions in the pore solution and (ii) the diffusivity of chloride ions through cover concrete [206, 207]. Assessments of the corrosion threshold at which chloride ions depassivate steel are related to $[Cl^-]/[OH^-]$ ratios in the pore solution [207-209]. Only the unbound fraction of the chloride dissolved in the aqueous phase of the concrete is deemed to interact destructively with the passivating layer on steel. Thus it is worthwhile to have precise information, preferably obtained using non-destructive techniques, on the partition of chloride between "free" and "bound" states.

Formation of Friedel's salt, containing essential chloride, is potentially a mechanism for retarding chloride diffusion and reducing aqueous $[Cl^-]/[OH^-]$ ratios along the profile.

5.1.2 Corrosion of reinforcing steel

Under alkaline conditions of pore solution, reinforcing steel tends to passivate with a thin adhering film of γ-Fe_2O_3 [210]. This protective thin layer is stable in the alkaline environment of hydrated cement which has pH generally higher than 12.5. The passivity of the film is destroyed by a drop in the alkalinity when pH < 11.5 [2]. This pH drop may occur when chloride ion migrates into concrete *e.g.* from sea water, or de-icing salt, or when carbonation occurs [2, 211], or some combination of processes. The corrosion of steel in concrete is an electrochemical process. Exposed steel will corrode in moist atmospheres due to local compositional or structural variations, some areas become positively and others negatively charged, and electrical cells are set up [2]. The metal oxidises at the anode where corrosion occurs according to (Eq. 5.1):

$$Fe\ (metal) \Rightarrow Fe^{2+} + 2e^- \qquad \textit{Eq. 5.1}$$

Simultaneously, reduction occurs at cathodic sites. The typical cathodic process is shown in (Eq. 5.2):

$$\tfrac{1}{2}O_2 + H_2O + 2e^- \Rightarrow 2OH^- \qquad \textit{Eq. 5.2}$$

The electrons produced during this process are conducted through the metal whilst the ions formed are transported via the pore water which acts as the electrolyte.

Thus in the presence of oxygen and water the ferrous ions released form ferrous hydroxide (Eq. 5.3):

$$Fe^{2+} + 2OH^- \Rightarrow Fe(OH)_2 \qquad \textit{Eq. 5.3}$$

From this initial product, a series of corrosion products such as chloro-complexes [212-215] may be produced. Some of these products are soluble and assist transport of corrosion products away from sites where they might otherwise give physical protection. Exposed steel will also corrode in moist atmospheres due to local compositional or structural variations, some areas become positively and others negatively charged, and

electrical cells are set up [2]. This differential corrosion also occurs in cement environments.

The permeability of the concrete is important in determining the extent and rate at which aggressive external substances can attack the steel. Concrete of low permeability is more likely to delay chloride ions from an external source from reaching the steel and causing depassivation.

5.1.3 Chloride salts as an accelerating admixtures

Accelerating admixtures are used in cold weather concreting operations and enable reduction in the curing and protection periods necessary to achieve specified strengths in concrete [176]. Chloride salts, and in particular calcium chloride, have been known to accelerate setting and hardening of Portland cement concrete. The addition of $CaCl_2$ increases heat evolution at early ages and affects such properties as strength, porosity, chemical composition and structure of the hydration products [2, 176]. The accelerating effect on the hydration of silicate phases C_3S and C_2S and possible mechanisms of acceleration have been discussed by several researchers [176, 216-220]. As addition of chloride salts increases the possibility of steel corrosion [176, 221, 222] in reinforced structures its use is prohibited in many countries.

5.1.4 Chloride hydrates

Friedel's salt ($3CaO{\cdot}Al_2O_3{\cdot}CaCl_2{\cdot}10H_2O$) has been first synthesized by Friedel [223] in 1897, who studied the reactivity of lime with aluminum chloride. Its crystal structure and unit cell parameters have been refined by Terzis et al. [80], Kuzel [148, 156], Renaudin et al. [78], and Rapin et al. [157]. Detailed information about unit cell parameters reported in these references is provided in Appendix I (subsections 51, 52 and 53). The compound transforms at around 35˚C from a rhombohedral, high-temperature form (β) to a monoclinic low-temperature form (α). The structural transition at 35˚C was studied by various methods, including polarized light optical microscopy [224] synchrotron powder diffraction [19] and 27Al MAS NMR [225]. The monoclinic distortion at < 35˚C was attributed to ordering of the orientation of the water molecules and changes in the hydrogen bond [19]. Friedel's salt is reported to be stable

within the pH range 11-12.5 [226, 227]. Formation of the iron analogue of Friedel's salt, $3CaO{\cdot}Fe_2O_3{\cdot}CaCl_2{\cdot}10H_2O$, and limited solid solution with $3CaO{\cdot}Al_2O_3{\cdot}CaCl_2{\cdot}10H_2O$ have been reported [2, 148, 158, 228, 229].

Kuzel's salt, $3CaO{\cdot}Al_2O_3{\cdot}½CaSO_4{\cdot}½\ CaCl_2{\cdot}12H_2O$, is an anion-ordered compound, ideally with the 2:1 molar ratio of Cl/SO_4 [2, 11, 13, 39, 148, 228, 230]. Kuzel who first synthesized and determined its crystal structure [13], concluded that SO_4 and Cl ions alternate in planes parallel to (001). The iron analogue of Kuzel's salt has been reported [148]. Detailed information about unit cell parameters is given in Appendix I (subsections 54 and 55).

Several oxychlorides ($3CaO{\cdot}CaCl_2{\cdot}H_2O$, $3CaO{\cdot}CaCl_2{\cdot}2H_2O$, $3CaO{\cdot}CaCl_2{\cdot}10H_2O$ $CaO{\cdot}CaCl_2{\cdot}12H_2O$, $CaO{\cdot}CaCl_2{\cdot}15H_2O$) have been reported and are stable in the range 3-8 M Cl^- [40, 176, 212, 214, 215]. Oxychlorides are highly soluble in comparison with chloroaluminate phases therefore, as long as aluminium is present, chloride will precipitate preferentially as a chloroaluminate phase. "Oxychlorides" will however only appear at very high chloride concentrations [40, 201]. The low-soluble phase likely to appear as a consequence of attack by sea water concentrations is the chloroaluminate.

Pöllmann [27] using the so called 'sugar method' attempted the synthesis of chlorine ettringite $3CaO{\cdot}Al_2O_3{\cdot}3CaCl_2{\cdot}30H_2O$ at "room temperature" and reported that the chloride content of the product was < 0.7% (compared with theoretical 17.7% for Cl-ettringite). Chloride ettringite has however been reported to occur stably only below 0^oC and usually at very high chloride concentrations (around 20 wt% of $CaCl_2$) [227-231].

Chloride has been reported to be sorbed/bound on the C-S-H [176, 184, 197, 202, 204, 205, 217] as an interlayer anion, chemisorbed as an oxychloride complex or substituted in the structure. Beaudoin et al. [205] investigated adsorption/desorption of chloride on the C-S-H depending on Ca/Si ratios. He established that reversible chloride sorption increases with increasing Ca/Si ratio of the C-S-H and that some of the chloride may be irreversibly lattice substituted into the C-S-H. The quantity of chemisorbed chloride equalled 0.6% for 0.68 Ca/Si ratio and [40, 201] increased to 1.5% for 1.91 Ca/Si ratio C-S-H. The amount of 'irreversibly'-bound chloride varied from 0.01% up to 0.25%. The conclusion was that chloride may exist on the surface of the C-S-H as well in

interlayer positions and that chloride may react with calcium to form strongly bound complexes. Vialis [204] investigated interactions of C-S-H with sodium, lithium and caesium chloride and established that chloride sorption is not only dependent on the Ca/Si ratio of the C-S-H but also on the cation associated with the chloride.

5.1.5 Chloride binding capacity of cement

The chloride binding capacity of cement depends on several factors: the mineralogical composition, temperature, pH, water/cement ratio and chloride concentration [188, 192, 193, 198, 202, 232-241]. Cements high in calcium aluminate and ferrite are able to bind relatively large amounts of chloride (giving pastes rich in AFm, which has ability to accommodate Cl^-) [180, 237, 242]. An increase of sulfate content in cement reduces the chloride binding capacity. Sulfates are more strongly bound with C_3A than chlorides therefore Friedel's salt is not stable in the presence of sulfate ions, and it is converted to ettringite [193, 232, 243]. Kuzel [244] found that Friedel's salt is stable from 0˚C up to 200˚C and noticed transition from monoclinic (M) to rhombohedral (R) symmetry occurring at around 28˚C. Jensen et al. [238] reported that more chloride was bound at 20˚C than at either 4˚C or 35˚C. Kuzel's salt is not stable at elevated temperatures, and at 60-90˚C monosulfoaluminate forms instead [185].

Nielsen [188, 245] reported that binding of chloride by cement pastes is dependent on pH. He concluded that alkalis have a negative impact on the binding of chlorides because they increase the concentration of chlorides in pore solution. Tritthart [192] suggested that competition between OH and Cl for AFm anion sites governed the distribution. Lower OH concentrations result in more chloride bound, therefore a higher pH pore fluid implies less chloride binding.

Arya et al. [233] noted that chloride binding also increased with increase in water/cement ratio, curing temperature and age. On the other hand Gégout et al. [197] also noted that action of chlorides is strongly related to the pH of aggressive solution, but that binding of chloride was the same for both pH 11.5 and 13, although leaching of portlandite was accelerated at pH 11.5 in the presence of chloride because portlandite solubility increases with decreasing pH [47].

Supplementary cementitious materials (SCM), such as blast furnace slag, fly ash, silica fume and natural pozzolans (volcanic ash, opaline shale, tuff, etc.), have a significant impact on the ability of concrete to resist penetration by chloride ions. This phenomenon is largely ascribed to the modified pore structure resulting in reduced permeability and ionic diffusivity. Supplementary cementitious materials also change the mineralogical composition and chloride binding capacity of the cement paste. The effect of SCM's on chloride binding and corrosion of reinforcement was studied by several researchers [181, 190, 197, 207, 246-251]. SCM's introducing additional alumina in general increased the chloride binding capacity of the cement paste. Granulated blast furnace slag and fly ash usually resulted in increased chloride binding [182, 233, 252] but silica fume showed a decrease in binding capacity in most experiments [242, 246].

Although an increase in the amount of C-S-H was generally considered to increase chloride uptake, chloride binding was generally reduced by the addition of silica fume despite increase in total amount of the C-S-H. As mentioned in section 5.1.4 some researchers associated degree of chloride binding in C-S-H with the Ca/Si ratio with a lower ratio resulting in a lower degree of binding, which may explain the reduction in binding when silica fume is present.

Contradictory to the above observations Mohammed [253] reported that increased replacement of cement by slag cement caused a decrease in the chloride-binding ability and Delagrave [181] noticed that 6% addition of silica fume did not markedly change binding capacity for chlorides. The conflict may be resolved by considering kinetics and mass balances: to reduce chloride, slag has to react and make alumina available to form a phase which is a good chloride sorber. More alumina may become available, but it may go to form a hydrotalcite like phase [254-256] or strätlingite [9, 255], which likely contribute little to Cl binding. Slag can lower the Ca/Si ratio of C-S-H resulting in higher alumina substitution into C-S-H, of which influence on chloride binding has not been reported [256].

5.2 Synthesis of chloride-aluminate hydrates

5.2.1 Friedel's salt

Tricalcium aluminate, $3CaO \cdot Al_2O_3$, was made by heating together a 3:1 molar ratio of reagent grades of $CaCO_3$ and Al_2O_3 at 1400°C. The heating was done in Pt crucibles and continued, with intermediate grinding of the product, until X-ray powder diffraction revealed that the product was phase pure. Portions of this solid were mixed with weighted amounts of reagent grade $CaCl_2 \cdot 2H_2O$ (molar ratio of C_3A:$CaCl_2$=1:1). The water content of $CaCl_2 \cdot 2H_2O$ was confirmed thermogravimetrically. The precursors were added to double distilled, CO_2-free water, at a w/s (water to solid) ratio ~10, and tightly sealed into plastic containers to prevent CO_2 uptake. Samples were equilibrated with agitation for 28 days at 23±2°C.

5.2.2 Kuzel's salt

C_3A, $CaCl_2 \cdot 2H_2O$ and $CaSO_4$ were mixed in stoichiometric amounts and slurried in double distilled, CO_2-free water at a water/solid ratio of ~10. The mixture was equilibrated with agitation for 3 months at 23±2°C. Thereafter the solid was filtered under nitrogen atmosphere and dried in a desiccator over saturated calcium chloride. The resulting bulk solid gave an X-ray powder pattern corresponding to Kuzel's salt, $Ca_4Al_2(SO_4)_{0.5}(Cl)(OH)_{12} \cdot 6H_2O$, with a basal spacing d = 8.32 Å.

5.2.3 Solid solutions amongst AFm phases

Samples were synthesized from initial supersaturation at 23±2°C. Stoichiometric amounts of appropriate reactants were mixed in and slurried in double distilled, CO_2-free water to a w/s ratio of ~10. Mixtures were equilibrated with agitation for 3 months, then dried over saturated calcium chloride (35% RH) and analysed by XRD.

5.2.4 Cl-ettringite

Attempts to prepare Cl-AFt were not successful. Mixtures of the appropriate composition, starting from C_3A and $CaCl_2$ and reacted at 5° and 25°C, instead formed

Friedel's salt. Preparations made using the so-called sucrose method also known as the 'sugar method'*, to enhance Ca solubility, gave an X-ray amorphous product. Damidot et al. [40] made similar observations but claimed possible metastable persistence of chloride ettringite at 25°C. As mentioned in section 5.1.4 chloride ettringite has been reported to occur stably below 0°C [227-231], but the conditions of the title study did not extend to < 5°C.

5.3 Results

5.3.1 Friedel's salt

The preparation gave an X-ray powder pattern at 25±2˚C corresponding to that reported for Friedel's salt with basal spacing d=7.93 Å. In some preparations, Friedel's salt giving a basal spacing of 7.89 Å and 7.83 Å was found. The lowered spacing is probably due to the presence of the rhombohedral (R) phase, *i.e.*, the preparation contained a mixture of polymorphs. At room temperature Friedel's salt is monoclinic (M) with a basal spacing around 7.91 Å [201]) but above ~35˚C [13, 19, 257] it is reported to transform to rhombohedral symmetry (basal spacing 7.77 Å [201]). Kuzel [13] gave the transformation temperature as 28˚±2C. It is probable that, depending upon bulk composition, and the OH/Cl ratio of the solid, the transformation temperature will extend over a range of temperatures implying the coexistence of both phases.

Rietveld analysis of Friedel's salt prepared by mixing C_3A:$CaCl_2$=1:1, revealed that even at room temperature, preparations consisted of a mixture of phases, approximately 93% monoclinic and 7% rhombohedral (Fig. 5.1). The existence of two phases over a range of temperatures can be explained by differing extents of substitution of Cl by OH, thereby creating a stable range of coexistence for solid solutions based on R and M phases. Independent bulk chemical analysis of the chloride content disclosed that its formula was $Ca_4Al_2Cl_{1.95}(OH)_{12.05}\cdot 4H_2O$. Previous researchers [201, 212] reported that, by reacting C_3A and $CaCl_2$ in 1:1 stoichiometric amounts with water, the maximum chloride content obtained for the final product was ~95% of the theoretical chloride content. In this study, about 2.5% OH was substituted for Cl in preparations made at pH~12.

** In which the Ca ion concentration is increased by adding sugar forming a soluble complex between sucrose and calcium*

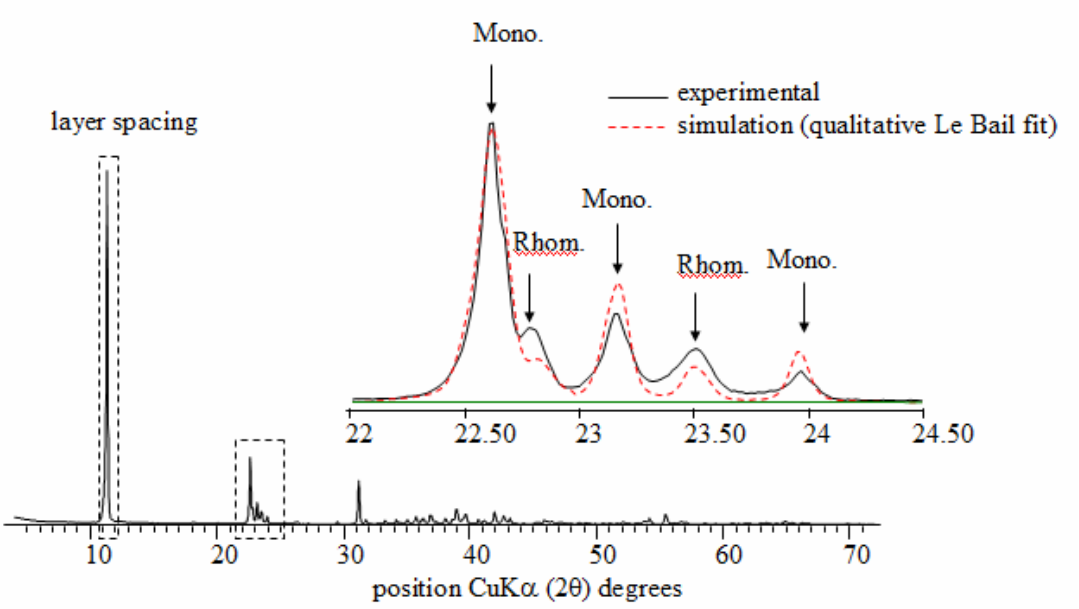

Figure 5.1: Powder pattern of Friedel's salt containing a mixture of monoclinic and rhombohedral polymorphs.

Solubility data are presented in Tab. 5.1. Powder patterns of Friedel's salt after equilibration at different temperatures are presented on Fig. 5.2.

Solubility products (K_{so}) of Friedel's salt were calculated according to the dissolution reactions presented in Eq. 5.4.

$$Ca_4Al_2(OH)_{12.05}(Cl)_{1.95}\cdot 4H_2O = 4\ Ca^{2+} + 2\ AlO_2^- + 1.95\ Cl^- + 4.05OH^- + 8H_2O \qquad \textit{Eq. 5.4}$$

Other numerical values of the solubility products of 'Friedel's salt' have been reported in the literature. Birnin-Yauri [18, 212] gave values of $\log K_{so}$ between -24.79 and -27.10. Hobbs [201] estimated $\log K_{so}$ as -27.57 ±0.86 and Bothe [258] calculated the solubility product to be within the range $-28.8 < \log K_{so} < -27.6$.

Thermal (TG/DTA) and infra red (FTIR) characteristics of Friedel's salt have been described in the literature [18, 212, 259, 260]. Birnin-Yauri [18, 212] reported double endothermal peaks centred at 120°C and 290°C matching two weight loss steps. The 120°C event was attributed due to removal of interlayer water while at 290°C, the remaining water was lost, giving a largely X-ray amorphous product. The anhydrous

product recrystallised exothermically at 670°C, yielding mainly calcium chloroaluminate ($11CaO \cdot 7Al_2O_3 \cdot CaCl_2$).

Vieille [260], using high-temperature X-ray diffraction, reported that Friedel's salt undergoes a three-step decomposition on heating (dehydration, dehydroxylation, and anion expulsion) over the following temperature ranges: 25–280°C, 280–400°C, and >400°C. Upon cooling to room temperature and exposure to the atmosphere, the dehydrated phase obtained by calcination between 80 and 280°C was found to rehydrate to Friedel's salt within a few minutes. Friedel's salt was found to become amorphous at 400°C, but above 750°C, it was said to recrystallize to a mixture of CaO and mayenite, $Ca_{12}Al_{14}O_{33}$. Exposure of the amorphous residue obtained at 400°C to aqueous solutions of KCl led to "reconstruction phenomena", which presumably means that Friedel's salt reformed.

Birnin Yauri performed an FTIR examination of Friedel's salt and assigned bonds as follows: the feature at 786 cm^{-1} was due to an Al-OH bending mode; the band at 1623 cm^{-1} was an H-O-H bending vibration of interlayer water, but the broad band at 3495 cm^{-1} was due to stretching vibration of OH in structural water. Chloride does not absorb in the range 400–4000 cm^{-1}*.

Thermal decomposition reactions and FTIR spectrum of Friedel's salt reported by Ahmed [259] were in relatively good agreement with results reported by Birnin-Yauri.

** Chloride in Friedel's salt is present in form of free Cl^- ions rather than in chloro-complexes. Infrared spectroscopy reveals information about the vibrational states of a molecule. For a nonlinear molecule (with n number of atoms), three degrees of freedom describe rotation and three describe translation. The remaining 3n - 6 degrees of freedom are vibrational degrees of freedom or fundamental vibrations. Free chloride ions are monoatomic so their vibrational degrees of freedom equal zero (3n-3 because we do not have any rotations) and therefore we do not observe any FTIR signal from chloride.*

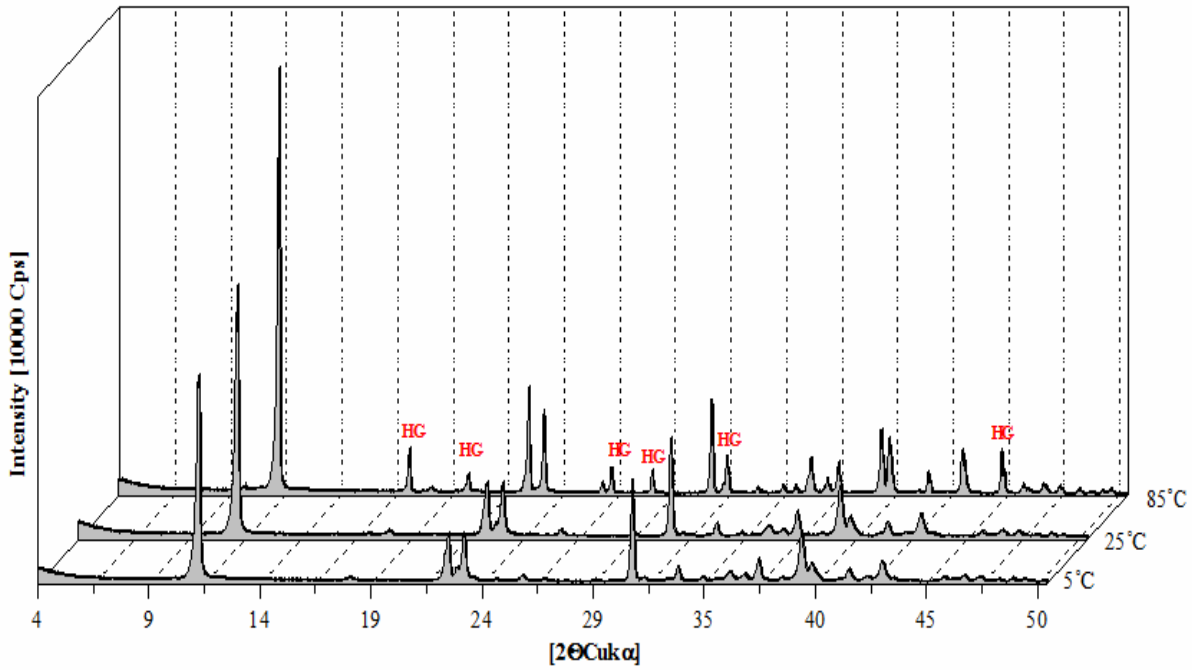

Figure 5.2: Powder patterns of Friedel's salt after 3 months of equilibration with water at different temperatures. HG peaks are attributed to hydrogarnet.

5.3.2 Kuzel's salt

Kuzel's salt $Ca_4Al_2(SO_4)_{0.5}(Cl)(OH)_{12}\cdot 6H_2O$ gave an X-ray powder pattern at 25±2˚C with a basal spacing of d=8.32 Å. It dissolves incongruently; solubility data are presented in Tab. 5.2. After dissolution, the X-ray diffraction pattern of the solid disclosed the presence of Kuzel's salt together with monosulfoaluminate and Friedel's salt (Fig. 5.3). The stability of Kuzel's salt relative to mixtures of monosulfoaluminate and Friedel's salt is considered to be proven because the two AFm end members, mixed in the 1:1 ratio, react at 25±2˚C to yield Kuzel's salt. That is, at 25ºC, two different phase assemblages react and converge on the same final state: Kuzel's salt [11].

Solubility products (K_{so}) of Kuzel's salt were calculated according to the dissolution reaction in Eq. 5.5.

$$Ca_4Al_2(SO_4)_{0.5}(Cl)\,(OH)_{12}\cdot 6H_2O = 4\,Ca^{2+} + 2\,AlO_2^- + Cl^- + 0.5SO_4^{2-} + 4OH^- + 10H_2O \qquad \textit{Eq. 5.5}$$

Table 5.1: Solubility data for Friedel's salt - $Ca_4Al_2(OH)_{12.05}(Cl)_{1.95}\cdot 4H_2O$.

Temp. [˚C]	Ca [mmol/l]	Al [mmol/l]	Cl [mmol/l]	$\log K_{so}$	pH measured	Equilbrium pH calc. by GEMS	Age-months	Phases present after dissolution
5	7.33	3.96	3.77	-29.53	12.40*	12.51	1	n.d.
5	7.30	2.93	3.86	-29.24	12.45*	12.56	3	Fs_{ss}
5	7.29	2.90	3.76	-29.24	12.45*	12.57	6	n.d.
5	7.20	2.85	3.70	-29.28	12.43*	12.56	8	Fs_{ss}
5	7.25	2.89	3.72	-29.26	12.44*	12.57	12	Fs_{ss}
25	9.19	4.52	4.95	-27.87	12.00	11.90	1	n.d.
25	9.09	2.48	4.89	-27.63	12.01	11.98	1	Fs_{ss}
25	9.13	2.63	4.97	-27.59	12.01	11.97	3	Fs_{ss}
25	8.92	2.73	4.89	-27.66	11.99	11.96	3	n.d.
25	8.95	2.35	4.98	-27.72	12.00	11.97	6	Fs_{ss}
25	9.11	2.78	5.02	-27.57	11.96	11.96	6	Fs_{ss}
25	8.99	2.69	4.98	-27.64	11.98	11.96	8	n.d.
25	8.77	2.97	5.50	-27.71	11.94	11.90	8	Fs_{ss}
25	*8.88*	*2.70*	*5.70*	*-27.69*	*11.94*	*11.92*	*12*	*Fs_{ss}*
25	8.82	2.39	5.79	-27.78	11.93	11.92	12	n.d.
55	13.25	2.31	14.31	-26.94	11.08*	10.99	3	Fs_{ss}, HG
55	13.66	2.45	15.10	-26.83	11.08*	10.98	6	n.d.
55	13.73	2.28	15.25	-26.85	11.09*	10.99	8	Fs_{ss}, HG
55	13.73	2.70	15.43	-26.82	11.06*	10.97	12	n.d.
85	16.05	2.90	19.46	-26.96	10.22*	10.24	3	Fs_{ss}, HG
85	16.68	2.57	19.06	-26.77	10.21*	10.32	6	n.d.
85	16.58	2.50	19.20	-26.83	10.20*	10.31	8	Fs_{ss}, HG
85	16.60	2.54	19.69	-26.86	10.19*	10.29	12	n.d.

**pH measured at 25˚C and corrected by calculation to measurement temperature (see 3.2.3). Abbreviations: Fs_{ss}-Friedel's salt in solid solution with OH-AFm, HG-hydrogarnet, n.d.-not determined. Italicised value from 12 month equilibration, was used as an input in Table 5.7.*

Data for the solubility product of Kuzel's salt have not been published previously in the literature. However from the solubility data given by Glasser et al. [11] the authors estimated $\log K_{so}$ to be -28.54.

Loss of molecular water is usually complete below 250˚C according to Taylor [2]. At room temperature and exposed to air, Kuzel's salt contains $6H_2O$ so its formula can be expressed as $Ca_4Al_2(SO_4)_{0.5}(Cl)(OH)_{12}\cdot 6H_2O$ (formula weight: 609.94 g/mol). This molecular water is lost in three stages upon heating, all below 200˚C (losses 1, 2 and 3 on Fig. 5.4). This loss should theoretically correspond to 17.7%. In this study, the measured cumulative weight loss at 200˚C was 17.37%, corresponding to 5.90 H_2O and close to the expected $6H_2O$. Further heating probably leads to dehydroxylation of the OH groups and decomposition of Kuzel's salt (peaks 4, 5 on Fig. 5.4) although detail analysis of the decomposition product was not performed for particular steps of degradation. Total weight loss at 1000˚C was 34.57%.

FTIR examination was carried in the mid-infra red range 4000-400 cm^{-1} (Fig. 5.5, Tab. 5.3). Peak #4 in Fig. 5.5, at 1410 cm^{-1}, indicates slight carbonation of the sample.
Similarly to Friedel's salt (as explained in section 5.3.1), chloride does not absorb in the range 400–4000 cm^{-1}. Sulfate stretching vibrations were recorded at 1110 cm^{-1} [261].

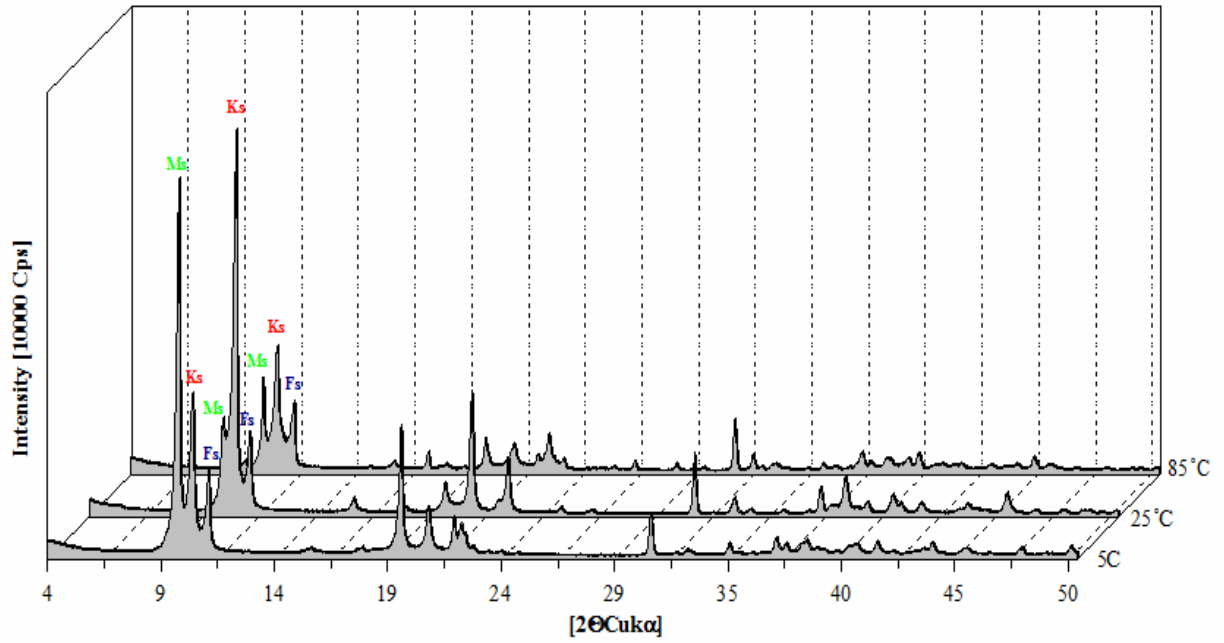

Figure 5.3: Powder patterns of Kuzel's salt after 3 months of equilibration with water at different temperature; Ms-monosulfoaluminate, Ks-Kuzel's salt, Fs-Friedel's salt.

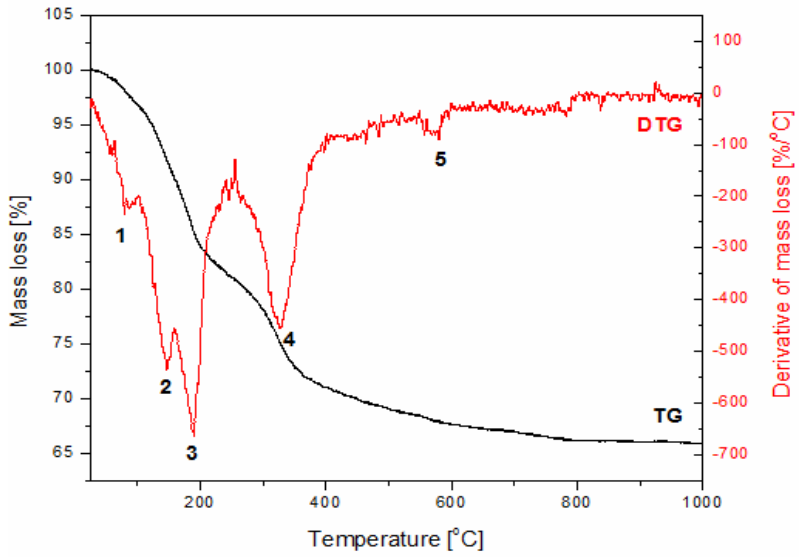

Temp. (˚C)	Cumulative % mass loss
90	2.95
150	9.61
200	17.37
330	27.13
580	32.25
1000	34.57

Figure 5.4: TG/DTG characteristics of Kuzel's salt values of the mass losses were determined from the TG curve by the points of deviation for the tangent lines of weight loss slopes versus temperature.

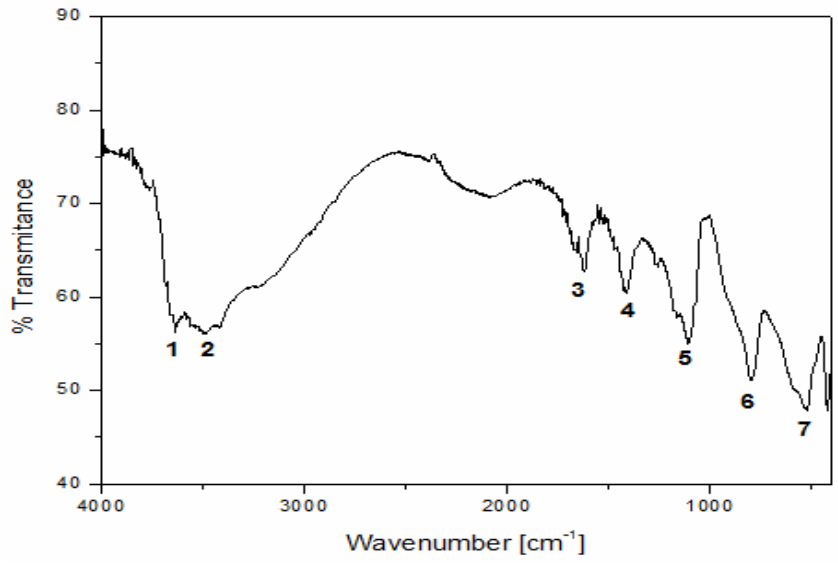

Figure 5.5: FTIR pattern of Kuzel's salt dried at 35% RH.

Table 5.3: FTIR identification of the Kuzel's salt.

Peak number	**Wavenumber (cm^{-1})**	**Assignment (see Fig. 5.5) [261]**
1	3636	O-H group (asymmetric stretching)
2	3490	O-H group (asymmetric stretching)
3	1620	O-H group (H-O-H bending)
4	1410	C-O symmetric stretching
5	1110	S-O stretching
6	793	Al-O (bending)
7	529	Al-O (bending)

Table 5.2: Solubility data for Kuzel's salt - $Ca_4Al_2(SO_4)_{0.5}(Cl)(OH)_{12}\cdot 6H_2O$.

Temp. [˚C]	Ca [mmol/l]	Al [mmol/l]	Cl [mmol/l]	SO_4 [mmol/l]	$\log K_{so}$	pH measured	Equilibrium pH calc. by GEMS	Age-months	Phases present after dissolution
5	5.25	3.26	3.85	0.005$^+$	-30.45	12.34*	12.20	1	Ks, Fs, Ms
5	5.47	3.16	3.89	0.005$^+$	-30.19	12.33*	12.26	3	Ks, Fs, Ms
5	5.45	3.10	3.99	0.005$^+$	-30.23	12.35*	12.25	6	n.d.
5	5.35	3.16	4.10	0.005$^+$	-30.40	12.31*	12.21	8	Ks, Ms, Fs
5	5.35	3.19	3.96	0.005$^+$	-30.35	12.26	12.22	12	n.d.
25	7.65	4.14	4.01	0.009$^+$	-28.53	11.76	11.77	1	Ks, Ms, Fs
25	8.73	2.61	5.96	0.009$^+$	-28.25	11.77	11.86	3	Ks, Ms, Fs
25	8.88	2.21	6.22	0.009$^+$	-28.28	11.80	11.88	3	Ks, Ms, Fs
25	8.64	2.26	5.89	0.009$^+$	-28.35	11.76	11.87	6	Ks, Ms, Fs
25	8.66	2.39	5.90	0.009$^+$	-28.32	11.88	11.87	6	n.d.
25	8.66	2.43	5.93	0.009$^+$	-28.31	11.87	11.86	8	Ks, Ms, Fs
25	8.68	2.40	5.98	0.009$^+$	-28.32	11.82	11.87	8	n.d.
25	*8.41*	*2.31*	*5.70*	*0.009$^+$*	*-28.53*	*11.76*	*11.79*	*12*	*Ks, Ms, Fs*
25	8.21	2.51	5.39	0.009$^+$	-28.51	11.74	11.86	12	n.d.
55	13.46	3.30	11.99	0.25$^+$	-26.64	11.07*	11.04	3	Ks, HG, Ms, Fs
55	12.71	3.31	11.38	0.25$^+$	-26.84	11.05*	11.01	6	n.d.
55	13.15	3.20	12.02	0.25$^+$	-26.77	11.08*	11.02	8	Ks, HG, Ms, Fs
55	12.88	3.49	11.89	0.25$^+$	-26.82	11.02*	10.99	12	n.d.
85	17.03	3.54	16.94	1.31$^+$	-26.50	10.41*	10.32	3	Ks, HG, Ms, Fs
85	17.49	3.71	16.51	1.31$^+$	-26.39	10.36*	10.34	6	Ks, HG, Ms, Fs
85	18.20	3.48	17.55	1.31$^+$	-26.32	10.37*	10.35	8	Ks, HG, Ms, Fs
85	18.15	3.55	17.41	1.31$^+$	-26.31	10.37*	10.35	12	n.d.

**pH measured at 25˚C and corrected by calculation to measurement temperature (see 3.2.3)*
$^+$Sulfate concentration determined assuming saturation with respect to monosulfoaluminate-data taken from Matschei et al [51]; Ks-Kuzel's salt, HG-hydrogarnet, Ms-monosulfoaluminate, Fs-Friedel's salt, n.d.-not determined. Italicised value from a 12 month equilibration, was used as an input in Table 5.7.

5.3.3 AFm solid solutions

5.3.3.1 Friedel's salt and hydroxy AFm

To investigate whether solid solutions are formed, a series of solids were analysed by XRD in the wet state (Fig. 5.6(a.b)) or following drying over saturated calcium chloride (35% RH) (Fig. 5.7(a.b)).

Solid solution formation between Friedel's salt (basal spacing d=7.93 Å) and hydroxy AFm (basal spacing d=7.99 Å) was investigated in the range 0-1 Cl/(Cl+OH). The extent of the miscibility gap has been variously reported: by Hobbs [201] to be below ratio 0.33 Cl/(Cl+OH), by Pöllmann and Kuzel [262] to be below 0.34 Cl/(Cl+OH), by Birnin-Yauri [212], below ratio 0.3 Cl/(Cl+OH) ratio and by Roberts [263], below ratio 0.4 Cl/(Cl+OH). However, and in contrast, Turriziani [264] claimed formation of complete solid solution. Previous researchers based the evidence of incomplete solid solution on the observation that changing bulk composition resulted in two separate sets of X-ray reflections, one for Friedel's salt, another for the high water variant of hydroxy AFm with a basal spacing d ~10.7 Å. In this investigation, only the lower water phase, C_4AH_{13} ($Ca_4Al_2(OH)_{14}\cdot 6H_2O$), with a basal spacing d=7.99 Å, was found after drying at 35% RH (Fig. 5.7(a,b)). The main reflections of chloride and hydroxy end-members coincided (close to 2 theta 11.40˚, Cu radiation) therefore the reflections at 2Θ~22˚ were analysed as they gave better discrimination. For members of solid solution peaks at 2Θ ~22˚ were investigated by Rietveld refinement but the signal/noise ratio was too low to establish solid solution limits. To define the miscibility gap without artefacts introduced by drying, X-ray characterisation of wet samples covered with 'Mylar' foil was done to prevent water evaporation and atmospheric carbonation. This preserved the higher water state of AFm. Two separate reflection types were still observed in the region below ratio 0.2 Cl/(Cl+OH) (Fig. 5.6(a,b)), indicating two hydrate states, each with discrete composition. Thus the coexisting solid solution of the (OH, Cl) AFm phases which are in different water states is inevitably incomplete. It is suspected that the presence of chloride stabilises the "13 H_2O" state at the expense of the "19 H_2O" state. A continuous solid solution between C_4AH_{13} and Cl-AFm (Friedel's salt) is not, however, precluded.

Dry (Cl, OH) AFm solid solution members were redispersed in double distilled water and equilibrated at 25˚C for 180 days. All the samples were periodically agitated. Aqueous solution compositions, measured after equilibration commencing from

undersaturation, are presented in Tab. 5.4. Experimental calcium, aluminium and chloride concentrations are plotted in Fig. 5.8 (a,b).

The best fit of the calculated solubilities for the Friedel's salt-hydroxy AFm solid solution series, relative to experimental solubility data at 25°C was obtained, assuming complete solid solution between hydroxy AFm and Friedel's salt. Calcium, aluminium and chloride concentrations simulated by GEMS are shown in Fig. 5.8 (a,b).

Although the best correlation between calculations and empirical data was obtained assuming an ideal solid solution, Guggenheim parameters used in the case of non-ideal binary solid solutions were derived. To enable calculation slight solid solution of Friedel's salt in hydroxy AFm (3%) was permitted. Assuming compositional boundaries of the miscibility gap 0.03-0.2 Cl/(Cl+OH) and applying MBSSAS software the resulting Guggenheim parameters equalled: a_0=0.669 and a_1=2.59. Using previously derived parameters a_0 and a_1, it was possible to determine the changes of the Gibbs energies of mixing; Fig. 5.9 compares the functions of the Gibbs energy of ideal mixing, ΔG_{id}, the estimated excess Gibbs energy of mixing ΔG_{ex} and the resulting estimated Gibbs energy of mixing, $\Delta G_{M,}$ of the Friedel's salt (Cl-AFm)-hydroxy AFm (OH-AFm) solid solution series, according to Eqns. 2.11-2.16. The molar Gibbs energy of the solid solution can be calculated according to Eq. 2.11 as the sum of the partial Gibbs energies of Friedel's salt, hydroxy AFm and ΔG_M.

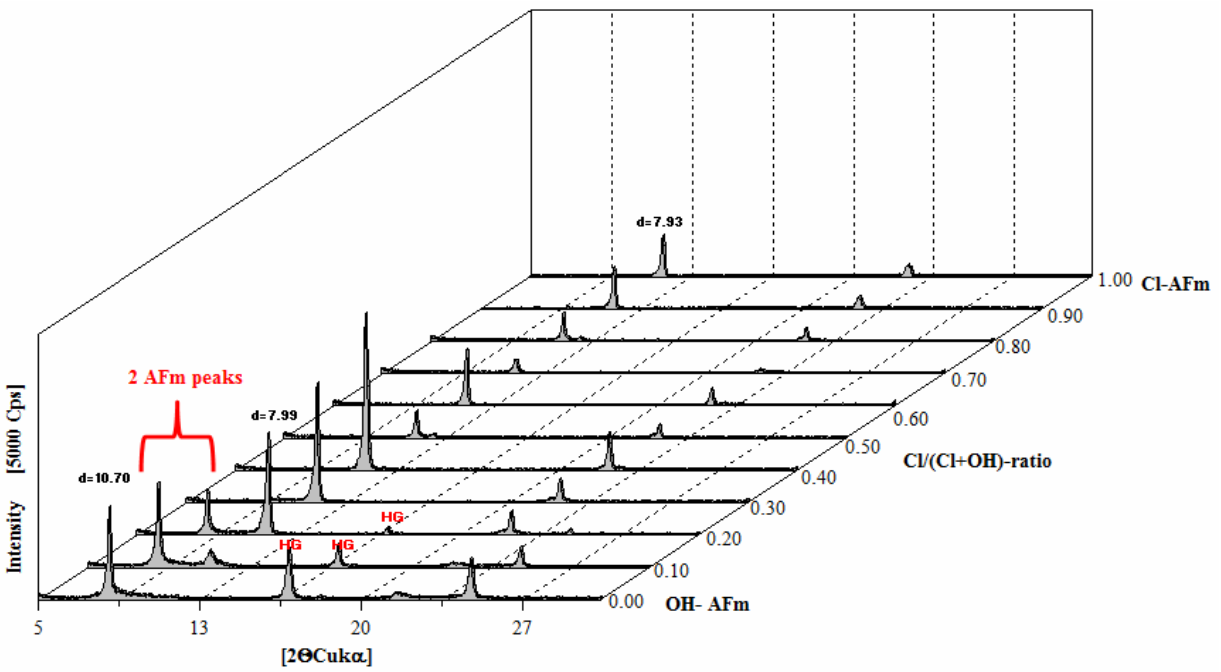

Figure 5.6(a): Partial XRD patterns of the solid solution formation at 25˚C between Friedel's salt and hydroxy AFm: wet samples. Reflections marked as HG are attributed to hydrogarnet.

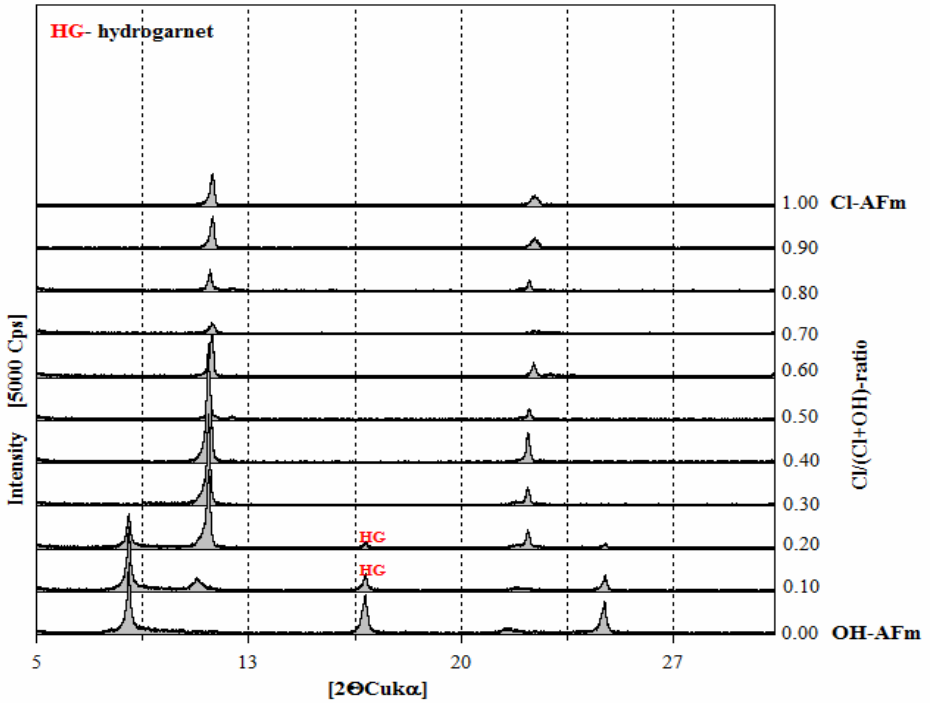

Figure 5.6(b): Partial XRD patterns of the solid solution formation at 25˚C between Friedel's salt and hydroxy AFm: wet samples. Reflections marked as HG are attributed to hydrogarnet.

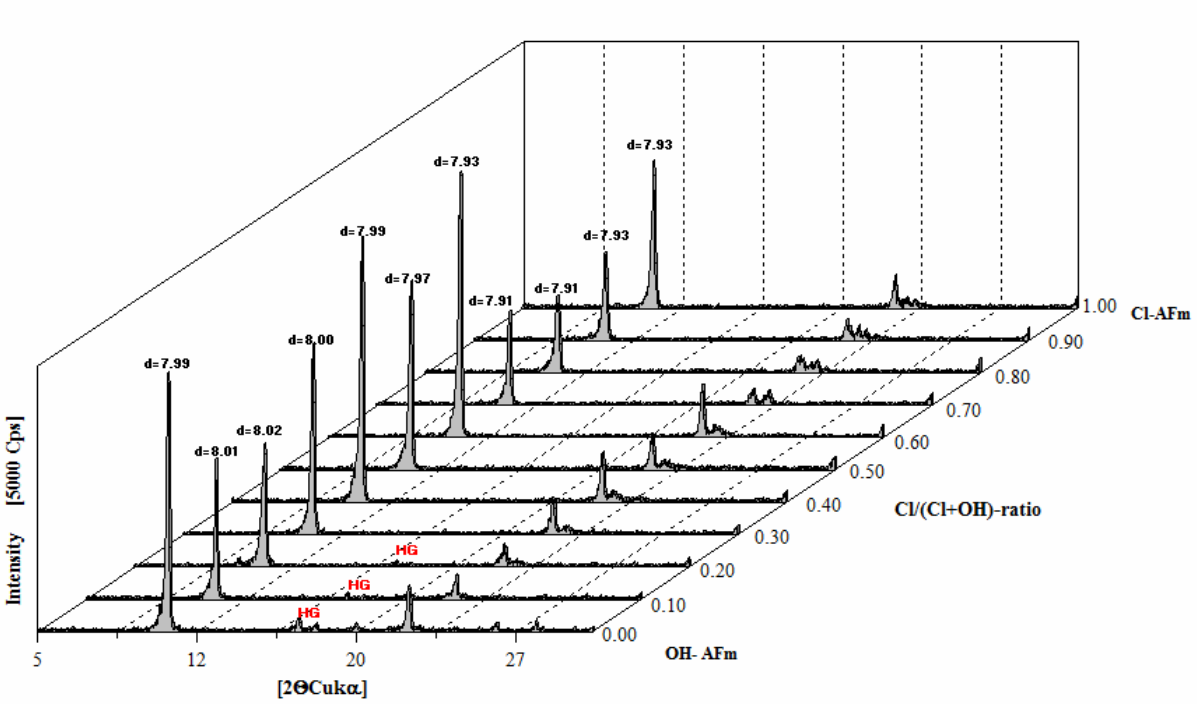

Figure 5.7(a): Partial XRD patterns of the solid solution formation at 25±2˚C between Friedel's salt and hydroxy AFm: samples dried at 35% RH. Reflections marked as HG are attributed to hydrogarnet.

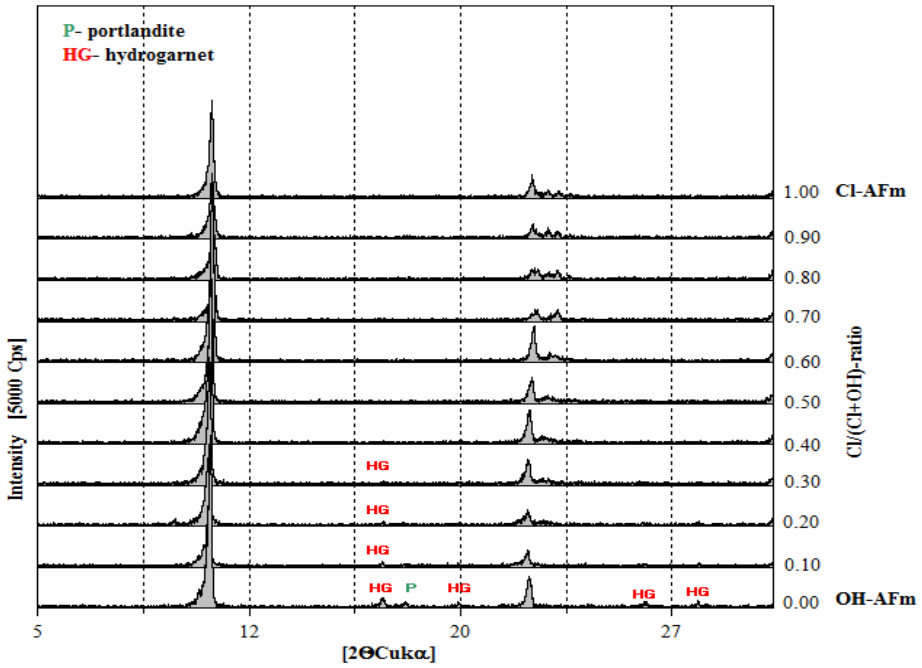

Figure 5.7(b): Partial XRD patterns of the solid solution formation at 25±2˚C between Friedel's salt and hydroxy AFm: samples dried at 35% RH; reflections marked "HG" are due to hydrogarnet, P due to portlandite.

Table 5.4: Aqueous solution compositions measured from undersaturation for samples between the hydroxy AFm (Cl/Al=0) and the Friedel's salt (Cl/Al=1) and with an excess of $CaCl_2$ (values >1); at 25±2ºC and after 180 days of equilibration. Data for hydrogarnet, $Ca_3Al_2(OH)_{12}$ are given for reference.

Calculated Cl/Al- ratio (total system)	Ca [mmol/l] (aq)	Al [mmol/l] (aq)	Cl [mmol/l] (aq)	pH	Solid phase at end of experiment
0.00	17.63	0.21	0.00	12.49	OH-AFm, HG, CH
0.10	17.19	0.24	0.72	12.47	FS_{ss}, HG
0.20	15.21	0.29	0.86	12.46	FS_{ss}, HG
0.30	12.68	0.79	1.29	12.41	Fs_{ss}, HG
0.40	10.53	1.87	1.73	12.33	FS_{ss}, HG(traces)
0.50	8.69	3.27	2.09	12.21	FS_{ss}
0.60	8.84	3.61	3.61	12.14	FS_{ss}
0.70	8.62	4.46	3.78	12.07	FS_{ss}
0.80	8.59	3.77	4.31	12.09	FS_{ss}
0.90	8.91	2.49	4.92	12.12	FS_{ss}
0.95	8.82	2.39	5.79	11.93	FS_{ss}
1.05	11.63	1.35	11.57	11.78	FS_{ss}
1.10	13.13	0.89	15.7	11.70	n.d.
1.20	16.78	0.93	24.5	11.62	n.d.
For pure hydrogarnet	6.31	5.07	0	11.81	HG

Abbreviations: FS_{ss}=solid solution between Cl-AFm and OH-AFm, CH=portlandite, HG=hydrogarnet (katoite); n.d.=not determined)

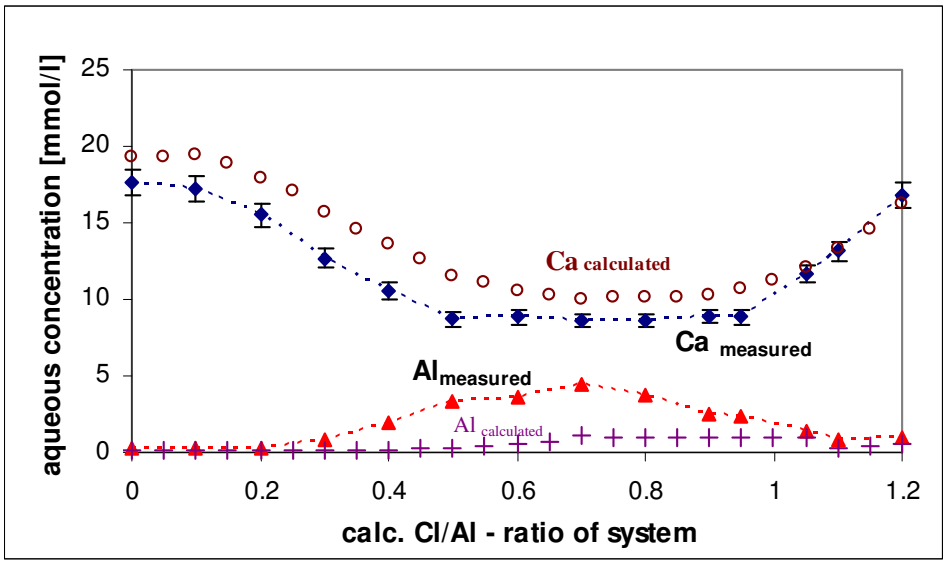

Figure 5.8(a): Equilibrium calcium and aluminium aqueous concentrations commencing from undersaturation for samples between hydroxy AFm (Cl/Al=0) - Friedel's salt (Cl/Al=1) and with an excess of calcium chloride (values > 1); at 25±2ºC and after 180 days of equilibration. Error bars are shown for Ca. Open circles represent calcium concentrations calculated by GEMS, crosses represent aluminium concentrations calculated by GEMS.

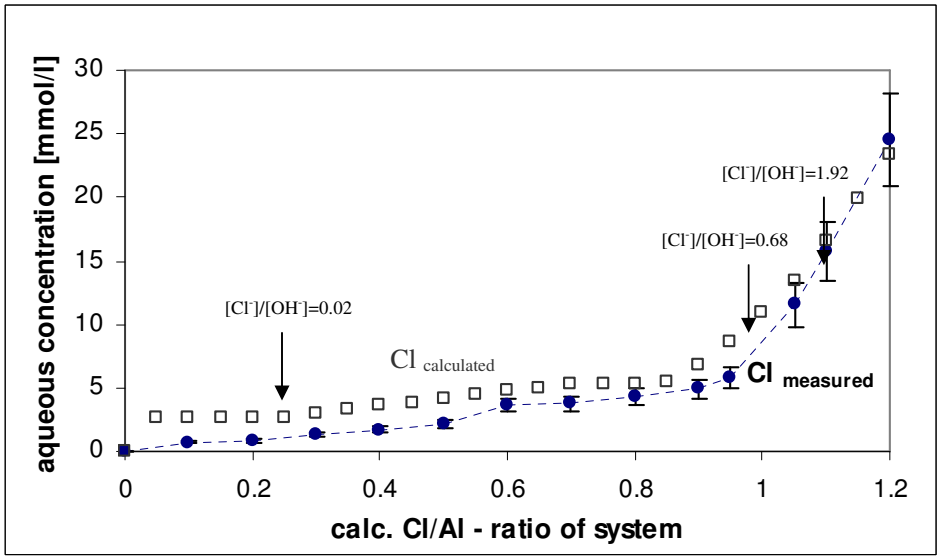

Figure 5.8(b): Equilibrium chloride aqueous concentrations commencing from undersaturation for samples between hydroxy AFm (Cl/Al=0) and Friedel's salt (Cl/Al=1) and with an excess of calcium chloride (values > 1); at 25±2ºC and after 180 days of equilibration. Error bars are shown for Cl. Variations in the measured aqueous [Cl⁻]/[OH⁻] ratios are shown at selected points: see discussion. Open squares represent chloride concentrations calculated by GEMS.

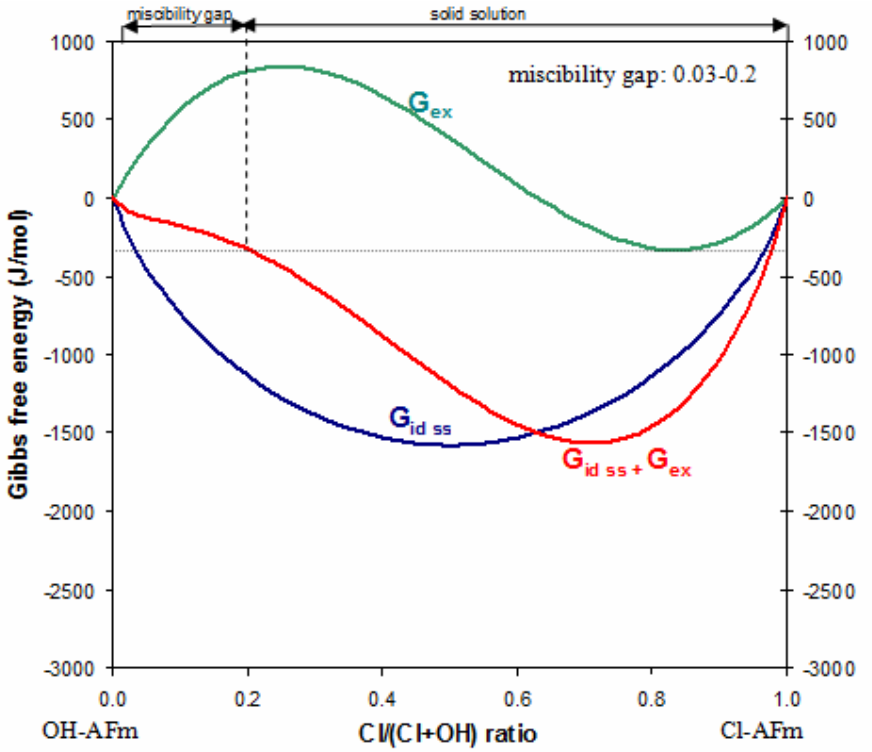

Figure 5.9: Gibbs energy of ideal mixing, ΔGid, excess Gibbs energy of mixing, ΔGex, and resulting molar Gibbs energy of mixing, ΔGM, calculated from Eq. for the Friedel's salt (Cl-AFm)-hydroxy AFm (OH-AFm) solid solution series assuming incomplete solid solution and Guggenheim parameters a_0=0.669 and a_1=2.59 for miscibility gap fractions 0.03 ≤ x ≤ 0.2.

5.3.3.2 Friedel's salt and monosulfoaluminate

No solid solution was found between monosulfoaluminate and Friedel's salt: instead an ordered compound containing both mono and divalent anions, $Ca_4Al_2(SO_4)_{0.5}(Cl)(OH)_{12}\cdot 6H_2O$ (Kuzel's salt), was encountered (Fig. 5.10(a,b)). These findings are similar to those of Kuzel [13] and Stronach [39] who additionally found a slight solid solution between monosulfoaluminate and Friedel's salt. Solubility data for Kuzel's salt are presented in Section 5.3.2. Dry (Cl, SO_4) AFm phases were redispersed in double distilled water and equilibrated at 25˚C for 180 days. All the samples were periodically agitated. Aqueous solution compositions, measured after equilibration commencing from undersaturation, are presented in Tab. 5.5. Experimentally-determined calcium, aluminium and chloride concentrations are plotted in Fig. 5.11(a,b).

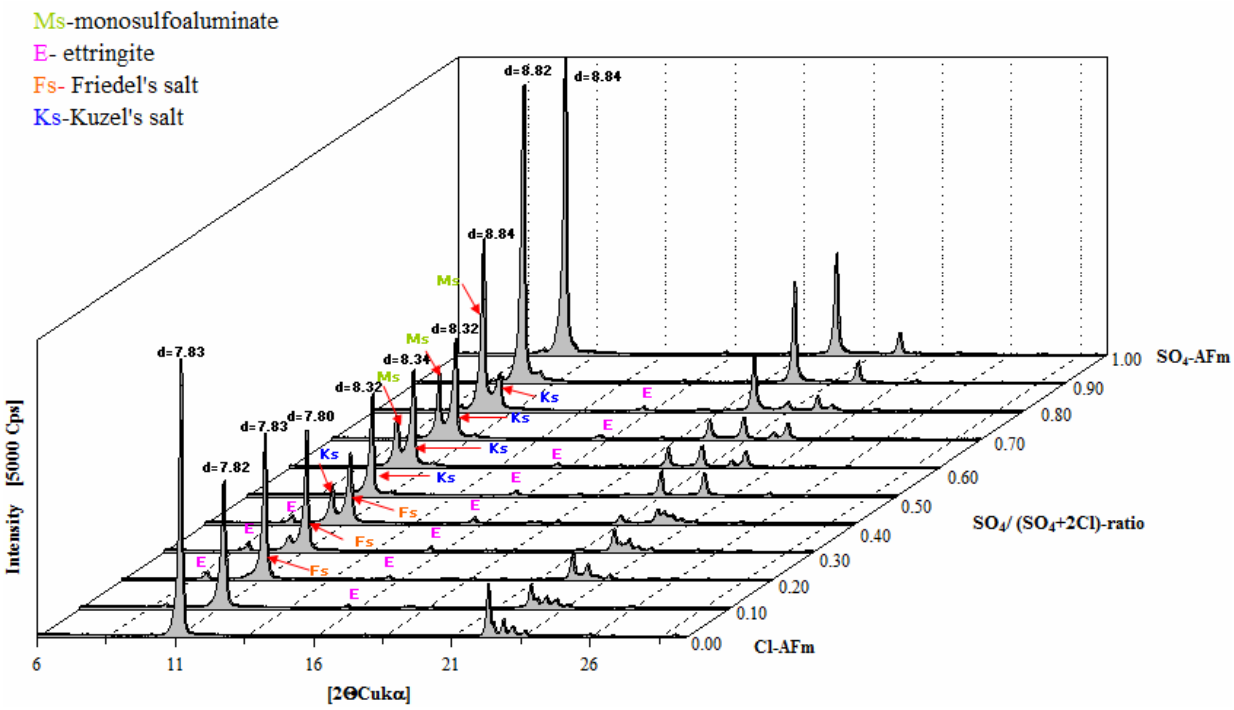

Figure 5.10(a): Partial XRD patterns of mixtures between Friedel's salt and monosulfoaluminate at 25±2˚C; note formation of Kuzel's salt at $SO_4/(SO_4+2Cl)$ ratio 0.5.

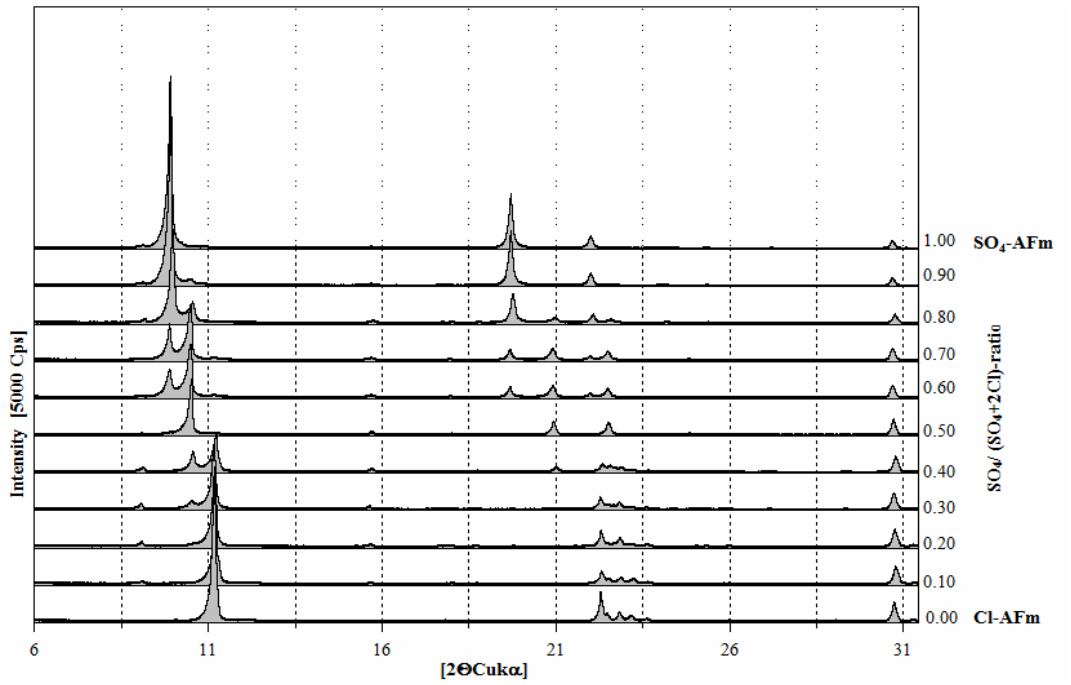

Figure 5.10(b): Partial XRD patterns of mixtures between Friedel's salt and monosulfoaluminate at 25±2˚C; note formation of Kuzel's salt at $SO_4/(SO_4+2Cl)$ ratio 0.5.

Table 5.5: Aqueous solution compositions measured from undersaturation for samples between monosulfoaluminate (Cl/Al=0) and Friedel's salt (Cl/Al=1) at 25±2ºC and after 180 days of equilibration.

Calculated Cl/Al- ratio (total system)	Ca [mmol/l] (aq)	Al [mmol/l] (aq)	Cl [mmol/l] (aq)	pH	Solid phase at end of experiment
0.00	5.51	2.90	0.00	11.75	Ms_{ss}, E
0.10	8.24	1.65	5.81	11.67	FS_{ss}, Ms_{ss}, Ks , E
0.20	8.98	1.70	5.35	11.68	FS_{ss}, Ms_{ss}, Ks, E
0.30	8.96	2.24	5.22	11.61	FS_{ss}, Ms_{ss}, Ks, E
0.40	8.67	1.74	6.22	11.61	FS_{ss}, Ms_{ss}, Ks, E
0.50	8.64	2.26	5.89	11.76	FS_{ss}, Ms_{ss}, Ks, E
0.60	8.65	2.50	6.85	11.60	FS_{ss}, Ms_{ss}, Ks, E
0.70	8.85	2.51	9.20	11.62	FS_{ss}, Ms_{ss}, Ks, E
0.80	8.98	2.26	9.12	11.68	FS_{ss}, Ms_{ss}, Ks, E
0.90	9.53	2.29	8.57	11.76	FS_{ss}, Ms_{ss}, Ks, E

Abbreviations: Ms_{ss} = monosulfoaluminate in solid solution with hydroxy AFm [9, 52], Ks = Kuzel's salt, FS_{ss} = Friedel's salt in solid solution with hydroxy AFm; E = ettringite; n.d.–not determined)

5.3.3.3 Friedel's salt and monocarboaluminate

Extensive solid solution was found between Friedel's salt and monocarboaluminate (Fig. 5.12(a,b)) although a miscibility gap exists at ≤ 0.1 $Cl/(Cl+1/2CO_3)$. One coexisting phase, Friedel's salt type, has a basal spacing d=7.72 Å and the other, monocarboaluminate type, has d=7.50 Å. This is in agreement with observations reported in the literature. From the appearance of XRD patterns Pöllmann [200] identified a miscibility gap ≤ 0.10 Cl and Hobbs [201] found a miscibility gap at ≤ 0.09 Cl. Samples were redispersed in double distilled water and equilibrated at 25˚C for 180 days. All the preparations were periodically agitated. Analysis of the solubility data for

particular members of solid solution as well as for some samples containing excess of calcium chloride are presented in Tab. 5.6.

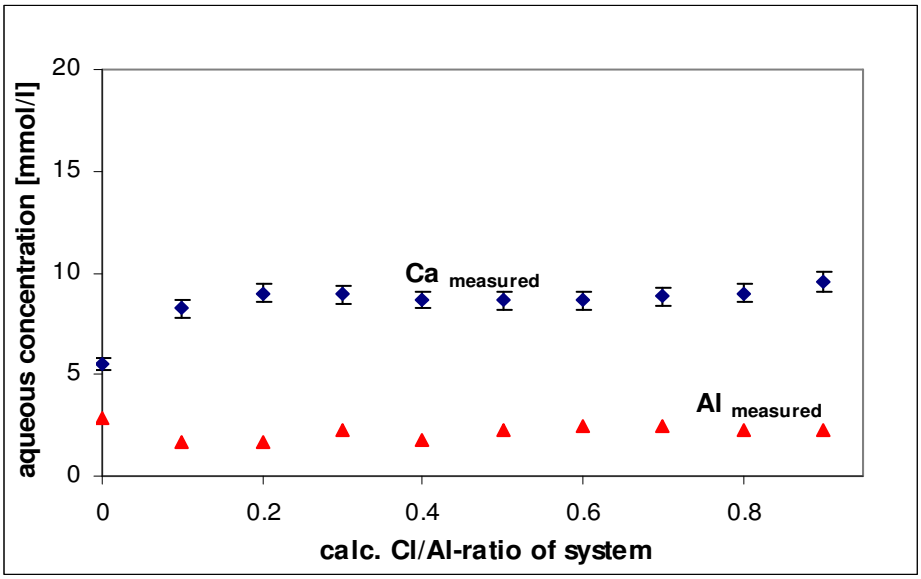

Figure 5.11(a): Equilibrium calcium and aluminium aqueous concentrations commencing from undersaturation for samples between monosulfoaluminate (Cl/Al=0) - Friedel's salt (Cl/Al=1) at 25±2ºC and after 180 days of equilibration. Error bars are shown for Ca.

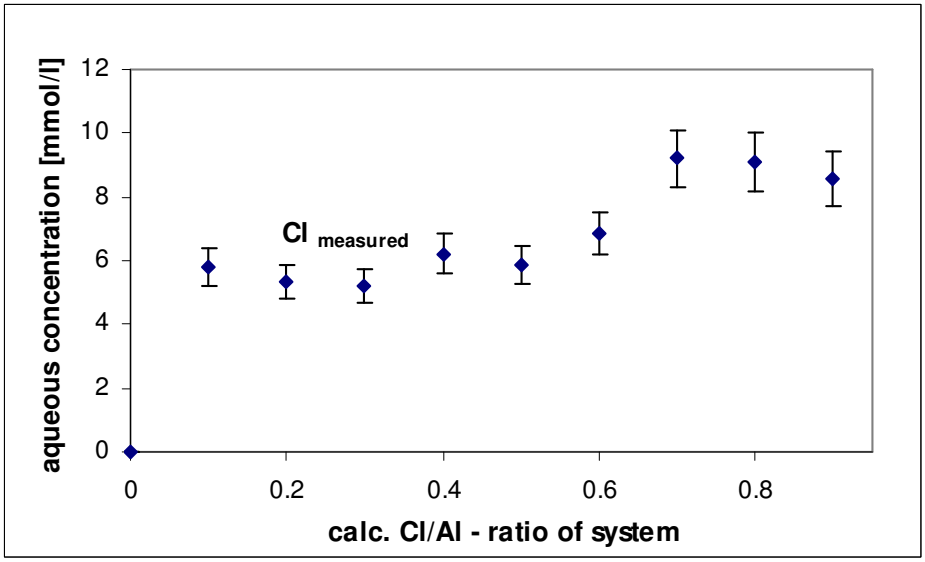

Figure 5.11(b): Equilibrium chloride aqueous concentrations commencing from undersaturation for samples between monosulfoaluminate (Cl/Al=0) and Friedel's salt (Cl/Al=1) at 25±2ºC and after 180 days of equilibration. Error bars are shown for Cl.

Aqueous: calcium, aluminium and chloride concentrations are plotted in Fig. 5.13(a,b). Assuming complete solid solution between monocarboaluminate, Friedel's salt and hydroxy AFm, the calcium, aluminium and chloride concentrations were simulated by GEMS and plotted on Fig. 5.13(a,b).

Although the best correlation between calculations and empirical data was obtained assuming ideal solid solution, an attempt to derive Guggenheim parameters was made. These are used in the case of non-ideal binary solid solutions. To enable calculation slight solid solution of Friedel's salt in monocarboaluminate (3%) was permitted. Assuming compositional boundaries of the miscibility gap 0.03-0.1 $Cl/(Cl+1/2CO_3)$ MBSSAS software was not able to derive Guggenheim parameters as the extent of the miscibility gap is probably too small.

5.4 Ion exchange experiments

To determine how the presence of other ions influences the stability of Friedel's salt, a series of ion exchange experiments were performed. Mixtures containing 1:1 molar ratios of Friedel's salt, portlandite and respectively calcite and various quantities of calcium sulfate were mixed with water and stirred for 180 days at 25˚C±2˚C. The results obtained clearly indicate that portlandite or calcite did not influence Friedel's salt but it is possible that, due to the existence of solid solution, some slight substitution of OH^- and/or CO_3^{2-} ions into the structure occurred (Figs. 5.14, 5.15). Figs. 5.16 and 5.17 show that increasing sulfate content destabilizes Friedel's salt and results in formation of ettringite. This is in agreement with data reported in the literature [193, 232]. Although in this study influence of alkalis has not been investigated as mentioned in section 5.1.5, from the data published by *e.g*. Nielsen [188, 245] it can be concluded that presence of alkalis results in lower chloride binding and increased chloride concentrations in the pore solution. This is interpreted as arising from the increased OH activity which favours OH substitution into Friedel's salt.

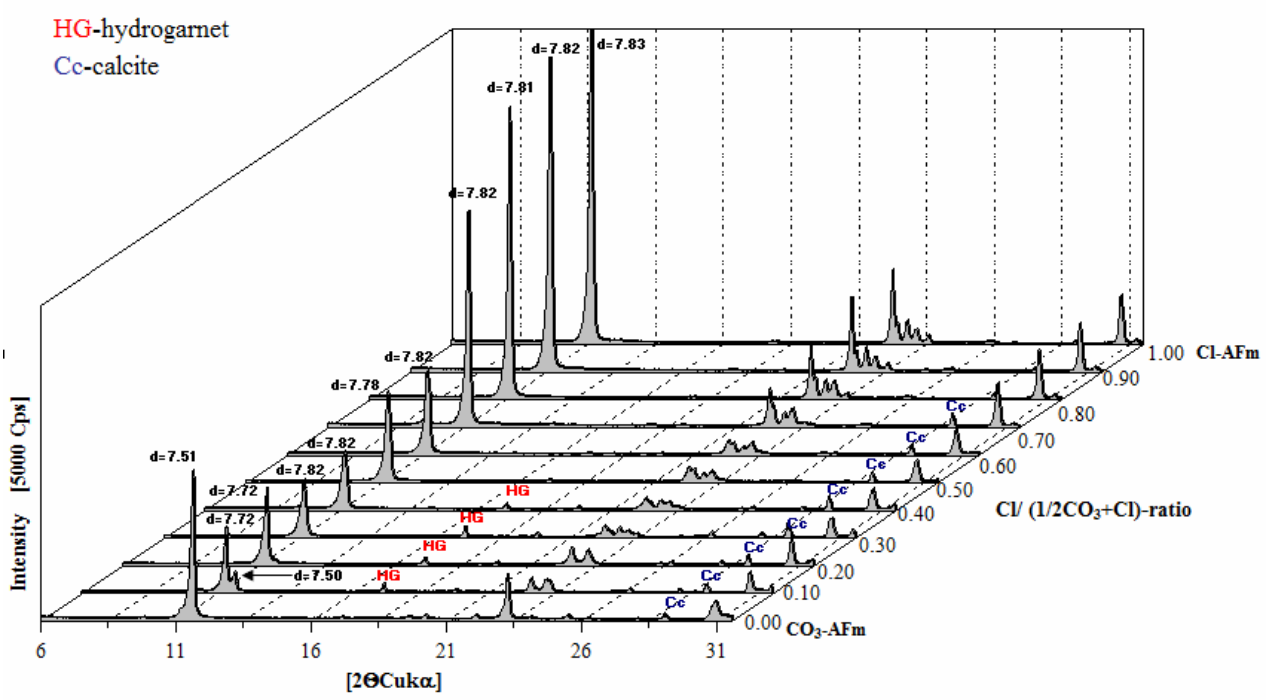

Figure 5.12(a): Partial XRD patterns of the solid solution formation at 25±2˚C between Friedel's salt and monocarboaluminate. Drying at 35% RH does not introduce phase changes. Reflections marked as: HG are attributed to hydrogarnet, Cc are attributed to calcite.

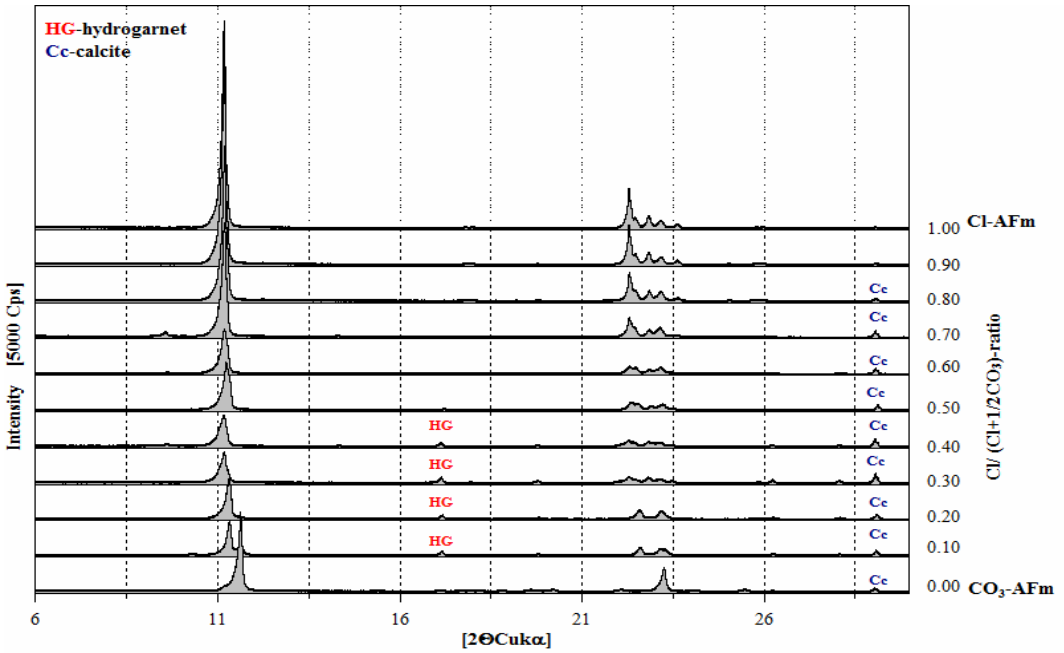

Figure 5.12(b): Partial XRD patterns of the solid solution formation at 25±2˚C between Friedel's salt and monocarboaluminate. Drying at 35% RH does not introduce phase changes. Reflections marked as: HG are attributed to hydrogarnet, Cc are attributed to calcite.

Table 5.6: Aqueous solution compositions measured from undersaturation for samples between monocarboaluminate (Cl/Al=0) and Friedel's salt (Cl/Al=1), and with an excess of $CaCl_2$ (values >1); at 25±2ºC and after 180 days of equilibration.

Calculated Cl/Al- ratio (total system)	Ca [mmol/l] (aq)	Al [mmol/l] (aq)	Cl [mmol/l] (aq)	pH	Solid phase at end of experiment
0.00	3.67	1.59	0.00	11.64	Mc, Cc
0.10	4.14	1.08	0.81	11.56	FS-Mc_{ss}, Mc, Cc
0.20	5.35	1.05	2.02	11.58	FS-Mc_{ss}, Cc
0.30	5.70	0.67	3.47	11.61	FS-Mc_{ss}, Cc
0.40	6.95	0.57	7.60	11.55	FS-Mc_{ss}, Cc
0.50	9.25	0.52	9.87	11.55	FS-Mc_{ss}, Cc
0.60	9.39	0.62	10.72	11.53	FS-Mc_{ss}, Cc
0.70	10.24	1.46	11.97	11.66	FS-Mc_{ss}, Cc
0.80	10.74	1.86	12.42	11.67	FS-Mc_{ss}, Cc
0.90	12.17	1.78	13.13	11.64	FS-Mc_{ss}, Cc
1.05	12.33	1.15	13.37	11.69	n.d.
1.1	13.73	0.91	15.77	11.72	n.d.
1.2	16.88	0.89	24.75	11.64	n.d.

Abbreviations: Mc=monocarboaluminate, Cc=calcite, FS-Mc_{ss} =Friedel's salt in solid solution with monocarboaluminate; n.d.–not determined)

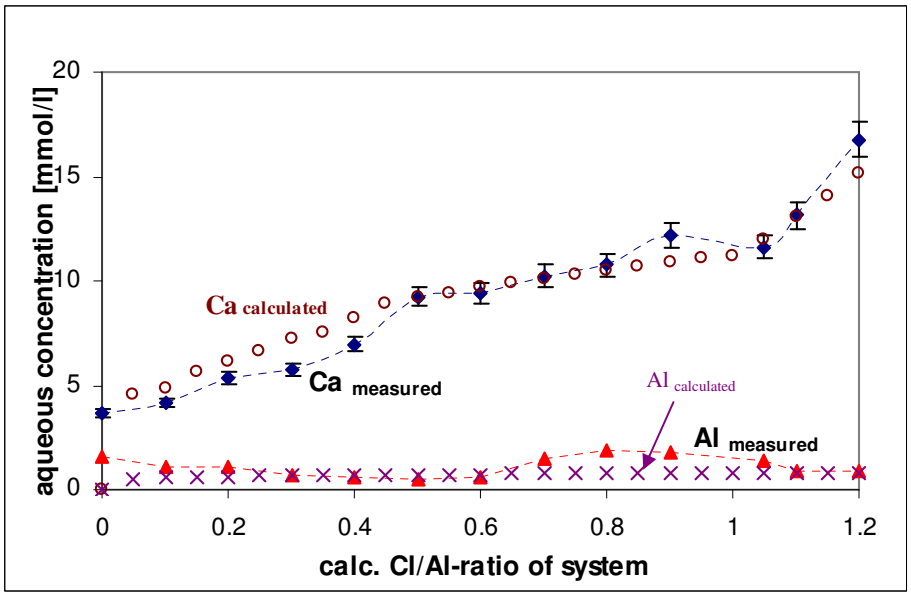

Figure 5.13(a): Equilibrium calcium and aluminium aqueous concentrations, commencing from undersaturation, for solids between monocarboaluminate (Cl/Al=0) - Friedel's salt (Cl/Al=1) and with an excess of calcium chloride (values > 1) at 25±2ºC and 180 days of equilibration. Error bars are shown for Ca. Open circles represent calcium concentrations calculated by GEMS, crosses represent aluminium concentrations calculated by GEMS.

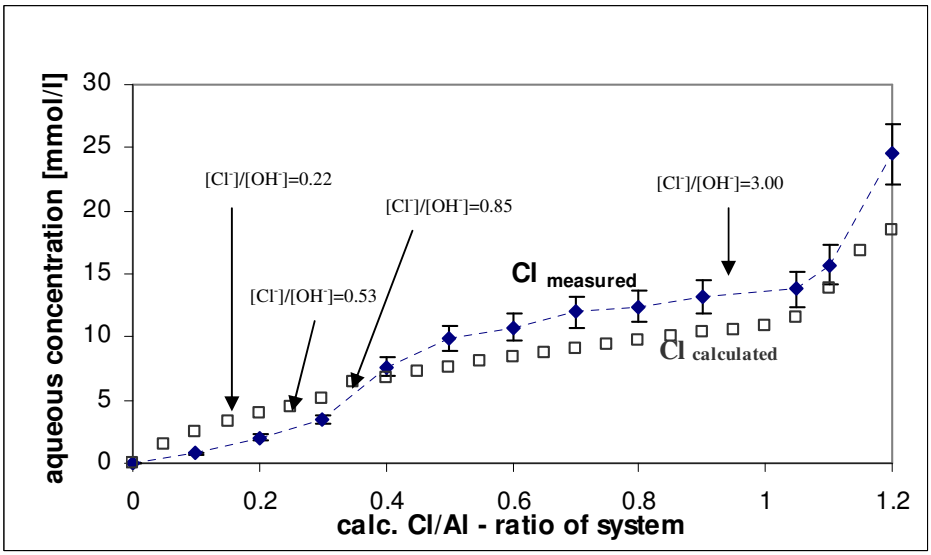

Figure 5.13(b): Equilibrium chloride aqueous concentrations, commencing from undersaturation for solids between monocarboaluminate (Cl/Al=0) - Friedel's salt (Cl/Al=1) and with an excess of calcium chloride (values > 1) at 25±2ºC and after 180 days of equilibration. Error bars are shown for Cl. Variations in the measured aqueous [Cl⁻]/[OH⁻] ratios are shown at selected points: see discussion. Open squares represent chloride concentrations calculated by GEMS.

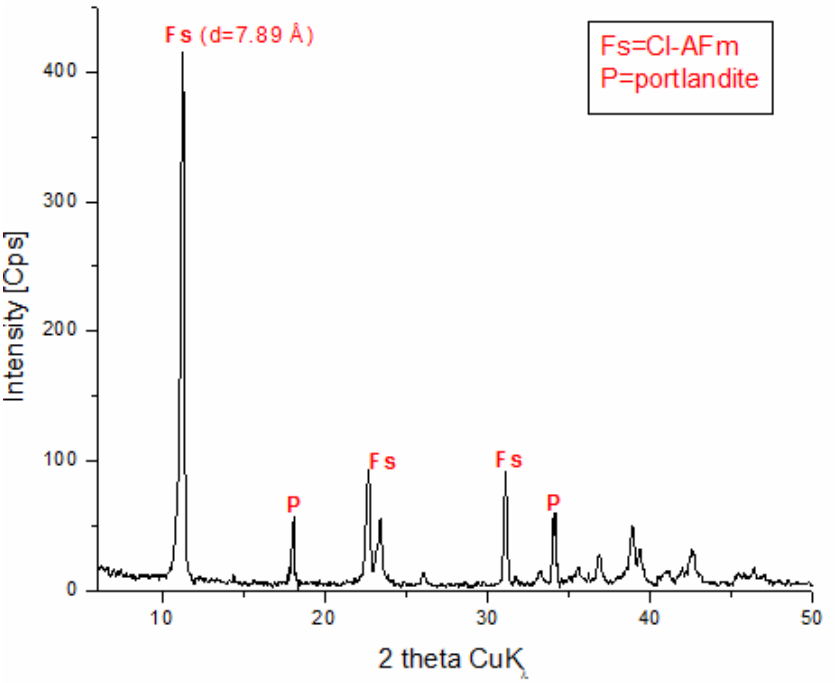

Figure 5.14: XRD patterns showing mineralogical phase assemblage of the mixture containing 0.01 moles Friedel's salt and 0.01 moles $Ca(OH)_2$ which was kept with continuous stirring in 60 ml H_2O at 25±2˚C for 180 days.

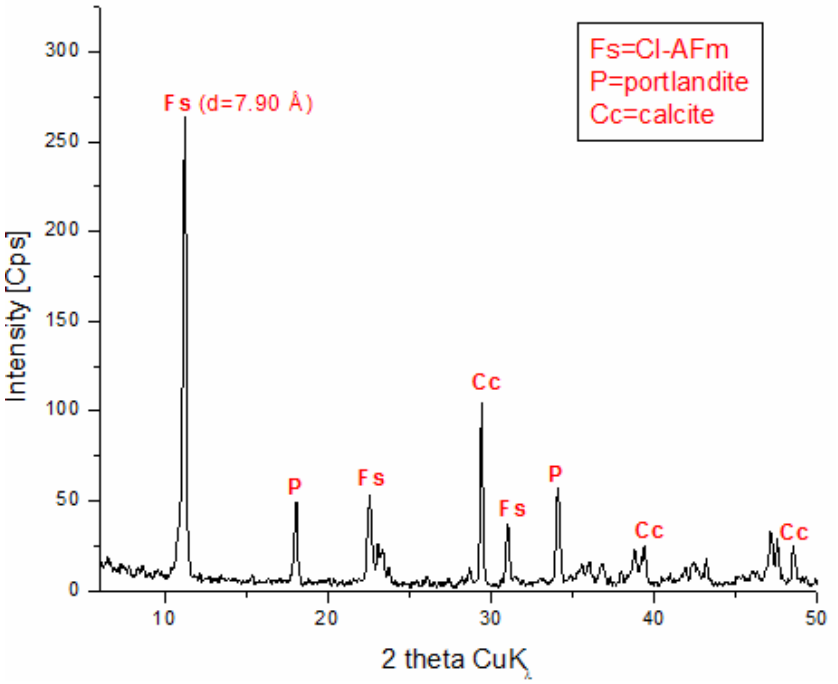

Figure 5.15: XRD patterns showing mineralogical phase assemblage of the mixture containing 0.01 moles Friedel's salt, 0.01 moles $Ca(OH)_2$ and 0.01 moles $CaCO_3$ which was kept with continuous stirring in 60 ml H_2O at 25±2˚C for 180 days.

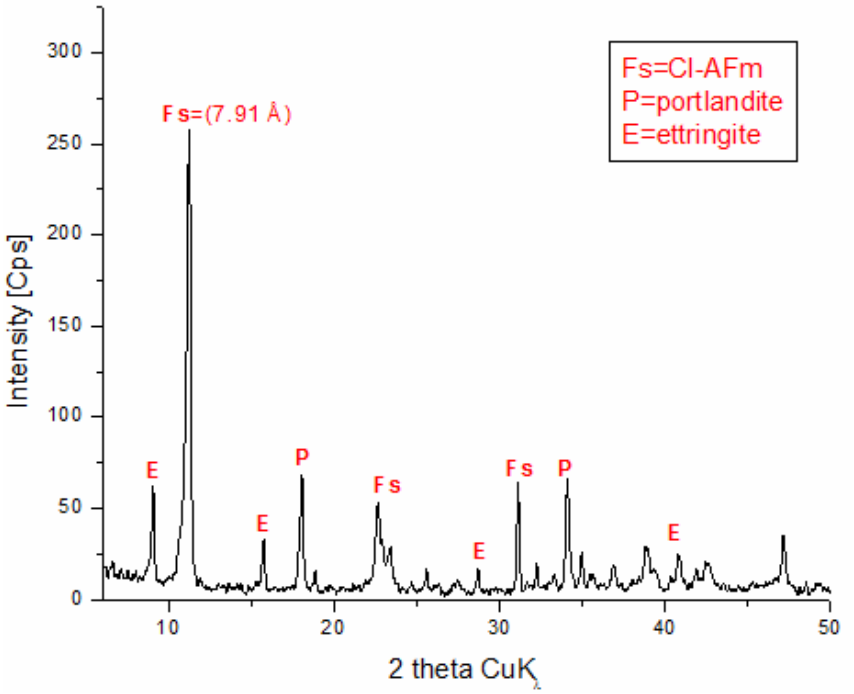

Figure 5.16: XRD patterns showing mineralogical phase assemblage of the mixture containing 0.01 moles Friedel's salt, 0.01 moles $Ca(OH)_2$ and 0.005 moles $CaSO_4$ which was kept with continuous stirring in 60 ml H_2O at 25±2˚C for 180 days.

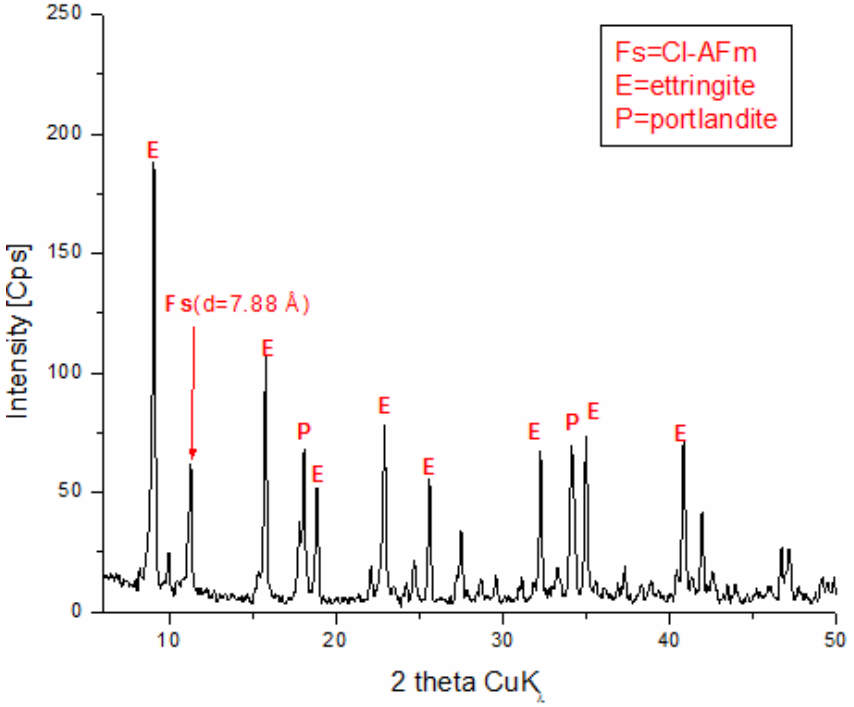

Figure 5.17: XRD patterns showing mineralogical phase assemblage of the mixture containing 0.01 moles Friedel's salt, 0.01 moles $Ca(OH)_2$ and 0.02 moles $CaSO_4$ which was kept with continuous stirring in 60 ml H_2O at 25±2˚C for 180 days.

5.5 Interactions of chloride within cement systems

Thermodynamic modelling was performed on the AFm phases in the systems C_3A-$CaSO_4$-$CaCl_2$-H_2O and C_3A-$CaSO_4$-$CaCO_3$-$CaCl_2$-H_2O. A key purpose of the calculation was to determine the binding power of AFm for chloride in competition with realistic concentrations of sulfate and carbonate and compare calculated data on anion fractionation with experiment.

The properties of chloride-containing hydrates used in the calculations are presented in Tab. 5.7. Experimental solubility products were determined using samples equilibrated for 12 months (Tabs. 5.1 and 5.2; values indicated in italic).

Table 5.7: Standard molar thermodynamic properties of Friedel's salt and Kuzel's salt at 25˚C.

	log K_{S0}	$\Delta_f G°$	$\Delta_f H°$	S°	a_0	a_1	a_2	a_3	$C°_p$	*d**
		[kJ/mol]	*[kJ/mol]*	*[J/K/mol]*	*[J/(mol·K)]*	*[J/(mol·K²)]*	*[J·K/mol]*	*[J/(mol·K^0.5)]*	*[J/K·mol]*	*[kg/m³]*
$C_4ACl_{1.95}H_{10.025}$	-27.69	-6814.6	-7609	731	503	0.89	-1.99e+06	1425	829	2064
$C_4As_{0.5}ClH_{12}$	-28.53	-7533.3	-8472	820	557	1.14	-1.01e+06	751.5	929	2114

** density values taken from [24]; K_{S0}-thermodynamic equilibrium constant at T_o=298 K; $\Delta_f G°$ - standard molar Gibbs energy of formation at T_o= 298 K; $\Delta_f H°$ - standard molar enthalpy at T_o= 298 K; S° - standard molar absolute entropy at T_o= 298 K; a_0, a_1, a_2, a_3 temperature independent empirical parameters characteristic for each solid; $C°_p$- heat capacity at T_o=298 K.*

For modelling purposes, an ideal solid solutions between Friedel's salt and hydroxy AFm, Friedel's salt and monocarboaluminate were assumed and Friedel's salt thermodynamic parameters were re-fitted assuming its ideal composition- $C_4ACl_2H_{10}$: log K_{S0}= -27.27, $\Delta_f G°$= -6810.9 kJ/mol, $\Delta_f H°$= -7604 kJ/mol, S°= 731 J/K/mol, a_o= 498 J/(mol·K), a_1=0.89 J/(mol·K²), a_2=-2.03e+06 J·K/mol, a_3= 1503 J/(mol·K$^{0.5}$), C_p = 829 J/K·mol, d= 2064 kg/m³. Changes in solids agreed well with changes observed in the aqueous phases (Figs. 5.8(b), 5.13(b), 5.19(b), 5.21(b)). The calculations assume alkali-free conditions.

5.5.1 Carbonate- free system

The model results shown in Fig. 5.18, depict the sequence of phase changes occurring in AFm with increasing molar ratio of chloride to alumina. This depiction usefully simulates phase changes occurring when for example chloride ingresses hardened cement paste. Chloride, introduced in the calculation as $CaCl_2$, readily displaces sulfate from "monosulfoaluminate" (Fig. 5.18) which is in solid solution with hydroxy-AFm, (designated as SO_4-AFm_{ss}) forming an intermediate compound Kuzel's salt, $Ca_4Al_2(SO_4)_{0.5}(Cl)(OH)_{12}\cdot 6H_2O$, at low $CaCl_2$ concentration (below molar ratio of $2Cl/Al_2O_3$~0.70) but Friedel's salt in solid solution with hydroxy AFm (designated as Friedel's $salt_{ss}$) at higher chloride concentration, above molar ratio $2Cl/Al_2O_3$~0.70.

The calculated results are in accordance with experimental data reported by Hirao [184, 265], Zibara [195], Csizmadia [180] and Kopecskó [185]. Sulfate ions, released from monosulfoaluminate, form ettringite and this additional ettringite formation results in significant increase in the molar volume of the solids, as shown in Fig 5.19(a).

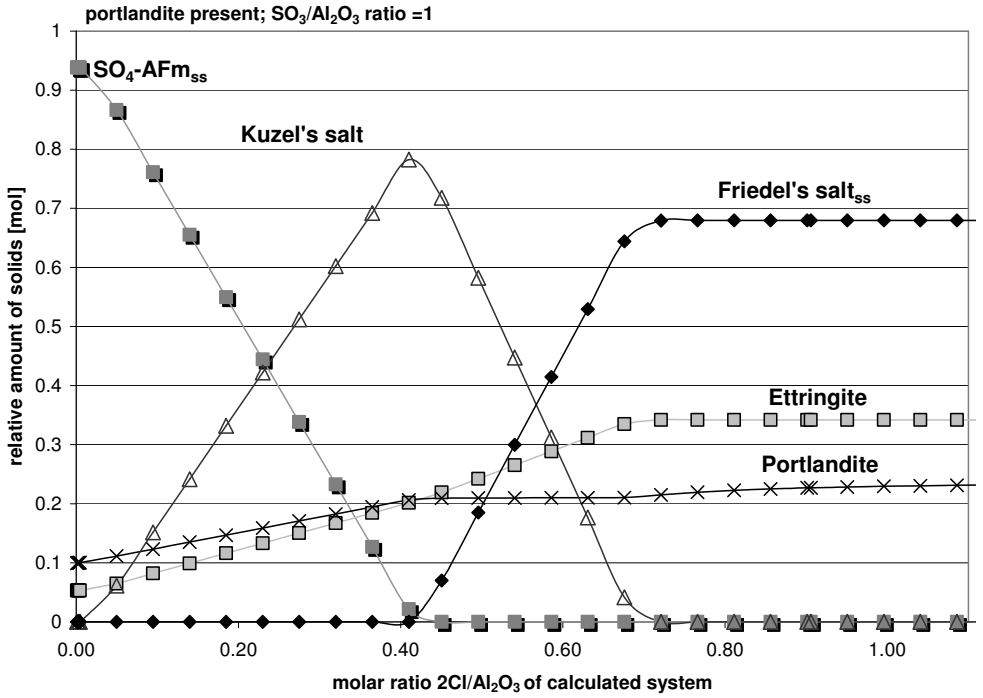

Figure 5.18: Relative amount of solid hydrate phases of a hydrated model mixture consisting of initially 1 mol C_3A, excess of portlandite and with fixed initial sulfate ratio (SO_3/Al_2O_3=1) showing phase development and its dependence on changing chloride ratio ($2Cl/Al_2O_3$) at 25°C.

Experimental results on a phase assemblage containing 0.01 moles C_3A-0.01 moles $CaSO_4$-0.015 moles $Ca(OH)_2$ and 60 ml H_2O are shown in Fig. 5.20, plot 1; the phases formed were identified as monosulfoaluminate (marked as Ms) in solid solution with hydroxy AFm, portlandite (P) and minor amounts of ettringite. In the course of reaction with $CaCl_2$, phase changes occur (plots 2-4): sulfate is displaced from monosulfoaluminate and, at lower chloride contents, Kuzel's salt forms (marked as Ks on plots 2 and 3). At higher chloride content (plot 4) Friedel's salt (in solid solution with hydroxy AFm), was found. Sulfate ions liberated from AFm form ettringite (marked as E in plots 1-4). Thus experiment confirms the calculated reaction sequence. Aqueous compositions (simulated and measured) are compared in Fig. 5.19(b) with generally satisfactory agreement. Note that the pH decreases in stepwise manner with rising $2Cl/Al_2O_3$ over the range of compositions included.

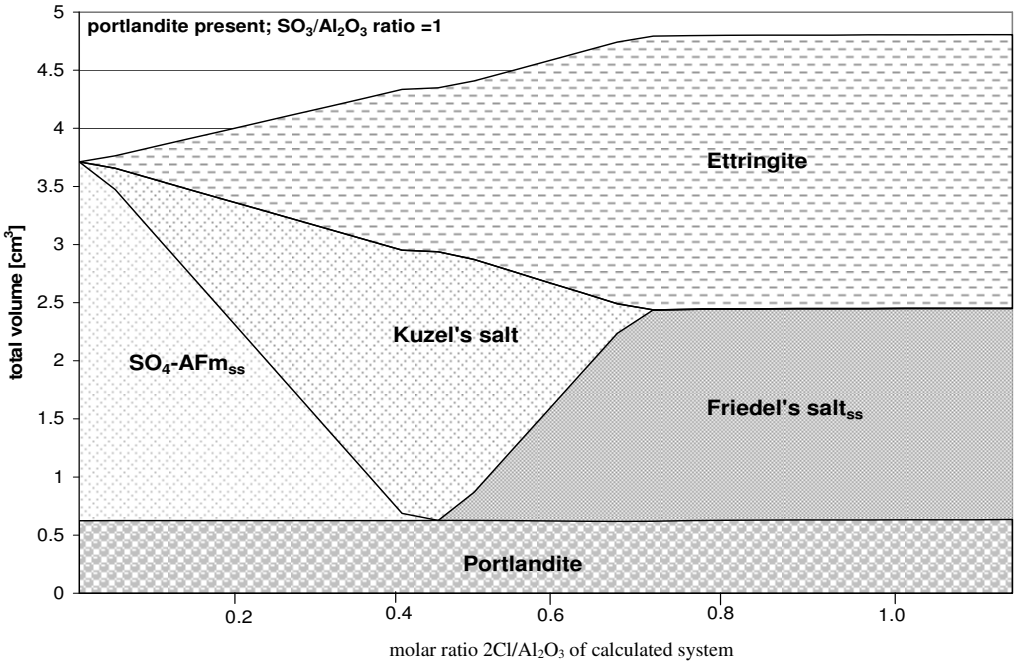

Figure 5.19(a): Calculated total volume of solid phases of a hydrated model mixture initially consisting of 0.01 moles C_3A, 60 ml H_2O, 0.015 moles portlandite and with fixed initial sulfate ratio (SO_3/Al_2O_3=1) showing phase development and its dependence on changing chloride ratios ($2Cl/Al_2O_3$) at 25°C. Minor changes in slope at $2Cl/Al_2O_3$ ~ 0.4 probably arise from rounding errors in the calculation.

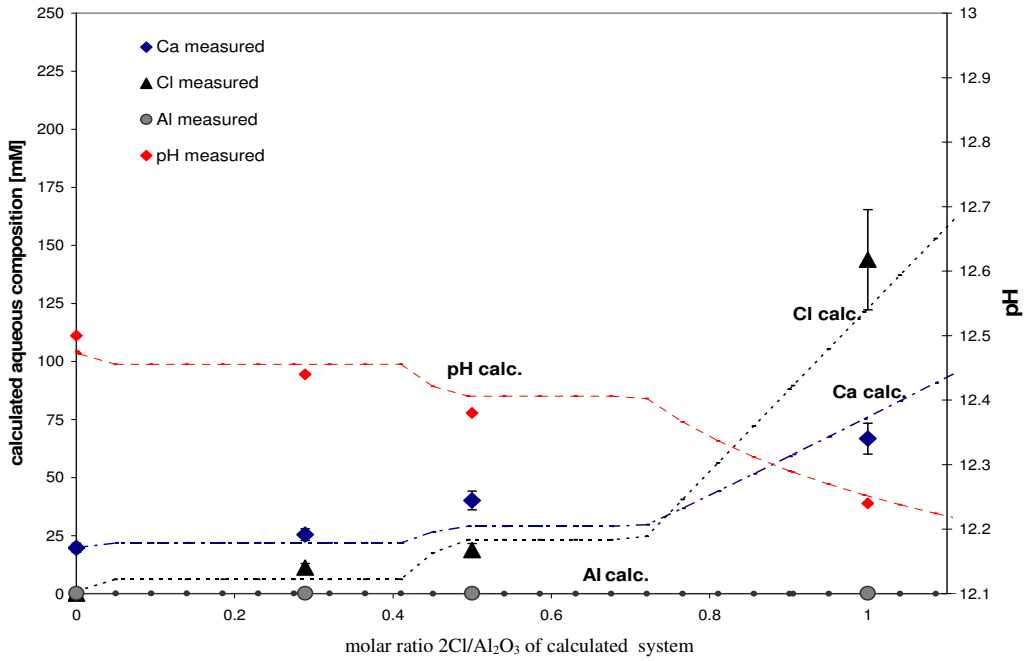

Figure 5.19(b): Calculated and experimental aqueous composition of hydrated model mixture initially consisting of 0.01 moles C_3A, 0.015 moles portlandite, 60 ml H_2O and with fixed initial sulfate ratio (SO_3/Al_2O_3=1) showing its dependence on changing chloride ratio ($2Cl/Al_2O_3$) at 25±2°C.

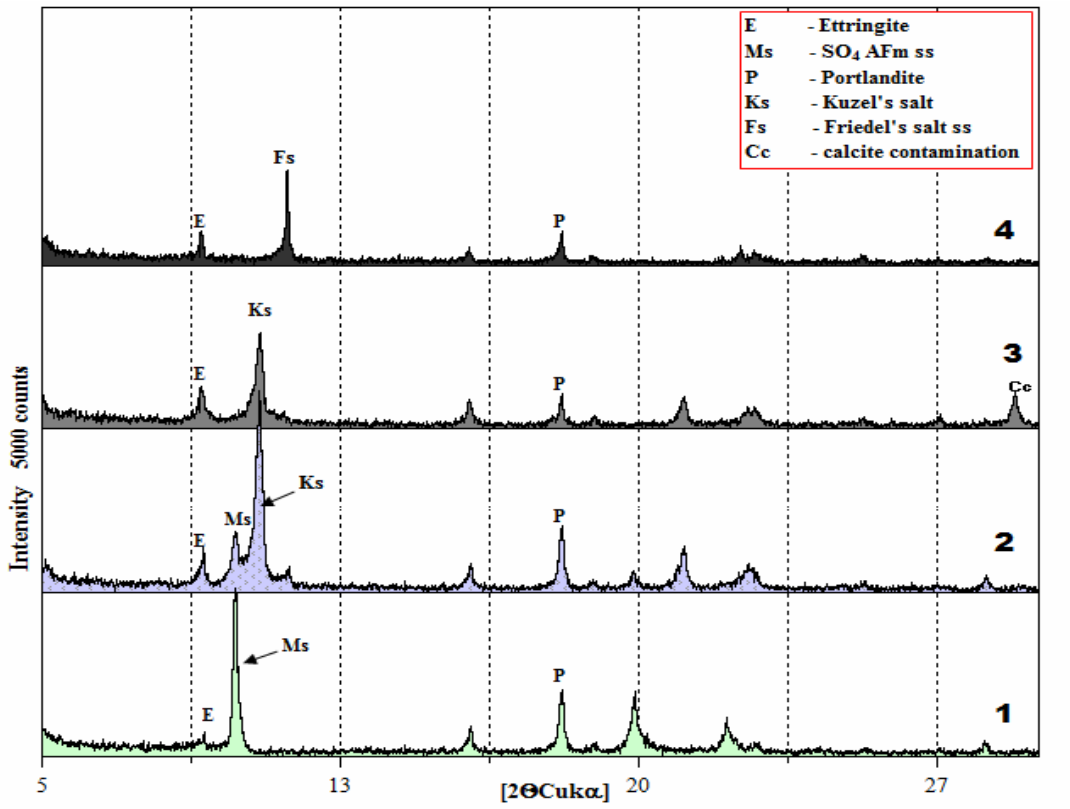

*Figure 5.20: XRD patterns showing mineralogical changes and influence of $CaCl_2$ addition for the system: 0.01 moles C_3A-0.01 moles $CaSO_4$-0.015 moles $Ca(OH)_2$- 60 ml H_2O at 25±2˚C; respectively plots: **1**-no $CaCl_2$ present; **2**-0.003 moles of $CaCl_2$ added; **3**-0.005 moles $CaCl_2$ added; **4**-0.01 moles $CaCl_2$ added.*

5.5.2 Carbonate- containing system

Calculated phase changes for the system C_3A-$CaSO_4$-$CaCl_2$-$CaCO_3$-H_2O are presented in Fig. 5.21(a). Calculations were done for mixtures of monocarboaluminate, portlandite and ettringite. With rising chloride content, carbonate ions in the AFm are substituted by chloride, forming Friedel's salt; the liberated carbonate ions are bound as calcite. Experimental verification was done by equilibrating for 45 days at 25ºC a mixture containing: 0.01 moles C_3A, 0.01 moles $CaSO_4$, 0.015 moles $Ca(OH)_2$, 0.0075 moles $CaCO_3$ and 60 ml H_2O. Fig. 5.22 shows the results. Initially-formed phases (plot 1) were identified as monocarboaluminate (marked as Mc) portlandite (P) and ettringite (E). In the course of admixing $CaCl_2$, a phase change occurs (plot 2). Friedel's salt appeared while carbonate, displaced from monocarboaluminate, formed calcite (marked as Cc). Thus calcite, $CaCO_3$, can be formed at constant carbonate content by adding chloride,

without introduction of additional carbonate from an external source, by displacement from carbonate-containing AFm solids. Kuzel's salt does not appear because its formation is suppressed by the greater stability of monocarboaluminate. Volume changes in this case are much reduced relative to those in the carbonate-free system: Fig. 5.21(b) compares calculated and measured aqueous compositions. Thus with rising chloride ratio, carbonate is displaced from monocarboaluminate (Fig. 5.22) forming calcite and Friedel's salt. These calculations are consistent with experimental results reported in the literature [10, 236, 245, 266].

Schematic phase relations at 25˚C, between Friedel's salt and other AFm phases are plotted in Figs. 5.23, 5.24. To construct diagram 5.23 it was assumed that the system contained an excess of both $CaCO_3$ and $Ca(OH)_2$. Limited solid solution between (i) SO_4-AFm/CO_3-AFm and (ii) between Kuzel's salt and either /SO_4-AFm or Friedel's salt are admitted. Since the AFm phases also contain minor hydroxide substituted for other anions the diagram is essentially a projection with (OH) substitution (not shown) adding a third dimension. This accords with the mineralogy of many Portland cements during early stages of alteration and has the advantage of fixing approximately the activities of calcium, carbonate and hydroxide. Phase relations and solid solutions between OH-AFm/ SO_4-AFm have been described in detail by Matschei [9].

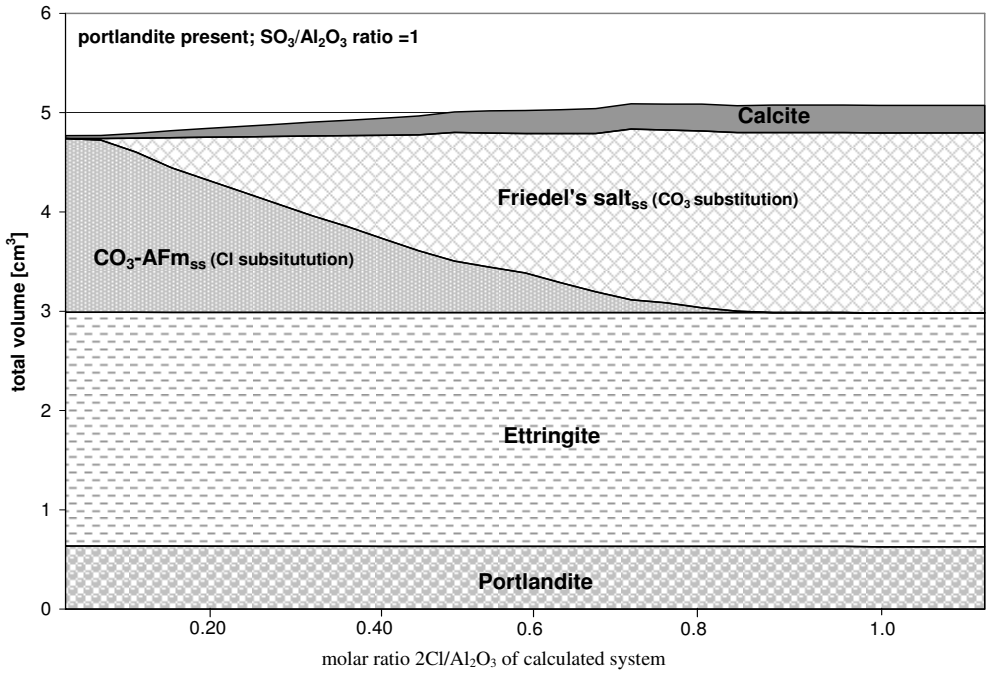

Figure 5.21(a): Total volume of solid phases of a hydrated model mixture initially consisting of 0.01 moles C_3A, 60 ml H_2O, 0.015 moles portlandite, 0.0075 moles $CaCO_3$ and with fixed initial sulfate ratio (SO_3/Al_2O_3=1) showing phase development and its dependence on changing chloride ratios ($2Cl/Al_2O_3$) at 25°C.

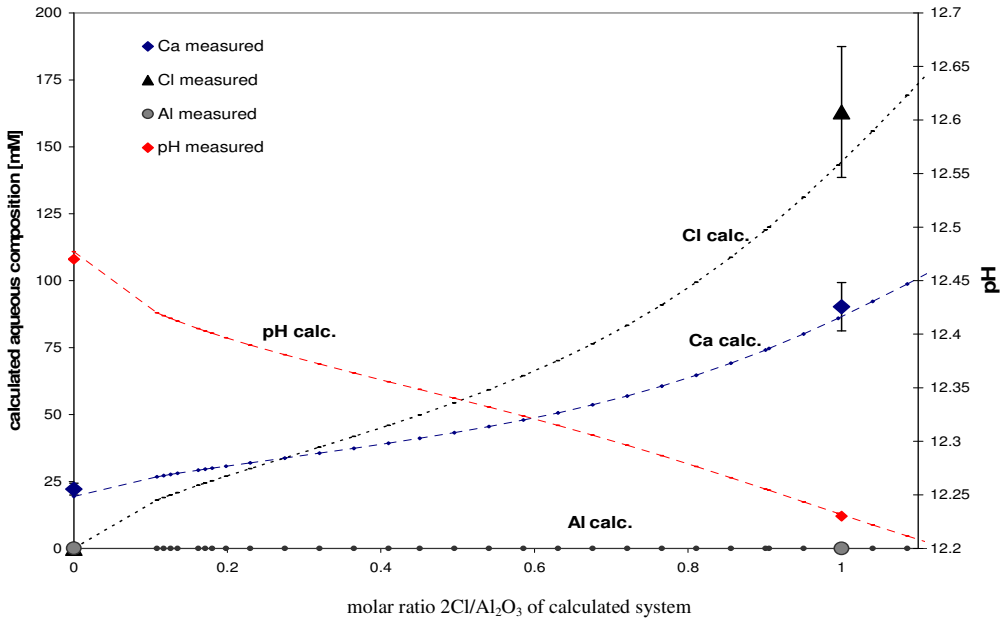

Figure 5.21(b): Calculated and experimental aqueous composition of hydrated model mixture initially consisting of 0.01 moles C_3A, 0.015 moles portlandite, 0.0075 mol $CaCO_3$, 60 ml H_2O and with fixed initial sulfate ratio (SO_3/Al_2O_3=1) showing its dependence on changing chloride ratios ($2Cl/Al_2O_3$) at 25±2°C.

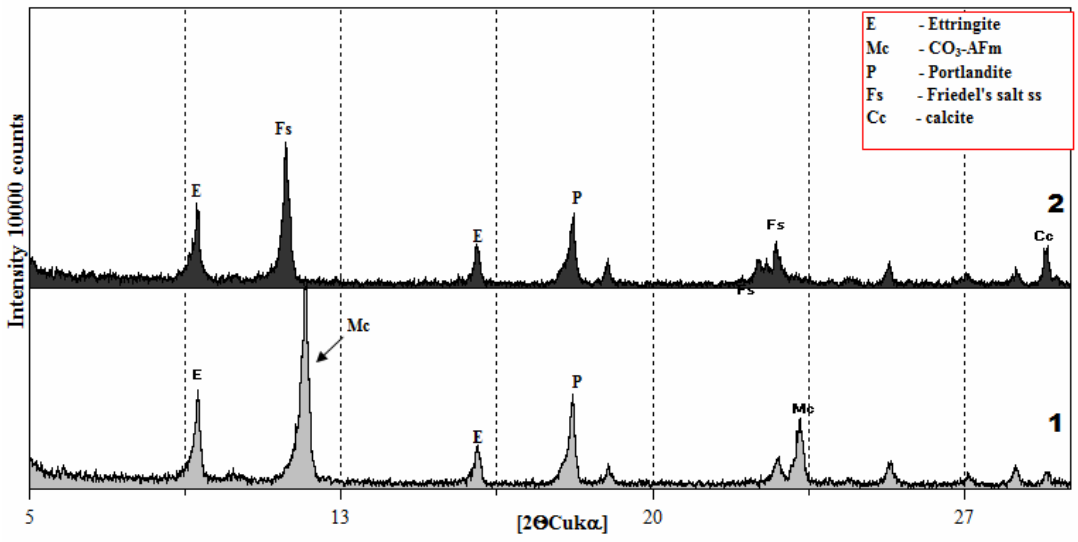

Figure 5.22: XRD patterns showing mineralogical changes and influence of $CaCl_2$ addition for the system 0.01 moles C_3A-0.01 moles $CaSO_4$-0.015 moles $Ca(OH)_2$-0.0075 moles $CaCO_3$- 60 ml H_2O at 25±2˚C; 1-no $CaCl_2$ present; 2-0.01 moles of $CaCl_2$ added.

5.5.3 Relationships of AFm phases

Some details of the phase boundaries are not known precisely but solid solution between SO_4-AFm and CO_3-AFm is known from previous studies to be negligible [9]. Kuzel's salt is also incompatible with CO_3-AFm. Taking into the account the above solid solution limits a region of three coexisting phases (SO_4-AFm + Kuzel's salt + Friedel's salt) must exist. However experiment shows that the range of compositions included in this assemblage must be physically small. This is because the greater stability of the extensive solid solution based on Friedel's salt and CO_3-AFm, shown at the right-hand edge on Fig. 5.23; the physical location of points a and b ensures that most of the ternary composition space is occupied by the coexistence of two AFm phases, SO_4-AFm and a carbonate –substituted Friedel's salt. This extensive range of Friedel's salt type solid solution and the resulting broad range of compositions included in this two phase region, explain why Kuzel's salt is only infrequently reported in chloride-containing cement pastes. Kuzel's salt is destabilised by even small amounts of carbonate, and will only be encountered in low-carbonate environments.

To visualise phase relation between monocarboaluminate, Friedel's salt and hydroxy AFm Fig. 5.24 was constructed assuming that the system did not contain any $CaSO_4$. A limited solid solution between Cl-AFm/CO_3-AFm and between Cl-AFm/OH-AFm is

admitted. But there is no solid solution between CO_3-AFm and OH-AFm; instead an ordered compound - hemicarboaluminate – has been reported in the literature [9, 45, 263]. Phase relations in this ternary diagram (Fig. 5.24) are complicated by the breakdown of OH-AFm at > 5˚C, which decomposes to hydrogarnet and portlandite [9]. Nevertheless previous studies have shown that on the join between Friedel's salt–OH-AFm, a miscibility gap occurs at high hydroxyl contents and that a miscibility gap also occurs on the join CO_3-AFm-Friedel's salt, with a gap at high carbonate contents. On the other hand, the literature claims [12] that continuous solid solution occurs between Friedel's salt and hemicarboaluminate. On the face of it, this seems unlikely.

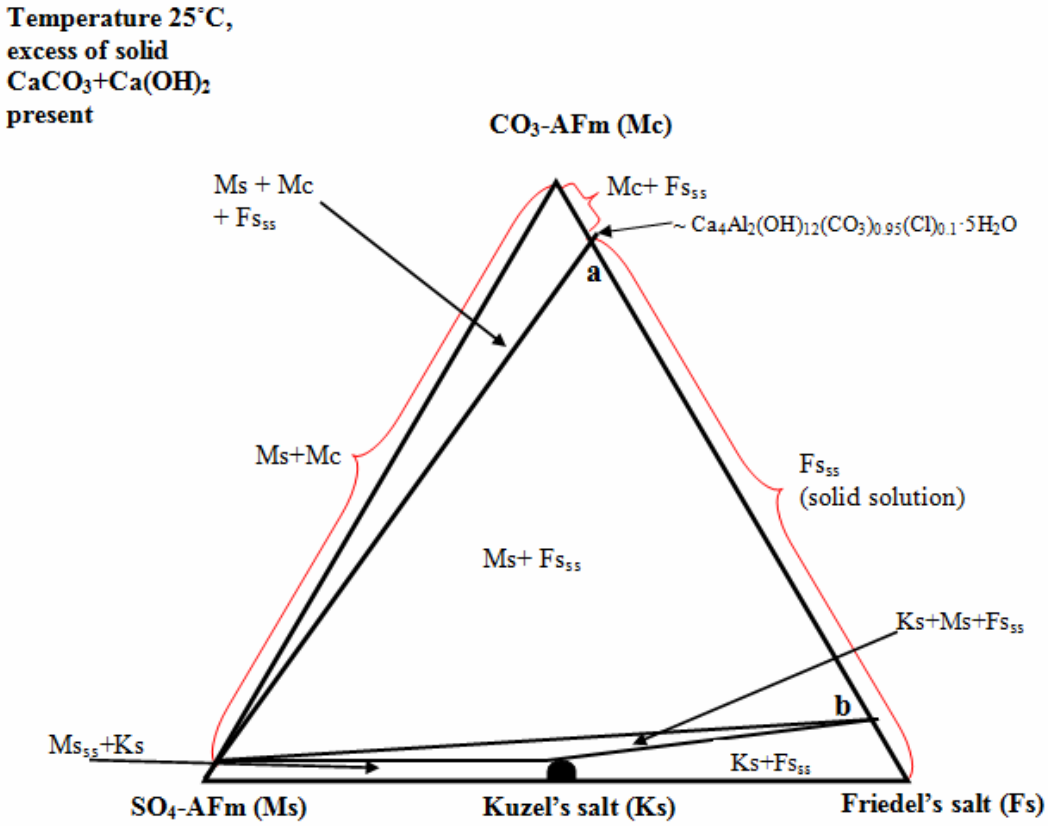

Figure 5.23: Schematic phase relations at 25˚C, between Friedel's salt, monosulfoaluminate and monocarboaluminate. Most of the composition range is dominated by the two solid phase region (Ms +FS$_{ss}$).

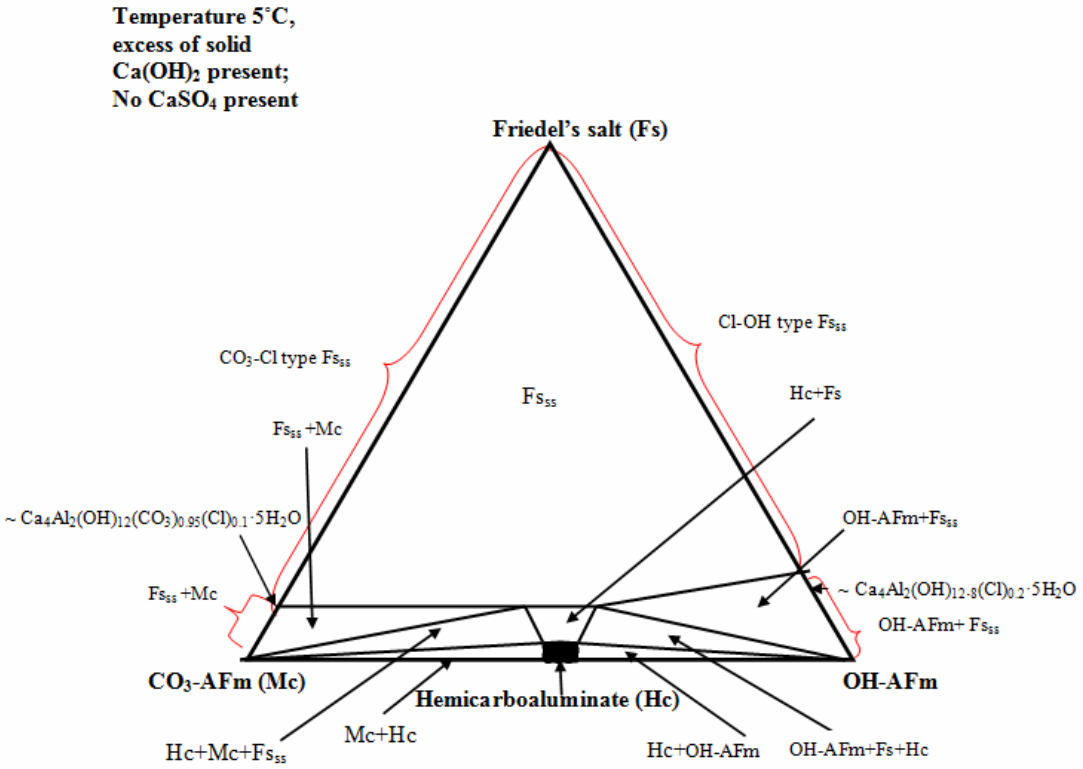

Figure 5.24: Schematic phase relations at 5˚C, between Friedel's salt, hydroxy AFm and monocarboaluminate.

Hemicarboaluminate-$Ca_4Al_2(CO_3)_{0.5}(OH)_{13}\cdot 5.5H_2O$ is characterised by having a fixed ratio of OH/CO_3. These two anions occupy separate crystallographic sites in the structure, allowing possibly only very slight solid solution. This contrasts with a ternary solid solution, in which the anions have to be disordered to explain ternary phase relations.

5.5.4 Influence of temperature

To evaluate potential influence of the temperature on the phase assemblages of investigated compositions, GEMS simulations were run at temperatures 5˚C, 55˚C and 85˚C (Figs. 5.25-5.27 and 5.30-5.32) as well as for selected compositions over the range of temperatures 0-99˚C (Figs. 5.28, 5.29, 5.33 and 5.34).

5.5.4.1 Carbonate free system

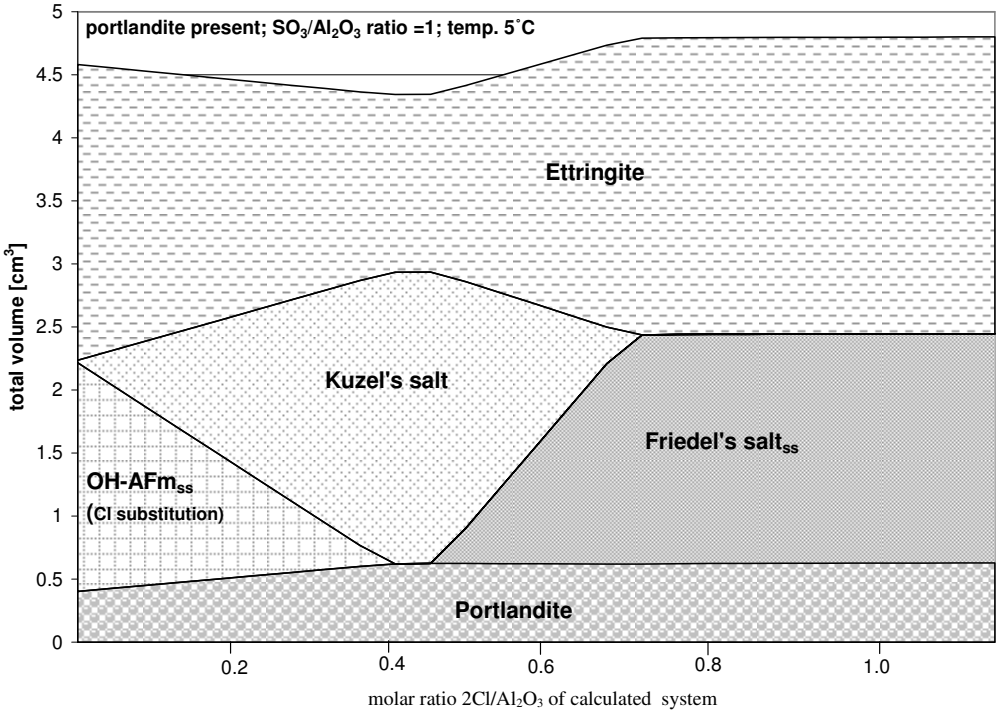

Figure 5.25: Calculated total volume of solid phases of a hydrated model mixture initially consisting of 0.01 moles C_3A, 60 ml H_2O, 0.015 moles portlandite and with fixed initial sulfate ratio (SO_3/Al_2O_3=1) showing phase development and its dependence on changing chloride ratios ($2Cl/Al_2O_3$) at 5°C.

The model results for 5˚C are shown in Fig. 5.25. If we compare results obtained at 25˚C (Fig. 5.19(a)), it can be clearly seen that at 5˚C, the monosulfoaluminate phase is not stable. Instead, at lower temperature hydroxy-AFm, slightly SO_4 substituted (designated as OH-AFm_{ss}) and ettringite form. Chloride, introduced in the calculation as $CaCl_2$, readily displaces hydroxide from "hydroxy AFm" (assuming solid solution between hydroxy AFm and Friedel's salt). Liberated OH^- ions react with calcium ions forming portlandite. Kuzel's salt forms below molar ratio $2Cl/Al_2O_3$~0.70 and Friedel's salt in solid solution with hydroxy AFm (designated as Friedel's $salt_{ss}$) above molar ratio $2Cl/Al_2O_3$~0.70. The general volume expansion tendency at 25˚C (Fig. 5.19(a)) is quite different than in the 5˚ C calculation and illustrates the importance of taking temperature into account.

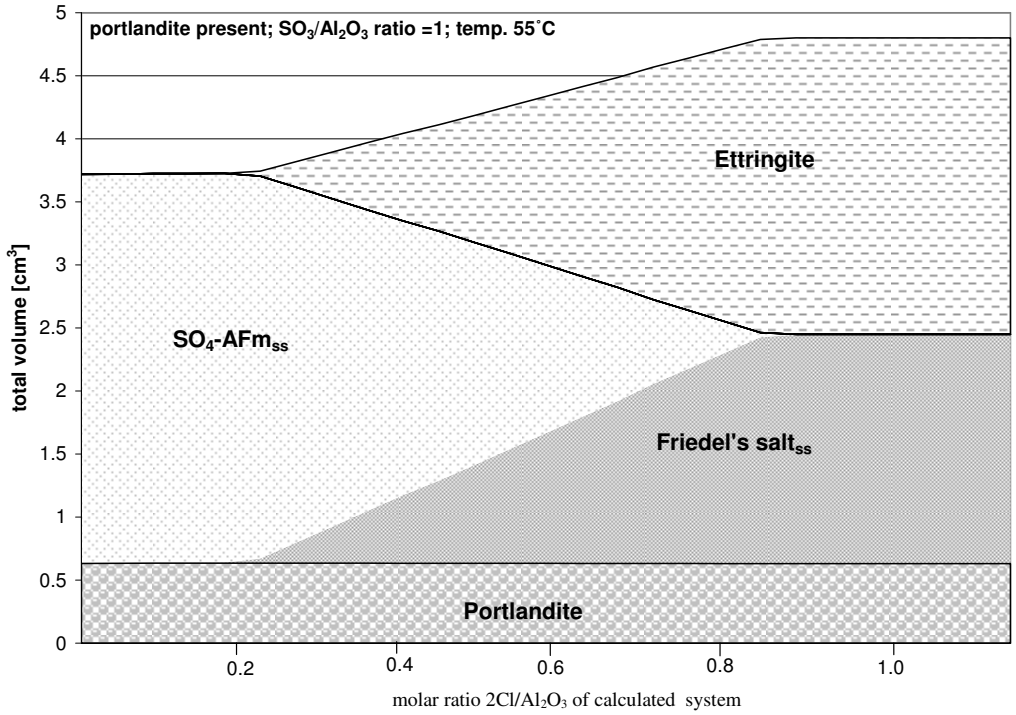

Figure 5.26: Calculated total volume of solid phases of a hydrated model mixture initially consisting of 0.01 moles C_3A, 60 ml H_2O, 0.015 moles portlandite and with fixed initial sulfate ratio (SO_3/Al_2O_3=1) showing phase development and its dependence on changing chloride ratios ($2Cl/Al_2O_3$) at 55°C.

Simulations were compared with data reported in the literature [9, 48, 56]. Hydroxy AFm is reported to be stable only in low temperatures: at room temperature it decomposes slowly to portlandite and hydrogarnet (katoite). Due to higher stability of hydroxy AFm at lower temperature, OH substitution in the Friedel's salt may be slightly higher that at room temperature. This would explain why Jensen et al. [238] reported that in their experiments more chloride was bound at 20˚C than at 4˚C.

Results of modelling at 55˚C and 85˚C are presented respectively on Figs. 5.26 and 5.27. At higher temperatures, the stability of Kuzel's salt decreases and at 55˚C, Kuzel's salt formation is completely supressed and Friedel's salt forms directly as Cl displaces sulfate from monosulfoaluminate (Fig. 5.26).

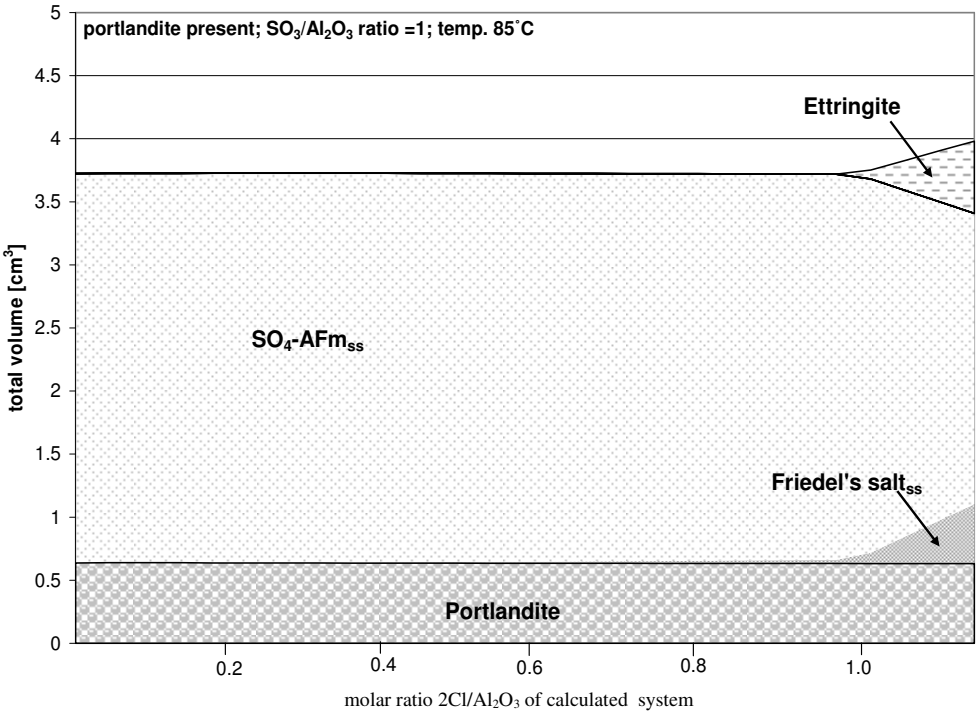

Figure 5.27: Calculated total volume of solid phases of a hydrated model mixture initially consisting of 0.01 moles C_3A, 60 ml H_2O, 0.015 moles portlandite and with fixed initial sulfate ratio (SO_3/Al_2O_3=1) showing phase development and its dependence on changing chloride ratios ($2Cl/Al_2O_3$) at 85°C.

Monosulfoaluminate (SO_4-AFm_{ss}) appears as a dominant phase at 85˚C in agreement with the literature [9, 48] and ettringite and Friedel's salt formation only occur at very high $2Cl/Al_2O_3$ ratios above 1.0 (Fig. 5.27).

To visualise influence of changing temperature for two particular compositions modelling was performed in the range 0-99˚C. Fig. 5.28 shows phase change for the initial composition containing: 0.01 moles C_3A, 0.015 moles portlandite, sulfate ratio (SO_3/Al_2O_3=1) and chloride ratio $2Cl/Al_2O_3$=0.5. Due to low initial chloride ratio, Kuzel's salt forms but is predicted to be stable only up to 28˚C. For this particular composition Friedel's salt persists below 70˚C. Monosulfoaluminate slightly substituted with OH (SO_4-AFm_{ss}) starts to appear at around 28˚C. As SO_4-AFm is stable at higher temperatures, it appears to be the dominant product above 70˚C.

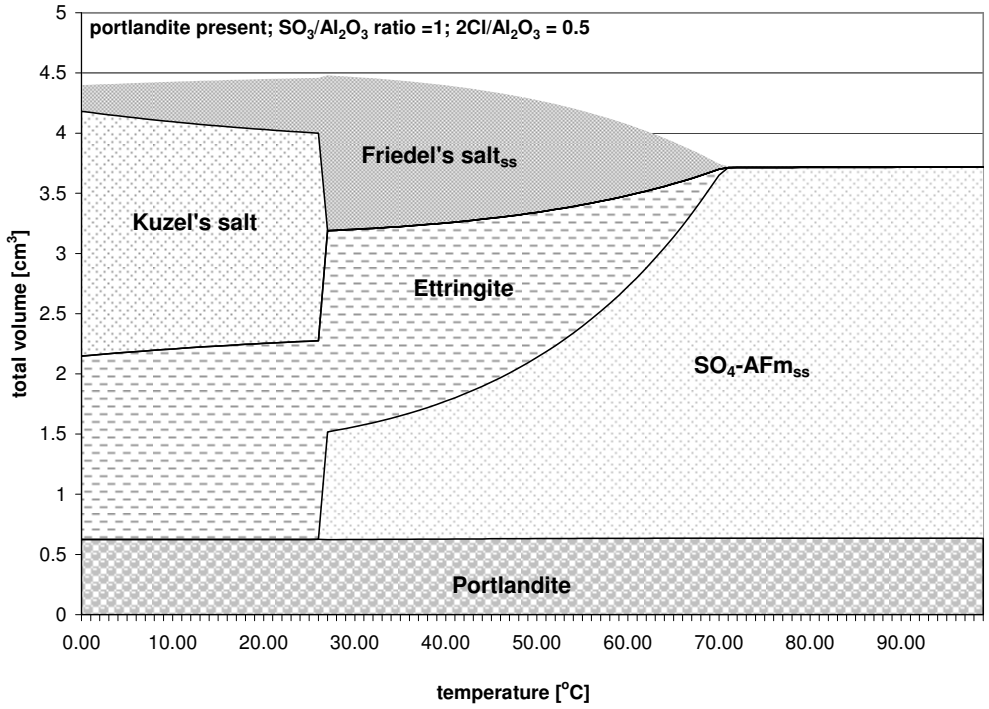

Figure 5.28: Calculated total volume of solid phases of a hydrated model mixture initially consisting of 0.01 moles C_3A, 60 ml H_2O, 0.015 moles portlandite and with fixed initial sulfate ratio (SO_3/Al_2O_3=1) and chloride ratio ($2Cl/Al_2O_3$=0.5) showing phase development and its dependence on changing temperature.

Fig. 5.29 shows phase change over a temperature range for the initial composition containing: 0.01 moles C_3A, 0.015 moles portlandite, sulfate ratio (SO_3/Al_2O_3=1) and higher than in the previous example chloride ratio $2Cl/Al_2O_3$=1. Kuzel's salt is initially supressed due to the high chloride content and Friedel's salt persists up to 80˚C, above which it decomposes. Monosulfoaluminate (SO_4-AFm_{ss}) only appears at >60˚C but by 80˚C it is a main phase. The literature discloses [2, 267, 268] that ettringite appears to be stable in water to at least 110-114˚C at atmospheric pressures and up to 70˚C in cement pastes because C-S-H competes strongly for sulfate ions but if sufficient sulfate is present it persists to higher temperatures.

As it can be seen from the graphs persistence of ettringite and conversion between monosulfoaluminate and ettringite is not only dependent on temperature but also on the initial composition of the system. Moreover, the decomposition extends across a range of temperatures.

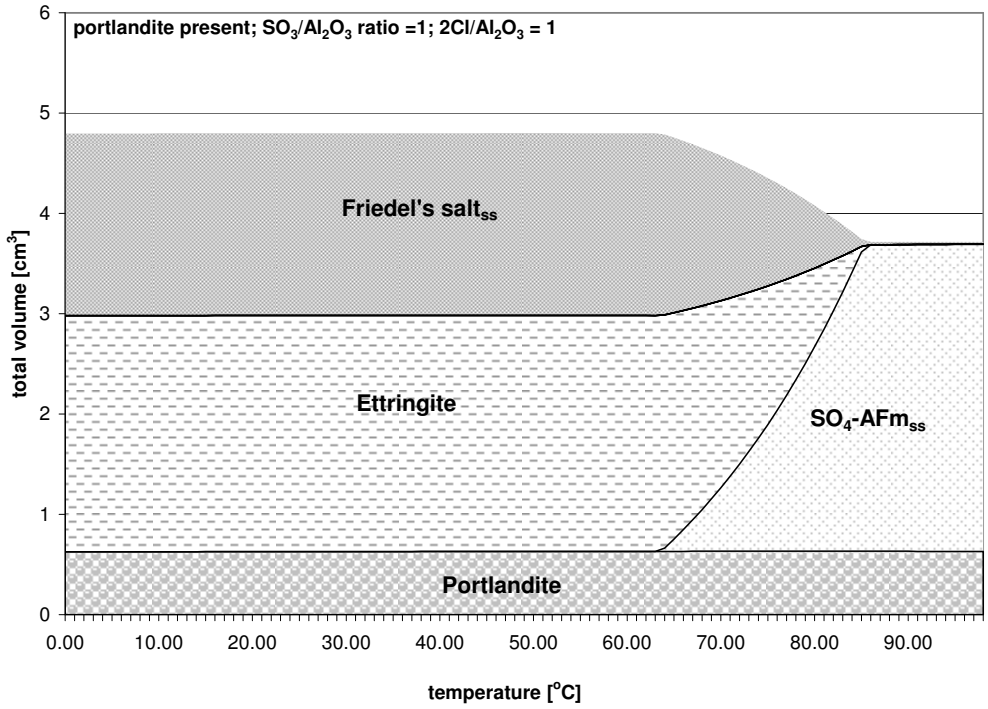

Figure 5.29: Calculated total volume of solid phases of a hydrated model mixture initially consisting of 0.01 moles C_3A, 60 ml H_2O, 0.015 moles portlandite and with fixed initial sulfate ratio (SO_3/Al_2O_3=1) and chloride ratio ($2Cl/Al_2O_3$=1) showing phase development and its dependence on changing temperature.

5.5.4.2 Carbonate containing system

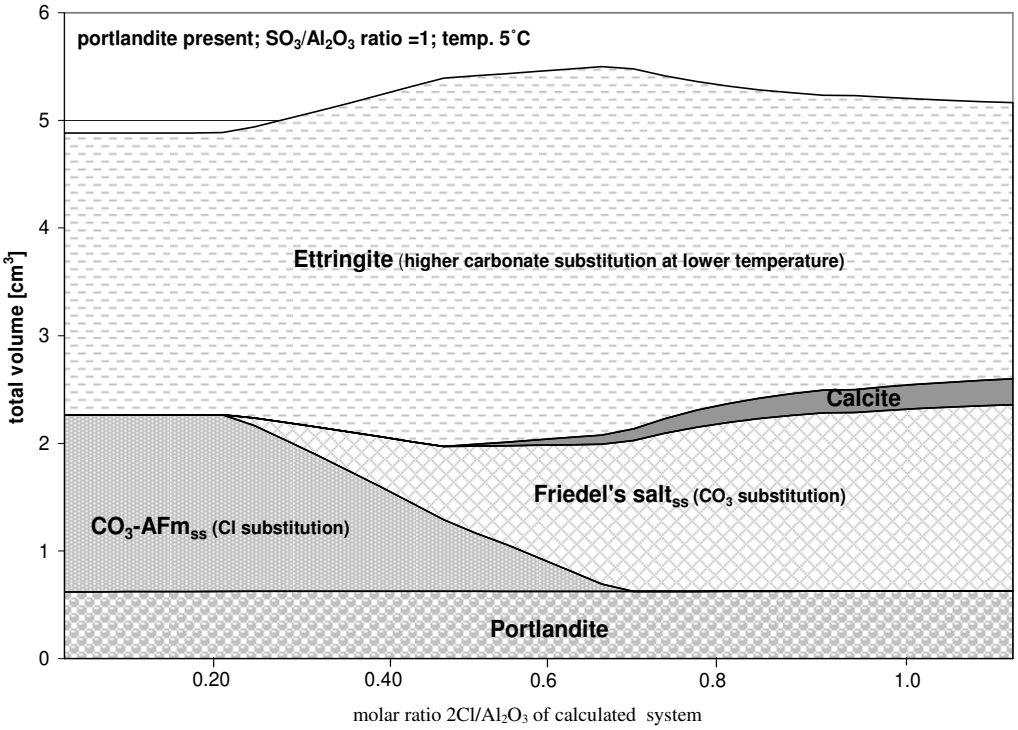

Figure 5.30: Total volume of solid phases of a hydrated model mixture initially consisting of 0.01 moles C_3A, 60 ml H_2O, 0.015 moles portlandite, 0.0075 moles $CaCO_3$ and with fixed initial sulfate ratio (SO_3/Al_2O_3=1) showing phase development and its dependence on changing chloride ratios ($2Cl/Al_2O_3$) at 5°C.

Simulation for the system initially containing carbonate (ratio CO_2/Al_2O_3=0.75) and hydrated at 5˚C are shown in Fig. 5.30. Chloride, introduced in the calculation as $CaCl_2$, readily displaces carbonate from "monocarboaluminate" and via solid solution forms Friedel's salt. Comparing results obtained at 25˚C (Fig. 5.21(a)) results do not much differ and the system looks very similar except between 0.25-0.7 $2Cl/Al_2O_3$ ratios, where GEMS predicts slightly elevated volume due to enhanced ettringite formation. For the ettringite the solid solution model proposed by Matschei et al. [56] has been adapted. As mentioned before with increasing chloride content, carbonate is displaced from monocarboaluminate. Carbonate ions displaced from ettringite with rising temperature form calcite. Calcite solubility increases with decreasing temperature.

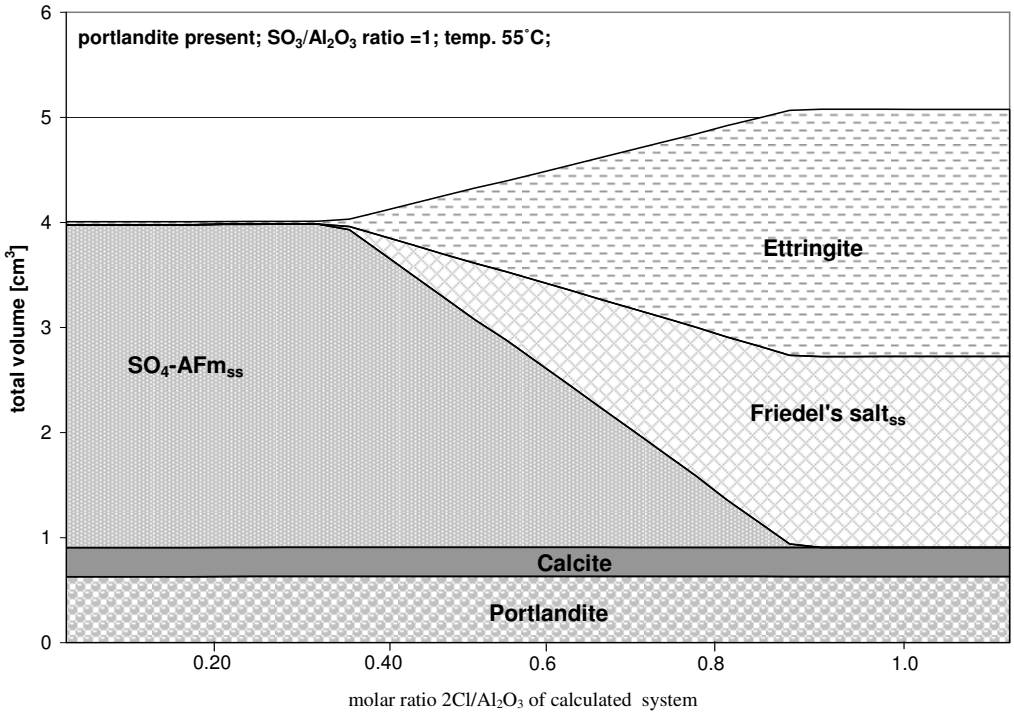

Figure 5.31: Total volume of solid phases of a hydrated model mixture initially consisting of 0.01 moles C_3A, 60 ml H_2O, 0.015 moles portlandite, 0.0075 moles $CaCO_3$ and with fixed initial sulfate ratio (SO_3/Al_2O_3=1) showing phase development and its dependence on changing chloride ratios ($2Cl/Al_2O_3$) at 55°C.

Matschei et al. [56] shown that in ettringite at 25˚C only a small percent of sulfate can be substituted by carbonate (maximum 9 mol%) but as the temperature decreases this substitution grows reaching 33 mol% at 5˚C and 50 mol% at 0˚C.

Fig. 5.30 predicts that carbonate substitution in ettringite will increase with $2Cl/Al_2O_3$ ratios (*e.g.* at 0.15 ratio= 18%, 0.25 ratio = 24%). Between ~0.35-0.7 ($2Cl/Al_2O_3$) ratios at 5˚C, 33 mol% of sulfate ions in ettringite will be substituted with carbonate which is the maximal amount of substitution that can be reached at this temperature. Above ratio 0.7 when all the carbonate has been displaced from monocarboaluminate model predicts that carbonate substitution in ettringite will be lower (*e.g.* at 0.8 ratio = 20%, and at ratio only ~12%).

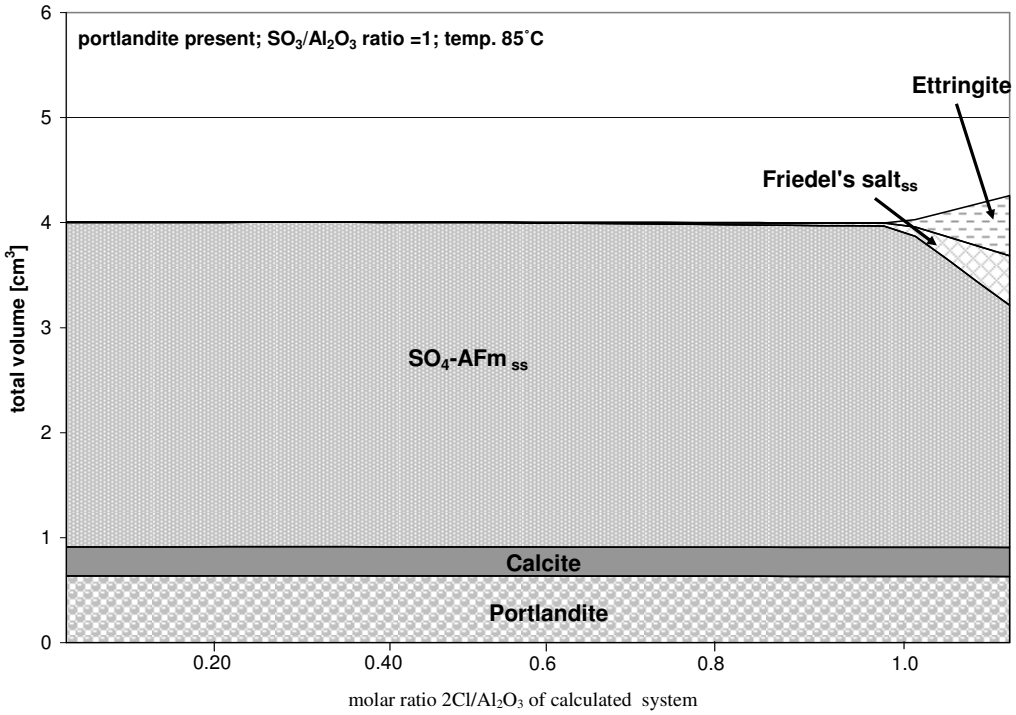

Figure 5.32: Total volume of solid phases of a hydrated model mixture initially consisting of 0.01 moles C_3A, 60 ml H_2O, 0.015 moles portlandite, 0.0075 moles $CaCO_3$ and with fixed initial sulfate ratio (SO_3/Al_2O_3=1) showing phase development and its dependence on changing chloride ratios ($2Cl/Al_2O_3$) at 85°C.

At 55˚C (Fig. 5.31) and in agreement with literature [9, 48, 56] simulation shows that monocarboaluminate will be no longer stable and carbonate ions are accommodated in calcite. Monosulfoaluminate (SO_4-AFm_{ss}) initially forms but with increasing $2Cl/Al_2O_3$ ratios sulfate is displaced from monosulfoaluminate, Friedel's salt is formed while liberated sulfate ions result in formation of ettringite. At 85˚C and slight Friedel's salt formation only occurs at very high $2Cl/Al_2O_3$ ratios above > 1.0 (Fig. 5.32). Trends modelled in Figs. 5.31 and 5.32 are very similar to those presented on Figs. 5.26 and 5.27. This is because monocarboaluminate phases are unstable in elevated temperatures [9] and calcite acts as an inert substance and therefore does not affect phase distribution.

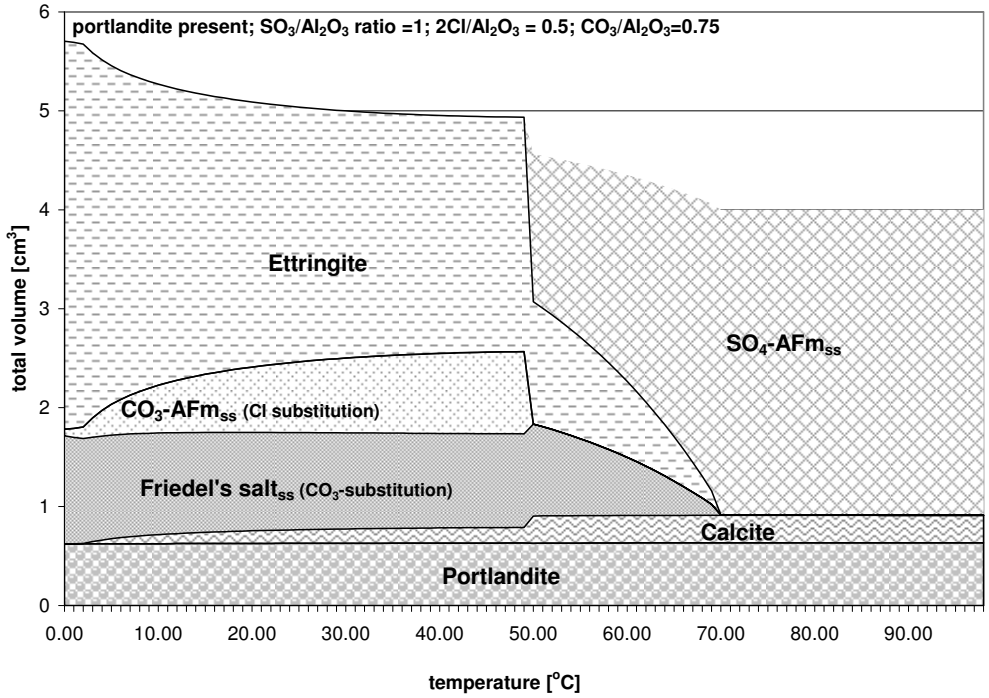

Figure 5.33: Total volume of solid phases of a hydrated model mixture initially consisting of 0.01 moles C_3A, 60 ml H_2O, 0.015 moles portlandite, 0.0075 moles $CaCO_3$ and with fixed initial sulfate ratio (SO_3/Al_2O_3=1) and chloride ratio ($2Cl/Al_2O_3$=0.5) showing phase development and its dependence on changing temperature.

Fig. 5.33 shows phase change for the initial composition containing: 0.01 moles C_3A, 0.015 moles portlandite, sulfate ratio (SO_3/Al_2O_3=1), carbonate ratio (CO_2/Al_2O_3=0.75) and chloride ratio $2Cl/Al_2O_3$=0.5 at various temperatures. CO_3-AFm substituted with chloride is stable up to ~50˚C. Above 50˚C all carbonate is predicted to form calcite. Friedel's salt persists up to 70˚C above which monosulfoaluminate forms (SO_4-AFm_{ss}). Fig. 5.34 shows phase change over a temperature range for the initial composition similar to those in Fig. 5.33 except that an input chloride content is higher ($2Cl/Al_2O_3$=1). Initial CO_3-AFm formation is supressed due to the high chloride content. Friedel's salt and ettringite persist up to ~90˚C.

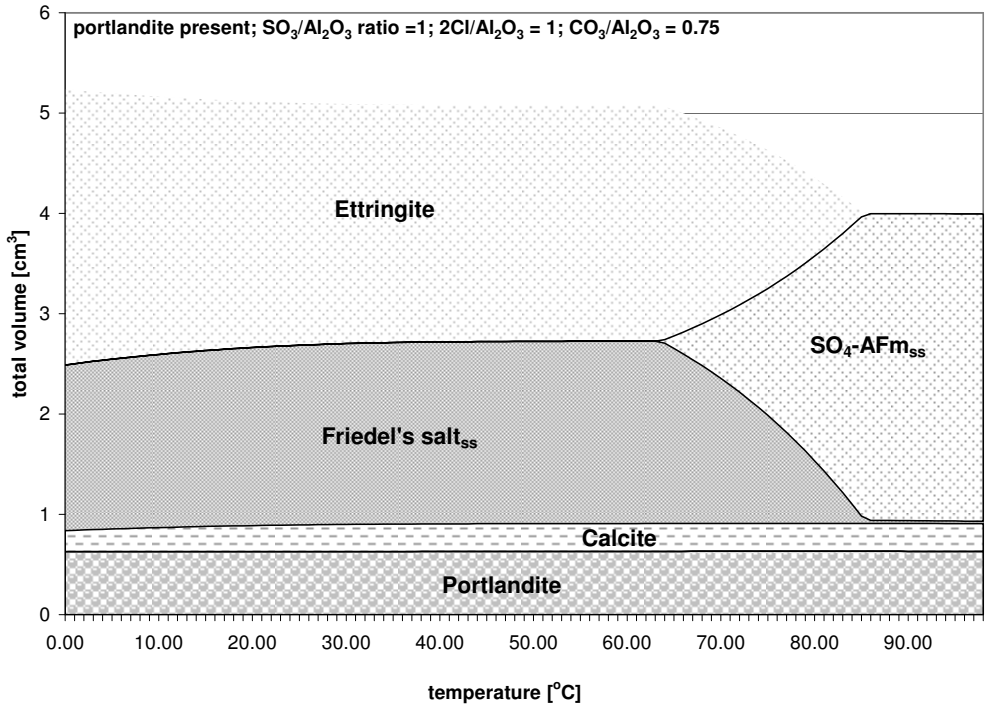

Figure 5.34: Total volume of solid phases of a hydrated model mixture initially consisting of 0.01 moles C_3A, 60 ml H_2O, 0.015 moles portlandite, 0.0075 moles $CaCO_3$ and with fixed initial sulfate ratio (SO_3/Al_2O_3=1) and chloride ratio ($2Cl/Al_2O_3$=1) showing phase development and its dependence on changing temperature.

5.6 Discussion

5.6.1 Structure of the phases: carbonate in Friedel's salt

Carbonate has ability to substitute for chloride in "Friedel's salt". Thus when Friedel's salt is reported it will not necessarily have its theoretical chloride content. Analysis of changes in the X-ray d-spacings of solid solution members enables us to predict the orientation of the carbonate group in Friedel's salt by analogy with the structures of other known AFm types. In hemicarboaluminate, the carbonate is oriented normal to the principal $(Ca_2Al(OH)_6)^+$ layers whereas in monocarboaluminate, it is co-planar [2]. Chloride behaves as a simple spherical ion, whereas carbonate is a trigonal planar group and, depending on carbonate orientation, the two possibilities differ in the effective molar volume of the anionic substituent and hence in their contribution to the basal spacing and density *e.g.,* the densities of hemi and monocarboaluminate are affected by

the orientation of the trigonal planar carbonate group. Carbonate is most efficiently packed in monocarboaluminate (basal spacing: d=7.5 Å), where it is sub-parallel to the principal layer spacing [173], hence its relatively high density, whereas in hemicarboaluminate (basal spacing: d=8.1 Å), carbonate is perpendicular to the principal layers [24]. In the case of Friedel's salt (spacing: d=7.8 Å) and associated monocarboaluminate solid solutions, we do not observe an increase in basal spacing value with increasing carbonate content we and therefore conclude that the carbonate group is essentially parallel or sub-parallel to the principal layer spacing.

5.6.2 Polymorphism of Friedel's salt

The polymorphism of Friedel's salt is possibly affected by solid solution with OH-AFm. The occurrence of Friedel's salt in M and R phases has been noted [13, 19, 78, 174]. The transformation temperature between M and R is possibly affected by solid solution, with R being stabilised to progressively lower temperatures by increasing substitution of Cl by OH, but the precise dependence of transformation temperature, or range of temperatures, on composition has not been studied.

5.6.3 Implication for solid solution formation

Experimental data recorded in the literature [8, 12] are often not directly comparable to those of the title study. This is partly because of the different restrains which were used. In [8, 12] species activities were controlled by weighted amounts of reactants whereas in the title study, buffer systems [56] were used to control the activities of selected species. For example, the carbonate activity was controlled by the solubility of solid calcite. Under these conditions, calcite and hemicarboaluminate are not compatible phases and hemicarboaluminate will not occur at equilibrium in calcium carbonate –saturated pastes. This situation approximates closely the situation in commercial pastes where the same carbonate buffers operate.

Another complication in the interpretation of data arises from the water state of AFm phases. It is known from the lime-alumina-water system that OH-AFm occurs in at least two discrete hydration states, with 13 and 19 H_2O, whereas Friedel's salt, the chloride AFm, seems to be stabilised in only one water state, 10 H_2O. Complete solid solution between Friedel's salt and OH-AFm, after allowing for partial substitution of OH by Cl,

could only occur between equivalent water states ("equivalent" allows for partial substitution of OH by Cl and *vice versa*). Thus where Friedel's salt type solid solution coexists with 19 H_2O AFm, as occurs in wet samples, difference in water states precludes complete solid solution. No definite evidence on the extent of solid solution between lower water states was obtained. Interpretations based on the limit of solid solution inferred from dried samples is suspect, as the lower water state encountered following drying at 35% RH is often an artefact induced by the drying process and cannot reliably be used to infer the hydration state in wet samples.

Friedel's salt formation is a potentially effective way of removing chloride from the pore fluid of a Portland cement. Tab. 5.1 shows that in the range of temperatures 5-25˚C, the minimum aqueous chloride concentration necessary to stabilise Friedel's salt is ~6 milimolar. This means that the ionic strength of the aqueous phase does not much differ from that of a model alkali-free cement and, on that account, the activity of water remains sufficiently high so that the water- rich (19 H_2O) variants of OH-AFm are likely to coexist with Friedel's salt type solid solution. Under these conditions, complete solid solution amongst OH and Cl-AFm will not occur.

5.6.4 Application to commercial Portland cement: binding capacity for chloride

Commercial Portland cement pastes generally start chloride-free: because they contain sulfate and/or carbonate, the initially-formed AFm phase is a SO_4-AFm type, with some sulfate replaced by OH at 25˚C [9], or CO_3-AFm, or mixtures. To estimate the capacity of cement to bind chloride, the contribution from Friedel's salt is limited by two factors: the maximum amount of Friedel's salt which can form and temperature, because Friedel's salt is destabilised with increasing temperature. At constant temperature, 25ºC, such that Friedel's salt is stable, the binding of chloride is still complex, as chloride must compete with other anions for binding sites in AFm. Moreover the role of C-S-H in Cl binding has to be assessed. To calculate the contribution of AFm to the binding potential, we must place restrictions on the calculations, nevertheless attempting to keep these as generic as possible. The first condition imposed is that the aqueous phase (cement pore fluid) pH is close to 12, as would occur if $Ca(OH)_2$ and/or high calcium C-S-H were present. The second condition is that the activity of sulfate and carbonate are fixed by the equilibration of pore fluid with ettringite, and with calcite, respectively.

These restrictions are realistic, and enable us to focus on the role of changing chloride concentration.

Where cement is in contact with water high in chloride, and once the AFm phase is saturated with chloride, the amount of Friedel's salt is maximised; no other chloride-binding phase appears until very high chloride concentrations, > 3M, such that oxychlorides become stable [40, 212]. Thus Tab. 5.1 should not be interpreted as implying that Friedel's salt can only coexist with the Cl molarity shown: it will also coexist to much higher concentrations: what is shown is the minimum critical chloride content necessary to stabilise the solids. However higher chloride concentrations may also destabilise other phases such as Kuzel's salt or monocarboaluminate and thereby increase the potential of the system to bind chloride.

Thus the diagrams presented here are *conditional*, implying that certain restrictions have been placed on their construction; these conditions have to be respected in order to make valid predictions. It will be appreciated that multi-component systems require more than two dimensions completely to show all features, hence the need for restrictions to generate accurate two-dimensional graphical representations. However the author has attempted to place reasonable sets of restrictions on constructions so as to preserve as many generic features as possible while, at the same time, depicting conditions likely to occur in Portland cements. A future modelling description should include additional factors *e.g.* chloride sorption on C-S-H and the influence of soluble alkalis on the distribution of chlorides.

The role of Friedel's salt in expansive processes has been discussed in the literature, often without conclusive results. From inspection of Fig. 5.19(a) the expansion is associated with enhanced ettringite formation as sulfate is displaced from AFm. Under conditions such that ettringite and Friedel's salt both increase in amount, significant increases in molar volume are predicted to occur. However the presence of reactive carbonate greatly reduces the change in molar volume in the course of Friedel's salt formation and hence lowers the potential for expansion (Fig. 5.21(a)). This is a possible positive argument for including carbonate in cement: to mitigate the expansive potential occurring with chloride ingress. The possibility of developing volume stable cements tailored for service in specific environments needs to be explored in more depth but

certainly simplistic association of particular phases as “expansive” or “non-expansive” should be avoided; what is important is the overall volume change associated with the redistribution of chemical substance in response to a flux-in this instance, of chloride.

Chloride-induced corrosion of steel is especially likely to occur at aqueous $[Cl^-]/[OH^-]$ ratios above 0.6 such that destruction of the passivating layer occurs [269]. Comparing data in Figs. 5.8(b) and 5.13(b), this threshold is achieved with less chloride substitution into the monocarboaluminate than in into hydroxy-AFm. This means that for the systems containing calcium carbonate and subject to chloride ingress, depassivation may occur more readily than for the carbonate-free compositions.

Tab. 5.8 shows the fraction of chloride per unit mass of cement substance from which it is apparent that the binding potential of C-S-H is not negligible, especially given that it is the most abundant paste constituent, but that idealised Friedel’s salt is still the most active chloride sorber on a mass basis.

Table 5.8: Fraction of chloride bound per g of phase.

Solid Phase	wt% Cl bound per gram of solid phase	Reference
$Ca_4Al_2(OH)_{13.8}(Cl)_{0.2}\cdot 4H_2O$	1.34	this work
$Ca_4Al_2(OH)_{12}(CO_3)_{0.95}(Cl)_{0.1}\cdot 5H_2O$	0.62	this work
$Ca_4Al_2(OH)_{12.05}(Cl)_{1.95}\cdot 4H_2O$	12.33	this work
$Ca_4Al_2(SO_4)_{0.5}(Cl)\ (OH)_{12}\cdot 6H_2O$	5.81	this work
0.68 C/S ratio C-S-H	0.6	[205]
1.91 C/S ratio C-S-H	1.5	[205]

6. Influence of calcium nitrate and nitrite on the constitution of cement hydrates

6.1 Nitrates and nitrites in cement

Portland cement is often modified by addition of water soluble or water dispersible chemicals, for example to protect embedded steel against corrosion [270-279]. Accelerating admixtures are added to concrete either to increase the rate of early strength development or to shorten the set time (*e.g.* to counteract low temperature conditions, which slow concrete hydration) [176, 280-283]. Inorganics used include soluble nitrates and nitrites. Nitrites are also used to inhibit corrosion of reinforcing steel in concrete. However the fate of nitrates and nitrites in cement and their impact on paste mineralogy is poorly quantified.

Concretes are usually formulated with an excess of water over that which is required to satisfy the chemical requirements for hydration. The chemical water demand, expressed as a weight ratio, water/cement (shorthand, w/c), is ~ 0.30 to 0.35. On the other hand, concretes are normally formulated to w/c ratios in the range 0.45 to 0.60. Water not combined into hydrates remains trapped in pores, termed “pore water”. But when normally soluble anions such as nitrate or nitrite are added to cement, they do not necessarily remain soluble in pore fluid. Firstly, the diminishing volume of free water as hydration proceeds, coupled with high pH and high ionic strength of the pore water, leads to “salting out” of many nominally soluble substances. But the ion uptake of cement substances also enables the solids to incorporate anions and thereby affect the stability of hydrates.

Several calcium nitroaluminates have been synthesized and reported in the literature [284-293]. According to [289, 290], $Ca_4Al_2(NO_3)_2{\cdot}10H_2O$ crystallizes in the trigonal space group P3*c*1 with a = 5.74 Å and c = 17.23 Å at ~ 20°C. Its crystal structure is typical for an AFm: it is built from positively charged layers $[Ca_2Al(OH)_6]^+$: the interlayer contents, water and nitrate ions, are reported to be strongly disordered [289]. Kuzel [284, 286] characterised a nitrate AFm with formula $Ca_4Al_2(NO_3)_2{\cdot}9.5\text{-}10\ H_2O$ and unit cell a = 5.74 Å and c = 17.24 Å. Ahmed et al. [259] reported a compound $Ca_4Al_2(NO_3)_2{\cdot}9H_2O$ with basal d-spacing 8.66 Å which agrees with the value 8.6 Å

given by Feitknecht for the same phase [294]. He also claimed that the numerical value of the layer thickness suggests that the NO_3^- groups lie with their planes perpendicular to $[Ca_2Al(OH)_6]^+$ layers. The thermal behaviour of nitrite AFm was investigated by Renaudin [289], Kuzel [284] and Ahmed [259], who indicated structural changes as a function of temperature. Renaudin, in the course of heating, distinguished an intermediate hydrate, $Ca_4Al_2(NO_3)_2(OH)_{12}\cdot 2H_2O$. Dumm et al. [285] created a schematic equilibrium phase diagram for the system $Ca(OH)_2$-Al_2O_3-$Ca(NO_3)_2$-H_2O for two temperatures, 25 and 85˚C, reporting various hydration states for the nitrate AFm. Rozenberg et al. [292] also investigated $Ca(OH)_2$-Al_2O_3-$Ca(NO_3)_2$-H_2O at temperatures, -10˚C and 20˚C, and reported different water states of nitrate AFm with basal spacing values varying from 8.0 to 10.5 Å.

Existence of nitrite AFm has been mentioned by Ramachandran [176]. Brown [295] reported synthesis of $3CaO\cdot Al_2O_3\cdot Ca(NO_2)_2\cdot xH_2O$, $3CaO\cdot Al_2O_3\cdot Ca(NO_3)_2\cdot xH_2O$ in their iron analogues $3CaO\cdot Fe_2O_3\cdot Ca(NO_2)_2\cdot xH_2O$, $3CaO\cdot Fe_2O_3\cdot Ca(NO_3)_2\cdot xH_2O$ with x varying stepwise from 10 to18 depending on relative humidity.

Using the so-called sucrose method, Pöllmann [27] prepared the nitrate AFt phase, $Ca_6Al_2O_6(NO_3)_6\cdot 32H_2O$. The synthesis of nitrite AFt has not been reported.

There is lack of quantitative characterization data regarding nitrate and nitrite cement hydrates in the literature and purpose of this chapter was to address this lack and model the distribution and retention of nitrate and nitrite in commercial cement pastes.

6.2 Synthesis of nitrite and nitrate AFm phases and their solid solutions with other AFm phases

Tricalcium aluminate, $3CaO\cdot Al_2O_3$, was made by heating together a 3:1 molar ratio of reagent grades of $CaCO_3$ and Al_2O_3 at 1400°C. The heating was done in Pt crucibles and continued, with intermediate grinding of the product, until X-ray powder diffraction revealed that the product was phase pure. $Ca_4Al_2(NO_3)_2(OH)_{12}\cdot xH_2O$ and $Ca_4Al_2(NO_2)_2(OH)_{12}\cdot xH_2O$ were synthesized by mixing C_3A and, respectively $Ca(NO_3)_2$ or $Ca(NO_2)_2$, in a 1:1 molar ratio. Additionally $Ca_4Al_2(NO_2)_2(OH)_{12}\cdot xH_2O$ was synthesized using: C_3A, CaO and analytical reagent purity sodium nitrite -$NaNO_2$ in a 1:1:1 molar ratio. All the samples were mixed with previously degassed double

distilled water (water/solid ratio ~10) at 23±2ºC subsequently stored with agitation in HDPE-bottles for 10 days until filtered at 23±2°C under nitrogen.

An attempt was made to prepare nitrate and nitrite AFm by mixing stochiometric amounts of CaO, $Ca(NO_3)_2$ or $Ca(NO_2)_2$ and gibbsite, $Al(OH)_3$, but the desired product was not obtained probably due to the low reactivity of gibbsite.

Attempts to prepare nitrate or nitrite AFt were not successful. Mixtures of the appropriate composition, starting from C_3A and either $(CaNO_3)_2$ or $(CaNO_2)_2$ and reacted at 5ºC, 25ºC, 55ºC and 85ºC instead formed respectively nitrate and nitrite AFm. Preparations made using the sucrose method, to enhance Ca solubility*, gave an X-ray amorphous solid product.

Solid solutions of nitrate AFm/nitrite AFm with other AFm phases were synthesized from initial supersaturation at 23±2˚C. Stoichiometric amounts of appropriate reactants (tricalcium aluminate, calcium nitrate, calcium nitrite, calcium sulfate, calcium oxide or calcium carbonate) were mixed and slurried in double distilled, CO_2-free water to a w/s ratio of ~10. The mixture was equilibrated with agitation for 3 months, then dried over saturated calcium chloride (35% RH) and analysed by XRD.

6.3 Characterisation of nitrate AFm

The water content of nitrate AFm $Ca_4Al_2(NO_3)_2(OH)_{12}\cdot xH_2O$, was found to be very sensitive to moisture conditions. Samples were examined in three different environments:~100% relative humidity (wet sample covered with Mylar foil to prevent water evaporation and atmospheric carbonation), 35% relative humidity (dried in a desiccator over saturated $CaCl_2$ at room temperature) and air dried at 85˚C. As can be seen from Fig. 6.1, the basal d spacing decreases from 10.49 Å for the wet sample, to 8.64 Å for 35% RH and to 8.60 Å for the sample dried at 85˚C. This is in agreement with data published in [285, 289].

** Ca ion concentration is increased by adding sugar because of the complex formation between sucrose and calcium*

Dumm found a basal spacing of 10.43 Å for a wet sample, $Ca_4Al_2(NO_3)_2(OH)_{12}\cdot 10H_2O$, but 8.64 Å for the "dry" sample, $Ca_4Al_2(NO_3)_2(OH)_{12}\cdot 4H_2O$, and 8.78 Å for the higher water variant, $Ca_4Al_2(NO_3)_2(OH)_{12}\cdot 6H_2O$; Renaudin gave data on the dry phase- $Ca_4Al_2(NO_3)_2(OH)_{12}\cdot 4H_2O$ - with a basal spacing of 8.61 Å.

In the course of drying, significant peak shift towards greater angles is observed. The first XRD peak, for the wet nitrate AFm - $Ca_4Al_2(NO_3)_2(OH)_{12}\cdot 10H_2O$ - appears at $2\Theta \sim 8.41^\circ$ but at 10.15° for the sample dried at 35% RH, $Ca_4Al_2(NO_3)_2(OH)_{12}\cdot 4H_2O$, and at 10.20° after air drying at 85°C, broadly in agreement with the literature [285-291]. Samples dried in 35% RH for 72 h gave peaks of basal spacing 8.77 Å, while the samples stored under the same conditions for 3 months resulted in a smaller basal spacing, 8.64 Å. Changes in basal spacing values are therefore explained mainly by differing water contents. Due to incomplete drying at 35% RH, nitrate AFm preparations often consisted of mixtures of different water states giving closely-spaced peaks at 8.77 Å and 8.64 Å. Dry nitrate AFm readily adsorbs water from the atmosphere. The sample dried in 85°C (basal spacing 8.60 Å) was found to re-equilibrate to the 8.64 Å state, after 1 day exposure to 35% RH. Thus at least some stages of dehydration and rehydration are approximately reversible [284, 289].

Unit cell parameters were refined from the powder diffraction patterns (29 reflections) using CELREF 2 software: $Ca_4Al_2(OH)_{12}(NO_3)_2\cdot 4H_2O$ cell dimensions for the trigonal space group P3*c*1 are a = 5.7434 Å, c = 17.241 Å. The calculated unit cell volume is 492.52 $Å^3$ and the density, 2071 kg/m^3. The morphology of the product consists of clusters of platelets (Fig. 6.7(a)).

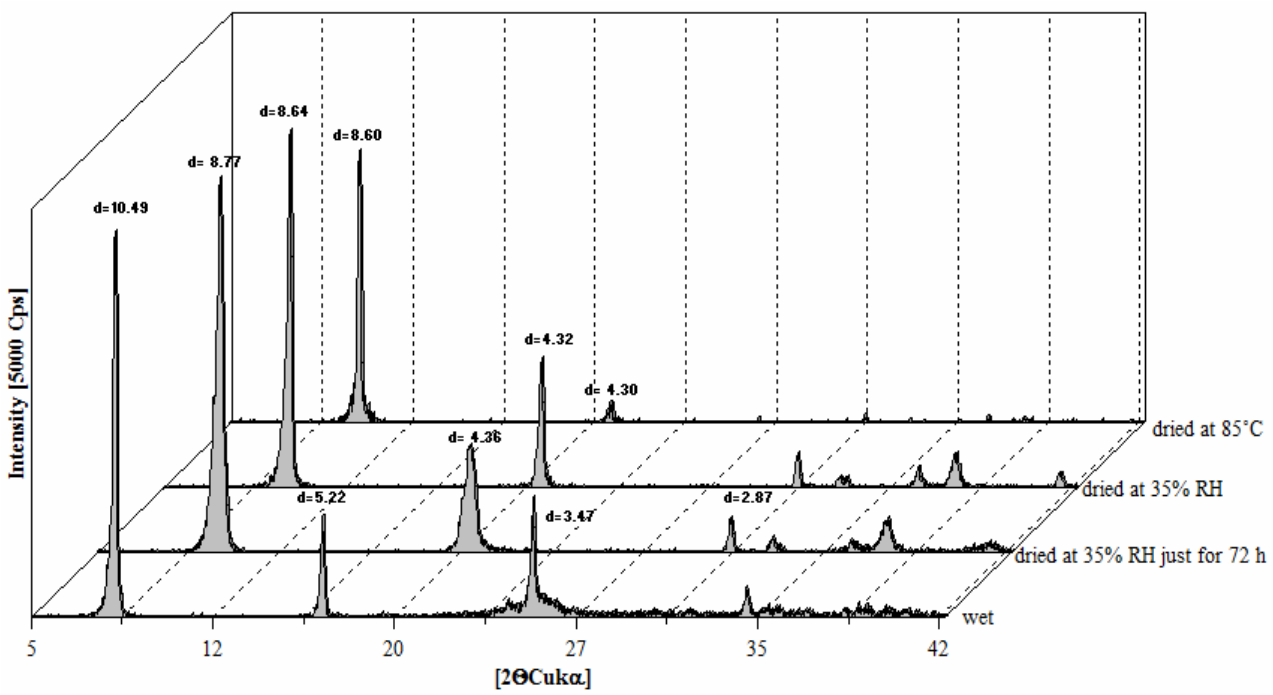

Figure 6.1: XRD powder patterns of nitrate AFm phases at different moisture conditions.

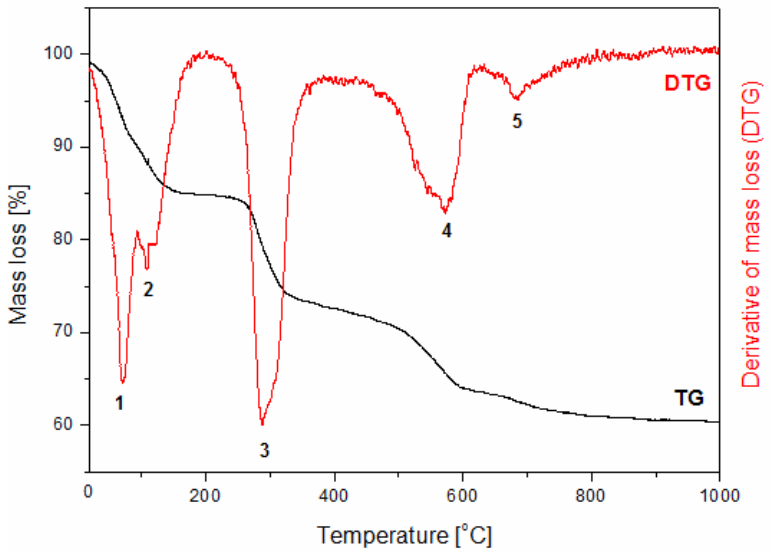

Temp (°C)	cumulative % mass loss
80	4.74
160	11.12
310	22.45
550	31.87
700	39.58
1000	41.84

Figure 6.2: TG/DTG characteristics of nitrate AFm. Values of the mass losses were determined from the TG curve by the points of deviation for the tangent lines of weight loss slope versus temperature. The initial sample had been dried at room temperature and 35% RH. See text for assignment of features.

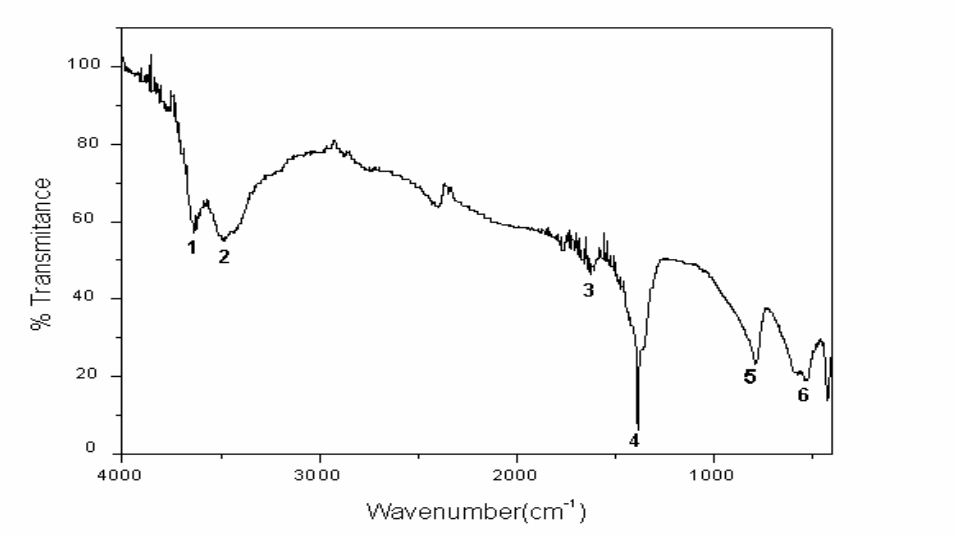

Figure 6.3: FTIR pattern of nitrate AFm dried at 35% RH.

Table 6.1: FTIR identification of the nitrate AFm.

Peak number	Wavenumber (cm^{-1})	Assignment (see Fig. 6. 3) [261, 306, 307]
1	3637	O-H group (asymmetric stretching)
2	3488	O-H group (asymmetric stretching)
3	1630	O-H group (H-O-H bending)
4	1384	N-O (asymmetric stretching)
5	788	Al-O; O-N-O (bending)
6	528	Al-O; O-N-O (bending)

Renaudin [289] reported that the dry nitrate AFm, at room temperature exposed to air contains $4H_2O$ so its formula can be expressed as $Ca_4Al_2(NO_3)_2(OH)_{12}\cdot 4H_2O$ (formula weight: 614.41 g/mol). All the molecular water is lost in two stages upon heating below 160˚C (losses 1 and 2, Fig. 6.2). This should theoretically correspond to a weight loss of 11.7%. In this thesis, measured cumulative weight loss to 160˚C was 11.12%, corresponding to 3.80 H_2O and close to the expected $4H_2O$. The first two water molecules removed result in formation of $Ca_4Al_2(NO_3)_2(OH)_{12}\cdot 2H_2O$, as reported by Renaudin [289].

According to Renaudin's [289] thermal studies on nitrate AFm, peaks 3, 4 and 5 (Fig. 6.2) correspond to dehydroxylation and nitrate reduction (peak 3), decomposition of nitrite and hydroxyl groups (peaks 4, 5). At around 540-560˚C, nitrite decomposition

overlaps with dehydroxylation of the OH groups. Total weight loss at 1300˚C reported by Renaudin, was 46.9%, resulting in the final solid product $Ca_4Al_2O_7$. In the title study measurement was carried up to 1000˚C and the final mass loss found to be 41.84%. However the final solid products of decomposition were found to be mayenite (ideally $Ca_{12}Al_{14}O_{33}$) and lime (CaO).

FTIR examination was carried in the mid-infra red range 4000-400 cm^{-1} (Fig. 6.3, Tab. 6.1). A characteristic sharp nitrate absorption, shown as #4 in Fig. 6.3, appeared at 1384 cm^{-1}.

Nitrate AFm dissolves incongruently. In all samples hydrogarnet (katoite) occurred as a solid product of dissolution. Solubility data are presented in Tab. 6.2 and solubility products (K_{so}) of nitrate AFm were calculated according to dissolution reaction defined by Eq. 6.1.

$$Ca_4Al_2(OH)_{12}(NO_3)_2\cdot 4H_2O = 4\ Ca^{2+} + 2\ AlO_2^- + 2\ NO_3^- + 4OH^- + 8H_2O \qquad \textit{Eq. 6.1}$$

Table 6.2: Solubility data for nitrate AFm-$Ca_4Al_2(OH)_{12}(NO_3)_2{\cdot}4H_2O$.

Temp [˚C]	Ca [mmol/l]	Al [mmol/l]	NO_3 [mmol/l]	logK_{so}	pH measured	Equilibium pH calc. by GEMS	Age-months	Phases present after dissolution
5	7.33	2.45	2.97	-28.47	12.65*	12.63	1	N, HG
5	7.11	2.35	2.33	-28.70	12.65*	12.65	3	n.d.
5	7.05	2.26	2.16	-28.79	12.63*	12.65	6	N, HG
5	7.09	2.25	2.16	-28.69	12.65*	12.66	8	n.d.
5	7.04	2.26	2.14	-28.80	12.66*	12.65	12	N.HG
25	8.81	2.87	3.80	-27.77	12.13	11.95	1	N, HG
25	7.05	3.24	3.90	-28.63	12.06	11.76	3	n.d.
25	6.95	3.17	3.96	-28.70	11.99	11.75	6	N, HG
25	7.03	2.45	4.44	-28.71	11.94	11.78	8	n.d.
25	*7.06*	*2.56*	*4.11*	*-28.67*	*11.99*	*11.79*	*12*	*N, HG*
55	17.80	2.58	26.74	-26.79	10.99*	10.76	1	N, HG
55	19.95	2.50	31.56	-26.70	10.98*	10.70	3	n.d.
55	20.02	2.58	32.00	-26.78	10.98*	10.69	6	N, HG
55	19.35	2.70	32.15	-26.87	10.95*	10.66	8	n.d.
55	20.35	2.70	31.40	-26.43	11.02*	10.77	12	N, HG
85	26.63	0.40	63.84	n.d.	10.4*	n.d.	1	N(decomp.), HG
85	36.76	3.60	76.78	n.d.	10.33*	n.d.	3	n.d.
85	35.17	3.66	71.12	n.d.	10.23*	n.d.	6	N(decomp.), HG
85	35.12	3.88	77.60	n.d.	10.20*	n.d.	8	n.d.
85	40.12	3.67	80.22	n.d.	10.27*	n.d.	12	N(decomp.),HG

** measured at 25˚C and corrected by calculation to measurement temperature (see 3.2.3). Abbreviations: N-nitrate AFm; HG- hydrogarnet; n.d-not determined. Italicised value from 12 month equilibration was used as an input in Table 6.16.*

6.4 Characterisation of nitrite AFm

Ramachandran [176] reported that nitrite AFm is formed by the action of calcium nitrite with the Al_2O_3-bearing phases of cement and that it may also crystallize by the action of aqueous sodium nitrite on C_3A in the presence of calcium hydroxide. Brown [295] synthesized nitrite AFm using stoichiometric amounts of C_3A, $Ca(NO_2)_2$ or $NaNO_2$ + $Ca(OH)_2$ and excess of water (water/solid ratio ~10) and reported various water states for the nitrite AFm. However no characterisation data were presented. In this study, two sets of synthesis were made: one using commercial calcium nitrate, nominally $Ca(NO_2)_2$, and the other using analytical reagent purity sodium nitrite - $NaNO_2$. Commercial calcium nitrite was found to be contaminated with calcium nitrate with the result that most of the preparations contained X-ray reflections attributed to both NO_2–AFm and NO_3–AFm: Fig. 6.4 shows the sample dried at 35% RH-prepared from ''$Ca(NO_2)_2$''. Apparently solid solution of nitrate in nitrite AFm is slight.

Nitrite AFm, $Ca_4Al_2(NO_2)_2(OH)_{12}\cdot xH_2O$, made from nitrate-free precursors was examined by XRD, thermal analysis, FTIR and SEM. Unlike nitrate AFm, the water state of NO_2-AFm seems to be relatively independent of moisture conditions. Nitrite AFm gave a main peak with basal spacing d=7.91 Å, corresponding to 2 theta: 11.23˚ (Cu K_α radiation) for the wet sample and 11.04˚ following drying at 35% RH (Fig. 6.4). The sample dried in more aggressive conditions, in air at 85˚C, gave a decreased d spacing (basal spacing d=7.85 Å). This sample also yielded much broader reflections which possibly indicates changed water content and, disorder and/or small crystallite size.

All nitrite AFm preparations had a pale yellowish colour similar to those of calcium or sodium nitrite.

Unit cell parameters were refined from the powder diffraction patterns (23 reflections) using CELREF 2 software. $Ca_4Al_2(OH)_{12}(NO_2)_2\cdot 4H_2O$ cell dimensions were determined assuming a trigonal space group R3*c* giving a = 5.7498 Å, c = 15.9306 Å: the calculated unit cell volume and density are 456.10 $Å^3$ and 2120 kg/m^3 respectively. The SEM image, Fig. 6.7(b), shows the typical AFm plate morphology of nitrite AFm. The crystals are, however, notably warped and have irregular leaf-like edges.

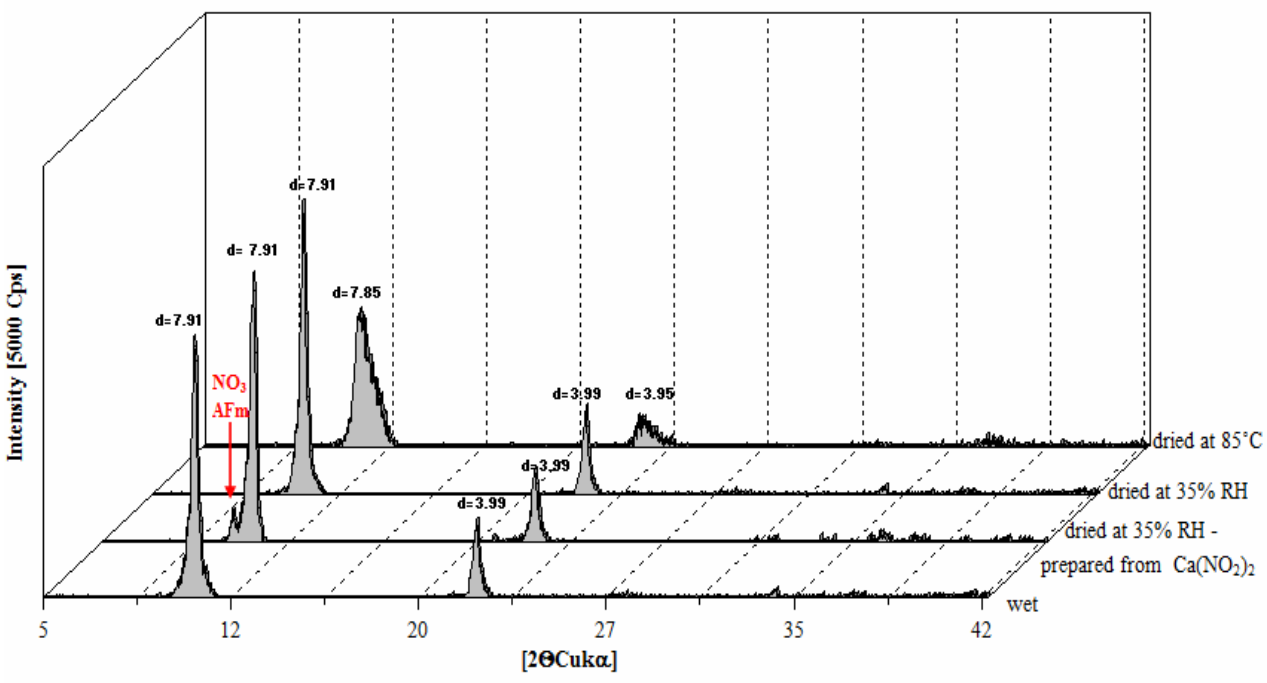

Figure 6.4: XRD powder patterns of nitrite AFm phases at different moisture conditions; note NO3-AFm impurity for the sample prepared from commercial Ca(NO2)2.

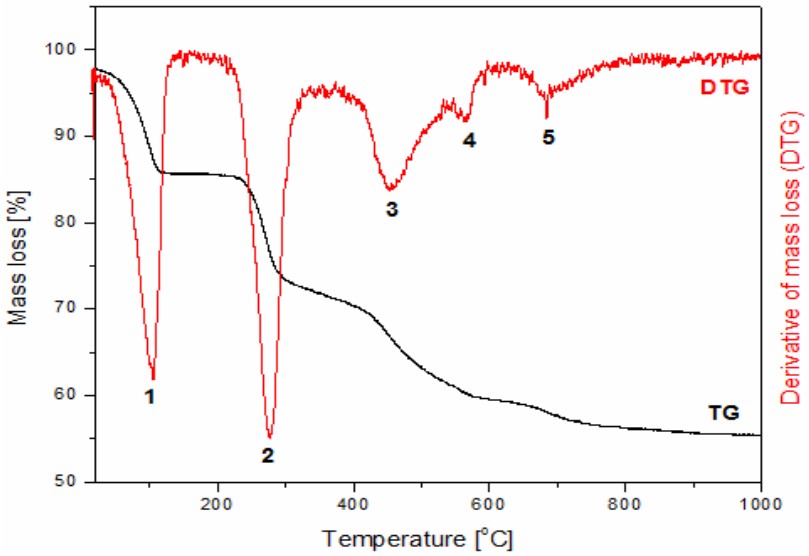

Temp (°C)	cumulative % mass loss
160	11.87
310	24.78
550	35.58
700	38.15
1000	41.42

Figure 6.5: TG/DTG characteristics of nitrite AFm. Values of the mass losses were determined from the TG curve by the points of deviation for the tangent lines of weight loss slope versus temperature. The initial sample was dried at 35% RH. See text for assignment of features.

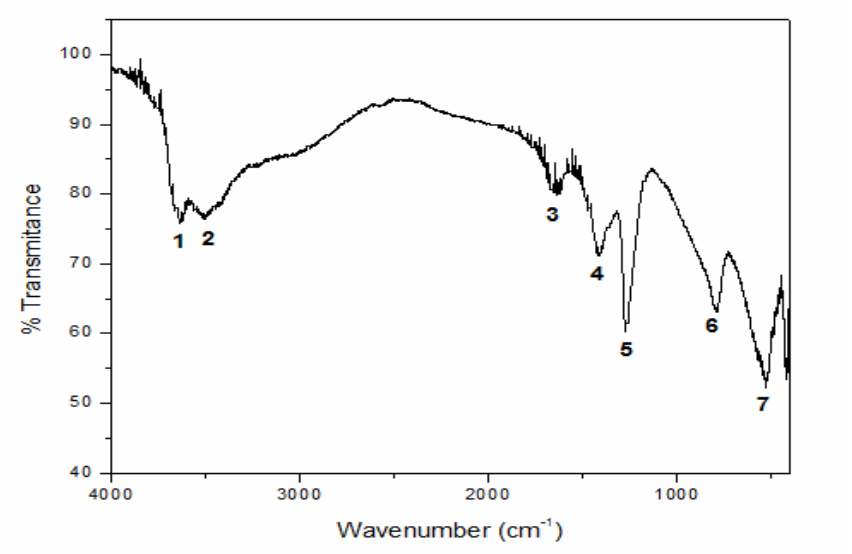

Figure 6.6: FTIR pattern of nitrite AFm dried at 35% RH.

Table 6.3: FTIR identification of the nitrite AFm.

Peak number	Wavenumber (cm^{-1})	Assignment (see Fig. 6.6) [261, 306, 307]
1	3639	O-H group (asymmetric stretching)
2	3514	O-H group (asymmetric stretching)
3	1730	O-H group (H-O-H bending)
4	1412	N-O symmetric stretching
5	1269	N-O asymmetric stretching
6	794	Al-O; O-N-O (bending)
7	527	Al-O; O-N-O (bending)

To calculate the water content of nitrite AFm, it was assumed that it contains initially 4 molecular water per formula *i.e.*, it is $Ca_4Al_2(NO_2)_2(OH)_{12}\cdot 4H_2O$ (formula weight: 582.41 g/mol). All the molecular water is lost below 160˚C (peak 1, Fig. 6.5). This should theoretically correspond to a weight loss of 12.36%; the measured loss at 160˚C was 11.96%, corresponding to 3.87 H_2O molecules. Unlike nitrate AFm, water molecules were lost in one step. Peaks 2-5 are ascribed to decomposition of hydroxyl and nitrite groups. Total weight loss at 1000˚C was 41.32%. At around 540-560˚C nitrite decomposition overlaps with loss of water from structural OH groups.

FTIR examination of $Ca_4Al_2(NO_2)_2(OH)_{12}\cdot 4H_2O$ was carried in the mid- infra red range 4000-400 cm^{-1} (Fig. 6.6, Tab. 6.3). Characteristic nitrite symmetric and asymmetric stretching vibrations appeared at 1269 and 1412 cm^{-1} respectively.

Solubility products (K_{so}) of nitrite AFm were calculated according to the dissolution reaction presented in Eq. 6.2.

$$Ca_4Al_2(OH)_{12}(NO_2)_2\cdot 4H_2O = 4\ Ca^{2+} + 2\ AlO_2^- + 2\ NO_2^- + 4OH^- + 8H_2O \qquad Eq.6.2$$

Nitrite AFm dissolves incongruently (Tab. 6.4). Hydrogarnet was found in trace amounts except at 85˚C, where it was abundant. Initially it was not known if hydrogarnet traces arose from the incongruent dissolution of NO_2-AFm or from the dissolution of the NO_3-AFm which was contaminating the nitrite AFm (as found on Fig. 6.4-sample dried at 35% RH and prepared from commercial $Ca(NO_2)_2$). Therefore solubility measurements were repeated on 'phase pure' nitrite AFm (prepared from: CaO, C_3A and analytical purity $NaNO_2$). Tab. 6.5 presents these solubility data which are the more appropriate to include in thermodynamic compilations because the preparation is not contaminated by nitrate. To remove sodium before equilibration, solids were flushed 5 times with small portions of double distilled water and the Na content subsequently checked by analysis. Measured sodium content was reduced to ~0.02 mmol/l and was assumed to have a negligible impact on solubility. No evidence of oxidation of nitrite ions to nitrate ions was found. This observation is in agreement with the literature [296, 297].

Table 6.4: Solubility data for nitrite AFm-$Ca_4Al_2(OH)_{12}(NO_2)_2 \cdot 4H_2O$, prepared from commercial $Ca(NO_2)_2$.

Temp. [˚C]	Ca [mmol/l]	Al [mmol/l]	NO_2 [mmol/l]	logKso	pH measured	Equilibrium pH calc. by GEMS	NO_3 Contami-nation in solution [mmol/l]	Age-months	Phases present after dissolution
5	9.50	2.95	11.07	-27.92	12.42*	12.35	0.58	1	Ni, HG(traces)
5	9.90	2.86	10.86	-27.58	12.48*	12.44	0.50	3	n.d.
5	10.11	3.01	9.19	-27.19	12.49*	12.56	0.36	6	Ni, HG(traces)
5	10.07	2.33	8.75	-27.25	12.51*	12.61	0.44	8	n.d.
5	9.81	2.69	10.01	-27.49	12.43*	12.50	0.47	12	Ni, HG(traces)
25	11.43	3.83	9.93	-26.71	11.89	11.86	0.43	1	Ni, HG(traces)
25	11.56	3.79	9.98	-26.66	11.92	11.87	0.68	3	n.d.
25	11.42	3.58	10.17	-26.75	11.99	11.86	0.58	6	Ni, HG(traces)
25	11.15	3.33	11.01	-26.99	11.90	11.80	0.62	8	n.d.
25	11.53	2.89	11.58	-26.87	12	11.85	0.46	12	Ni, HG(traces)
55	25.35	2.45	35.55	-25.18	11.10*	11.04	0.58	1	Ni, HG
55	30.77	2.30	49.01	-25.18	11.03*	10.92	0.55	3	n.d.
55	32.38	2.21	52.40	-25.14	11.01*	10.91	0.43	6	Ni, HG
55	33.41	2.20	54.65	-25.12	11.00*	10.90	0.59	8	n.d.
55	33.52	2.16	54.55	-25.08	11.03*	10.92	0.49	12	Ni, HG
85	29.28	1.59	57.83	n.d.	10.25*	n.d.	0.51	1	Ni(decomp.), HG
85	33.18	1.89	61.22	n.d.	10.26*	n.d.	0.49	3	n.d.
85	37.14	2.01	68.99	n.d.	10.25*	n.d.	0.69	6	Ni(decomp.); HG
85	41.22	2.12	72.13	n.d.	10.23*	n.d.	0.63	8	n.d.
85	42.32	2.45	74.32	n.d.	10.20*	n.d.	0.52.	12	Ni(decomp.), HG

** measured at 25˚C and corrected by calculation to measurement temperature (see 3.2.3). Abbreviations: Ni-nitrite AFm; HG- hydrogarnet; n.d-not determined.*

Table 6.5: Solubility data for nitrite AFm-$Ca_4Al_2(OH)_{12}(NO_2)_2 \cdot 4H_2O$, prepared from the analytical purity $NaNO_2$.

Temp. [˚C]	Ca [mmol/l]	Al [mmol/l]	NO_2 [mmol/l]	logKso	pH measured	Equilibrium pH calc. by GEMS	Age-months	Phases present after dissolution
5	10.05	2.05	8.45	-27.30	12.52*	12.64	1	Ni
5	9.90	2.06	8.59	-27.38	12.58*	12.62	3	n.d.
5	10.31	2.99	8.79	-27.14	12.53*	12.59	12	Ni, HG(traces)
25	12.10	2.02	9.34	-26.66	11.94	12.01	1	Ni
25	12.16	2.89	9.25	-26.48	11.96	11.98	3	n.d.
25	*12.93*	*2.87*	*9.93*	*-26.24*	*12*	*12.01*	*12*	*Ni, HG(traces)*
55	28.18	1.19	47.83	-26.38	10.99*	10.79	1	Ni , HG
55	30.49	1.47	49.01	-25.53	10.98*	10.94	3	n.d.
55	30.15	1.56	51.33	-26.03	10.96*	10.78	12	Ni , HG
85	39.80	2.13	67.98	n.d.	10.20*	n.d.	1	Ni(decomp.), HG
85	42.17	1.49	76.87	n.d.	10.11*	n.d.	3	n.d.
85	45.76	2.09	79.80	n.d.	10.26*	n.d.	12	Ni(decomp.), HG

** measured at 25˚C and corrected by calculation to measurement temperature (see 3.2.3) Abbreviations: Ni-nitrite AFm; HG- hydrogarnet; n.d-not determined. Italicised value from 12 month equilibration, was used as an input in Table 6.16.*

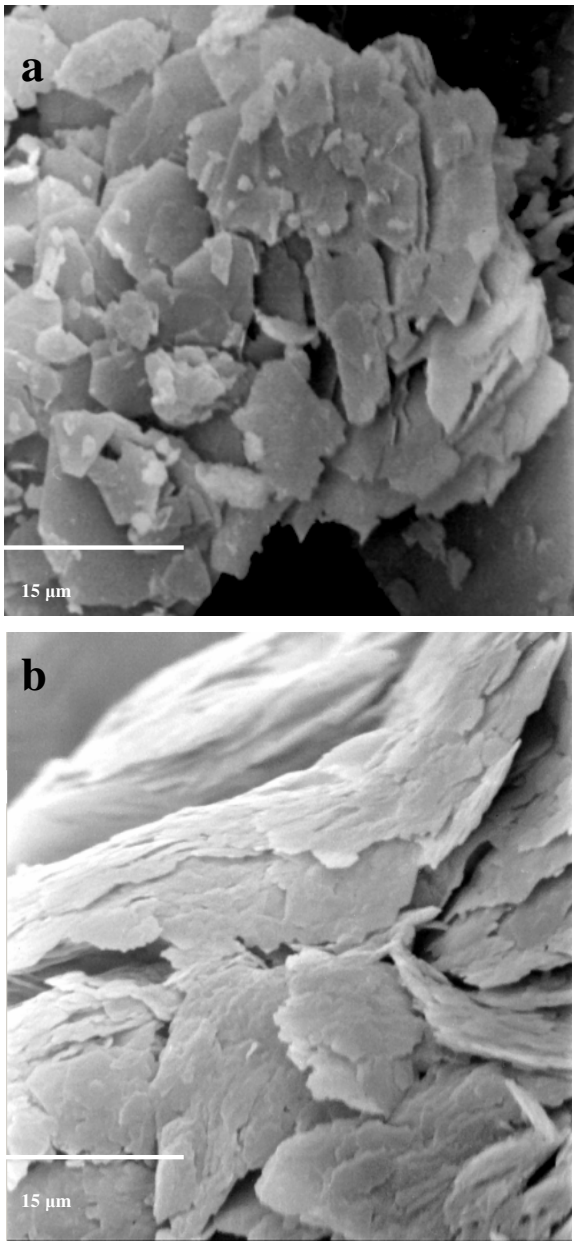

Figure 6.7: SEM micrographs of the nitrate (a) and nitrite (b) AFm phases.

6.5 AFm solid solutions

6.5.1 Nitrate AFm and hydroxy AFm

To investigate whether solid solutions are formed, a series of solids were analysed by XRD after drying over saturated calcium chloride (35% RH, room temperature) (Fig. 6.8(a.b)). The purpose of drying was to avoid carbonation. Solid solution formation between nitrate AFm (basal spacing d=8.64 Å) and hydroxy AFm (basal spacing d=7.99 Å) was investigated in the range 0-1 OH/(NO_3+OH). Solid solution was found in a range of compositions around 0-0.5 OH/(NO_3+OH) meaning that up to 50% of nitrate in NO_3-AFm can be substituted by OH. With increasing OH substitution the basal spacing of nitrate AFm decreased, from d=8.64 Å for pure $Ca_4Al_2(OH)_{12}(NO_3)_2 \cdot 4H_2O$ to d= 8.46 Å for $Ca_4Al_2(OH)_{13}NO_3 \cdot 4H_2O$. Above ratio 0.5 OH/($NO_3$+OH) a miscibility gap occurred and two separate sets of X-ray reflections were found, one for nitrate AFm, another for hydroxy AFm (itself probably slightly substituted by NO_3^- ions).
Dry (NO_3, OH) AFm solid solution members were redispersed in double distilled water and equilibrated at 25˚C for 180 days. All the samples were periodically agitated. Aqueous solution compositions, measured after equilibration commencing from undersaturation, are presented in Tab. 6.6. Experimental calcium, aluminium and nitrate concentrations are plotted on Fig. 6.9(a,b).

Guggenheim parameters used in the case of non-ideal binary solid solutions were derived (see section 2.4). To enable calculation slight solid solution (3%) of nitrate AFm in hydroxy AFm was permitted. Assuming compositional boundaries of the miscibility region 0.03-0.5 OH/(NO_3+OH) and applying MBSSAS software, the resulting Guggenheim parameters equalled: a_0=0.188 and a_1=2.49. Using the previously derived parameters a_0 and a_1, it was possible to determine the changes of the Gibbs energies of mixing. Fig. 6.10 compares the functions of the Gibbs energy of ideal mixing, ΔG_{id}, the estimated excess Gibbs energy of mixing ΔG_{ex} and the resulting estimated Gibbs energy of mixing ΔG_M of the nitrate AFm (NO_3-AFm)-hydroxy AFm (OH-AFm) solid solution series, according to Eqns. 2.11-2.16. The molar Gibbs energy of the solid solution can be calculated according to Eq. 2.11 as the sum of the partial Gibbs energies of nitrate AFm, hydroxy AFm and ΔG_M.

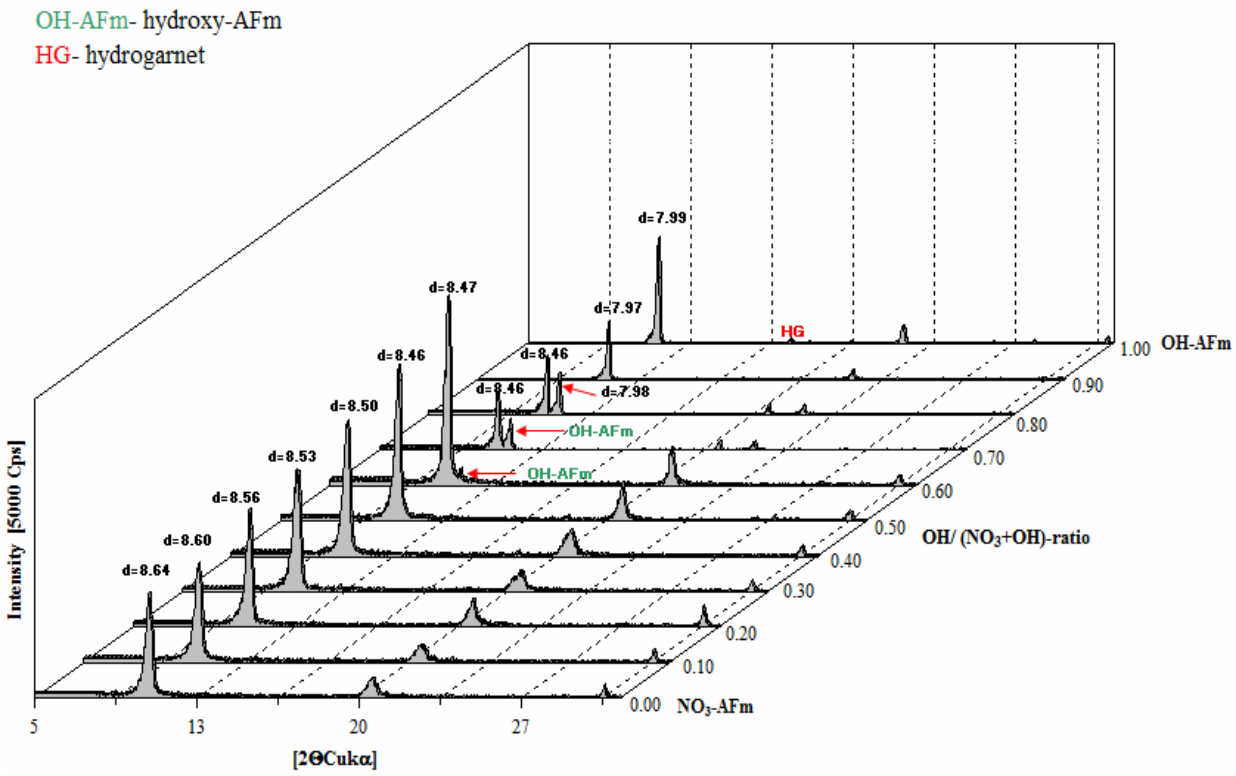

Figure 6.8(a): Partial XRD patterns of the solid solution formation at 25˚C between nitrate AFm and hydroxy AFm. Reflections marked as HG are attributed to hydrogarnet.

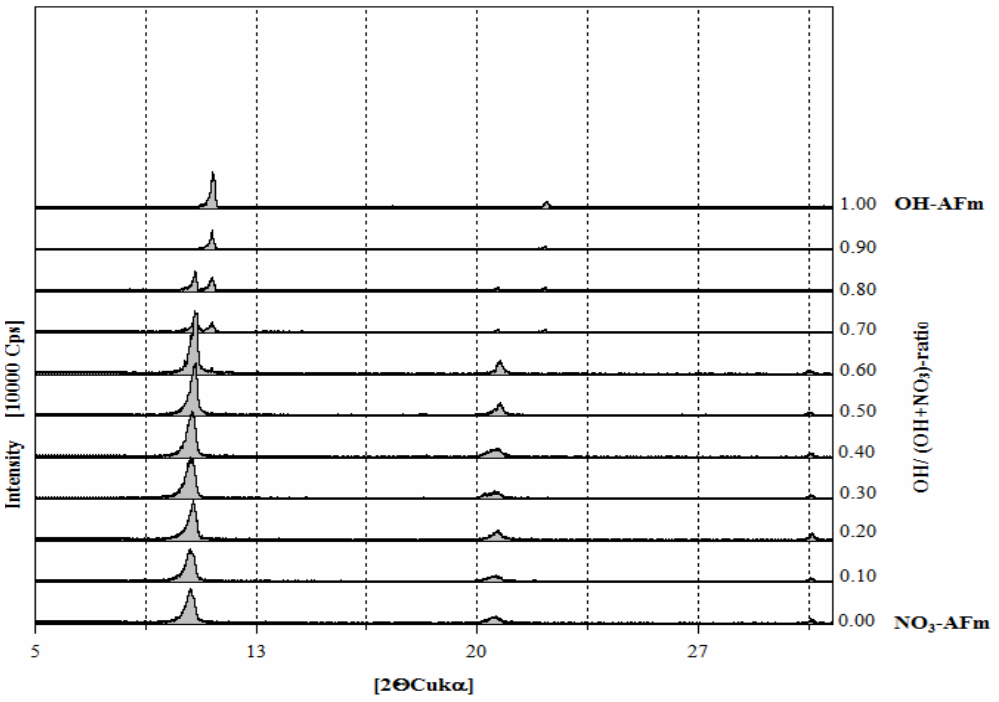

Figure 6.8(b): Partial XRD patterns of the solid solution formation at 25˚C between nitrate AFm and hydroxy AFm.

Table 6.6: Aqueous solution compositions measured from undersaturation for samples between the hydroxy AFm (NO_3/Al=0) and the nitrate AFm (NO_3/Al=1) at 25±2ºC and after 180 days of equilibration.

Calculated NO_3/Al- ratio (total system)	Ca [mmol/l] (aq)	Al [mmol/l] (aq)	NO_3 [mmol/l] (aq)	pH	Solid phase at end of experiment
0.00	17.63	0.21	0.00	12.49	OH-AFm, HG, CH
0.10	12.25	0.14	0.49	12.24	n.d.
0.20	10.05	0.18	0.85	12.23	N_{ss}, HG, $CH_{(traces)}$, Hc
0.30	9.55	0.48	0.93	12.10	n.d.
0.40	8.35	0.22	1.59	12.09	n.d
0.50	8.28	1.79	1.46	12.08	N_{ss}
0.60	7.49	2.39	2.37	12.05	n.d.
0.70	7.25	3.25	2.72	12.03	$N_{ss,}$ $HG_{(traces)}$
0.80	7.00	3.48	3.23	11.99	n.d.
0.90	6.99	3.49	3.69	11.98	N_{ss}, HG
1.00	6.95	3.17	3.96	11.99	N ,HG

Abbreviations: N=NO_3-AFm (nitrate AFm), N_{ss}=solid solution between NO_3-AFm and OH-AFm, CH=portlandite, HG=hydrogarnet (katoite), Hc=hemicarboaluminate, n.d.=not determined

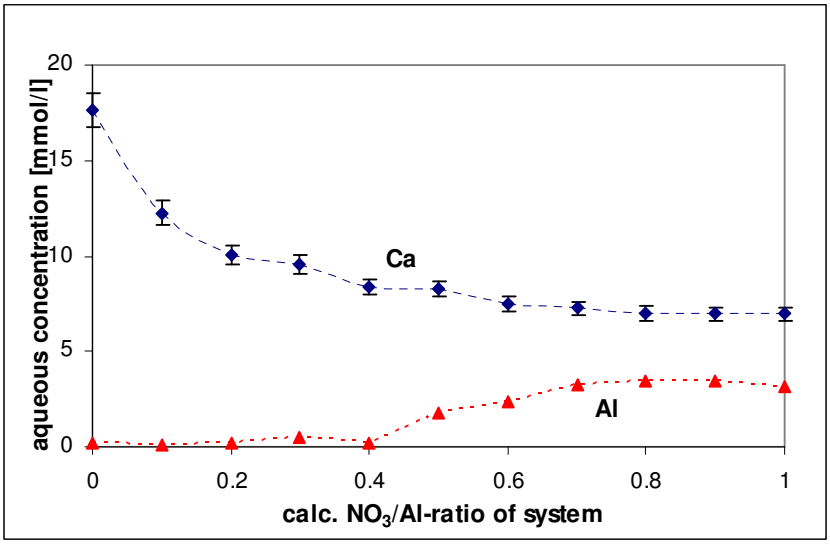

Figure 6.9(a): Equilibrium calcium and aluminium aqueous concentrations commencing from undersaturation for samples between hydroxy AFm (NO_3/Al=0)– nitrate AFm (NO_3/Al=1) at 25±2°C after 180 days of equilibration. Error bars are shown for Ca.

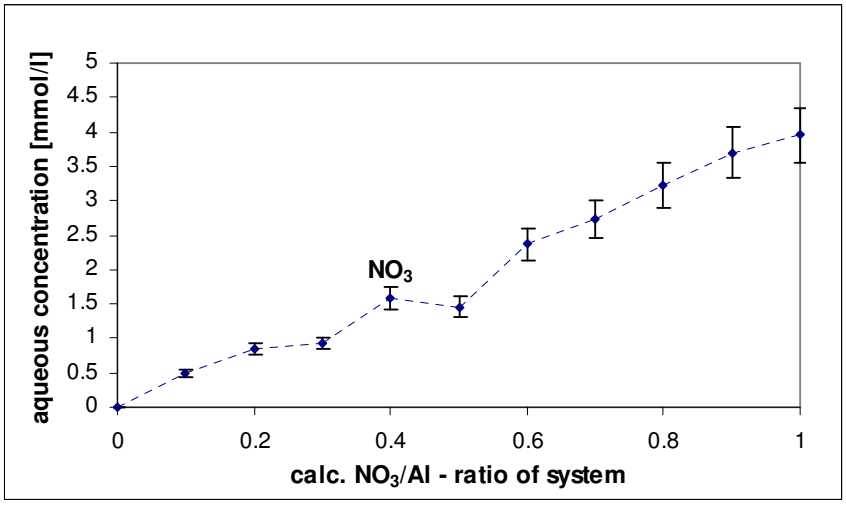

Figure 6.9(b): Equilibrium nitrate aqueous concentrations commencing from undersaturation for samples between hydroxy AFm (NO_3/Al=0) – nitrate AFm (NO_3/Al=1) at 25±2°C and after 180 days of equilibration.

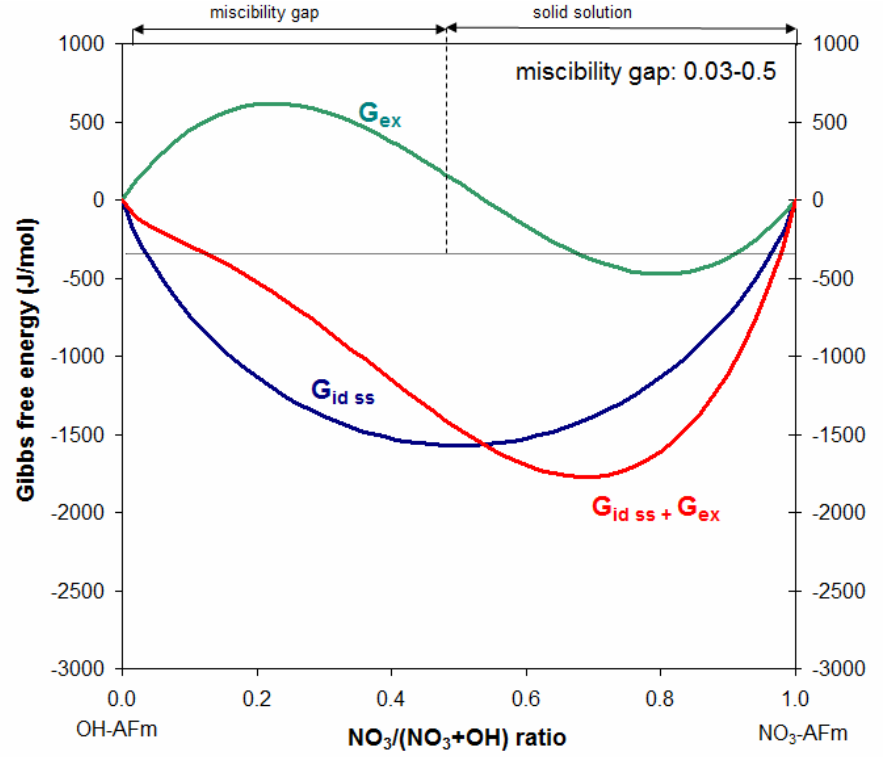

Figure 6.10: Gibbs energy of ideal mixing, ΔGid, excess Gibbs energy of mixing, ΔGex, and resulting molar Gibbs energy of mixing, ΔGM, calculated for the nitrate AFm (NO_3-AFm)-hydroxy AFm (OH-AFm) solid solution series assuming Guggenheim parameters a_0=0.188 and a_1=2.49 for miscibility gap fractions $0.03 \leq x \leq 0.5$.

6.5.2 Nitrate AFm and monosulfoaluminate

No solid solution was found between monosulfoaluminate and nitrate AFm. Two separate sets of XRD peaks were observed through all range of compositions, Fig. 6.11(a,b). The samples were redispersed in double distilled water and periodically agitated. Aqueous solution compositions, measured after equilibration commencing from undersaturation, are presented in Tab. 6.7. Calcium, aluminium and nitrate concentrations are plotted on Fig. 6.12(a,b). Sulfate concentrations were below detection limit: < 0.5 ppm (see section 3.2.1).

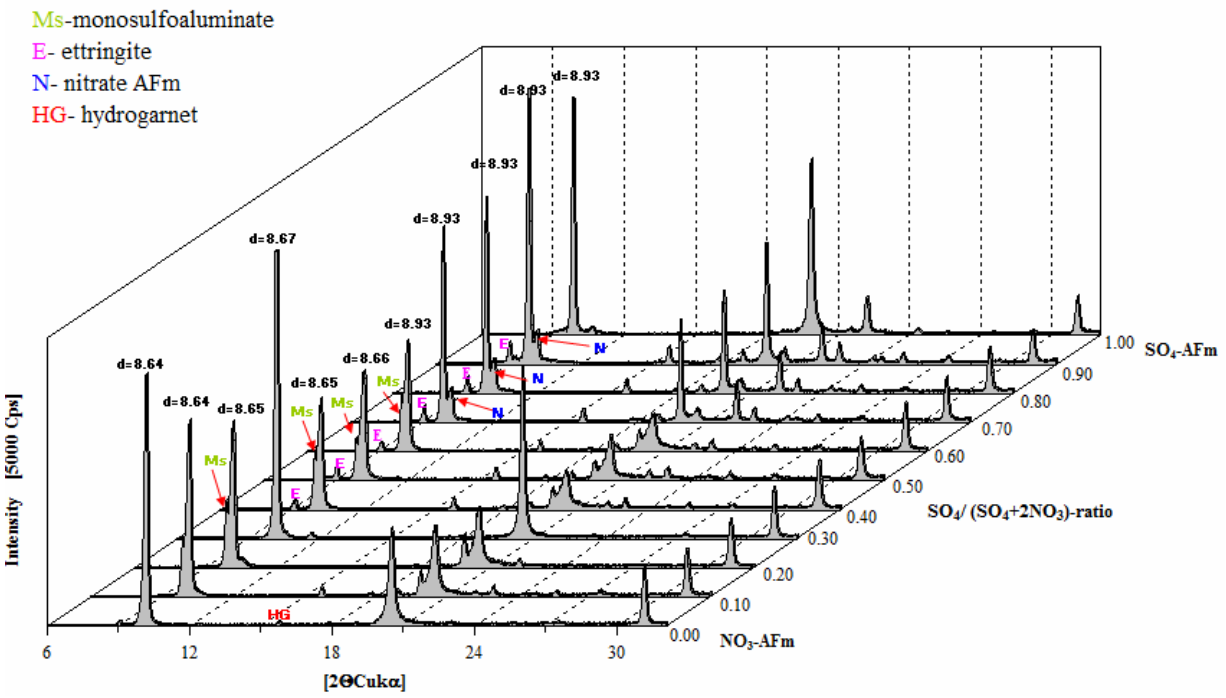

Figure 6.11(a): Partial XRD patterns of mixtures between nitrate AFm and monosulfoaluminate at 25±2˚C; note separate peaks through all range of compositions.

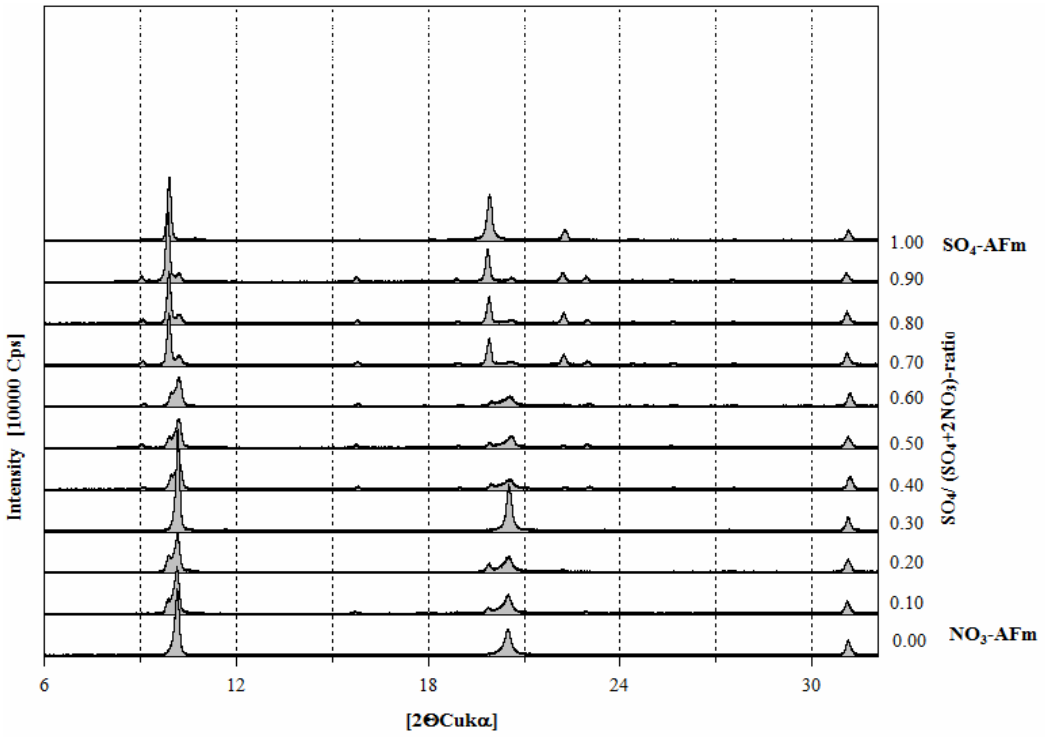

Figure 6.11(b): Partial XRD patterns of mixtures between nitrate AFm and monosulfoaluminate at 25±2˚C; note separate peaks through all range of compositions.

Table 6.7: Aqueous solution compositions measured from undersaturation for samples between the monosulfoaluminate (NO_3/Al=0) and the nitrate AFm (NO_3/Al=1) at 25±2ºC and after 180 days of equilibration.

Calculated NO_3/Al- ratio (total system)	Ca [mmol/l] (aq)	Al [mmol/l] (aq)	NO_3 [mmol/l] (aq)	pH	Solid phase at end of experiment
0.00	5.51	2.90	0.00	11.75	M_{ss}, E
0.10	5.45	2.98	2.69	11.74	Ms_{ss}, CH, Hc_{traces}
0.20	7.08	2.69	2.91	11.93	n.d.
0.30	7.06	2.48	2.99	11.98	M_{ss}, N, E, Hc_{traces}
0.40	6.35	3.22	3.58	11.96	M_{ss}, N, E
0.50	7.08	3.29	3.44	12.01	n.d.
0.60	7.09	2.82	3.37	12.01	$M_{ss,}$ N, E
0.70	7.25	3.25	3.73	12.03	n.d.
0.80	6.93	3.28	3.64	12.03	$M_{ss,}$ $HG_{(traces),}$ N, E
0.90	6.94	3.29	3.29	12.02	n.d.
1.00	6.95	3.17	3.96	11.99	N, HG

Abbreviations: Ms_{ss} = monosulfoaluminate in solid solution with hydroxy-AFm [9, 52], N=NO_3-AFm (nitrate AFm), CH=portlandite, HG=hydrogarnet (katoite), E- ettringite, Hc= hemicarboaluminate, n.d.= not determined

6.5.3 Nitrate AFm and monocarboaluminate

No solid solution was found between monocarboaluminate and nitrate AFm. Two separate sets of XRD peaks were observed through the all range of compositions (Fig 6.13(a,b)). The samples were redispersed in double distilled water and periodically agitated. Aqueous solution compositions, measured after equilibration for 180 days commencing from undersaturation, are presented in Tab. 6.8. Calcium, aluminium and nitrate concentrations are plotted on Fig. 6.14(a,b). Carbonate concentrations were below detection limit (see section 3.2.1) and are not shown.

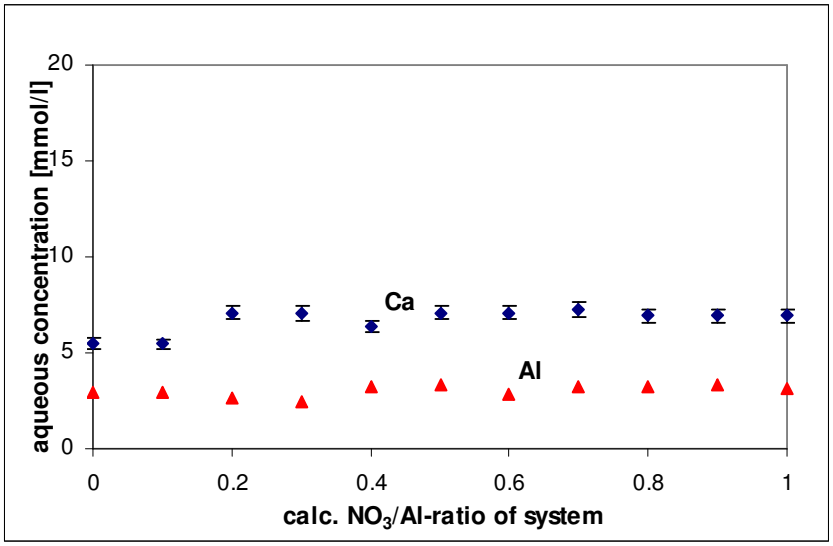

Figure 6.12(a): Equilibrium calcium and aluminium aqueous concentrations commencing from undersaturation for samples between monosulfoaluminate (NO_3/Al=0) – nitrate AFm (NO_3/Al=1) at 25±2ºC and after 180 days of equilibration. Error bars are shown for Ca.

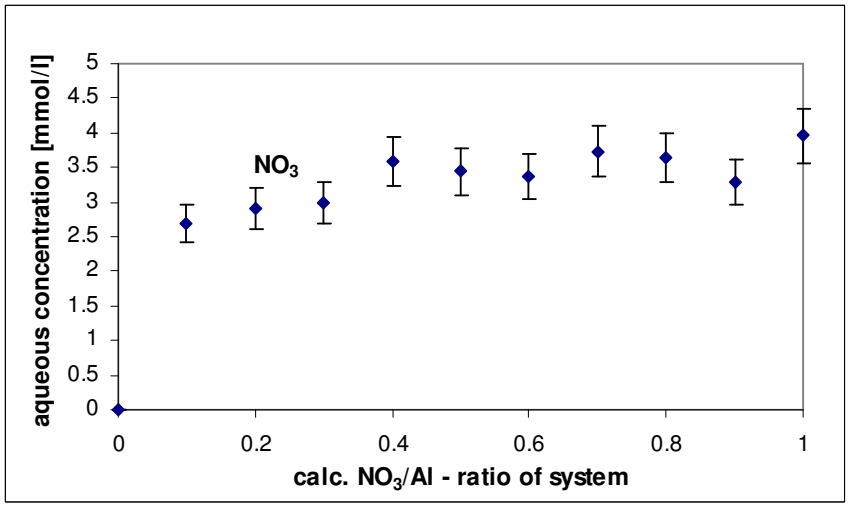

Figure 6.12(b): Equilibrium nitrate aqueous concentrations commencing from undersaturation for samples between monosulfoaluminate (NO_3/Al=0) and nitrate AFm (NO_3/Al=1) at 25±2ºC and after 180 days of equilibration. Error bars are shown for NO_3.

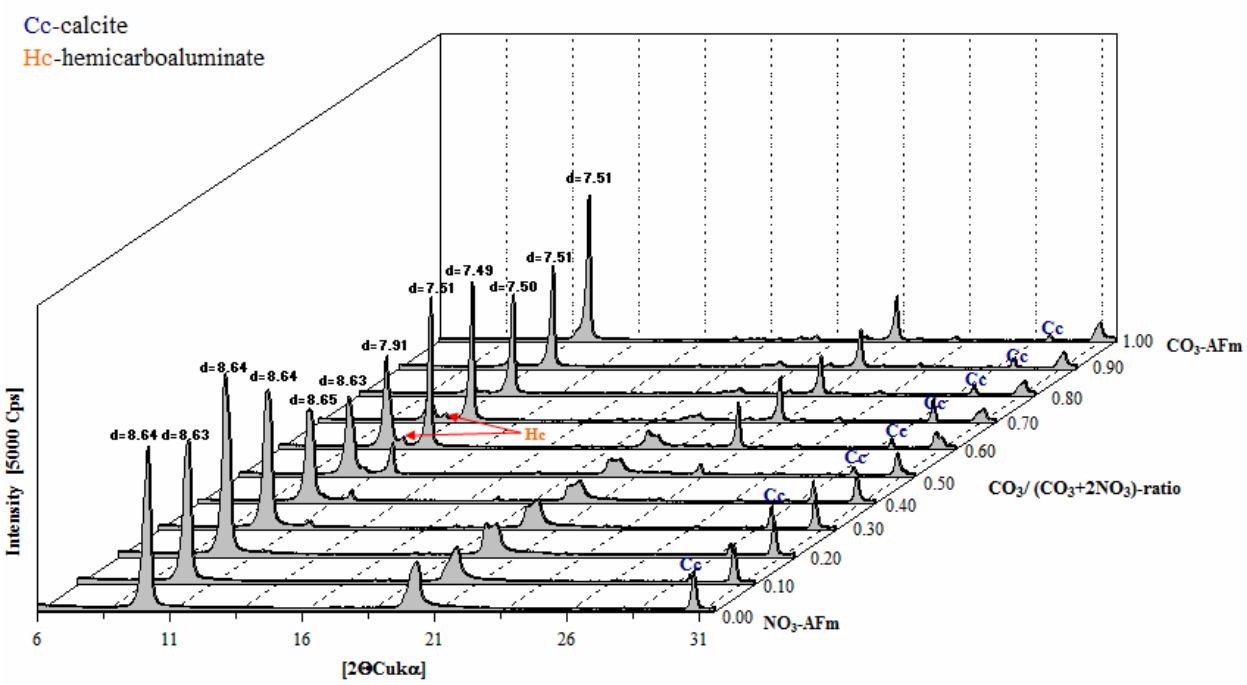

Figure 6.13(a): Partial XRD patterns of mixtures between nitrate AFm and monocarboaluminate at 25±2˚C; note separate peaks through all range of compositions; Cc peaks are attributed to calcite, Hc to hemicarboaluminate.

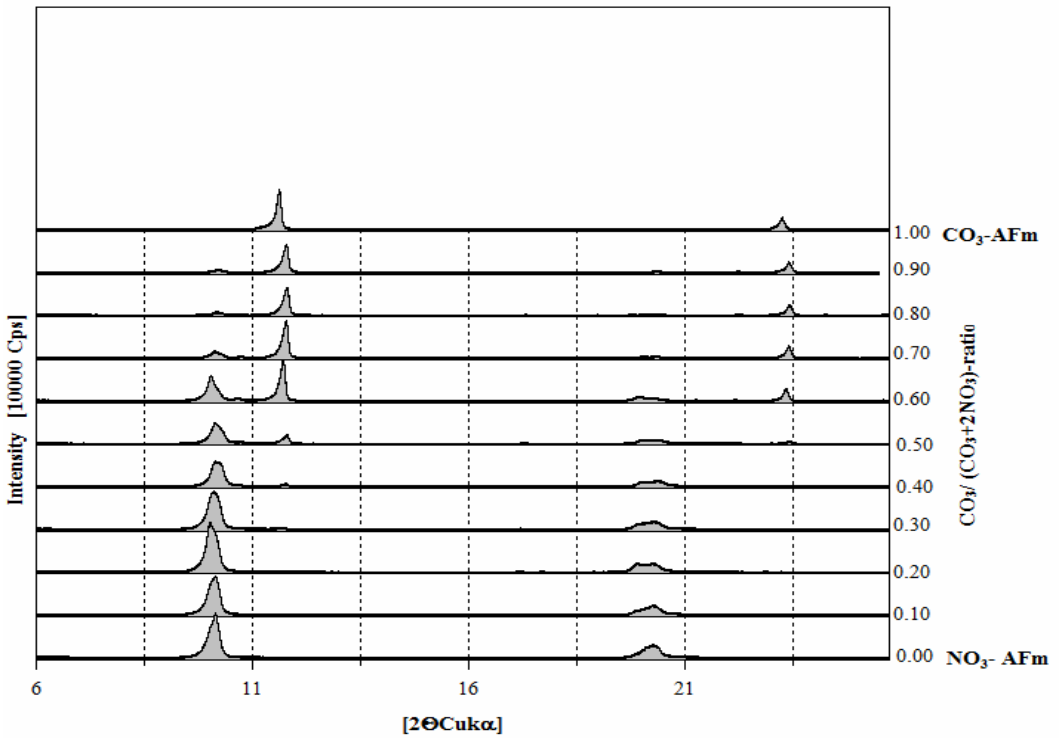

Figure 6.13(b): Partial XRD patterns of mixtures between nitrate AFm and monocarboaluminate at 25±2˚C; note separate peaks through all range of compositions.

Table 6.8: Aqueous solution compositions measured from undersaturation for samples between the monocarboaluminate (NO_3/Al=0) and the nitrate AFm (NO_3/Al=1) at 25±2ºC and after 180 days of equilibration.

Calculated NO_3/Al- ratio (total system)	Ca [mmol/l] (aq)	Al [mmol/l] (aq)	NO_3 [mmol/l] (aq)	pH	Solid phase at end of experiment
0.00	3.67	1.59	0.00	11.64	Mc, Cc
0.10	5.65	1.28	2.80	11.68	n.d.
0.20	5.19	1.23	2.62	11.69	N_{traces}, Mc, Cc
0.30	6.98	1.52	3.30	11.68	n.d.
0.40	6.35	2.02	3.34	11.76	N, Mc, Cc, Hc_{traces}
0.50	6.43	2.85	3.19	11.89	n.d.
0.60	6.29	2.49	3.61	11.81	N, HG, Mc, Cc
0.70	6.26	2.77	3.87	11.83	n.d.
0.80	6.93	3.29	3.58	11.83	N, HG, Mc, Cc
0.90	6.94	3.18	3.73	11.86	n.d.
1.00	6.95	3.17	3.96	11.99	N, HG

Abbreviations: Mc = monocarboaluminate, N=NO_3-AFm (nitrate AFm), HG=hydrogarnet (katoite), Cc- calcite, Hc= hemicarboaluminate, n.d.= not determined

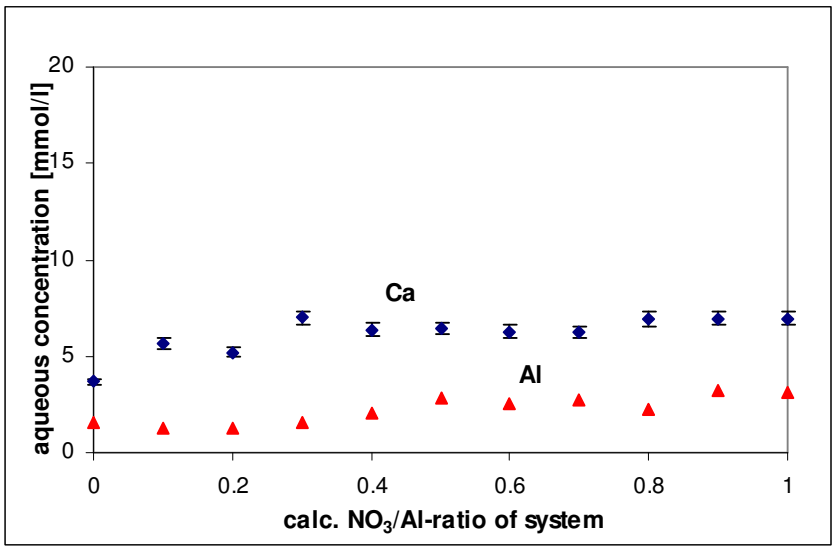

Figure 6.14(a): Equilibrium calcium and aluminium aqueous concentrations commencing from undersaturation for samples between monocarboaluminate (NO_3/Al=0) – nitrate AFm (NO_3/Al=1) at 25±2ºC and after 180 days of equilibration. Error bars are shown for Ca.

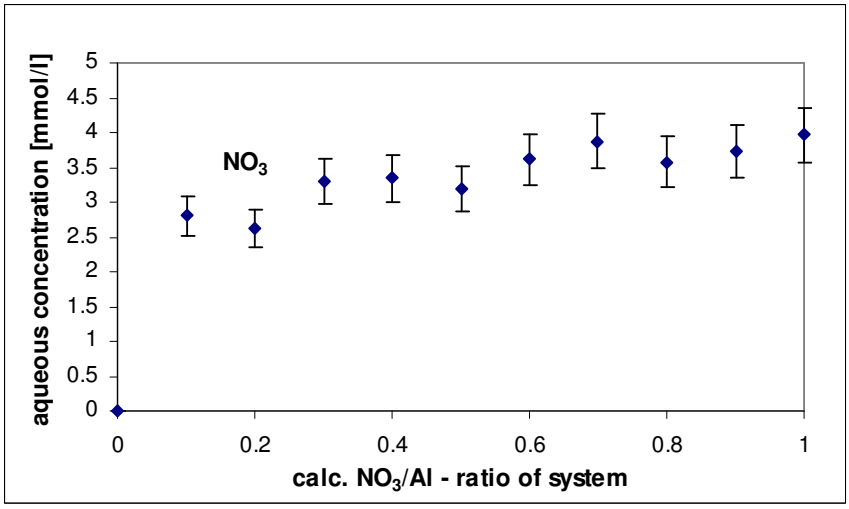

Figure 6.14(b): Equilibrium nitrate aqueous concentrations commencing from undersaturation for samples between monocarboaluminate (NO_3/Al=0) and nitrate AFm (NO_3/Al=1) at 25±2ºC and after 180 days of equilibration. Error bars are shown for NO_3.

6.5.4 Nitrate AFm and Friedel's salt

Kuzel [244] reported hydrothermal synthesis of $3CaO \cdot Al_2O_3 \cdot ½CaCl_2 \cdot ½Ca(NO_3)_2 \cdot 10H_2O$, containing traces of unknown polytypic modifications.

In this thesis solid solution formation between nitrate AFm (basal spacing d=8.64 Å) and Friedel's salt (basal spacing d=7.93 Å) was investigated in the range 0-1 $Cl/(NO_3+Cl)$ (Fig. 6.15(a.b)). Solid solution was found in a range of compositions in the range 0-0.5 $Cl/(NO_3+Cl)$ meaning that nitrate AFm can be substituted up to 50% by Cl ions. With increasing Cl substitution the basal spacing of nitrate AFm decreases, from d=8.64 Å for pure $Ca_4Al_2(OH)_{12}(NO_3)_2 \cdot 4H_2O$ to d=8.53 Å for the $Ca_4Al_2(OH)_{12}(NO_3)Cl \cdot 4H_2O$. Above ratio 0.5 $Cl/(NO_3+Cl)$ a miscibility gap occurs and two separate sets of X-ray reflections, one for nitrate AFm, another one for Friedel's salt (itself probably slightly substituted by NO_3^- ions).

Samples were redispersed in double distilled water and periodically agitated. Aqueous solution compositions, measured after equilibration commencing from undersaturation, are presented in Tab. 6.9. Calcium, aluminium, chloride and nitrate concentrations are plotted on Fig. 6.16(a,b). Guggenheim parameters used in the case of non-ideal binary solid solutions were derived (see section 2.4). To enable calculation slight solid solution (3%) of nitrate AFm in Friedel's salt was permitted. Assuming a miscibility region 0.03-0.5 $Cl/(NO_3+Cl)$ and applying MBSSAS software the resulting Guggenheim parameters were: a_0=0.188 and a_1=2.49.

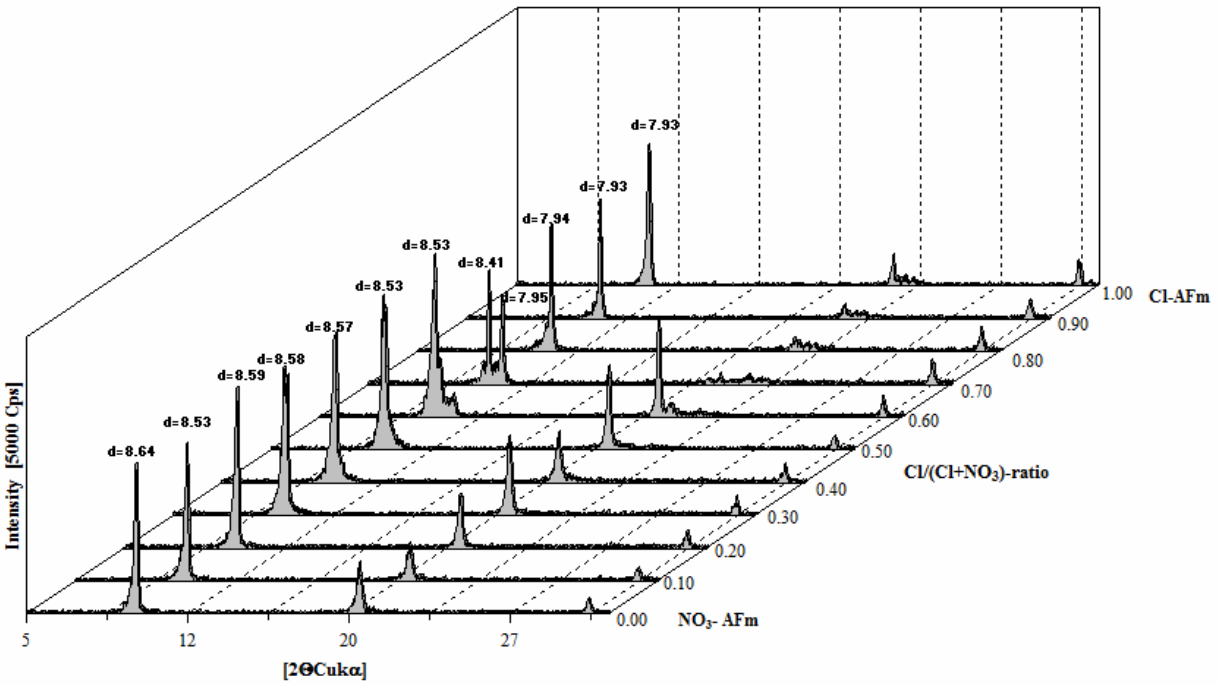

Figure 6.15(a): Partial XRD patterns of the solid solution formation at 25˚C between nitrate AFm and Friedel's salt.

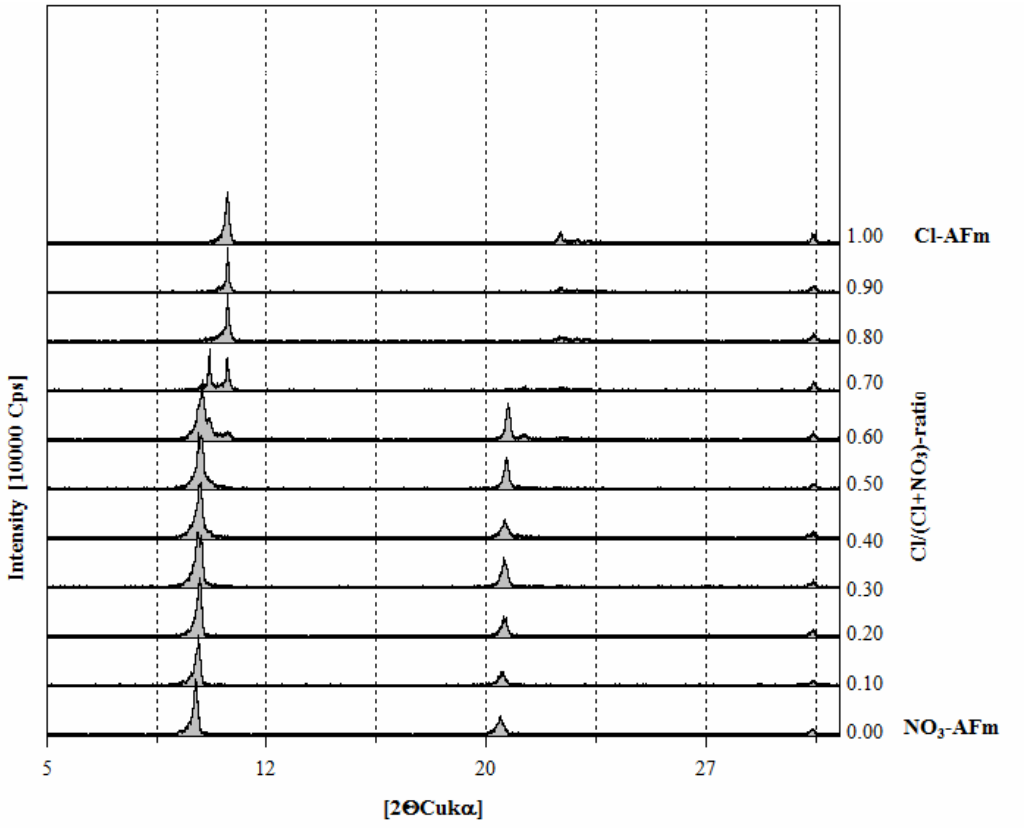

Figure 6.15(b): Partial XRD patterns of the solid solution formation at 25˚C between nitrate AFm and Friedel's salt.

Table 6.9: Aqueous solution compositions measured from undersaturation for samples between the Friedel's salt (NO_3/Al=0) and the nitrate AFm (NO_3/Al=1) at 25±2ºC and after 180 days of equilibration.

Calculated NO_3/Al- ratio (total system)	Ca [mmol/l] (aq)	Al [mmol/l] (aq)	NO_3 [mmol/l] (aq)	Cl [mmol/l] (aq)	pH	Solid phase at end of experiment
0.00	8.82	2.39	0.00	5.79	11.93	Fs
0.10	8.86	2.61	4.14	5.55	11.98	n.d
0.20	8.46	2.74	4.16	5.50	12.02	Fs, N,
0.30	8.36	2.72	4.33	5.47	12.06	n.d
0.40	8.49	2.11	3.88	5.10.	12.02	Fs, N
0.50	8.19	3.30	3.70	4.55	11.97	N-$Fs_{ss,}$
0.60	8.06	2.88	3.29	4.22	11.96	n.d
0.70	7.98	2.94	3.14	3.63	12.04	N-$Fs_{ss,}$ HG
0.80	7.12	3.34	3.04	2.24	12.03	n.d.
0.90	6.56	3.05	2.79	0.80	12.01	N-$Fs_{,ss}$, HG
1.00	6.95	3.17	3.96	0.00	11.99	N, HG

Abbreviations: N=NO_3-AFm (nitrate AFm probably slightly substituted with OH), HG=hydrogarnet (katoite), Fs=Friedel's salt (slightly substituted with OH), N-Fs_{ss}= nitrate-AFm in solid solution with Friedel's salt, n.d.= not determined

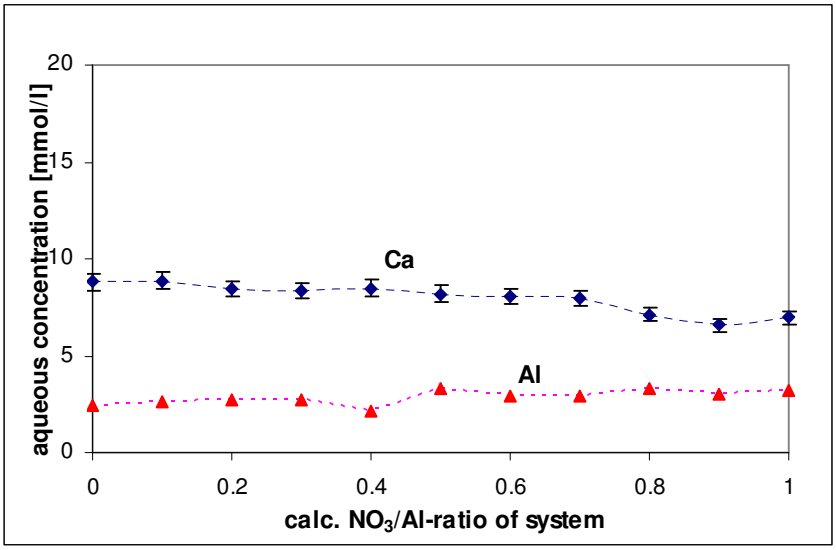

Figure 6.16(a): Equilibrium calcium and aluminium aqueous concentrations commencing from undersaturation for samples between Friedel's salt (NO_3/Al=0)– nitrate AFm (NO_3/Al=1) at 25±2ºC and after 180 days of equilibration. Error bars are shown for Ca.

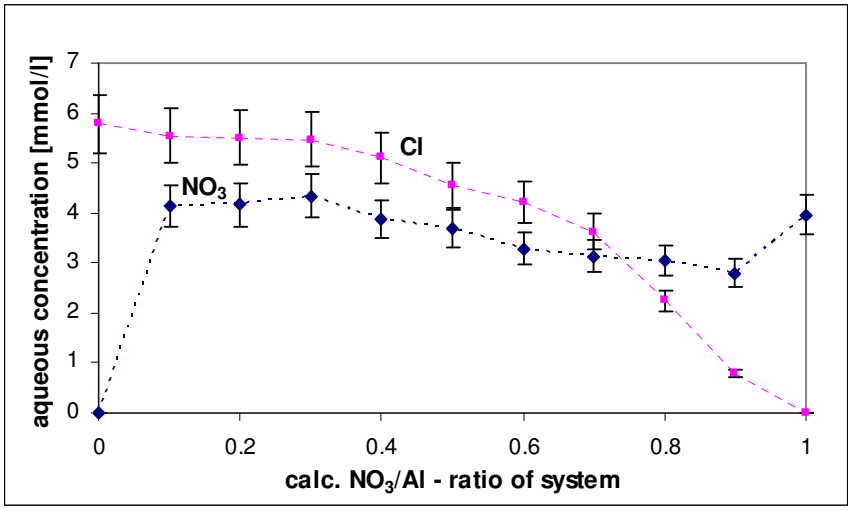

Figure 6.16(b): Equilibrium nitrate and chloride aqueous concentrations commencing from undersaturation for samples between Friedel's salt (NO_3/Al=0) – nitrate AFm (NO_3/Al=1) at 25±2ºC and after 180 days of equilibration. Error bars are shown for Ca.

6.5.5 Nitrite AFm and hydroxy AFm

Solid solution formation between nitrite AFm (basal spacing d=7.91 Å) and hydroxy AFm (basal spacing d=7.99 Å) was investigated in the range 0-1 OH/(NO_2+OH) (Figs. 6.17(a,b), 6.18(a.b)). The main reflections of nitrite and hydroxy end members coincided after drying in 35% RH (Fig. 6.18(a,b)).

To define the miscibility gap without artefacts introduced by drying, for X-ray characterisation wet samples were covered with 'Mylar' foil to prevent water evaporation and avoid atmospheric carbonation. This preserved the higher water state of AFm; two separate peaks were observed in the region above ratio 0.5 OH/(NO_2+OH) (Fig. 6.17(a,b)). Thus the coexisting solid solution of the (OH, NO_2) AFm phases, which are in different water states during the equilibration, is inevitably incomplete. Dry (OH, NO_2) AFm solid solution members were redispersed in double distilled water and equilibrated at 25˚C for 180 days. All the samples were periodically agitated. Aqueous solution compositions, measured after equilibration commencing from undersaturation, are presented in Tab. 6.10. Experimental calcium, aluminium and nitrite concentrations are plotted in Fig. 6.19. Guggenheim parameters used in the case of non-ideal binary solid solutions were derived (see section 2.4). To enable calculation slight solid solution (3%) of nitrite AFm in hydroxy AFm was permitted. Assuming miscibility region: 0.03-0.5 OH/(NO_2+OH) and applying MBSSAS software the resulting Guggenheim parameters were: a_0=0.188 and a_1=2.49.

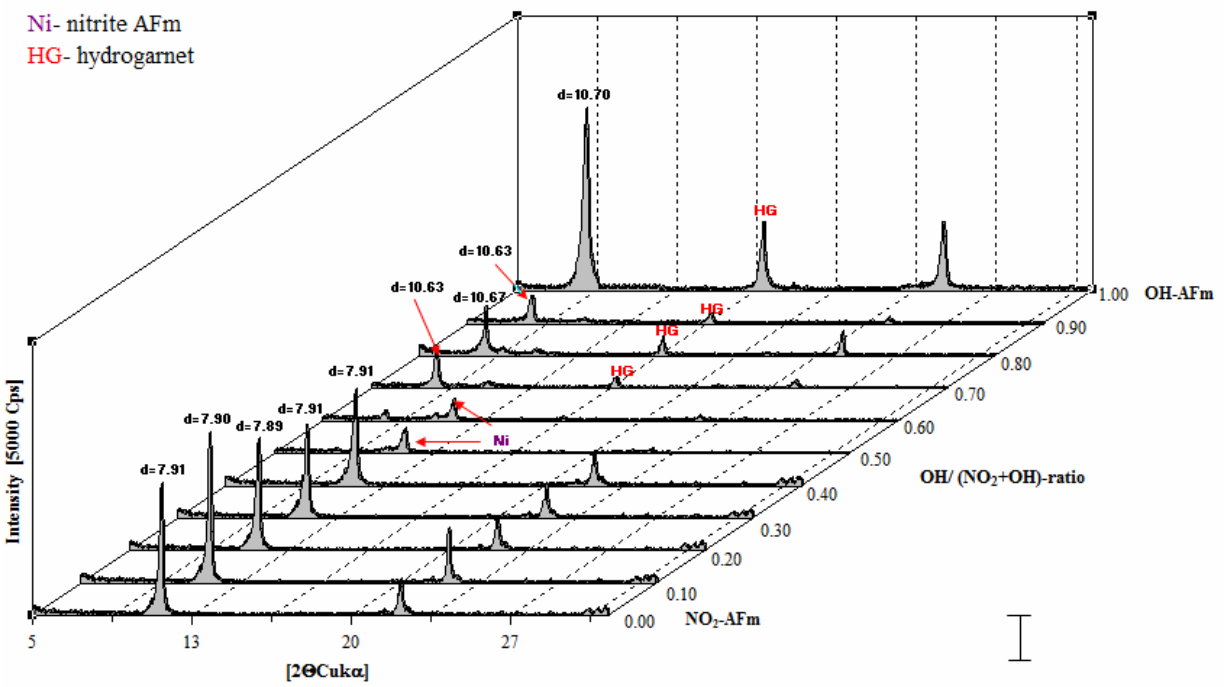

Figure 6.17(a): Partial XRD patterns of the solid solution formation at 25˚C between nitrite AFm and hydroxy AFm: wet samples. Reflections marked as HG are attributed to hydrogarnet.

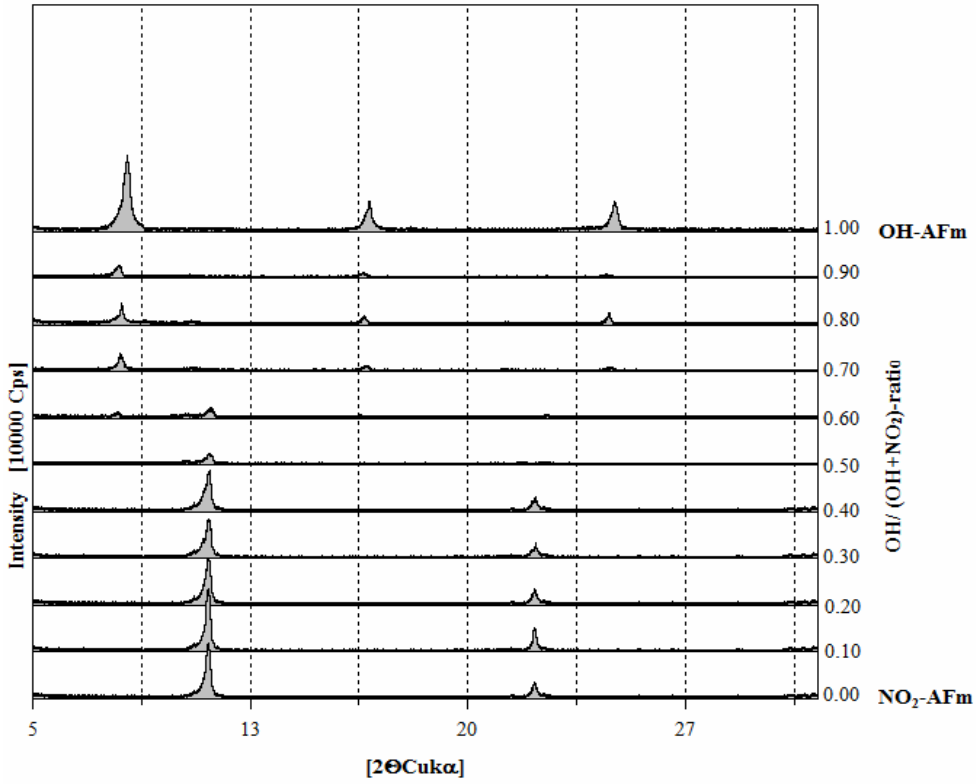

Figure 6.17(b): Partial XRD patterns of the solid solution formation at 25˚C between nitrite AFm and hydroxy AFm: wet samples.

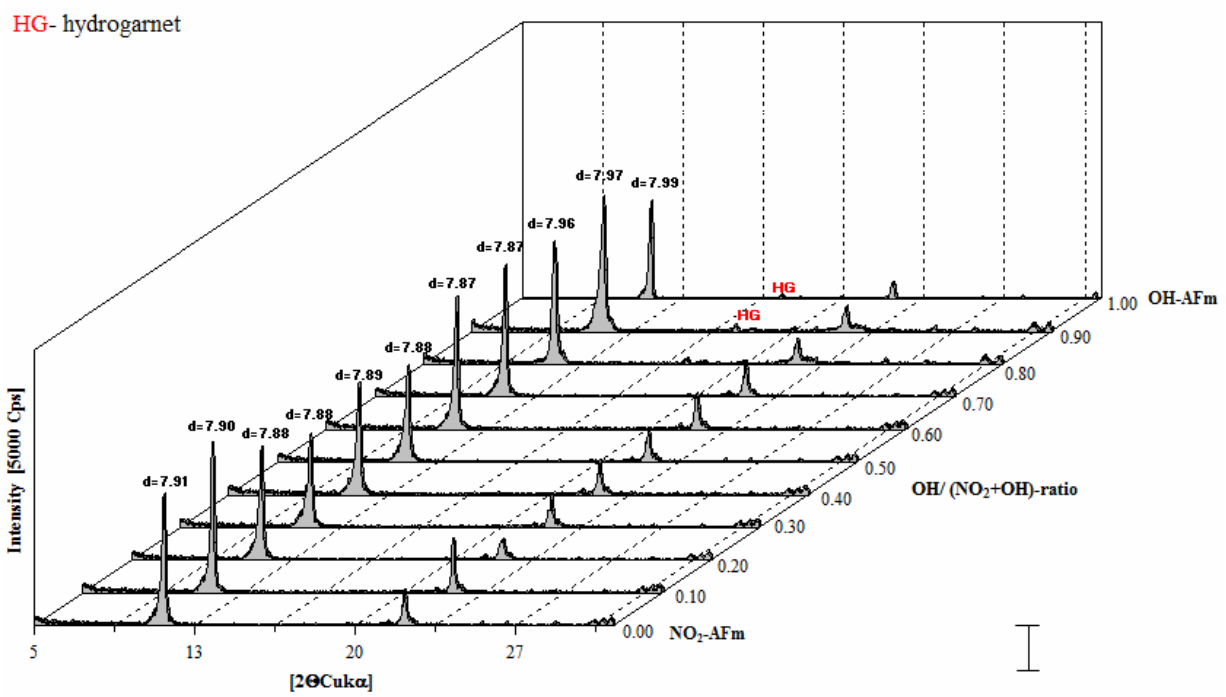

Figure 6.18(a): Partial XRD patterns of the solid solution formation at 25±2˚C between nitrite AFm and hydroxy AFm: samples dried at 35% RH. Reflections marked as HG are due to hydrogarnet.

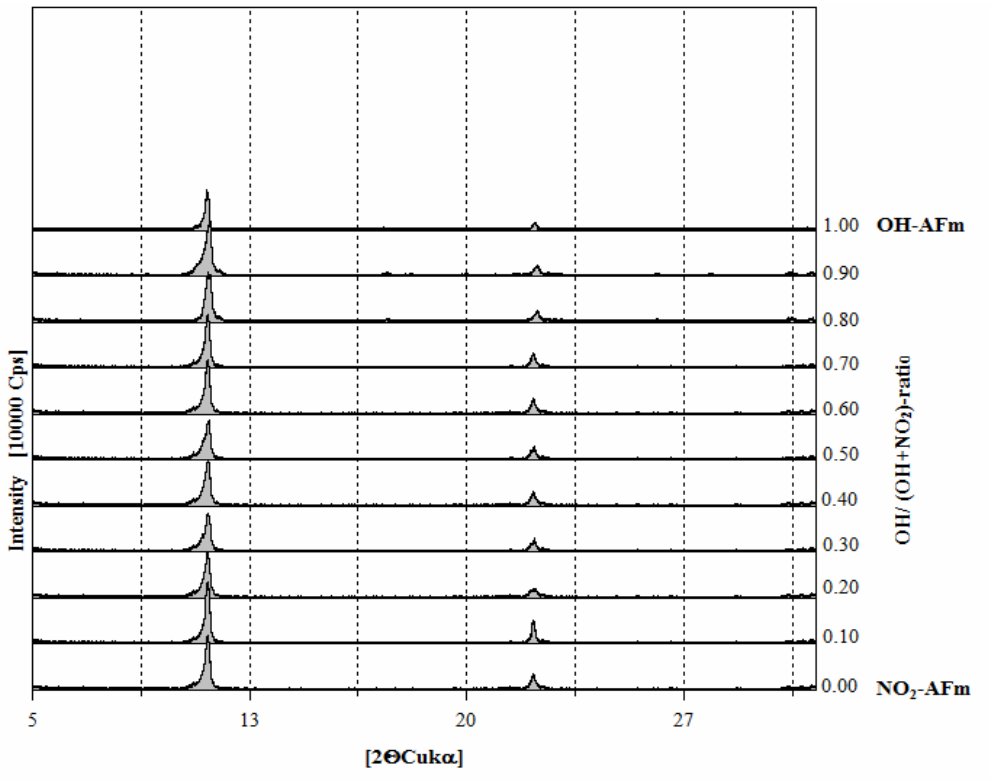

Figure 6.18(b): Partial XRD patterns of the solid solution formation at 25±2˚C between nitrite AFm and hydroxy AFm: samples dried at 35% RH.

Table 6.10: Aqueous solution compositions measured from undersaturation for samples between the hydroxy AFm (NO_2/Al=0) and the nitrite AFm (NO_2/Al=1) at 25±2ºC and after 180 days of equilibration.

Calculated NO_2/Al- ratio (total system)	Ca [mmol/l] (aq)	Al [mmol/l] (aq)	NO_2 [mmol/l] (aq)	pH	Solid phase at end of experiment
0.00	17.63	0.21	0.00	12.49	OH-AFm, HG, CH
0.10	13.21	0.27	6.10	12.20	n.d
0.20	12.42	0.34	7.79	12.18	Ni, HG, CH
0.30	11.91	0.48	8.72	12.11	n.d
0.40	11.64	0.72	9.56	12.02	Ni_{ss}/OH-AFm
0.50	12.03	1.98	10.07	12.01	n.d.
0.60	12.70	2.75	9.76	12.05	n.d.
0.70	12.25	2.80	9.43	12.04	$Ni_{ss,}$ HG
0.80	11.70	2.98	9.54	11.98	n.d.
0.90	11.45	3.03	10.05	11.99	Ni_{ss}, HG
1.00	12.93	2.87	9.93	12.00	Ni ,HG

Abbreviations: Ni=NO_2-AFm (nitrite AFm), Ni_{ss}=solid solution between NO_2-AFm and OH-AFm, OH-AFm= hydroxy-AFm, CH=portlandite, HG=hydrogarnet (katoite); n.d.=not determined

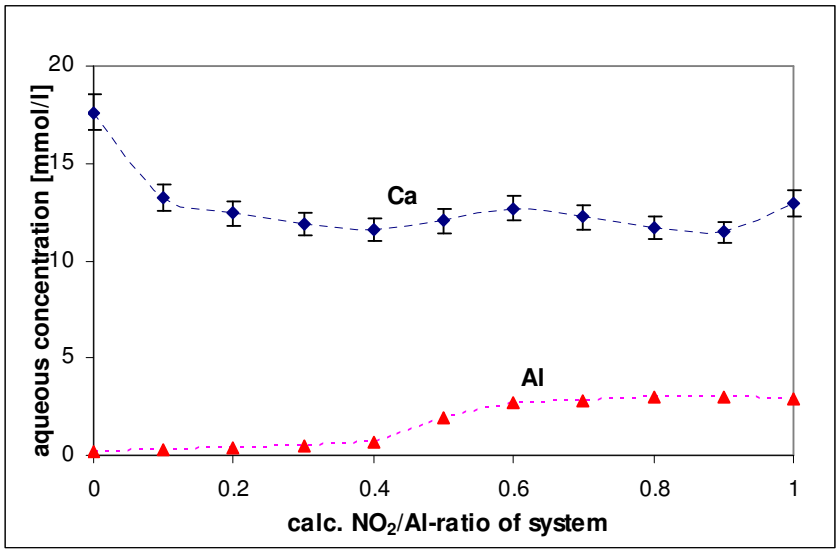

Figure 6.19(a): Equilibrium calcium and aluminium aqueous concentrations commencing from undersaturation for samples between hydroxy AFm (NO_2/Al=0)–nitrite AFm (NO_2/Al=1) at 25±2ºC and after 180 days of equilibration. Error bars are shown for Ca.

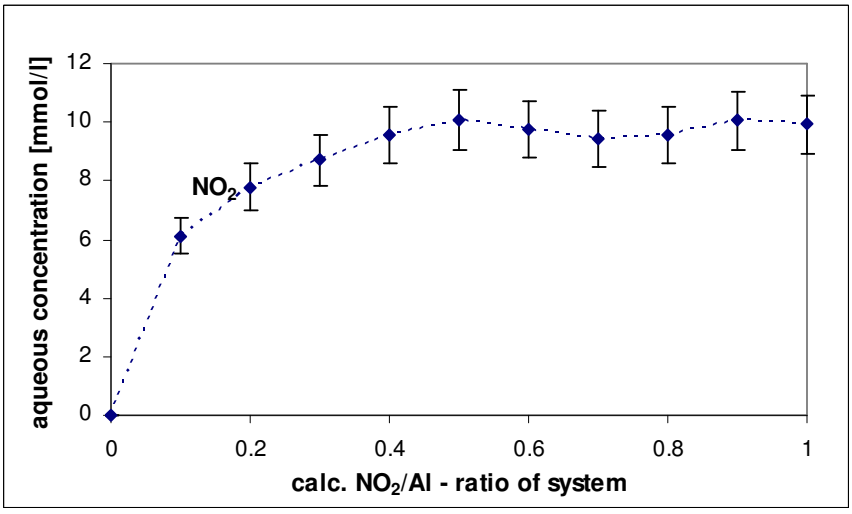

Figure 6.19(b): Equilibrium nitrite aqueous concentrations commencing from undersaturation for samples between hydroxy AFm (NO_2/Al=0) – nitrite AFm (NO_2/Al=1) at 25±2ºC and after 180 days of equilibration. Error bars are shown for Ca.

6.5.6 Nitrite AFm and monosulfoaluminate

No solid solution was found between monosulfoaluminate and nitrite AFm. Two separate XRD peaks were observed through the all range of compositions (Fig. 6.20(a,b)). At higher sulfate contents, some ettringite precipitation was detected. The samples were redispersed in double distilled water and periodically agitated. Aqueous solution compositions, measured after equilibration commencing from undersaturation, are presented in Tab. 6.11. Calcium, aluminium and nitrite concentrations are plotted in Fig. 6.22. Sulfate concentrations were below detection limit: < 0.5 ppm (see section 3.2.1). After 180 days of dissolution reaction reflections at 2 theta ~ 10.5º (between monosulfoaluminate and nitrite AFm phase peaks) an additional peak of unknown phase 'X' of basal d spacing 8.42 Å appeared (Fig. 6.20(c)). Formation of an ordered compound was suspected and an attempt to synthesize the phase was made. Two routes of synthesis were carried. One (I) consisted of mixing monosulfoaluminate and nitrite AFm in 1:1 molar ratios in distilled water with continues agitation for 6 months at 25˚C; another, (II), by mixing stoichiometric amounts of C_3A, $CaSO_4$, $Ca(NO_2)_2$ with distilled water with continued agitation for 6 months at 25˚C. The target composition was set by analogy to Kuzel's salt as $Ca_4Al_2(SO_4)_{0.5}(NO_2)(OH)_{12}\cdot 6H_2O$. It was initially thought that ordered compound did not appear on Fig. 6.20(a,b) because synthesis was carried out just for 3 months with periodic agitation therefore it was extended up to 6 months and to continous stirring. After six months samples were dried over saturated $CaCl_2$ and X-ray diffraction was performed. Batch II consisted only of monosulfoaluminate and nitrite AFm. However in batch I, peak of phase with basal d value 8.42 Å appeared. Unfortunatately the product was not phase pure (Fig. 6.21) and reflections associated with monosulfoaluminate and nitrite AFm were also detected. It is possible that between monosulfoaluminate and nitrite AFm an ordered compound forms $Ca_4Al_2(SO_4)_x(NO_2)_y(OH)_z\cdot aH_2O$ but its exact composition is not known and it may be a subject for further research.

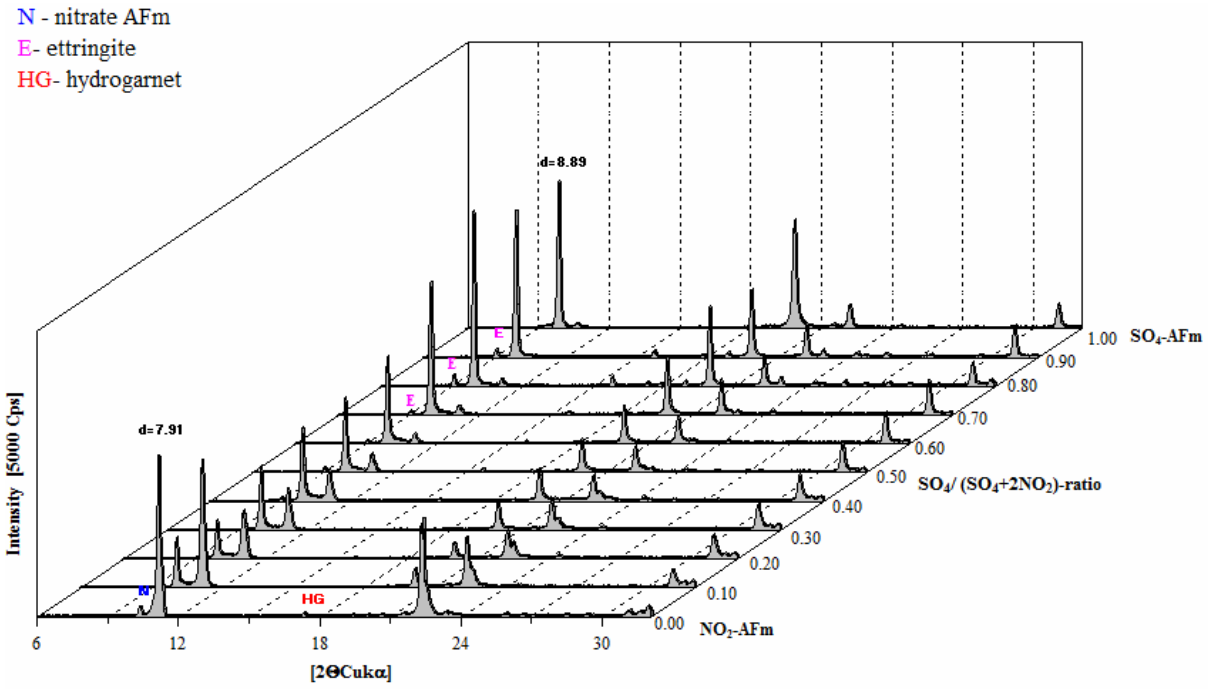

Figure 6.20(a): Partial XRD patterns of mixtures between nitrite AFm and monosulfoaluminate at 25±2˚C; note separate peaks through all range of compositions.

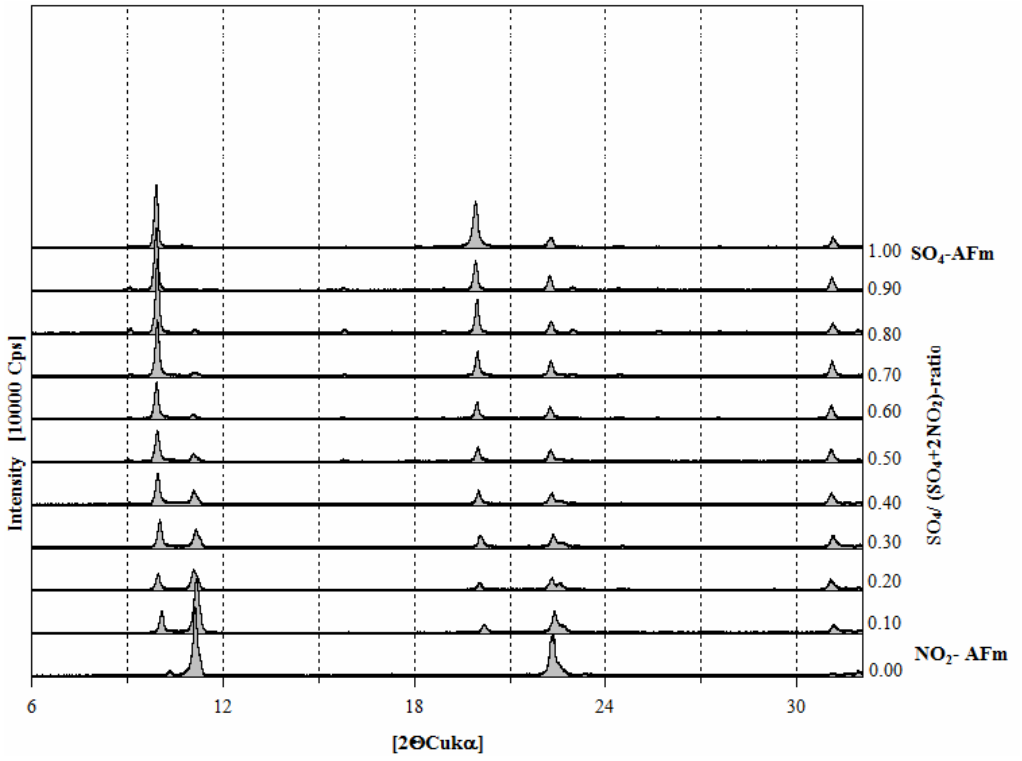

Figure 6.20(b): Partial XRD patterns of mixtures between nitrite AFm and monosulfoaluminate at 25±2˚C; note separate peaks through all range of compositions.

Table 6.11: Aqueous solution compositions measured from undersaturation for samples between the monosulfoaluminate (NO_2/Al=0) and the nitrite AFm (NO_2/Al=1) at 25±2ºC and after 180 days of equilibration.

Calculated NO_2/Al- ratio (total system)	Ca [mmol/l] (aq)	Al [mmol/l] (aq)	NO_2 [mmol/l] (aq)	pH	Solid phase at end of experiment
0.00	5.51	2.90	0.00	11.75	M_{ss}, E
0.10	10.42	0.27	5.10	11.74	n.d.
0.20	7.91	0.34	8.31	11.93	n.d.
0.30	7.06	0.43	7.79	11.98	M_{ss}, Ni, 'X' phase (8.42Å)
0.40	7.57	0.72	8.72	11.96	n.d.
0.50	6.08	1.98	10.05	12.01	M_{ss}, Ni, 'X' phase (8.42Å)
0.60	6.64	2.75	10.04	12.01	M_{ss}, Ni, 'X' phase (8.42Å)
0.70	7.03	2.98	10.43	12.03	n.d.
0.80	7.70	3.03	10.10	12.03	M_{ss}, Ni, 'X' phase (8.42Å)
0.90	7.97	3.21	10.54	12.02	M_{ss}, Ni, 'X' phase (8.42Å)
1.00	12.93	2.87	9.93	12.00	Ni, HG

Abbreviations: Ms_{ss}=monosulfoaluminate in solid solution with hydroxy-AFm [9, 52], Ni=NO_2-AFm (nitrite AFm), HG=hydrogarnet (katoite), E- ettringite, n.d.= not determined, 'X' *phase (8.42 Å) = unknown phase of basal d spacing 8.42 Å which appears after dissolution of samples containing monosulfoaluminate and nitrite AFm (see Fig. 6.20(c))*

6.5.7 Nitrite AFm and monocarboaluminate

No solid solution was found between monocarboaluminate and nitrite AFm. Two separate sets of XRD peaks were observed through the range of compositions (Fig. 6.23(a,b)).

All the samples were redispersed in double distilled water and periodically agitated. Aqueous solution compositions, measured after equilibration commencing from undersaturation, are presented in Tab. 6.12. Calcium, aluminium and nitrite concentrations are plotted in Fig. 6.24 (a,b). Carbonate concentrations were below detection limit (see section. 3.2.1)

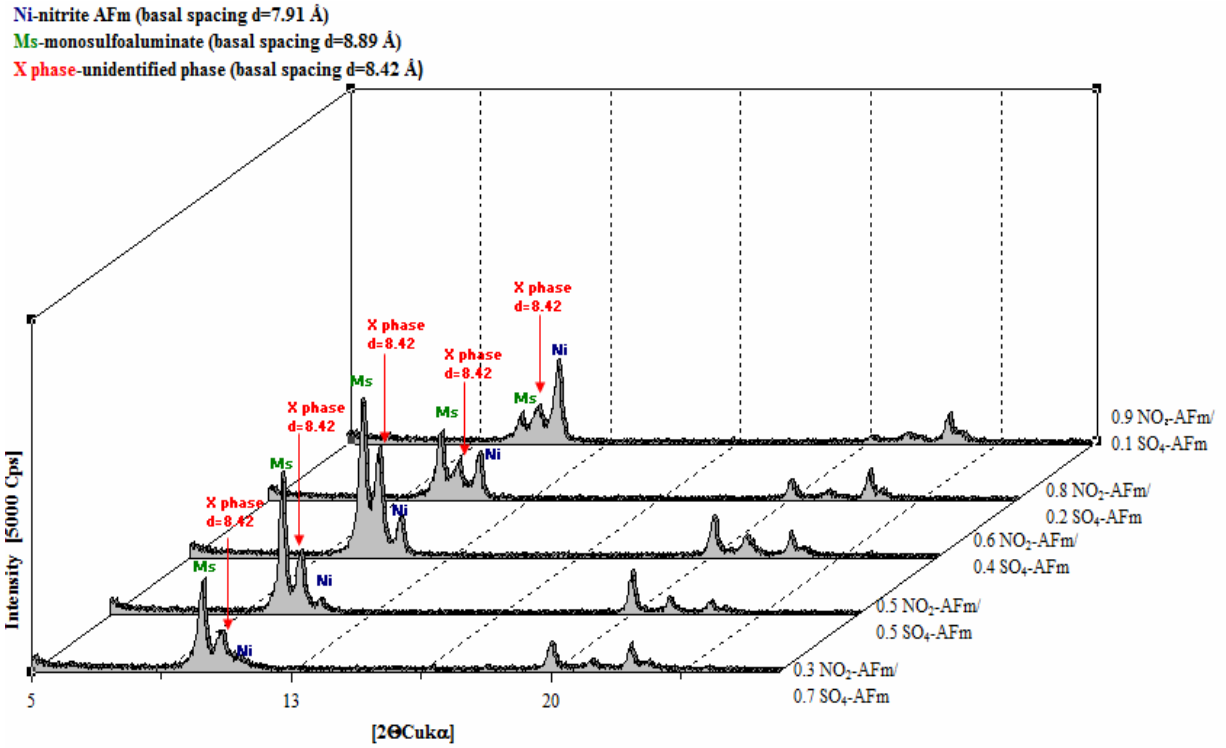

Figure 6.20(c): Partial XRD patterns of selected mixtures between nitrite AFm and monosulfoaluminate measured after 180 days of equilibration in distilled water at 25±2˚C; note unidentified 'X' phase (unknown phase of basal d spacing 8.42 Å which appears after dissolution of samples containing monosulfoaluminate and nitrite AFm).

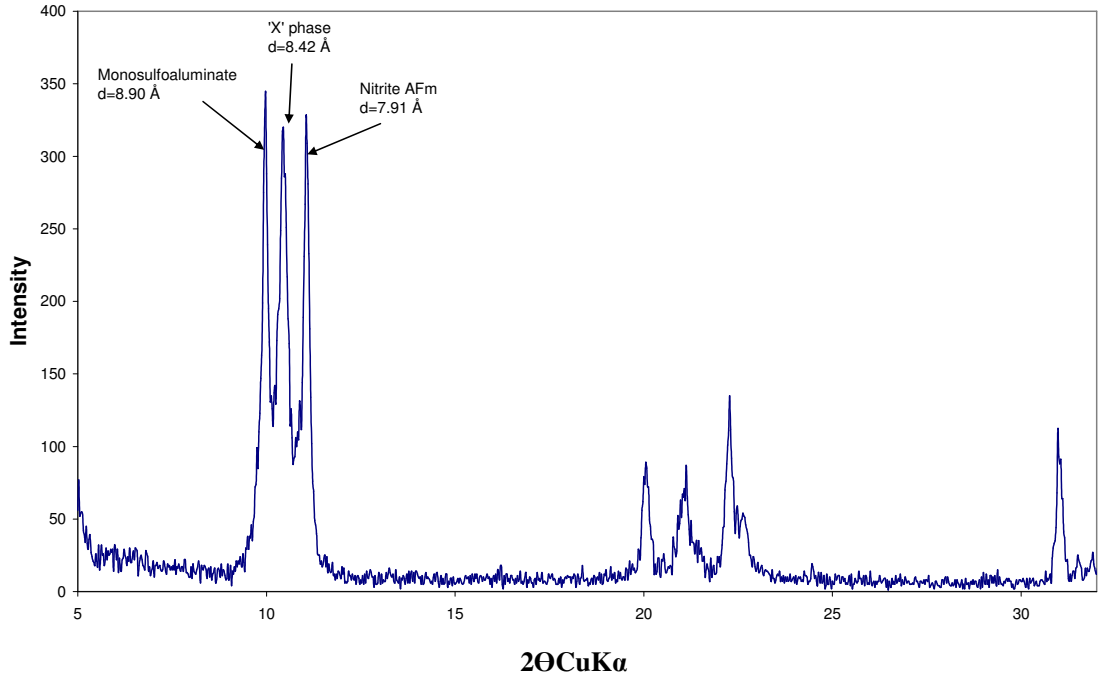

Figure 6.21: XRD pattern showing formation of potential ordered compound ('X' phase) after mixing monosulfoaluminate and nitrite AFm in 1:1 molar ratios in distilled water with continuous agitation for 6 months at 25˚C.

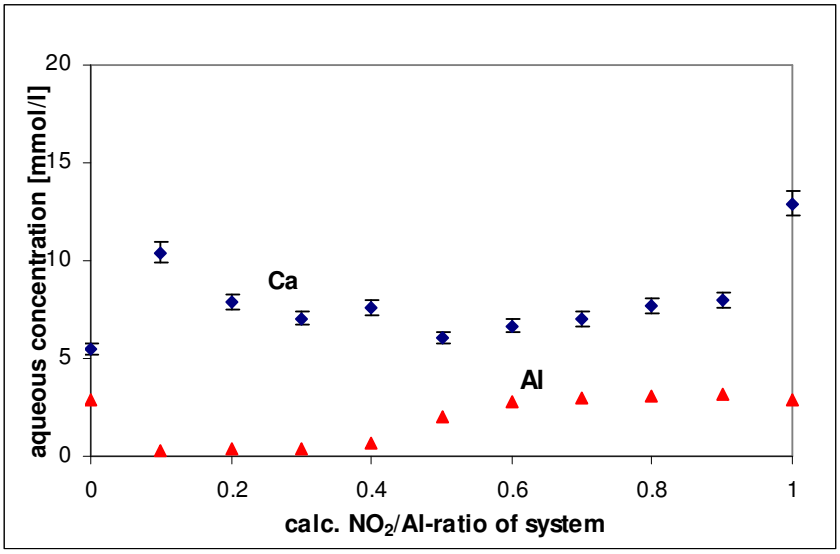

Figure 6.22(a): Equilibrium calcium and aluminium aqueous concentrations commencing from undersaturation for samples between monosulfoaluminate (NO_2/Al=0)–nitrite AFm (NO_2/Al=1) at 25±2ºC and after 180 days of equilibration. Error bars are shown for Ca.

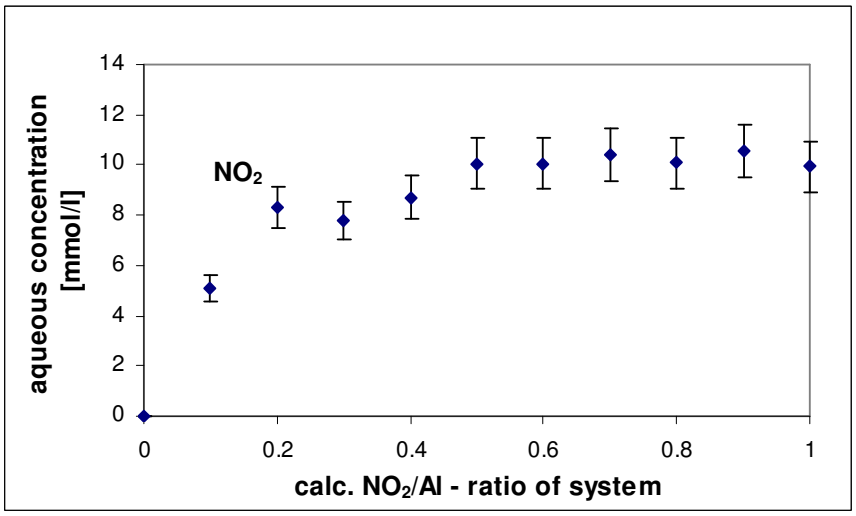

Figure 6.22(b): Equilibrium nitrite aqueous concentrations commencing from undersaturation for samples between monosulfoaluminate (NO_2/Al=0) and nitrite AFm (NO_2/Al=1) at 25±2ºC and after 180 days of equilibration. Error bars are shown for NO_2.

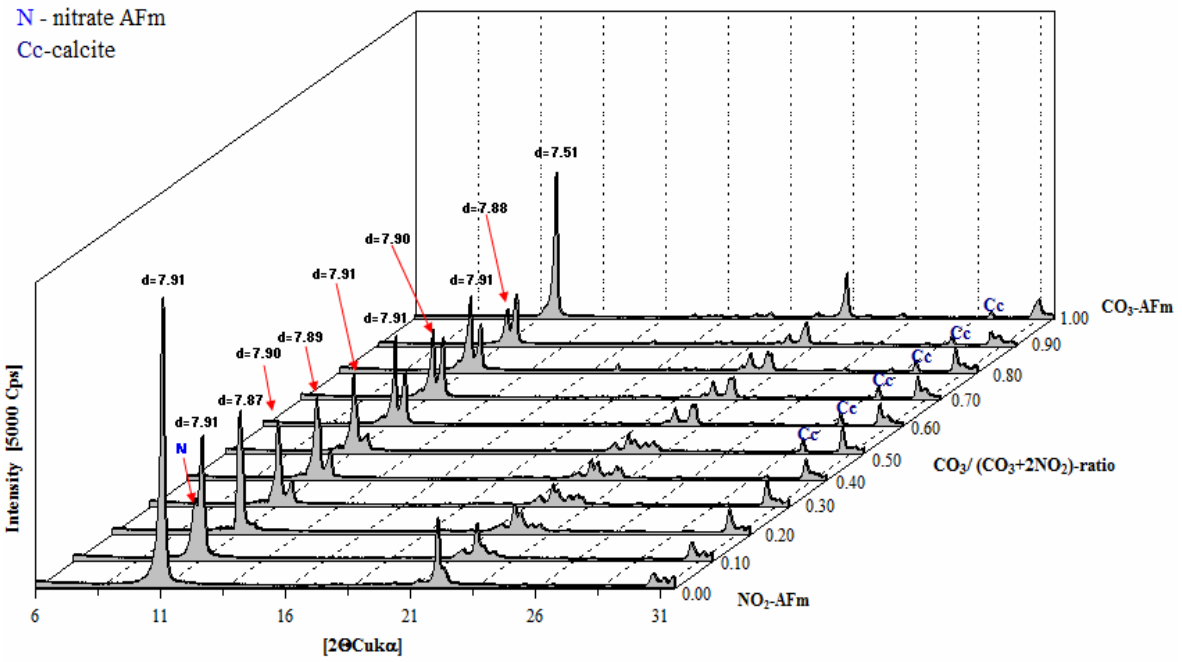

Figure 6.23(a): Partial XRD patterns of mixtures between nitrite AFm and monocarboaluminate at 25±2˚C; note separate peaks through all range of compositions; Cc peaks are attributed to calcite, N to nitrate AFm contamination.

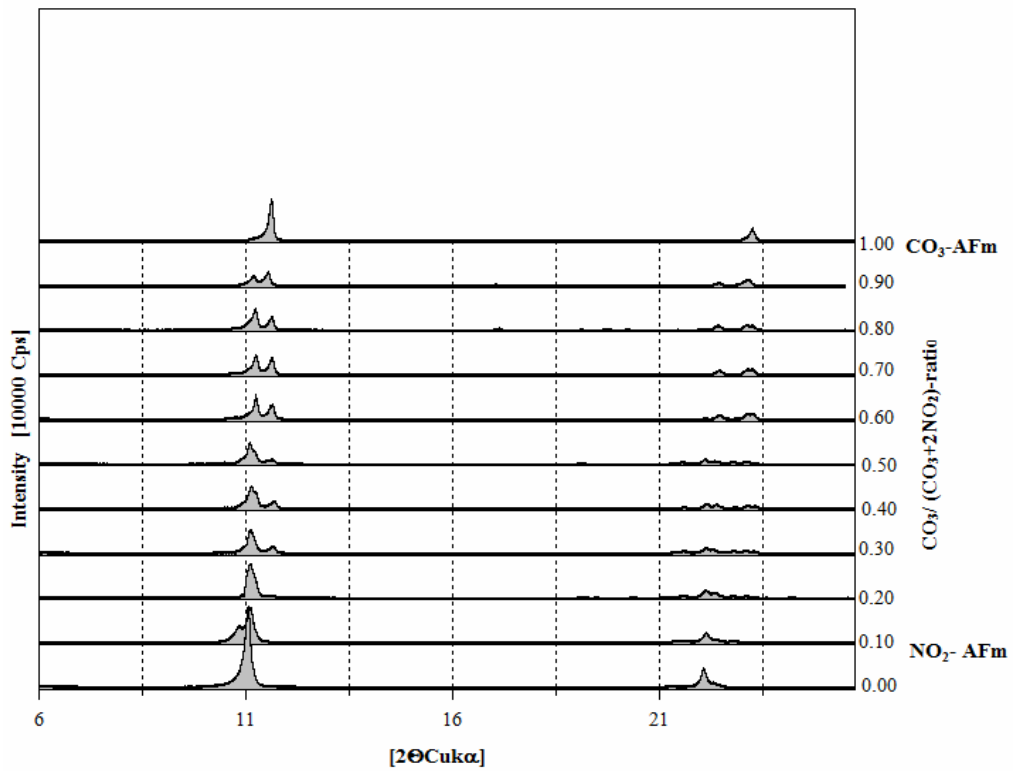

Figure 6.23(b): Partial XRD patterns of mixtures between nitrite AFm and monocarboaluminate at 25±2˚C; note separate peaks through all range of compositions.

Table 6.12: Aqueous solution compositions measured from undersaturation for samples between the monocarboaluminate (NO_2/Al=0) and the nitrite AFm (NO_2/Al=1) at 25±2ºC and after 180 days of equilibration.

Calculated NO_2/Al- ratio (total system)	Ca [mmol/l] (aq)	Al [mmol/l] (aq)	NO_2 [mmol/l] (aq)	pH	Solid phase at end of experiment
0.00	3.67	1.59	0.00	11.64	Mc, Cc
0.10	8.51	0.75	3.92	11.69	n.d.
0.20	12.38	0.87	7.92	11.64	Ni, Mc, Cc
0.30	12.28	0.63	8.40	11.66	n.d.
0.40	13.82	1.78	9.59	11.67	Ni, Mc, Cc,
0.50	14.66	0.99	8.99	11.85	n.d.
0.60	14.28	1.89	8.82	11.77	n.d.
0.70	14.34	1.98	9.29	11.76	n.d.
0.80	14.29	1.99	9.40	11.75	Ni, HG, Mc, Cc, $N_{(traces)}$
0.90	13.07	2.60	9.88	11.86	n.d.
1.00	12.93	2.87	9.93	12.00	Ni, HG

Abbreviations: Mc=monocarboaluminate, Ni=NO_2-AFm (nitrite AFm), HG=hydrogarnet (katoite), Cc- calcite, n.d.= not determined

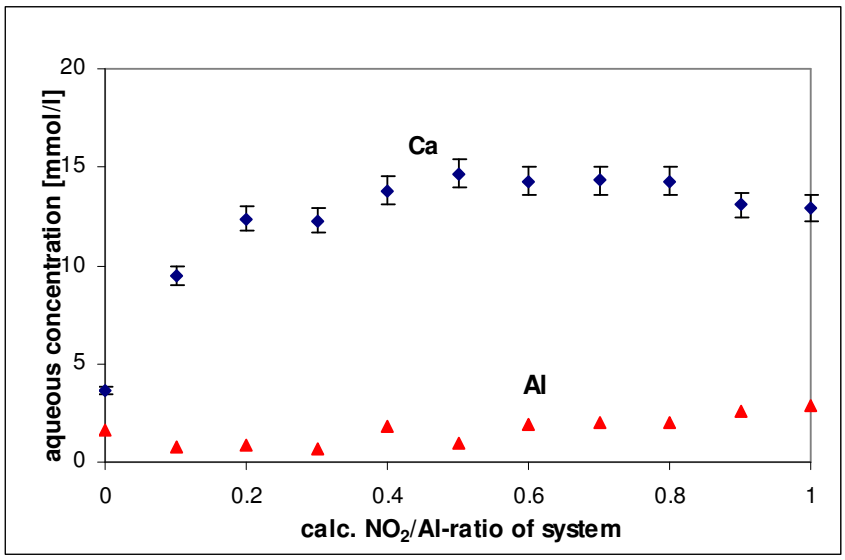

Figure 6.24(a): Equilibrium calcium and aluminium aqueous concentrations commencing from undersaturation for samples between monocarboaluminate (NO_2/Al=0)–nitrite AFm (NO_2/Al=1) at 25±2°C and after 180 days of equilibration. Error bars are shown for Ca.

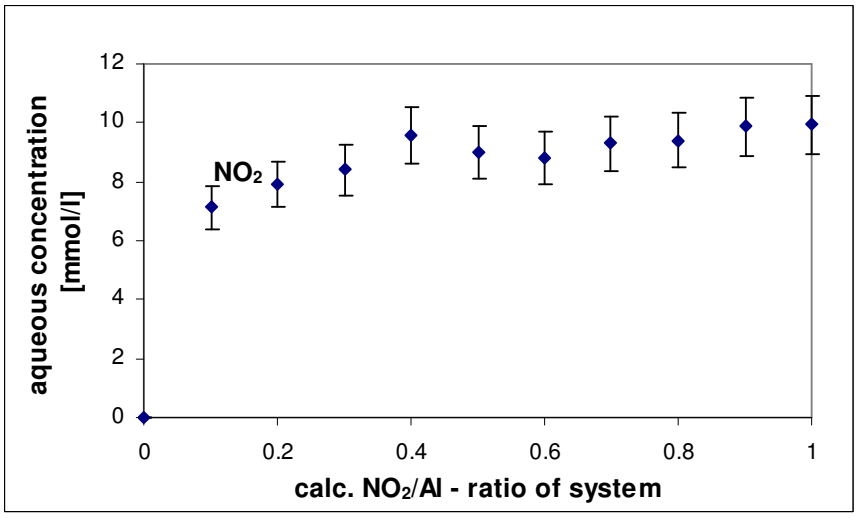

Figure 6.24(b): Equilibrium nitrite aqueous concentrations commencing from undersaturation for samples between monocarboaluminate (NO_2/Al=0)–nitrite AFm (NO_2/Al=1) at 25±2°C and after 180 days of equilibration. Error bars are shown for Ca.

6.5.8 Nitrite AFm and Friedel's salt

It was difficult to determine if there is or there is not solid solution formation between nitrite AFm and Friedel's salt because the end members gave main reflections at essentially identical 2 theta (samples dried at 35% RH); (Fig. 6.25(a,b)), shows the similar basal d-spacings. Also, nitrite AFm and Friedel's salt do not have a higher water variant therefore investigation for wet samples was not diagnostic. FTIR investigation was carried to reveal possible solid solution formation (Fig. 6.26). The infrared spectrum of Friedel's salt was compared with the spectrum reported in [18, 212]. Similar to the conclusion of Birnin-Yauri, no chloride signal was observed (chloride is FTIR inactive: see section 5.3.1). In the case of Friedel's salt peaks around 3400- 3600 cm^{-1} are ascribed O-H asymmetric stretching vibrations; 1620 cm^{-1} is due to H-O-H bending; The wavebands at 786 and 530 cm^{-1} are attributed to Al-O bending mode.

Regarding nitrite AFm, characteristic peaks appear around 1269 $cm^{-1.}$ These are attributed to-asymmetric stretching of N-O while that at 1412 cm^{-1} is due to symmetric stretching of N-O [306]. Those last two peaks diminish with increasing $Cl/(Cl+NO_2)$ which is logical due to a lower nitrite AFm content in the mixtures. No other differences were noticed *e.g.* peak shifts, broadening (Fig. 6.26).

Aqueous solution compositions, measured after equilibration commencing from undersaturation, are presented in Tab. 6.13. Calcium, aluminium, nitrite and chloride concentrations are plotted in Fig. 6.27(a,b). From the solution composition it was also difficult to clearly identify solid solution limits. Chloride and nitrite concentrations seem to change continuously which accordingly to the phase rule* indicates solid solution formation, but calcium values starting from range > 0.5 NO_2/Al are constant what can suggest miscibility gap.

**The Gibbs phase rule is relationship used to determine the number of state variables F, usually chosen from among temperature, pressure, and species composition in each phase, which must be specified to fix the thermodynamic state of a system in equilibrium: P+F=C+2 where P is the number of phases in thermodynamic equilibrium with each other and C is the number of components, F equals degrees of freedom. For investigated two component system at constant temperature and pressure equals P+F=2+0 so when we have 2 phases F =0 and assemblage is invariant (therefore Ca, NO_2, Cl concentrations should be constant), when only one (solid solution formation) F=1 and with increasing ion substitution variation in aqueous Ca, Cl, NO_2 concentrations should be observed.*

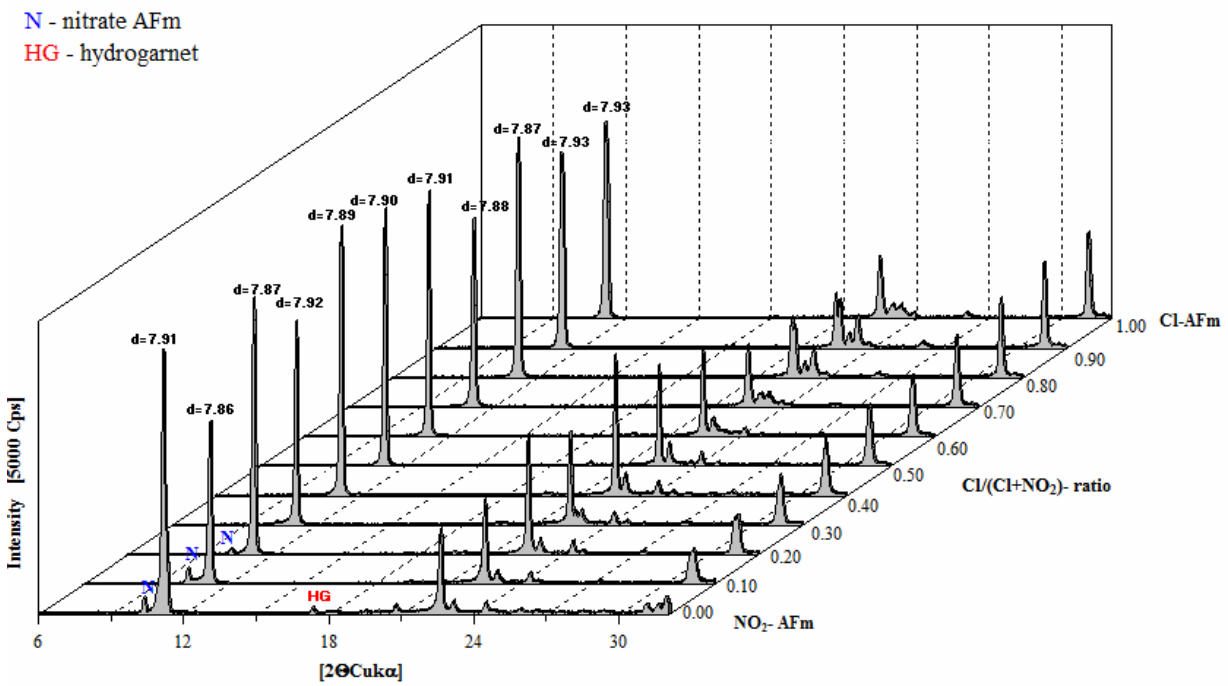

Figure 6.25(a): Partial XRD patterns investigating potential solid solution formation at 25˚C between nitrite AFm and Friedel's salt, HG is attributed to hydrogarnet, N-nitrate AFm contamination.

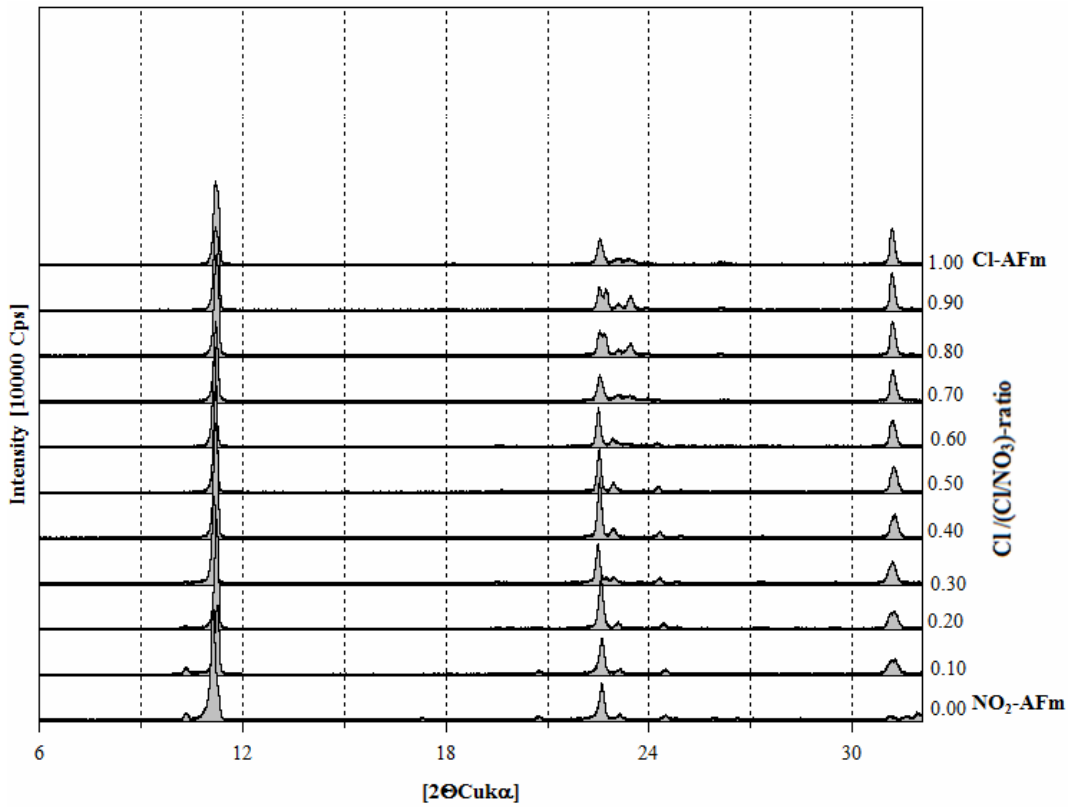

Figure 5.25(b): Partial XRD patterns investigating potential solid solution formation at 25˚C between nitrite AFm and Friedel's salt.

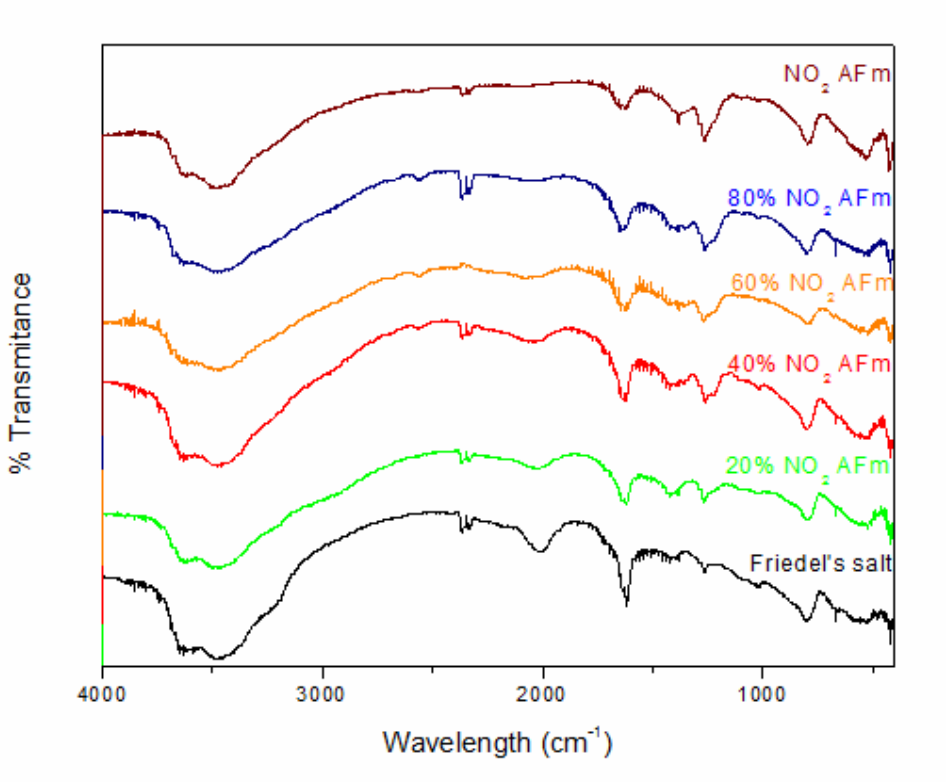

Figure 6.26: FTIR patterns of the NO_2-AFm and Friedel's salt mixtures.

6.5.9 Nitrate AFm and nitrite AFm

XRD data indicate solid solution formation between nitrate and nitrite AFm in a range $NO_2/(NO_3 + NO_2)$ = 0-0.4, *i.e.*, nitrate AFm may be substituted by nitrite up to 40% (Fig. 6.28(a,b)). The basal d-spacing decreases from 8.64 Å phase to 8.50 Å for the composition with 40% nitrate substituted by nitrite. All the samples were redispersed in double distilled water and periodically agitated. Aqueous solution compositions, measured after equilibration commencing from undersaturation, are presented in Tab. 6.14. Calcium, aluminium, nitrate and nitrite concentrations are plotted in Fig. 6.29(a,b). Guggenheim parameters used in the case of non-ideal binary solid solutions were derived (see section 2.4). To enable calculation slight solid solution (5%) of nitrate AFm in nitrite AFm was permitted. Assuming miscibility region 0.05-0.4, and applying MBSSAS software the resulting Guggenheim parameters equalled: a_0=0.673 and a_1= 2.61.

Table 6.13: Aqueous solution compositions measured from undersaturation for samples between the Friedel's salt (NO_2/Al=0) and the nitrite AFm (NO_2/Al=1) at 25±2ºC and after 180 days of equilibration.

Calculated NO_2/Al- ratio (total system)	Ca [mmol/l] (aq)	Al [mmol/l] (aq)	NO_2 [mmol/l] (aq)	Cl [mmol/l] (aq)	pH	Solid phase at end of expriment
0.00	8.82	2.39	0.00	5.79	11.93	Fs
0.10	8.07	2.04	4.61	8.67	11.96	n.d
0.20	9.55	1.85	5.02	8.82	12.09	Ni, Fs
0.30	10.18	1.82	5.53	8.51	12.09	n.d.
0.40	11.16	1.94	6.99	8.42	12.07	n.d.
0.50	11.96	1.93	7.80	8.08	12.08	Ni/Fs
0.60	11.99	2.00	7.32	7.51	12.06	n.d.
0.70	11.72	2.47	7.45	1.59	12.03	Ni/Fs
0.80	11.81	3.84	8.35	1.30	12.04	n.d.
0.90	12.20	2.93	8.33	1.19	12.02	Ni/Fs, $HG_{(traces)}$
1.00	12.93	2.87	9.93	0.00	12.00	Ni, HG

Abbreviations: Ni=NO_2-AFm (nitrite AFm probably slightly substituted with OH), HG=hydrogarnet (katoite), Fs=Friedel's salt (slightly substituted with OH)

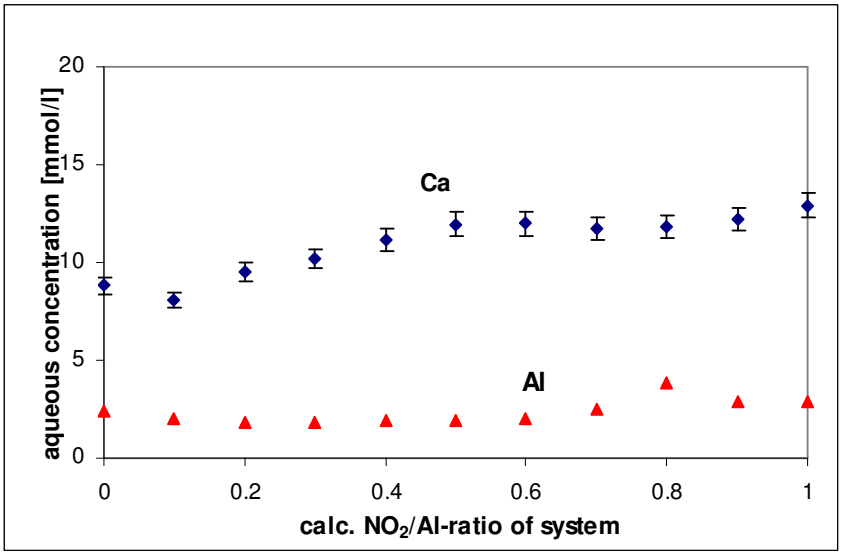

Figure 6.27(a): Equilibrium calcium and aluminium aqueous concentrations commencing from undersaturation for samples between Friedel's salt (NO_2/Al=0)– nitrite AFm (NO_2/Al=1) at 25±2ºC and after 180 days of equilibration. Error bars are shown for Ca.

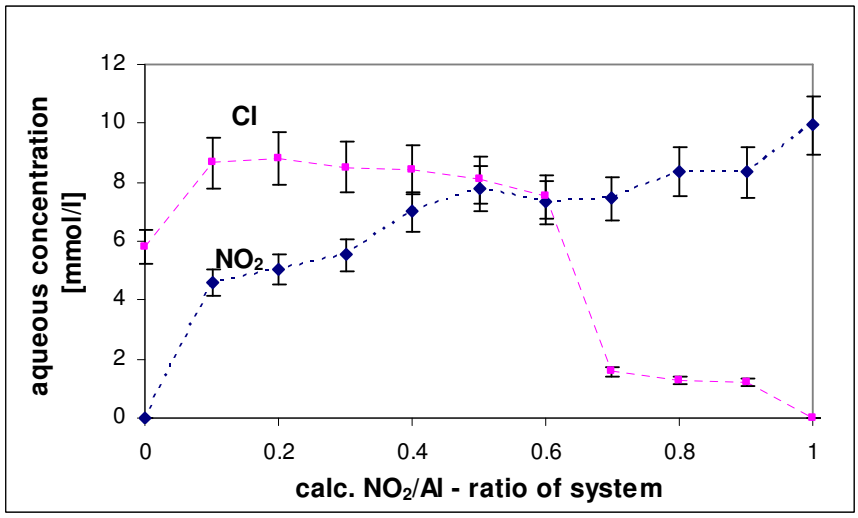

Figure 6.27(b): Equilibrium nitrite and chloride aqueous concentrations commencing from undersaturation for samples between Friedel's salt (NO_2/Al=0) – nitrite AFm (NO_2/Al=1) at 25±2ºC and after 180 days of equilibration.

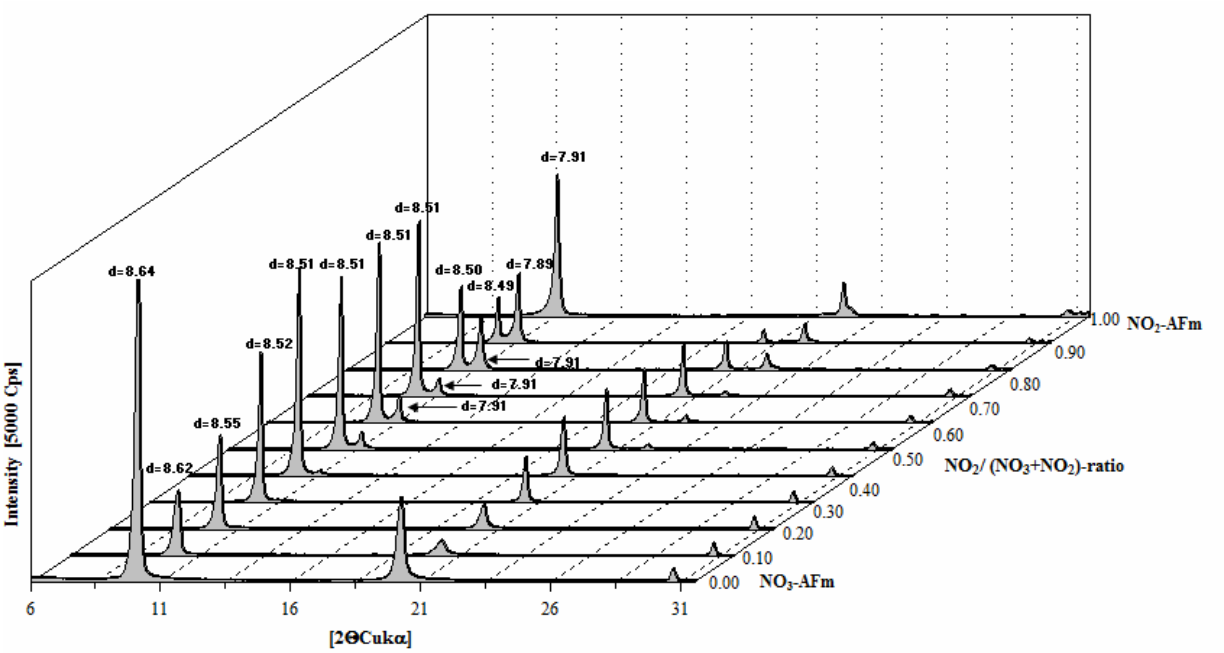

Figure 6.28(a): Partial XRD patterns showing solid solution formation at 25˚C between nitrate AFm and nitrite AFm.

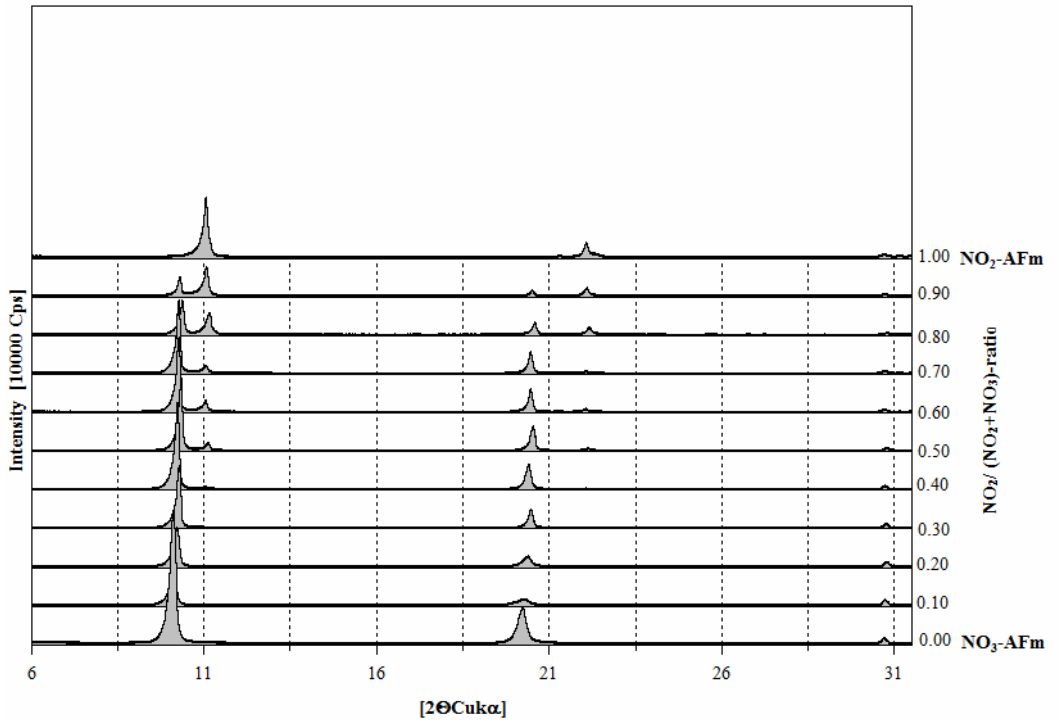

Figure 6.28(b): Partial XRD patterns showing solid solution formation at 25˚C between nitrate AFm and nitrite AFm.

Table 6.14: Aqueous solution compositions measured from undersaturation for samples between the nitrite AFm (NO_3/Al=0) and the nitrate AFm (NO_3/Al=1) at 25±2ºC and after 180 days of equilibration.

Calculated NO_3/Al- ratio (total system)	Ca [mmol/l] (aq)	Al [mmol/l] (aq)	NO_3 [mmol/l] (aq)	NO_2 [mmol/l] (aq)	pH	Solid phase at end of experiment
0.00	12.93	2.87	0.00	9.93	12.00	Ni, HG
0.10	12.61	2.30	2.91	9.45	12.01	n.d
0.20	12.65	2.58	3.02	9.62	12.03	Ni, N, $HG_{(traces)}$
0.30	12.50	1.86	3.69	9.13	12.04	n.d.
0.40	12.32	2.14	3.98	8.42	12.04	n.d.
0.50	12.96	2.88	4.69	8.62	12.03	Ni-N_{ss}
0.60	12.54	2.33	3.82	10.14	12.03	n.d.
0.70	12.01	2.91	4.07	7.96	12.02	n.d.
0.80	8.20	2.80	3.40	2.32	12.01	n.d.
0.90	7.89	2.93	3.18	1.50	12.00	Ni-N_{ss}, HG
1.00	6.95	3.17	3.96	0.00	11.99	N, HG

Abbreviations: Ni=NO_2-AFm (nitrite AFm probably slightly substituted with OH), HG=hydrogarnet (katoite), N=NO_3-AFm (nitrate AFm probably slightly substituted with OH) Ni-N_{ss} =solid solution between NO_2-AFm and NO_3-AFm

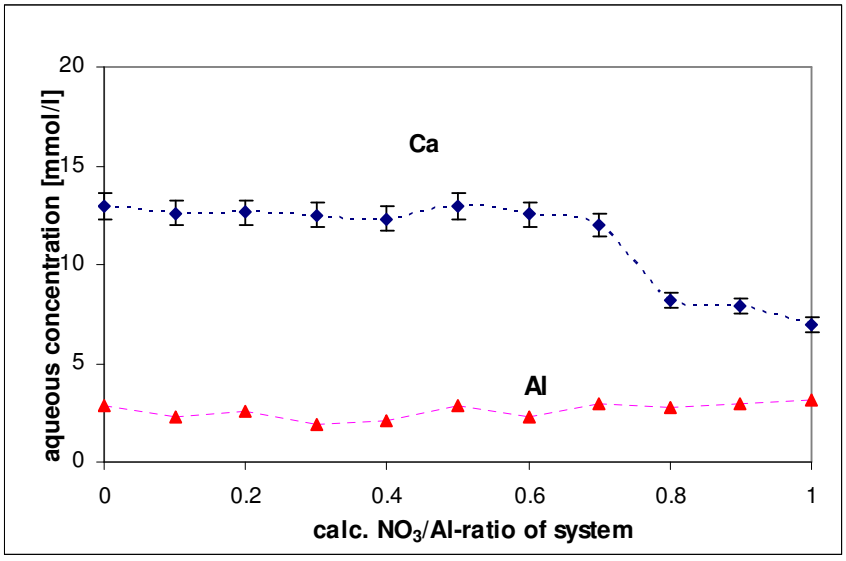

Figure 6.29(a): Equilibrium calcium and aluminium aqueous concentrations commencing from undersaturation for samples between nitrite AFm (NO_3/Al=0)– nitrate AFm (NO_3/Al=1) at 25±2ºC and after 180 days of equilibration.

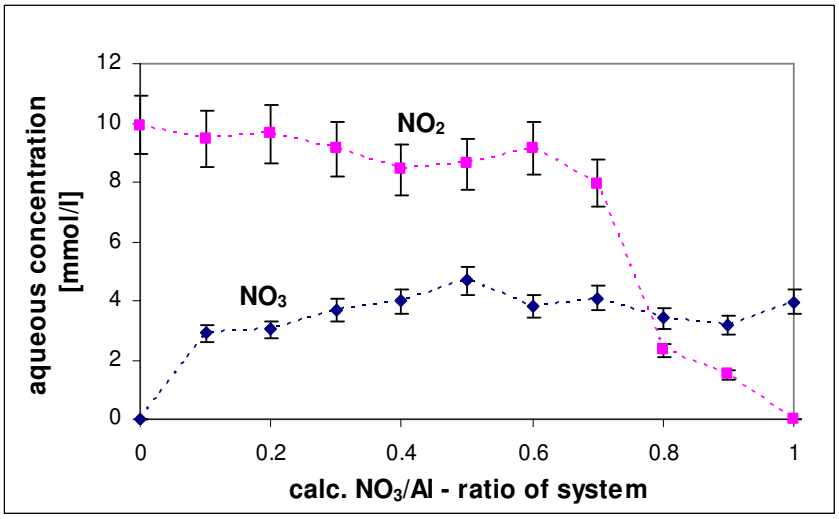

Figure 6.29(b): Equilibrium nitrate and nitrite aqueous concentrations commencing from undersaturation for samples between nitrite AFm (NO_3/Al=0) – nitrate AFm (NO_3/Al=1) at 25±2ºC and after 180 days of equilibration.

Tab. 6.15 was constructed to summarise investigations on solid solutions amongst nitrate/nitrite AFm and other AFm phases.

Table 6.15: Summary of the solid solution investigations amongst nitrate/nitrite AFm and other AFm phases.

Phases	**Phase composition**	**Solid solution**
nitrate AFm and hydroxy AFm	$Ca_4Al_2(OH)_{12}(NO_3)_2 \cdot 4H_2O$ and $Ca_4Al_2(OH)_{14} \cdot 6H_2O$	Incomplete solid solution; NO_3^- in nitrate AFm can be up to around 50% substituted by OH^-; NO_3^- substitution in hydroxy AFm is very slight, < 5%
nitrate AFm and monosulfoaluminate	$Ca_4Al_2(OH)_{12}(NO_3)_2 \cdot 4H_2O$ and $Ca_4Al_2(OH)_{12}(SO_4) \cdot 6H_2O$	No solid solution
nitrate AFm and monocarboaluminate	$Ca_4Al_2(OH)_{12}(NO_3)_2 \cdot 4H_2O$ and $Ca_4Al_2(OH)_{12}(CO_3) \cdot 5H_2O$	No solid solution
nitrate AFm and Friedel's salt	$Ca_4Al_2(OH)_{12}(NO_3)_2 \cdot 4H_2O$ And $Ca_4Al_2(OH)_{12}(Cl)_2 \cdot 4H_2O$	Incomplete solid solution; NO_3^- in nitrate AFm can be up to 50% substituted by Cl^-; NO_3^- substitution in Friedel's salt very slight, < 5%
nitrite AFm and hydroxy AFm	$Ca_4Al_2(OH)_{12}(NO_2)_2 \cdot 4H_2O$ and $Ca_4Al_2(OH)_{14} \cdot 6H_2O$	Incomplete solid solution, NO_2^- in nitrate AFm can be up to around 50% substituted by OH^-; NO_2^- substitution in hydroxy AFm very slight, < 5%
nitrite AFm and monosulfoaluminate	$Ca_4Al_2(OH)_{12}(NO_2)_2 \cdot 4H_2O$ and $Ca_4Al_2(OH)_{12}(SO_4) \cdot 6H_2O$	No solid solution but formation of an ordered compound possible (basal d= 8.42 Å); further research needed
nitrite AFm and monocarboaluminate	$Ca_4Al_2(OH)_{12}(NO_2)_2 \cdot 4H_2O$ and $Ca_4Al_2(OH)_{12}(CO_3) \cdot 5H_2O$	No solid solution
nitrite AFm and Friedel's salt	$Ca_4Al_2(OH)_{12}(NO_2)_2 \cdot 4H_2O$ and $Ca_4Al_2(OH)_{12}(Cl)_2 \cdot 4H_2O$	Solid solution formation but not enough information to define miscibility limits
nitrate AFm and nitrite AFm	$Ca_4Al_2(OH)_{12}(NO_3)_2 \cdot 4H_2O$ and$Ca_4Al_2(OH)_{12}(NO_2)_2 \cdot 4H_2O$	Incomplete solid solution; NO_3^- in nitrate AFm can be up to around 40% substituted by NO_2^-; NO_3^- substitution in nitrite AFm very slight, < 5%

6.6 Ion exchange experiments

To determine how the presence of other ions influence the stability of the nitrate/nitrite AFm, a series of ion exchange experiments were performed. The results are shown in Figs. 6.30-6.41. Mixtures containing 1:1 molar ratios of nitrate AFm/nitrite AFm, portlandite and respectively, calcite, various quantities of calcium sulfate or calcium chloride, calcium nitrite/calcium nitrate were mixed with water and stirred for 180 days at 25˚C±2˚C. The results indicate that portlandite did not influence nitrate/nitrite AFm phases but, due to slight substitution of OH^- into the structures, some ion exchange occurred (Figs. 6.30, 6.36).

Calcite slightly destabilised nitrate/nitrite AFm's and after equilibration some monocarboaluminate was detected (Figs. 6.31, 6.37).

Increasing sulfate content destabilizes nitrate/nitrite AFm phases and results in formation of ettringite (Figs. 6.32, 6.33, 6.38, 6.39). In the case of nitrite AFm at lower calcium sulfate content 'X' phase (see section 6.3.6) was detected which as discussed before may lead to formation of an ordered compound between nitrite AFm and monosulfoaluminate.

Chloride displaces nitrate/nitrite from the AFm structure forming Friedel's salt (Figs 6.34, 6.40). As in the case of nitrite AFm and Friedel's salt, the strongest XRD reflections overlap (see section 6.5.8) an analysis of aqueous phase for nitrite was performed to confirm that displacement occurred. For pure nitrite-AFm/portlandite mixture, nitrite concentration equalled 108 mM [NO_2^-] but after adding calcium chloride, it increased to 398 mM [NO_2^-]. Nitrate AFm is 'more resistant' to chloride displacement and although Friedel's salt formed, some nitrate AFm persisted. Chloride probably needs to be use in an excess to fully displace nitrate from the nitrate AFm.
Nitrite (calcium nitrite) did not displace nitrate from the nitrate AFm (Fig. 6.35). Nitrate (introduced as calcium nitrate) can displace nitrite form the nitrite AFm (Fig. 6.41) and form nitrate AFm.

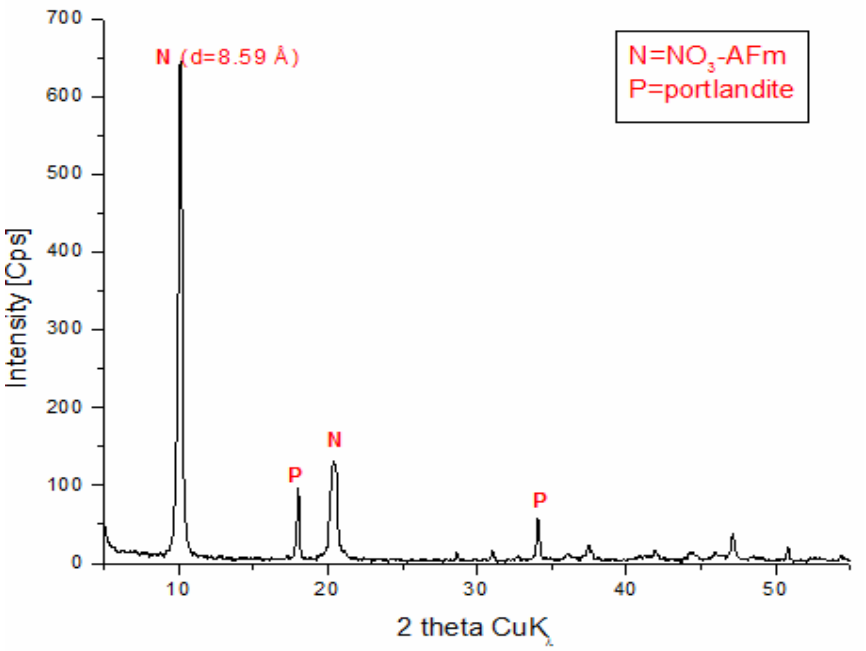

Figure 6.30: XRD patterns showing mineralogical phase assemblage of the mixture containing 0.01 moles nitrate AFm and 0.01 moles $Ca(OH)_2$ which was kept with continuous stirring in 60 ml H_2O at 25±2˚C for 180 days.

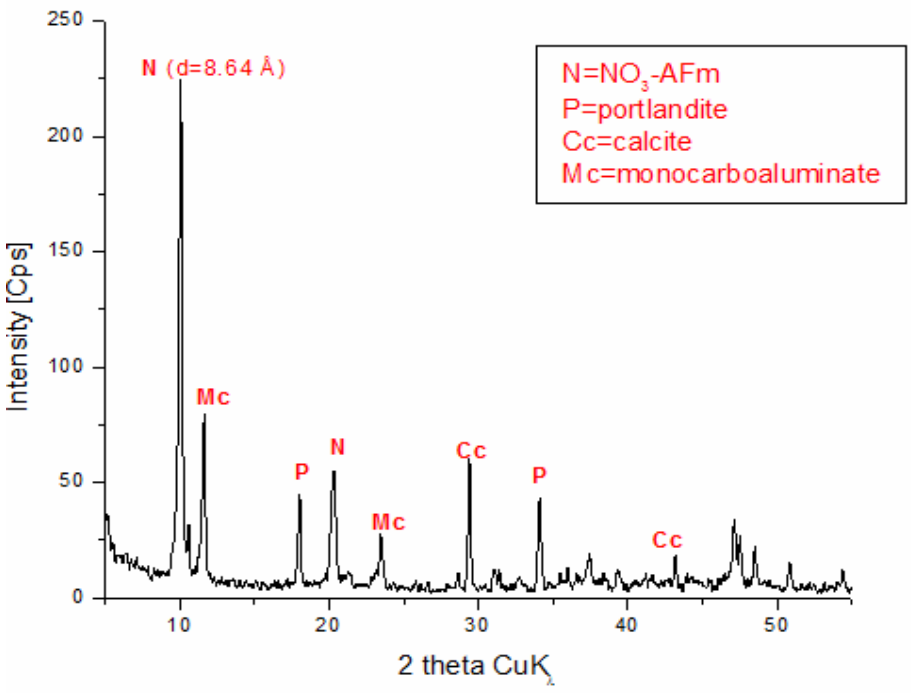

Figure 6.31: XRD patterns showing mineralogical phase assemblage of the mixture containing 0.01 moles nitrate AFm, 0.01 moles $Ca(OH)_2$ and 0.01 moles $CaCO_3$ which was kept with continuous stirring in 60 ml H_2O at 25±2˚C for 180 days.

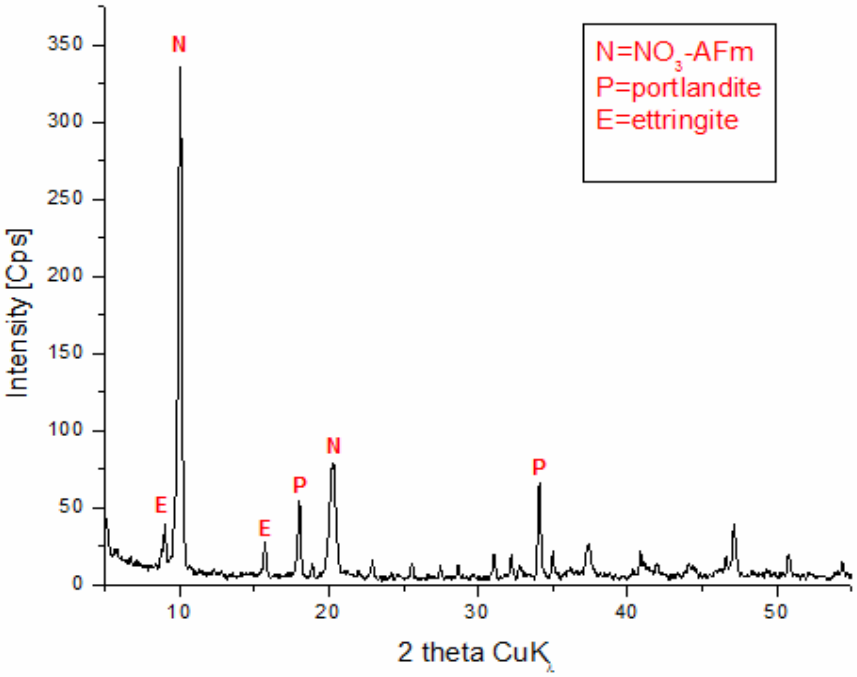

Figure 6.32: XRD patterns showing mineralogical phase assemblage of the mixture containing 0.01 moles nitrate AFm, 0.01 moles $Ca(OH)_2$ and 0.005 moles $CaSO_4$ which was kept with continuous stirring in 60 ml H_2O at 25±2˚C for 180 days.

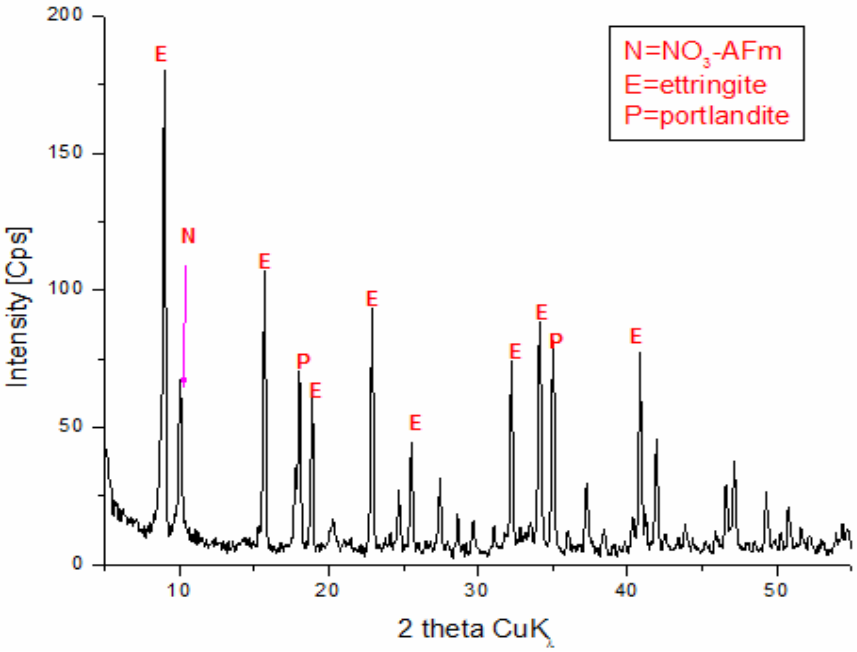

Figure 6.33: XRD patterns showing mineralogical phase assemblage of the mixture containing 0.01 moles nitrate AFm, 0.01 moles $Ca(OH)_2$ and 0.02 moles $CaSO_4$ which was kept with continuous stirring in 60 ml H_2O at 25±2˚C for 180 days.

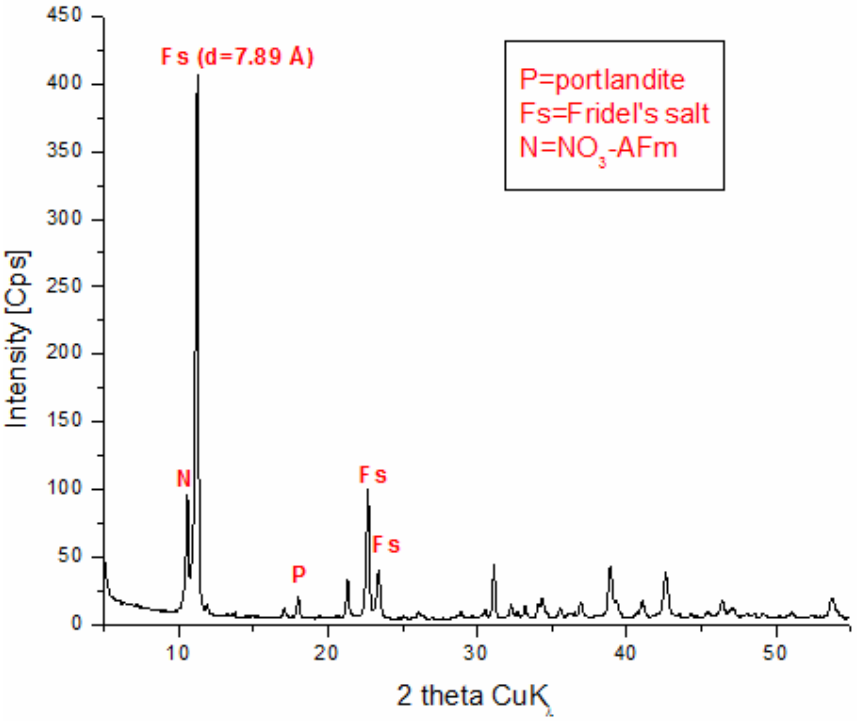

Figure 6.34: XRD patterns showing mineralogical phase assemblage of the mixture containing 0.01 moles nitrate AFm, 0.01 moles $Ca(OH)_2$ and 0.01 moles $CaCl_2$ which was kept with continuous stirring in 60 ml H_2O at 25±2˚C for 180 days.

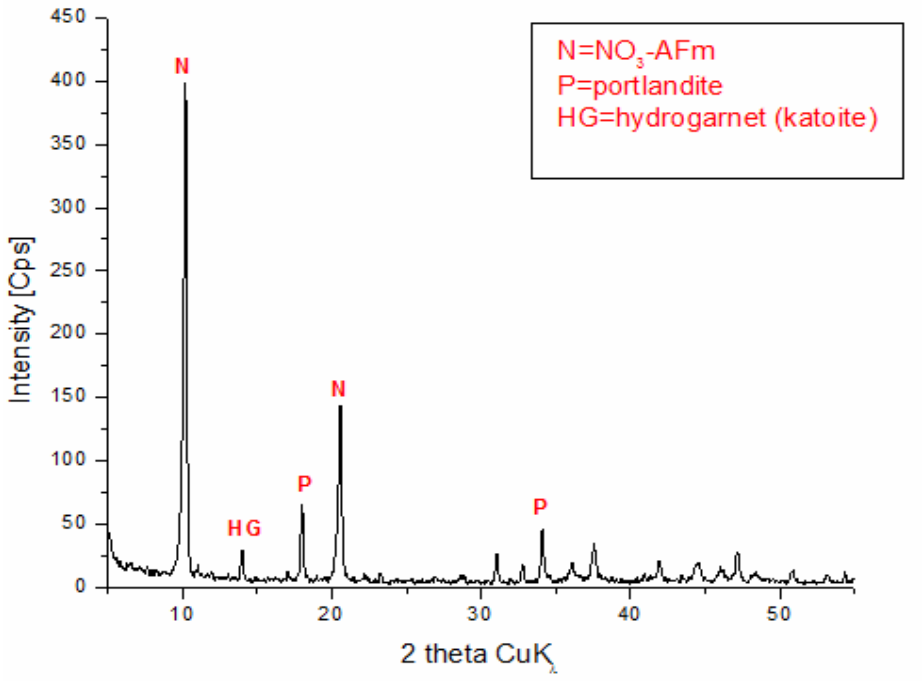

Figure 6.35: XRD patterns showing mineralogical phase assemblage of the mixture containing 0.01 moles nitrate AFm, 0.01 moles $Ca(OH)_2$ and 0.01 moles $Ca(NO_2)_2$ which was kept with continuous stirring in 60 ml H_2O at 25±2˚C for 180 days.

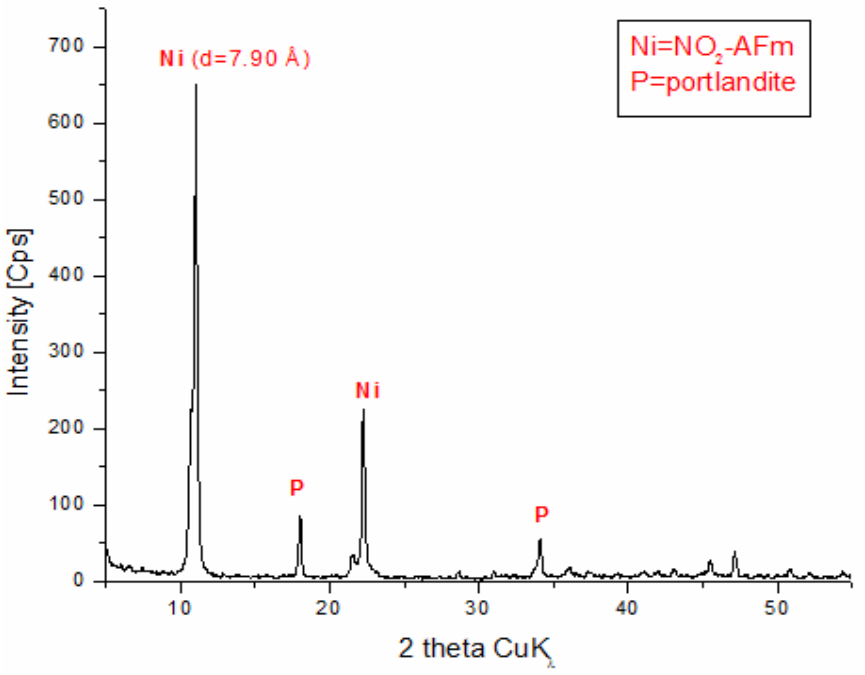

Figure 6.36: XRD patterns showing mineralogical phase assemblage of the mixture containing 0.01 moles nitrite AFm and 0.01 moles $Ca(OH)_2$ which was kept with continuous stirring in 60 ml H_2O at 25±2˚C for 180 days.

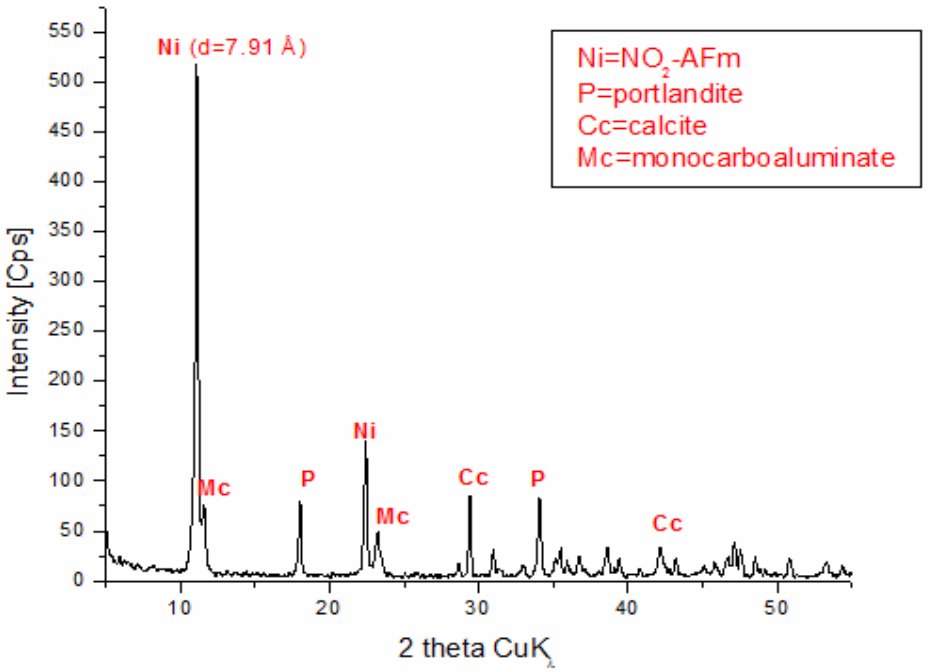

Figure 6.37: XRD patterns showing mineralogical phase assemblage of the mixture containing 0.01 moles nitrite AFm, 0.01 moles $Ca(OH)_2$ and 0.01 moles $CaCO_3$ which was kept with continuous stirring in 60 ml H_2O at 25±2˚C for 180 days.

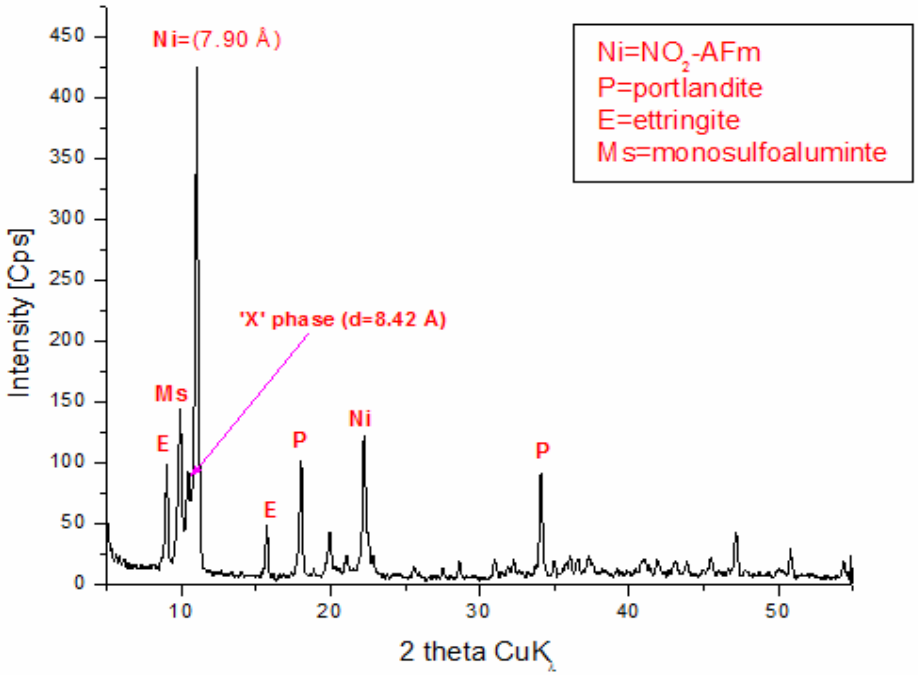

Figure 6.38: XRD patterns showing mineralogical phase assemblage of the mixture containing 0.01 moles nitrite AFm, 0.01 moles $Ca(OH)_2$ and 0.005 moles $CaSO_4$ which was kept with continuous stirring in 60 ml H_2O at 25±2˚C for 180 days.

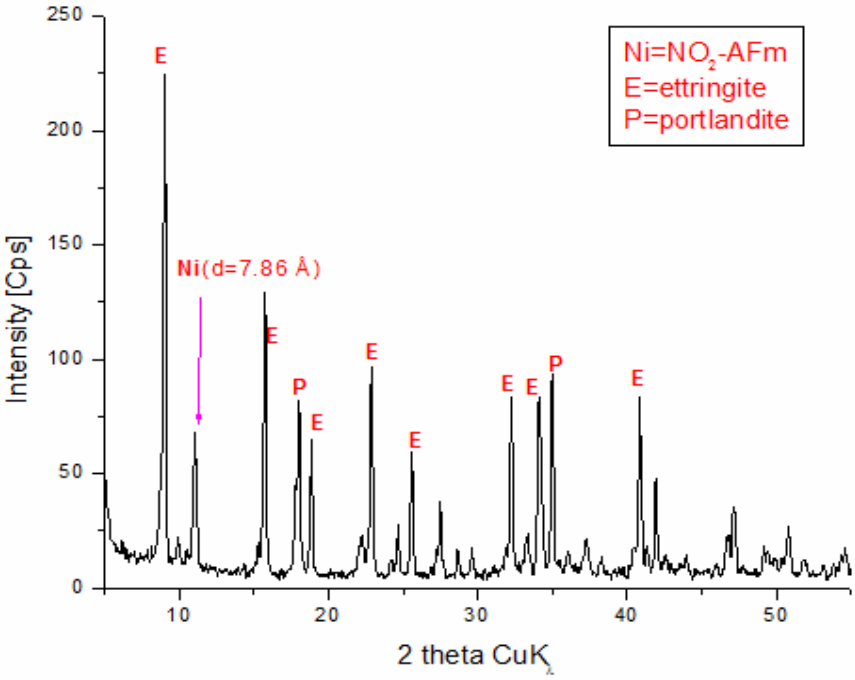

Figure 6.39: XRD patterns showing mineralogical phase assemblage of the mixture containing 0.01 moles nitrite AFm, 0.01 moles $Ca(OH)_2$ and 0.02 moles $CaSO_4$ which was kept with continuous stirring in 60 ml H_2O at 25±2˚C for 180 days.

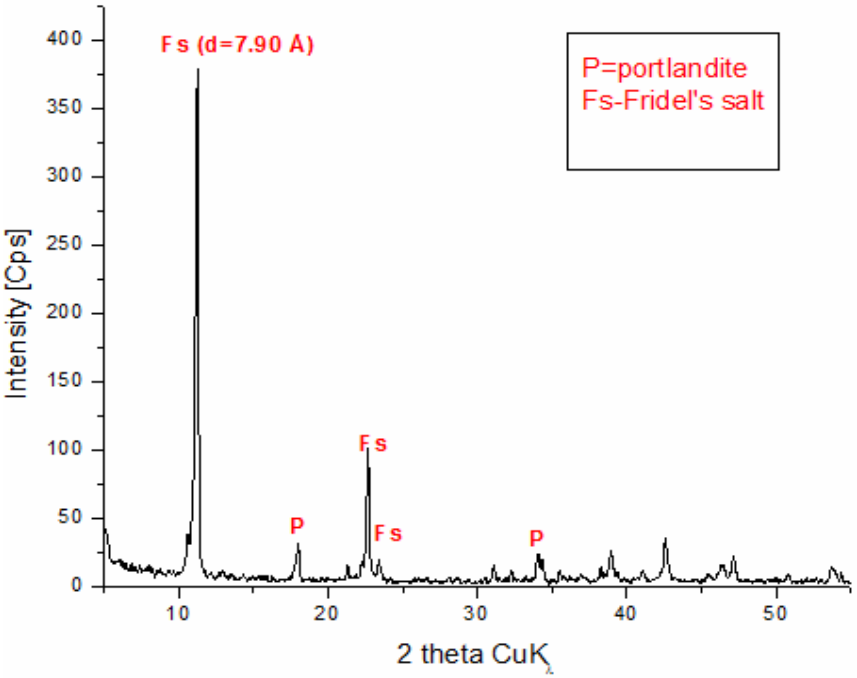

Figure 6.40: XRD patterns showing mineralogical phase assemblage of the mixture containing 0.01 moles nitrite AFm, 0.01 moles $Ca(OH)_2$ and 0.01 moles $CaCl_2$ which was kept with continuous stirring in 60 ml H_2O at 25±2˚C for 180 days.

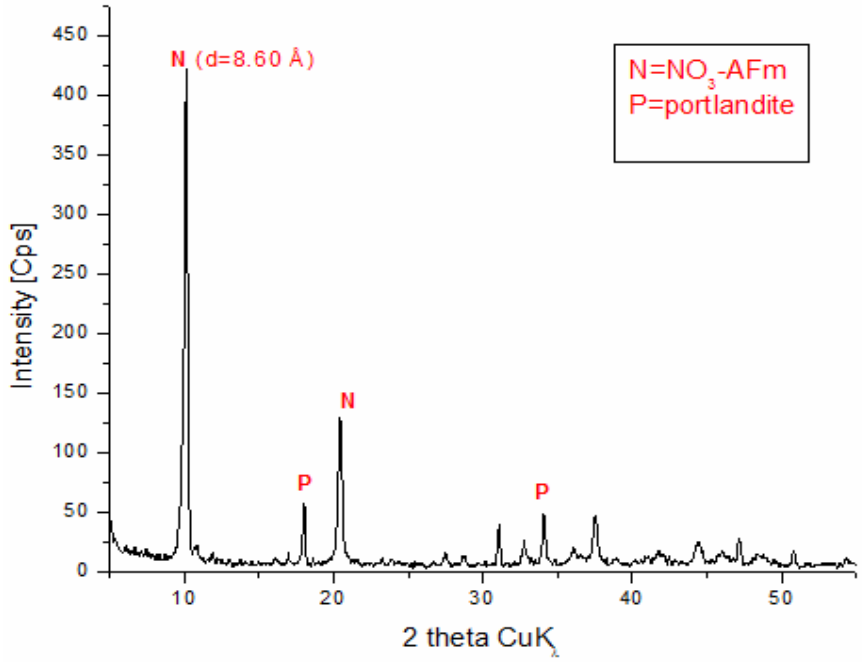

Figure 6.41: XRD patterns showing mineralogical phase assemblage of the mixture containing 0.01 moles nitrite AFm, 0.01 moles $Ca(OH)_2$ and 0.01 moles $Ca(NO_3)_2$ which was kept with continuous stirring in 60 ml H_2O at 25±2˚C for 180 days.

6.7 Interactions of nitrate and nitrite within cement systems

Thermodynamic modelling was performed on the AFm phases in the systems C_3A-$CaSO_4$-$Ca(NO_3)_2$-H_2O, C_3A-$CaSO_4$-$Ca(NO_2)_2$-H_2O and C_3A-$CaSO_4$-$CaCO_3$-$Ca(NO_3)_2$-H_2O, C_3A-$CaSO_4$-$CaCO_3$-$Ca(NO_2)_2$-H_2O. A key purpose of the calculation was to determine the binding power of AFm for nitrate and nitrite in competition with hydroxide, sulfate and carbonate, and compare calculated data on anion distribution with experiment. All calculations assumed alkali-free conditions. The properties of nitrate/nitrite-containing hydrates used in the calculation are presented in Table 6.16. Experimental solubility products were determined using samples equilibrated for 12 months (Tabs. 6.2, 6.5).

Table 6.16: Standard molar thermodynamic properties of nitrate AFm and nitrite AFm at 25˚C.

	log K_{S0}	$\Delta_f G°$ *[kJ/mol]*	$\Delta_f H°$ *[kJ/mol]*	$S°$ *[J/K/mol]*	a_0 *[J/(mol·K)]*	a_1 *[J/(mol·K²)]*	a_2 *[J·K/mol]*	a_3 *[J/(mol·K^0.5)]*	$C°_p$ *[J/K·mol]*	*d* *[kg/m³]*
$C_4A(NO_3)_2H_{10}$	-28.67	-6778	-7719	821	580	1.02	-2.77e+06	872.2	905	2071
$C_4A(NO_2)_2H_{10}$	-26.24	-6606	-7493	799	565	0.99	-2.24e+06	703.3	876	2120

** calculated density; K_{S0}-thermodynamic equilibrium constant at T_o=298 K; $\Delta_f G°$ - standard molar Gibbs energy of formation at T_o= 298 K; $\Delta_f H°$ - standard molar enthalpy at T_o= 298 K; $S°$ - standard molar absolute entropy at T_o= 298 K; a_0, a_1, a_2, a_3 temperature independent empirical parameters characteristic for each solid, $C°_p$- heat capacity at T_o=298 K*

6.7.1 Carbonate- free systems

Calculated phase changes are shown in Figs. 6.42(a) and 6.43(a). They depict the sequence of phase changes occurring in AFm with increasing molar ratio of nitrate (or nitrite) to alumina. Nitrate or nitrite, introduced in the calculation respectively as $Ca(NO_3)_2$ or $Ca(NO_2)_2$, readily displace sulfate from "monosulfoaluminate" which is in solid solution with hydroxy AFm, (designated as SO_4-AFm_{ss}) forming nitrate AFm or nitrite AFm (substituted with OH therefore designated as NO_3-AFm_{ss} NO_2-AFm_{ss}). The reaction is more complex than ion exchange because sulfate, displaced from "monosulfoaluminate'', increases the amount of ettringite and this reaction is thus accompanied by significant volume increase amongst the solids. These calculations find experimental confirmation from data reported by Asaga [288] and Park [298].

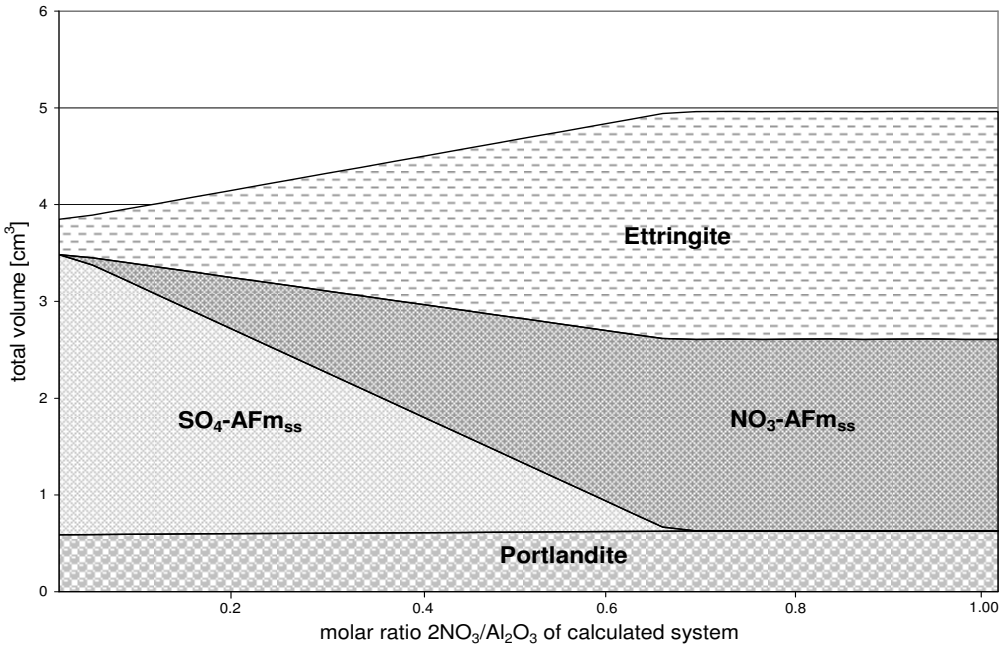

Figure 6.42(a): Calculated total volume of phases of a hydrated model mixture consisting of 0.01 moles C_3A, 60 ml H_2O, 0.015 moles portlandite and with fixed initial sulfate ratio (SO_3/Al_2O_3=1) showing phase development and its dependence on changing nitrate ratios ($2NO_3/Al_2O_3$) at 25°C.

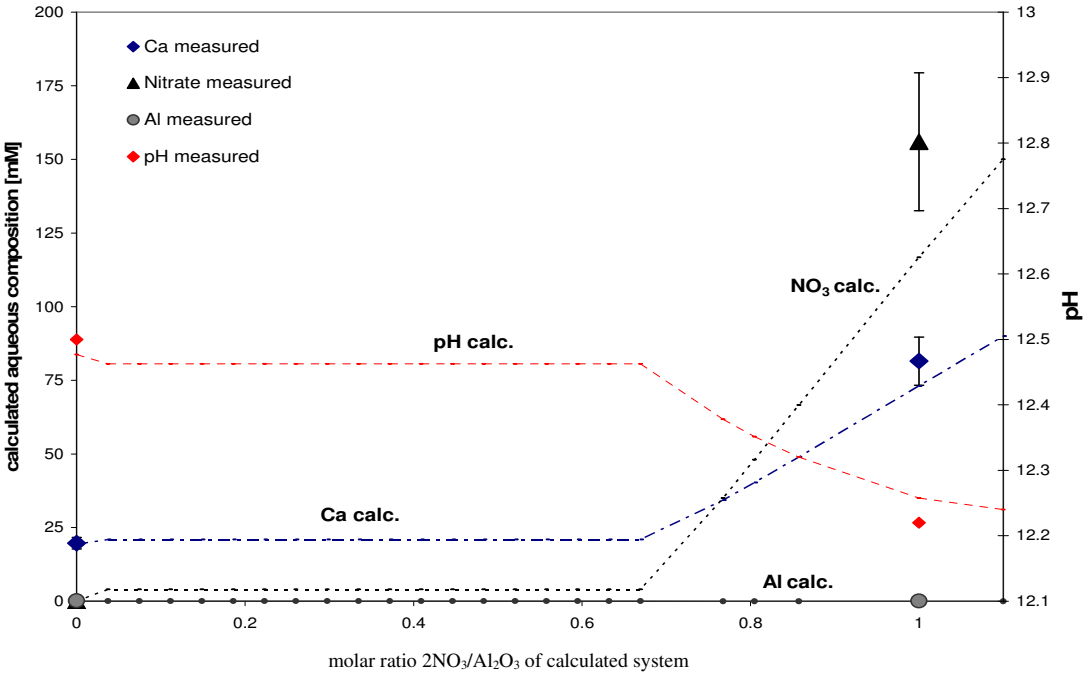

Figure 6.42(b): Calculated and experimental aqueous composition of hydrated model mixture consisting of 0.01 moles C_3A, 0.015 moles portlandite, 60 ml H_2O and with fixed initial sulfate ratio (SO_3/Al_2O_3=1) showing its dependence on changing nitrate ratios ($2NO_3/Al_2O_3$) at 25±2°C. Error bars are shown where appropriate. Note the strong insolubilisation of nitrate at low nitrate: alumina ratios.

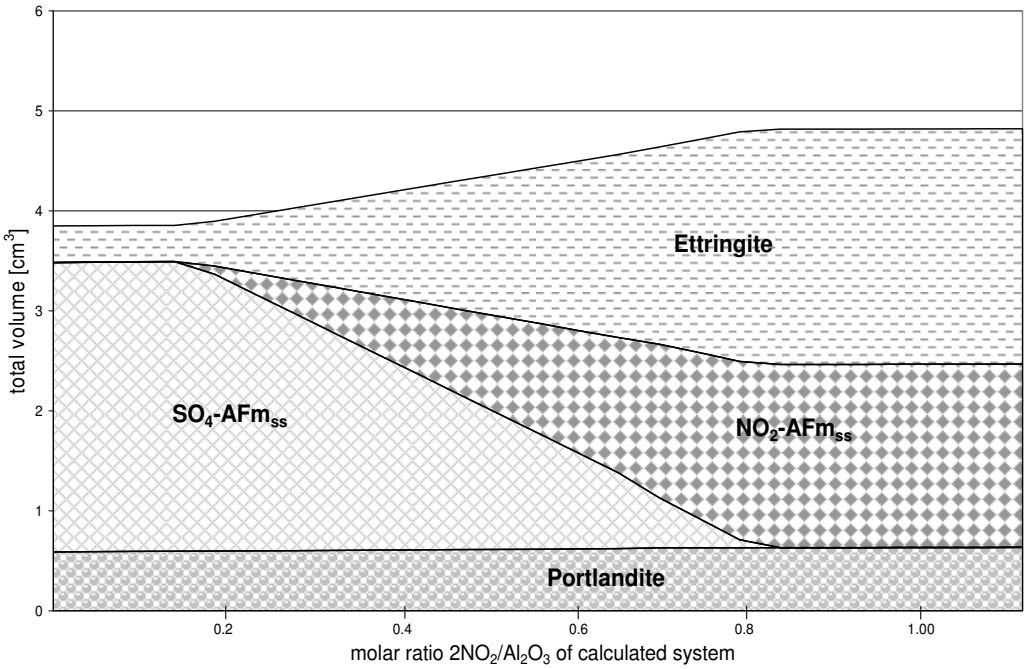

Figure 6.43(a): Calculated total volume of phases of a hydrated model mixture consisting of 0.01 moles C_3A, 60 ml H_2O, 0.015 moles portlandite and with fixed initial sulfate ratio (SO_3/Al_2O_3=1) showing phase development and its dependence on changing nitrite ratios ($2NO_2/Al_2O_3$) at 25°C.

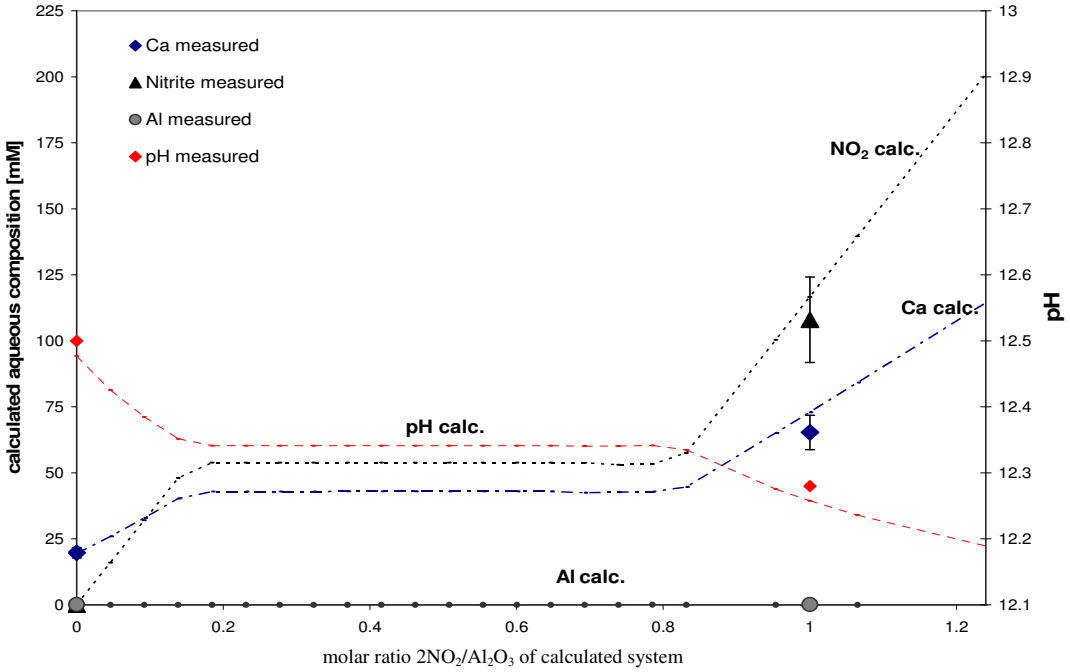

Figure 6.43(b): Calculated and experimental aqueous composition of hydrated model mixture consisting of 0.01 moles C_3A, 0.015 moles portlandite, 60 ml H_2O and with fixed initial sulfate ratio (SO_3/Al_2O_3=1) showing its dependence on changing nitrite ratios ($2NO_2/Al_2O_3$) at 25±2°C. Error bars are shown where appropriate.

Experimental results on a phase assemblage containing: 0.01 moles C_3A, 0.01 moles $CaSO_4$, 0.015 moles $Ca(OH)_2$ and equilibrated at 25˚C for 45 days in 60 ml H_2O are shown in Fig. 6.44, plot 1; the phases formed were identified as monosulfoaluminate in solid solution with hydroxy AFm, (marked as Ms), portlandite (P) and minor amounts of ettringite. In the course of reaction with $Ca(NO_3)_2$ or $Ca(NO_2)_2$, phase changes occur (plots 2-3): sulfate is displaced from monosulfoaluminate while nitrate AFm (plot 2)/nitrite AFm (plot 3) form. Sulfate ions liberated from AFm form ettringite (marked as E in plots 2-3). Thus experiment confirms the calculated reaction sequence. Aqueous compositions (simulated and measured) are compared in Figs. 6.42(b) and 6.43(b).

Changes in the slope of concentrations (Fig. 6.42(b), 6.43(b)) result from the changes in the nature of the solid phases (see Fig. 6.42(a), 6.43(a)).

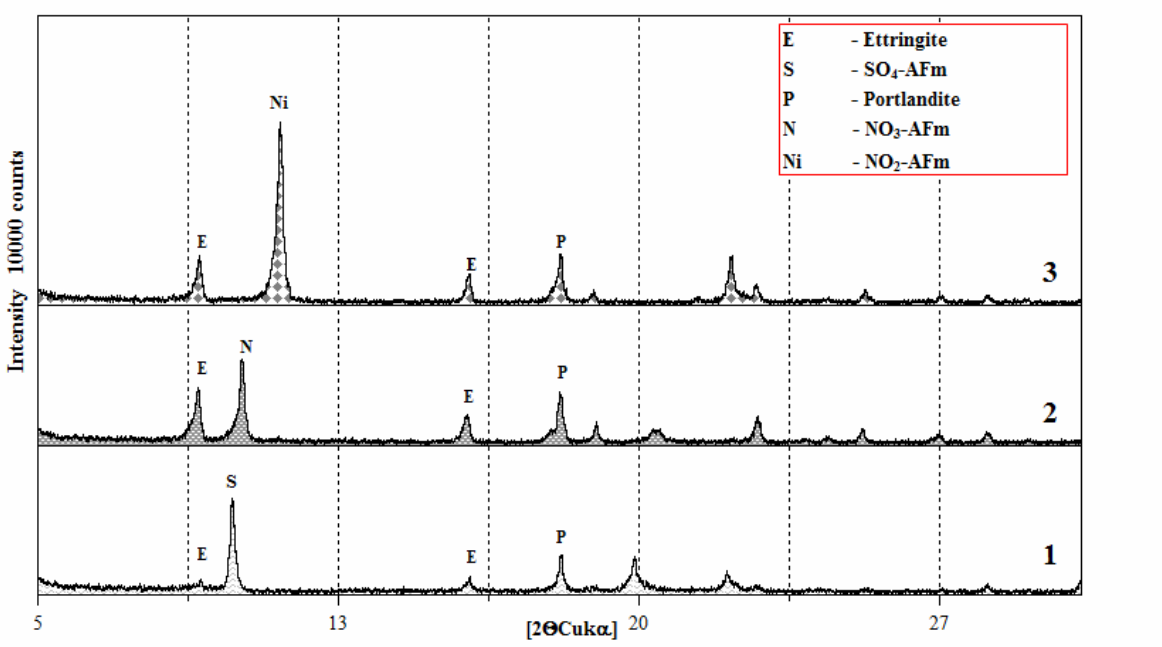

*Figure 6.44: XRD patterns showing mineralogical changes and influence of $Ca(NO_3)_2$/$Ca(NO_2)_2$ addition for the system: 0.01 moles C_3A-0.01 moles $CaSO_4$-0.015 moles $Ca(OH)_2$- 60 ml H_2O at 25±2˚C; respectively plots: **1**-no $Ca(NO_3)_2$/$Ca(NO_2)_2$ present; **2**-0.01 moles of $Ca(NO_3)_2$ added; **3**-0.01 moles $Ca(NO_2)_2$ added.*

6.7.2 Carbonate- containing systems

Calculated phase changes for the system C_3A-$CaSO_4$-$Ca(NO_3)_2$-$CaCO_3$-H_2O and C_3A-$CaSO_4$-$Ca(NO_2)_2$-$CaCO_3$-H_2O are presented in Figs. 6.45(a) and 6.46(a). Calculations commenced with mixtures of monocarboaluminate, portlandite and ettringite and reveal the impacts of nitrite and nitrate on the model compositions. With rising nitrate/nitrite content, carbonate ions are displaced from monocarboaluminate, forming nitrate AFm /nitrite AFm respectively (slightly substituted with OH therefore designated as NO_3-AFm_{ss} NO_2-AFm_{ss}); carbonate ions thus liberated from AFm form calcite. An experimental verification was made by equilibrating, for 45 days at 25ºC, a mixture containing: 0.01 moles C_3A, 0.01 moles $CaSO_4$, 0.015 moles $Ca(OH)_2$, 0.0075 moles $CaCO_3$ and 60 ml H_2O: Fig. 6.47 shows the results. Initially-formed phases (plot 1) were identified as monocarboaluminate (marked as Mc) portlandite (P) and ettringite (E). In the course of admixing $Ca(NO_3)_2$/$Ca(NO_2)_2$, carbonate is displaced from monocarboaluminate and nitrate AFm (plot 2)/nitrite AFm (plot 3) form instead. Carbonate displaced from monocarboaluminate, forms calcite (marked as Cc). Thus calcite can be formed even at constant carbonate content, *i.e.*, without introduction of additional carbonate from an external source, by displacement of CO_3^{2-} from carbonate-containing AFm solids and interaction with $Ca(OH)_2$. Although nitrate and nitrite have the same formal impact on calcium monocarboaluminate, the energetics of the situation is that nitrate much more readily displaces carbonate than does nitrite. Also, volume changes for both nitrate and nitrite are much reduced relative to those calculated to occur in the carbonate -free system: Figs. 6.45(b) and 6.46(b) compare calculated and measured aqueous compositions. Changes in the slope of concentrations (Figs. 6.45(b), 6.46(b)) result from the changes in the nature of the solid phases (see Figs. 6.45(a), 6.46(a)).

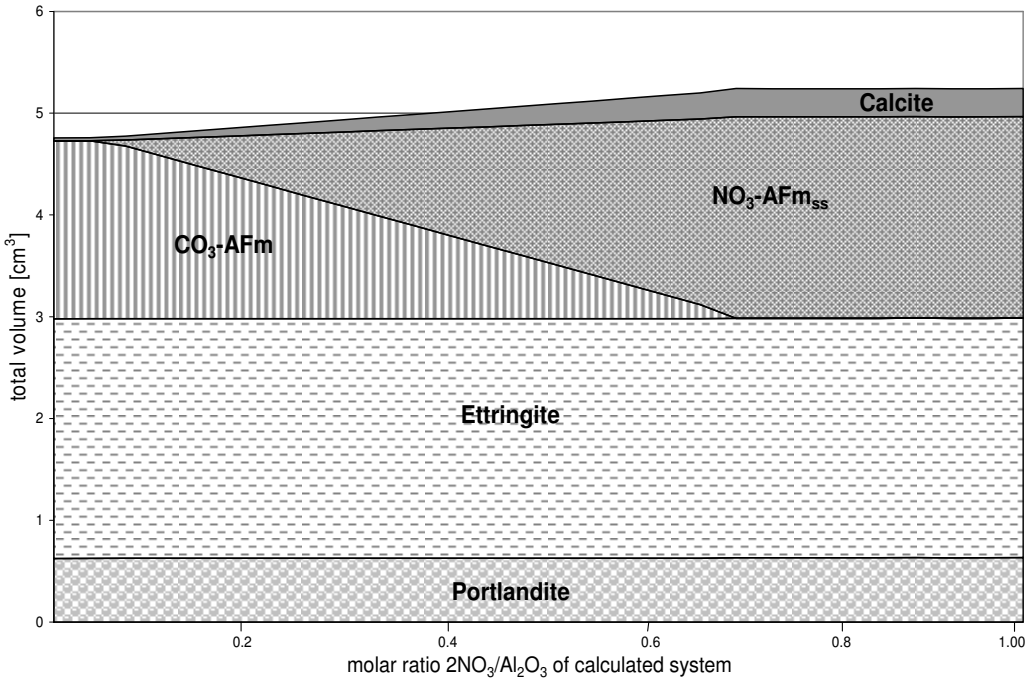

Figure 6.45(a): Total volume of phases of a hydrated model mixture consisting of 0.01 moles C_3A, 60 ml H_2O, 0.015 moles portlandite, 0.0075 moles $CaCO_3$ and with fixed initial sulfate ratio (SO_3/Al_2O_3=1) showing phase development and its dependence on changing nitrate ratios ($2NO_3/Al_2O_3$) at 25°C.

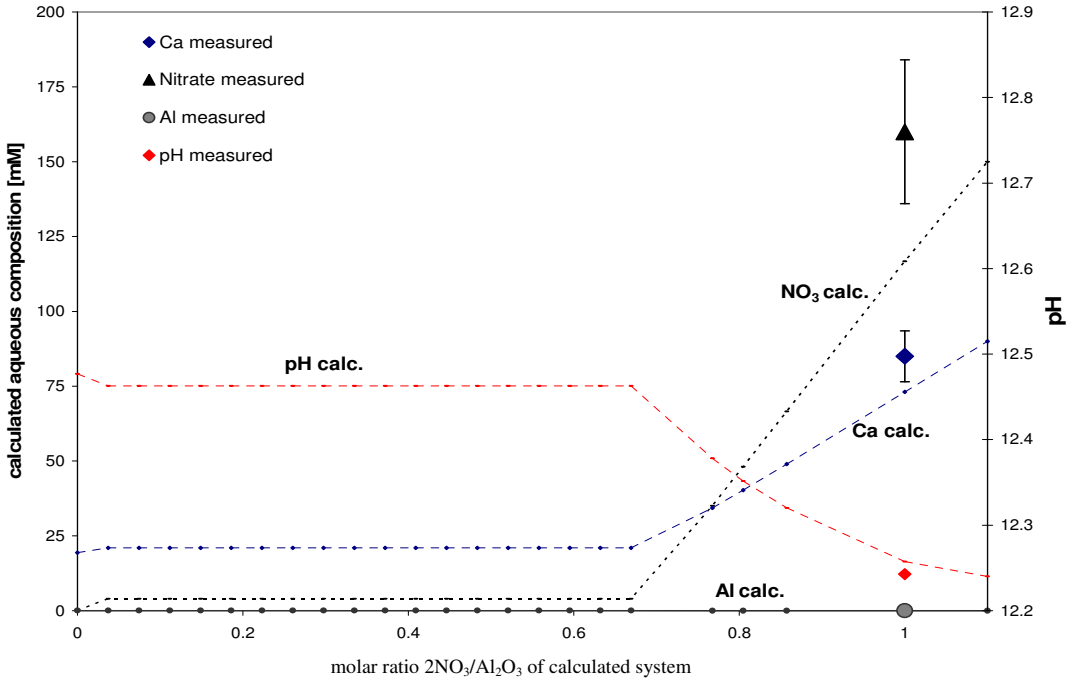

Figure 6.45(b): Calculated and experimental aqueous composition of hydrated model mixture consisting of 0.01 moles C_3A, 0.015 moles portlandite, 0.0075 mol $CaCO_3$, 60 ml H_2O and with fixed initial sulfate ratio (SO_3/Al_2O_3=1) showing its dependence on changing nitrate ratios ($2NO_3/Al_2O_3$) at 25±2°C. Error bars are shown where appropriate.

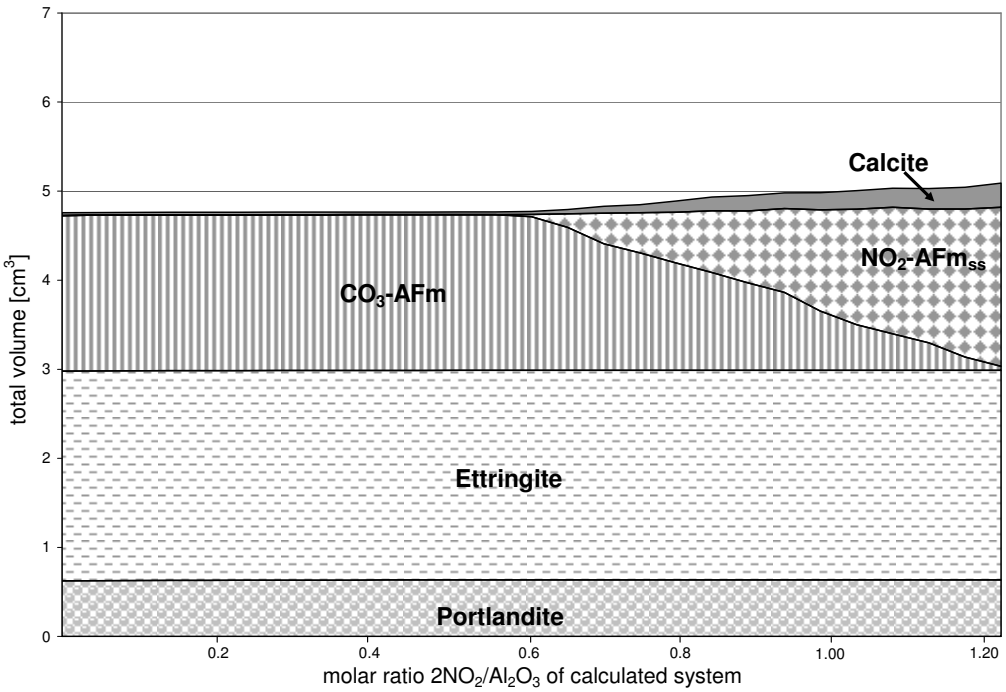

Figure 6.46(a): Total volume of phases of a hydrated model mixture consisting of 0.01 moles C_3A, 60 ml H_2O, 0.015 moles portlandite, 0.0075 moles $CaCO_3$ and with fixed initial sulfate ratio (SO_3/Al_2O_3=1) showing phase development and its dependence on changing nitrite ratios ($2NO_2/Al_2O_3$) at 25°C.

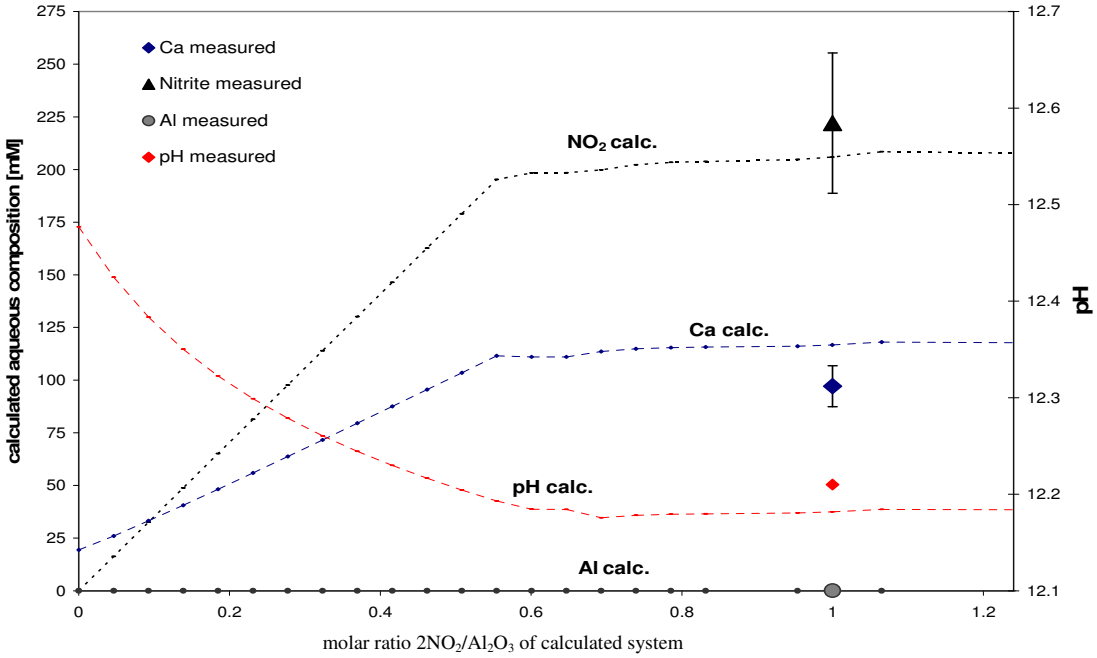

Figure 6.46(b): Calculated and experimental aqueous composition of hydrated model mixture consisting of 0.01 moles C_3A, 0.015 moles portlandite, 0.0075 mol $CaCO_3$, 60 ml H_2O and with fixed initial sulfate ratio (SO_3/Al_2O_3=1) showing its dependence on changing nitrite ratios ($2NO_2/Al_2O_3$) at 25±2°C. Error bars are shown where appropriate.

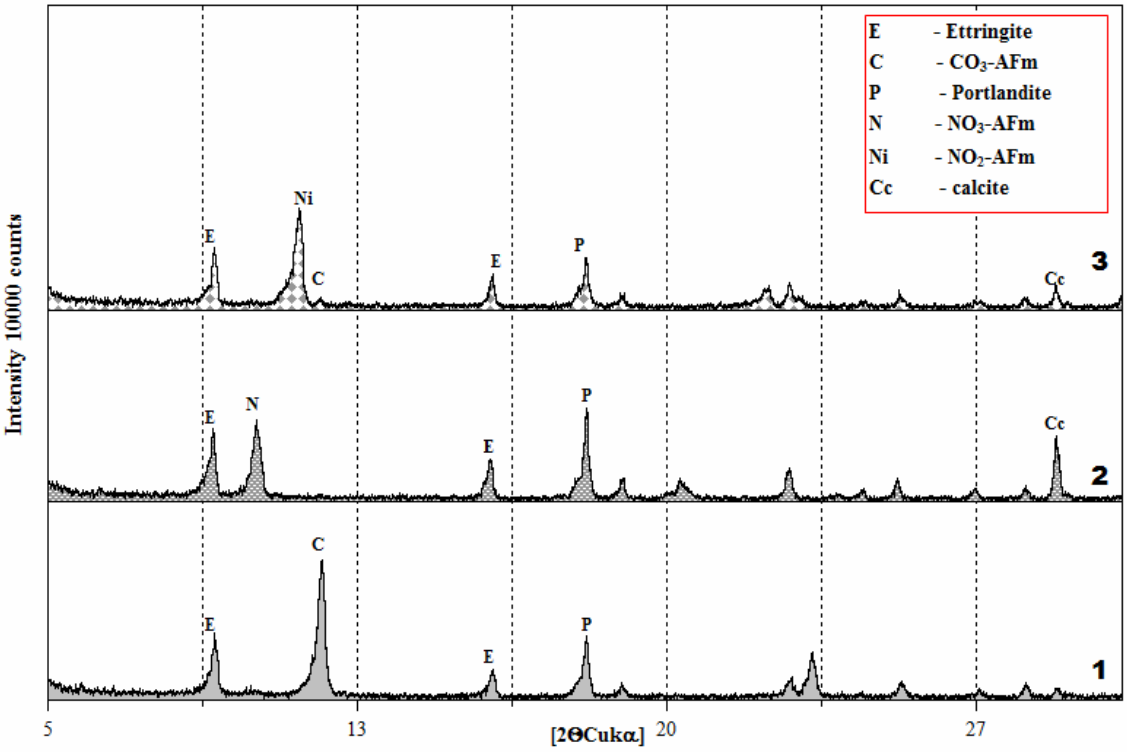

*Figure 6.47: XRD patterns showing mineralogical changes and influence of $Ca(NO_3)_2/Ca(NO_2)_2$ addition for the system 0.01 moles C_3A-0.01 moles $CaSO_4$-0.015 moles $Ca(OH)_2$-0.0075 moles $CaCO_3$- 60 ml H_2O at 25±2˚C; **1**-no $Ca(NO_3)_2/Ca(NO_2)_2$ present; **2**-0.01 moles of $Ca(NO_3)_2$ added; **3**-0.01 moles of $Ca(NO_2)_2$ added.*

6.7.3 Influence of temperature

To illustrate the influence of temperature on the phase assemblages, GEMS simulations were run for selected compositions over the range of temperatures 0-99˚C (Figs. 6.48, 5.29-6.51). Calculations were performed for carbonate-free systems assuming SO_2/Al_2O_3 ratio of 1.0 and initial $2NO_3/Al_2O_3$ $2NO_2/Al_2O_3$ of 0.5 (Figs. 6.48, 6.50) and 1.0 (Figs. 6.49, 6.51). At lower $2NO_3/Al_2O_3$ ratios of 0.5, nitrate AFm persists up to around 58˚C (Fig. 6.48) but at higher ratio, 1.0, up to 70˚C (Fig. 6.49) above which only monosulfoaluminate and portlandite are present. At ratio 0.5 (Fig. 6.50), nitrite AFm disappears at ~35˚C and AFt reduces leaving mainly monosulfoaluminate. Nitrite AFm persists at higher $2NO_2/Al_2O_3$ ratio of 1.0 up to 60˚C. It is worth remembering that conversion is not fixed to particular temperature but strongly depends on the initial composition of the system especially the SO_3/Al_2O_3 ratios.

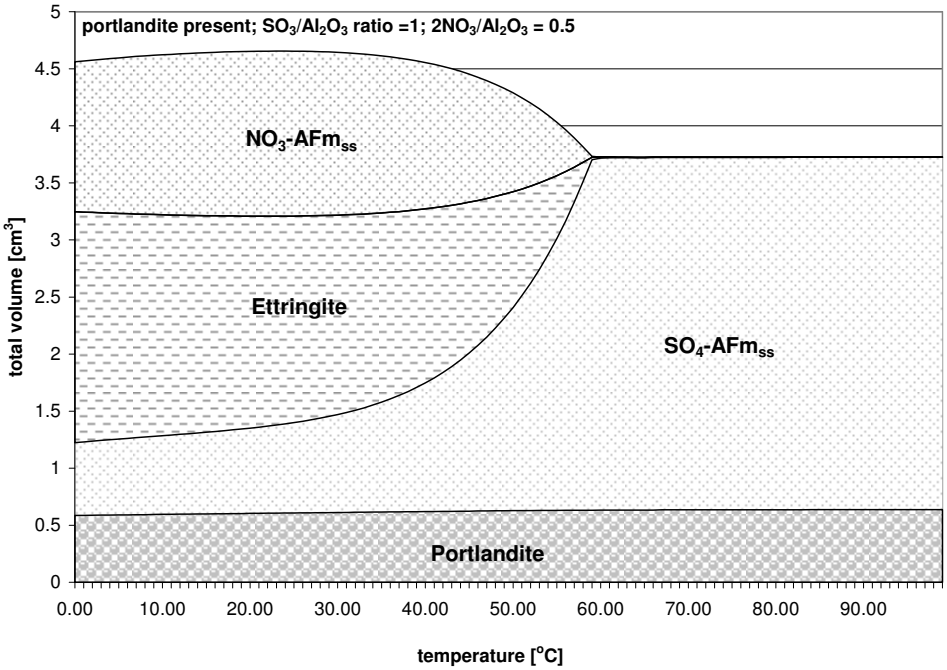

Figure 6.48: Calculated total volume of solid phases of a hydrated model mixture initially consisting of 0.01 moles C_3A, 60 ml H_2O, 0.015 moles portlandite and with fixed initial sulfate ratio (SO_3/Al_2O_3=1) and nitrate ratio ($2NO_3/Al_2O_3$=0.5) showing phase development and its dependence on changing temperature.

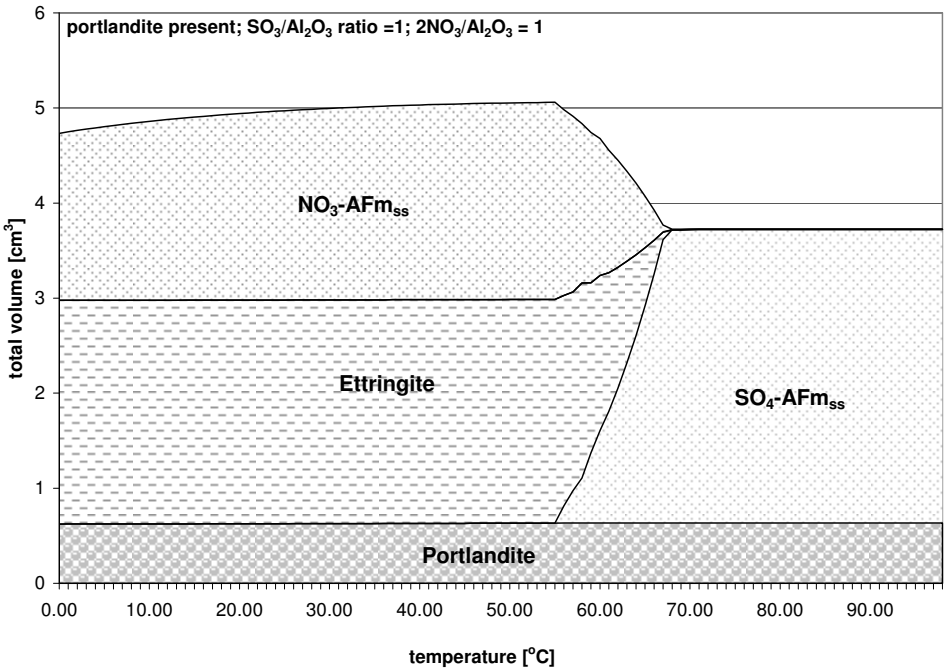

Figure 6.49: Calculated total volume of solid phases of a hydrated model mixture initially consisting of 0.01 moles C_3A, 60 ml H_2O, 0.015 moles portlandite and with fixed initial sulfate ratio (SO_3/Al_2O_3=1) and nitrate ratio ($2NO_3/Al_2O_3$=1) showing phase development and its dependence on changing temperature.

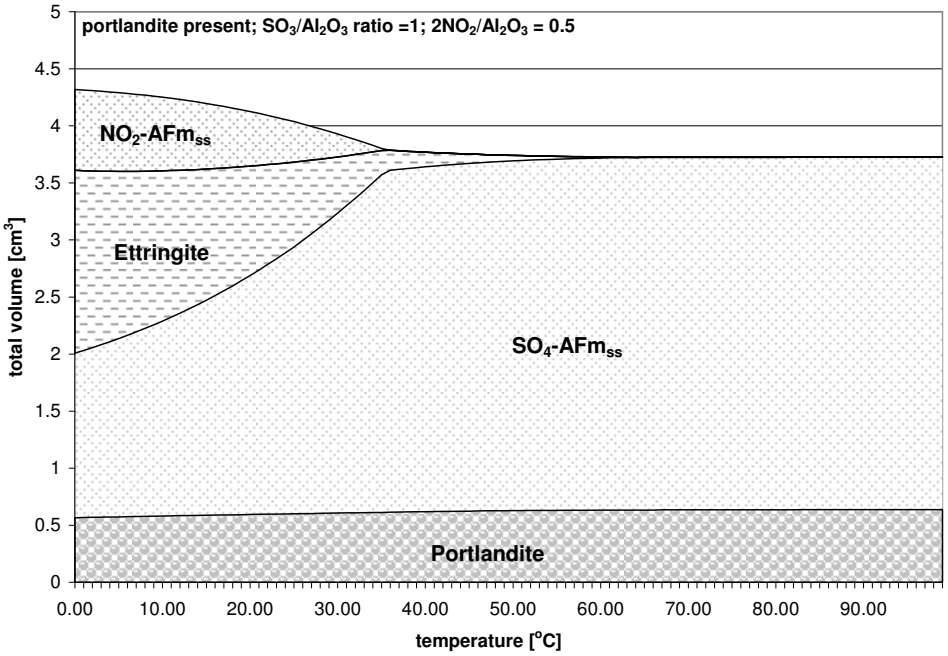

Figure 6.50: Calculated total volume of solid phases of a hydrated model mixture initially consisting of 0.01 moles C_3A, 60 ml H_2O, 0.015 moles portlandite and with fixed initial sulfate ratio (SO_3/Al_2O_3=1) and nitrite ratio ($2NO_2/Al_2O_3$=0.5) showing phase development and its dependence on changing temperature.

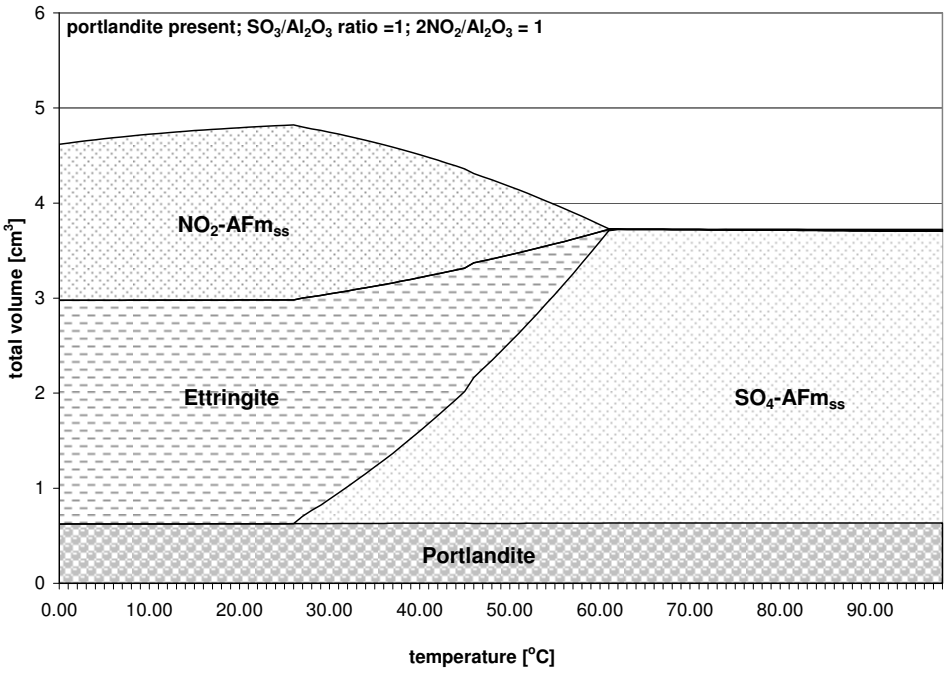

Figure 6.51: Calculated total volume of solid phases of a hydrated model mixture initially consisting of 0.01 moles C_3A, 60 ml H_2O, 0.015 moles portlandite and with fixed initial sulfate ratio (SO_3/Al_2O_3=1) and nitrite ratio ($2NO_2/Al_2O_3$=1) showing phase development and its dependence on changing temperature.

6.7.4 Practical implications

To assess the impact of nitrate and nitrite on cement properties, Tab. 6.17 has been constructed to show the relationships between dose rate and the units used in calculations. The Table is calculated for several cement alumina contents and assumes a uniform sulfate content, as SO_3, of 3.15 wt% and an added 1 wt% of either $Ca(NO_3)_2$ or $Ca(NO_3)_2$. The calculated ratio can then be transposed to the relevant Figures. Since the Figures are calculated for SO_3/Al_2O_3 ratio =1, only the first dataset can be transposed without correction. Other SO_3/Al_2O_3 ratios commence with different initial AFt/AFm balances but thereafter, upon addition of nitrate/nitrite, will exhibit similar trends. In the specimen calculation, nitrate and nitrite ratios are low, 0.155 and 0.19 respectively. Transposing the nitrate ratio to Fig. 6.42(a) for carbonate-free cement shows that the process of conversion of SO_4-AFm to NO_3-AFm is underway and the amount of conversion is sensitive to the % nitrate added. It is unlikely that sufficient nitrate or nitrite will be added in commercial practise to complete the process of maximising ettringite unless the cement has a high initial SO_3/Al_2O_3 ratio. Other factors being equal, more AFm will equate with greater binding capacity of the paste for nitrate and nitrite.

Using a carbonate-containing cement, Figs. 6.45(a) and 6.45(b) discloses that the pore fluid composition is very low in nitrate while the rate of volume change attending changing nitrate ratios is also low.

Table 6.17: Example of conversion factors for cements with various Al_2O_3 content, constant of SO_3=3.15 wt%, plus added $Ca(NO_3)_2$ or $Ca(NO_3)_2$ at 1 wt%.

Al_2O_3	SO_3/Al_2O_3	$2NO_3/Al_2O_3$	$2NO_2/Al_2O_3$
4 wt%	1	0.155	0.19
6 wt%	0.66	0.10	0.12
8 wt%	0.5	0.077	0.096

6.8 Discussion

$Ca_4Al_2(NO_3)_2(OH)_{12}\cdot 4H_2O$ and $Ca_4Al_2(NO_2)_2(OH)_{12}\cdot 4H_2O$ dissolve incongruently. The water content of nitrate AFm was found to be very sensitive to humidity conditions. This can influence the amount of bound water and the physical density of the AFm

phase. Nitrite AFm, on the other hand, has a relatively stable water content over a normal range of moisture conditions. As estimated and observed experimentally, cement has the capability to bind both nitrate/nitrite. This capacity is limited by several factors but the maximum amount of nitrate AFm/nitrite AFm which can form will be limited by the alumina content of cement and by temperature, because both nitrate AFm and nitrite AFm are destabilised with increasing temperature. At constant temperature 25ºC, such that nitrate AFm or nitrite AFm are stable, the binding is still complex, as nitrate or nitrite ions must compete with other anions for binding sites in AFm. To calculate the contribution of AFm to the binding potential, we placed restrictions on the calculations, to keep them as generic as possible. The first condition imposed is that the aqueous phase (cement pore fluid) pH is > 12, as would occur if $Ca(OH)_2$ and/or high calcium C-S-H were present. The second condition is that the activity of sulfate and carbonate are fixed by the equilibration of pore fluid with ettringite and calcite, respectively.

The disposition of nitrite and nitrate in a hydrated cement paste depends on the presence or absence and, if present, on the amount of carbonate. Carbonate may be added to the cement, perhaps as a blending agent, but if not added, it may subsequently be gained in service conditions (from unavoidable pre-hydration and carbonation during grinding, transport, and storage).

The impacts arising from the presence or absence of carbonate in the presence of varying nitrate can be seen by comparing Figs. 6.42(a) and 6.45(a). The explanation assumes that sufficient carbonate is added to saturate and react with all the alumina forming CO_3-AFm; the 5 wt% frequently added is sufficient and will leave a surplus of $CaCO_3$ which is neglected here. The carbonate free cement will start with an AFm phase which is essentially SO_4-AFm but with some OH substituting for sulfate: Matschei, et al. [9] give a “finder” diagram with which to predict the AFm composition. As the nitrate ratio, $2NO_3/Al_2O_3$, increases, sulfate AFm rapidly decreases in amount while ettringite develops. The better space filling properties of ettringite contribute to densification of the matrix: the more nitrate is added (up to a point) the stronger will be the densification process.

If instead we follow the evolution of a carbonate-blended cement, the initial AFm state would consist of monocarboaluminate and a rather high threshold of the nitrate ratio is required to initiate its conversion to NO_3-AFm. Ettringite is not significantly affected by the process although at low temperatures (the calculations are done for 25˚C) ettringite

may well be able to expand its range of compositions by absorbing the $CaCO_3$ formed upon progressive addition of nitrate [53, 56].

At 25˚C, the specific volume attending nitrate additions increases, but only slightly, in the presence of calcite. As noted, carbonate liberated from AFm forms calcite thereby decreasing the $Ca(OH)_2$ content (not shown on diagrams, but assumed to be present in excess). It can also be seen that the overwhelming fraction of nitrate must be in the solid: reference to Figs. 6.42(b) and 6.45(b) shows that the nitrate content of the pore fluid is less than 10 mM at all nitrate ratios up to ~0.7. However nitrite solubility is always much higher. This has the advantage that it is chemically available in pore fluid but has the potential disadvantage of being more leachable than nitrate. Fig. 6.46(b) indicates that a fixed proportionality exists between nitrite added and soluble nitrite up to about 200 mM. Thus in commercial cements, nitrite will be available in pore fluid to act as a corrosion inhibitor, in contrast to nitrate which is effectively locked into solids.

Where cement is in contact with water high in nitrate/nitrite concentrations, and once the AFm phase is saturated with nitrate/nitrite, the amount of nitrate AFm or nitrite AFm is maximised; no other nitrate/nitrite-binding phase appears until very high concentrations such that oxynitrates or oxynitrites become stable [176]. Some sources also report that below 55°C, at concentrations above 20 wt%, calcium nitrite, combines with calcium hydroxide to form a double salt $Ca(NO_2)_2 \cdot Ca(OH)_2 \cdot 2H_2O$ [297].

At low activities of nitrate and nitrite as *e.g.* produced by photocatalytic oxidation of NO_x on concrete containing TiO_2 [299, 300], most probably and the nitrite/nitrate will be contained in dilute solid solution in AFm and formation of either nitrate or nitrite AFm will not be observed. However higher nitrate/nitrite concentrations may influence cement paste mineralogy, destabilise monosulfoaluminate or monocarboaluminate in favour of nitrite or nitrate AFm and increase binding especially of nitrate. This replacement may also occur when nitrite and nitrate ingress from agricultural wastes. The role of cement in water treatment, to remove nitrate, has been assessed in the past [298] and data given here may be used to calculate the effectiveness of cement in this application. It would however be desirable to have data of the impact of soluble alkali and role of the C-S-H on the binding potential of hydrated cements.

7 Influence of calcium nitrite corrosion inhibitor on chloride binding in Portland cement

7.1 Introduction about corrosion inhibition

Steel-reinforced concrete is a vital component of the infrastructure. But an important limitation on the service lifetime of steel-concrete composite structures is imposed by corrosion of embedded steel. Much remains to be learnt about the nature and rates of processes leading to corrosion but practical experience reveals a number of corrosion promoters such as chloride but also, the existence of inhibitors. Calcium nitrite is widely used to counteract the harmful impact of chloride as a corrosion accelerator.

Chloride typically migrates into concrete from the service environment and, upon reaching embedded steel and exceeding a certain critical concentration, destroys its normally passivated surface state and initiates an active corrosion regime [174, 175]. Chloride migration in the cover concrete is partly rate-limited by binding, such that chloride is partly soluble in the cement pore fluid and partly bound into cement solids, particularly in AFm (see chapter 5).

Nitrite is added to the cement mix water typically as its calcium salt. The action of nitrite ions in delaying the onset of corrosion has been studied [270-279]. Chloride destroys the passivating oxide layer on steel forming complexes with ferrous ion giving rise to a complex cycle of transport and oxidation, leading to formation of expansive corrosion products [213-215] (see section 5.1.1, Eqs. 5.1-5.3)). This cycle can be suppressed by using an appropriate dose of nitrite ions, which react with and complex ferrous ions, an important intermediate species. Calcium nitrite is an anodic inhibitor, quickly oxidizing ferrous ions-the first product of corrosion- to ferric ions, which then precipitate in the alkaline pH environment of concrete thus interrupting the corrosion cycle [301] (Eq. 7.1):

$$Fe^{2+} + 2OH^- + 2NO_2^- = Fe_2O_3 + 2NO + H_2O \qquad \textit{Eq. 7.1}$$

Only those nitrite ions dissolved in the pore solution of the cement matrix are free to migrate to the steel and able to inhibit corrosion. Nitrite dosages, derived from the threshold $[NO_2]/[Cl]$ values necessary to inhibit corrosion, are determined empirically.

The numerical $[NO_2^-]/[Cl^-]$ ratio above which corrosion is suppressed differ according to source: reported values range from 0.5 Berke [272] to higher levels > 1.0, recommended by Andrade [301]. This latter value is consistent with results reported by Gaidis and Rosemberg [302], who obtained the maximum inhibitory efficiency of nitrites at a $[NO_2^-]/[Cl^-]$ ratio in the range above 0.7–1. Gonzalez [273] reported that a $[NO_2^-]/[Cl^-] = 1.5$ was adequate to preserve the passive layer of the reinforcement. However there is no reason to believe that the corrosion threshold has a single fixed value but that it may vary with cement composition, particularly pore fluid pH and temperature. The author in this work accepts that the ratio has physical significance and is not concerned about differences in reported values.

However other concerns exist. $Ca(NO_2)_2$ is a soluble salt and might be expected readily to leach from cement in the course of exposure, thus it could afford only transient corrosion protection. Other components of chemically-complex cement could notionally interfere with protection and the somewhat empirical nature of proof of its action have led to reservations about relying on nitrite for long- term corrosion control, as for example in major infrastructure developments and ageing nuclear structures.

To this end, the binding mechanisms of nitrite have been studied (chapter 6) [67, 303]. Nitrites are found readily to displace hydroxide, sulfate and carbonate from the AFm, so AFm is confirmed as mainly responsible for storing nitrite in cement solids [67]. It is also reported that bound nitrite can be released into the pore fluid by chloride ingress [303] but the underlying release mechanism has not been quantified. Brown [295] reported that when $3CaO{\cdot}Al_2O_3{\cdot}Ca(NO_2)_2{\cdot}10H_2O$ is added to fresh concrete as a pre-formed particulate solid, chloride from de-icing salts, applied to hardened concrete in service conditions, reacted with formation of Cl-AFm (Friedel's salt). Cl-AFm, which sequesters the chloride, in addition, releases nitrite which is available to oxidize any Fe^{2+}. In chapter 6 the author reported broader study of the chemical-mineralogical impacts of nitrite on cement paste, together with nitrate, a common impurity in commercial nitrite products, and in this chapter study explore quantitatively mechanisms for nitrite retention and release.

7.2 Experimental procedure

7.2.1 Phase assemblage experiments

Mixtures of $CaSO_4$, $Ca(NO_2)_2$, $CaSO_4$ and $CaCl_2$ were reacted at molar ratios shown in Tabs. 7.1 and 7.2 with previously degassed double distilled water (60 ml) at 25±2ºC and stored with agitation in HDPE-bottles for 45 days until reaction was quenched by filtration under N_2 at 25±2°C. Solutions for analysis were obtained by filtering 20 ml of liquid phase through a 0.22 μm MF "Millipore" membrane syringe filter.

Table 7.1: Molar ratios of mixtures: carbonate-free compositions.

Designation	C_3A [mol]	$CaSO_4$ [mol]	$Ca(NO_2)_2$ [mol]	$CaCl_2$ [mol]
A_1	0.01	0.01	0.01	0
B_1	0.01	0.01	0.01	0.005
C_1	0.01	0.01	0.01	0.0075
D_1	0.01	0.01	0.01	0.01

Table 7.2: Molar ratios of mixtures: carbonate-containing compositions.

Designation	C_3A [mol]	$CaSO_4$ [mol]	$Ca(NO_2)_2$ [mol]	$CaCO_3$ [mol]	$CaCl_2$ [mol]
A_2	0.01	0.01	0.01	0.0075	0
B_2	0.01	0.01	0.01	0.0075	0.005
C_2	0.01	0.01	0.01	0.0075	0.0075
D_2	0.01	0.01	0.01	0.0075	0.01

7.2.2 Thermodynamic modelling

Thermodynamic modelling was performed on the AFm phases in the systems: C_3A-$CaSO_4$-$Ca(NO_2)_2$-$CaCl_2$-H_2O and C_3A-$CaSO_4$-$CaCO_3$-$Ca(NO_2)_2$-$CaCl_2$-H_2O. Thermodynamic properties of relevant hydrates were taken from Tabs. 2.1, 5.7, 6.16. A key purpose of the calculation was to determine the binding power of AFm for chloride in competition with nitrite and other abundant anions of cement systems, hydroxide, carbonate and sulfate. Calculated and experimental data on anion fractionation are compared. All calculations assumed alkali-free conditions. For modelling purposes, an ideal solid solutios (marked on Figs. 7.1(a)-7.6(a) as Friedel's $salt_{ss}$) between Friedel's salt and hydroxy AFm, monocarboaluminate and hydroxy AFm, was assumed. Thermodynamic parameters were re-fitted assuming ideal composition of Friedel's salt: $C_4ACl_2H_{10}$ and no initial OH substitution (see section 5.5). AFm solid solutions between SO_4-AFm and OH-AFm (marked on Fig. 4(a) as SO_4-AFm_{ss}) [9], NO_2-AFm and OH-AFm (marked on Figs. 7.1(a)-7.6(a) as NO_2-AFm_{ss}) were admitted in simulations (chapter 6), but the composition of AFt was assumed to be ideal ettringite. Although potentially there is a solid solution formation between NO_2-AFm and Friedel's salt (section 6.3.8), because of existing uncertainty of its limits, in calculation nitrite AFm and Friedel's salt were treated as two separate phases.

7.3 Results

At the low nitrite concentrations used in this study, reaction between nitrite and cement solids is largely confined to AFm. Reaction is, however, complicated by the presence of several ions that compete for structural sites in the AFm phases: sulfate, hydroxyl, carbonate and chloride. Their ion activity determines the type and number of AFm phases and their anion content(s) and thus strongly affects the anion distribution between solid and aqueous phases (chapter 6). In order to present quantitative results in two dimensions, restraints have to been placed on calculations. These have been chosen to preserve as much as possible generic features and trends but without introducing approximations. Thus data presented are for 1 bar total pressure, a fixed temperature (25˚C) and fixed ratios of selected components to

visualise the impact of changing nitrite and chloride concentrations on paste mineralogy.

The restrictions applied enable solid phase relations correctly to be depicted in two dimensions and phase proportions to be estimated using the lever rule. For several key points, those at which phase changes are calculated to occur, aqueous phase composition, have been determined by experiment as a check on the accuracy of calculations.

Cement sulfate/alumina ratios (the "sulfate ratio") range as a consequence of cement formulation as well as gain of sulfate which may occur in service conditions. The calculations and experimental verification were therefore obtained for three SO_3/Al_2O_3 ratios 0.5, 1.0 and 1.5, with 0.5 being used as a model for as- produced Portland cement. Data for each ratio are shown twice, once assuming a carbonate - free cement, the other assuming enough $CaCO_3$ having been added to saturate the cement with respect to calcite and leave a slight excess (the amount of the excess is not important except for calculating amounts of phases). Tab. 7.3 is presented to coordinate the Figures, which should be used in conjunction with each other. In these Figures, the Cl/NO_2 ratio is treated as a variable to simulate ingress of chloride, as may occur in service conditions. Six figures are needed to compare permutations of three SO_3/Al_2O_3 ratios and at each ratio, the presence or absence of carbonate. Also two diagrams are needed for each set of conditions, one to depict solid phase compositions, the other to depict functions of the coexisting aqueous phase (composition, pH). Both calculated and experimental data are included for the aqueous phase while selected confirmation data for solids are shown in Figs. 7.7 and 7.8. Thus the impacts of selected changes can be determined by choosing the relevant pairs of Figures. For example, the calculations for carbonate- free systems with changing SO_3/Al_2O_3 ratios are shown by comparing Figs. 7.1(a,b), 7.3(a,b) and 7.4(a,b) while the corresponding calculation but made for carbonate -saturated systems, is shown in Figs. 7.2(a,b), 7.5(a,b) and 7.6(a,b).

Table 7.3: Guide to data presentation: Cl/NO_2 mole ratio is the system variable.

Figure #	SO_3/Al_2O_3 ratio	$CaCO_3$ presence	Solids, aqueous phase (composition and pH)
1(a)	1.0	Absent	Solids
1(b)	1.0	Absent	Aqueous phase
2(a)	1.0	Saturated	Solids
2(b)	1.0	Saturated	Aqueous phase
3(a)	1.5	Absent	Solids
3(b)	1.5	Absent	Aqueous phase
4(a)	0.5	Absent	Solids
4(b)	0.5	Absent	Aqueous phase
5(a)	1.5	Saturated	Solids
5(b)	1.5	Saturated	Aqueous phase
6(a)	0.5	Saturated	Solids
6(b)	0.5	Saturated	Aqueous phase

In this manner, the mineralogy of the systems are seen to differ at the outset, "outset" being defined as chloride-free conditions projecting at the left-hand side, and depending on conditions selected for calculations: the sulfate ratio and the presence or absence of carbonate. For example, at sulfate ratio 1.0, without carbonate, ettringite coexists with NO_2-AFm (Fig. 7.1(a)) whereas in the presence of carbonate, and even at the low carbonate activity conditioned by the solubility of $CaCO_3$ at high pH, CO_3-AFm and NO_2-AFm coexist with ettringite (Fig. 7.2(a)): the presence of carbonate expels sulfate from the AFm structure increasing the amount of ettringite. Under the conditions calculated, sulfate released form AFm must appear in AFt because gypsum, $CaSO_4.2H_2O$, remains undersaturated in all conditions. On the other hand, had the SO_3/Al_2O_3 ratio been less than 0.5, as is typically encountered in commercial cements, and in the absence of carbonate (Figs. 7.4(a,b)), SO_4-AFm and NO_2-AFm would have coexisted with ettringite. But if calcite had been present sufficient to saturate the solids with respect to calcite precipitation, the initial equilibrium state would have consisted of two AFm phases: CO_3-AFm and NO_2-AFm. Comparison of volume change calculations attending subsequent addition of chloride show that at low sulfate ratios, subsequent volume changes are quite sensitive to the potential for further ettringite formation stimulated by chloride ingress. Under a broad range of conditions, Friedel's

salt is more stable than SO_4-AFm, (monosulfoaluminate) and the sulfate thus liberated enhances ettringite formation (chapter 5). Thus more ettringite can form even though the sulfate content of the system remains constant or even undergoes dilution by chloride. The amount of ettringite present, as well as its potential for formation in the course of chloride ingress, is one factor controlling the partition of alumina between AFm and AFt phases, so is sensitive to the starting composition. This helps explain the many and varied reports in the literature concerning changes in the mineralogical balances attending changes in formulation and subsequent exposure in service to chloride, sulfate and carbonate: a broad range of responses are possible in terms of changing mineralogy and consequently, of volume occupied by the solids.

A common feature of all systems is that as chloride is progressively introduced to the system, it is necessary to reach a certain critical concentration before reaction with solids will commence. The Figures are calculated to reveal this effect by depicting molar Cl/NO_2 ratio on the horizontal scale. A common feature of the reaction between chloride and solids is that as chloride is progressively introduced to the system, it is necessary to reach a certain critical concentration before reaction will commence. The Figures are calculated to reveal this effect by depicting molar Cl/NO_2 on the horizontal scale. Note that the horizontal scale uses molar Cl/NO_2 ratio to show increasing chloride content with respect to nitrite (typically, the nitrite content is fixed), but aqueous $[NO_2^-]/[Cl^-]$ ratios have been added to Figs. 7.1(b)-7.6(b) to accord with the convention used in corrosion science to evaluate inhibition threshold: ratios >1.0 approximately indicate passivation.

Most of the nitrite is initially bound into the paste solids, mainly into AFm, from which it has displaced or partly displaced, other potential anionic substituents (OH^-, SO_4^{2-} or CO_3^{2-}). The main reaction resulting from chloride addition is, initially, conversion of nitrite AFm to chloride AFm (Friedel's salt). As the aqueous chloride concentration is increased, nitrite is progressively displaced from AFm and the nitrite thus displaced accumulates in the pore fluid, as shown for example in Fig. 7.1(b), giving aqueous compositions in equilibrium with the solids of Fig. 7.1(a). Numerical values of aqueous concentrations as well as changes in the slope of the data for aqueous nitrite and chloride are correlated. Fig. 7.1(b), thus correlates with the phase changes shown in Fig 7.1(a) and the two figures should be used in conjunction. This correlation, between pairs of figures, should also be made for other grouped (a+b) pairs of Figures. Note also that as chloride is added, pH decreases and although the pH change is numerically

small, this is deceptive as pH is plotted on a log scale- unlike other aqueous concentration, which are on an arithmetic scale.

Critical concentration necessary to initiate chloride uptake by AFm is variable, depending upon initial mineralogy. The diagrams enable reaction sequences and aqueous concentrations of key species to be read directly from the appropriate pair of Figures.

The diagrams also record the total molar volumes of the solids and its changes with rising chloride concentration. The calculations apply strictly to $CaCl_2$, and predict a range of changes. The volume expansion attending chloride penetration is never large but is at its highest for a paste made to a low sulfate ratio, 0.5, and without carbonate.

To verify the influence of chloride ions on solid phases, X-ray diffraction measurements were also performed for selected mixtures with and without calcite both in the presence and absence of calcium chloride (Figs. 7.7 and 7.8 respectively). Fig. 7.7 shows the results for the calcite-free system and can be considered to benchmark calculations in chemically more complex systems. Plot 1 on Fig. 7.7 represents the initial phase assemblage without chloride. Phases formed were identified as NO_2-AFm, probably slightly substituted with OH ions (marked as Ni), portlandite (P) and ettringite (E). This phase distribution is thus in agreement with experimental observations presented in chapter 6. In the course of reaction with $CaCl_2$, phase changes occurs (plot 2): nitrite is displaced from NO_2-AFm while Friedel's salt (Cl-AFm, marked as Fs on plot 2, is formed. Nitrite ions are liberated to the aqueous phase and result in increased nitrite concentrations in the aqueous phase.

Fig. 7.8 shows the results for a calcite-containing system. Initially-formed phases (plot 1) were identified as NO_2-AFm, probably slightly substituted by OH ions (marked as Ni) monocarboaluminate (marked as Mc) portlandite (P) and ettringite (E), in agreement with the findings in [67]. In the course of admixing $CaCl_2$, a phase change occurs (plot 2): Friedel's salt (Cl-AFm, marked as Fs) appeared while nitrite from NO_2-AFm was displaced to the aqueous phase. Carbonate, displaced from monocarboaluminate, forms calcite (marked as Cc). In the example calculation, sufficient carbonate was added to form only small amounts of CO_3-AFm. However a generic conclusion is that adding chloride to a paste containing monocarboaluminate results in the formation of calcite: the appearance of calcite can be isochemical and is not necessarily due to uptake of additional CO_2 from the service environment [67].

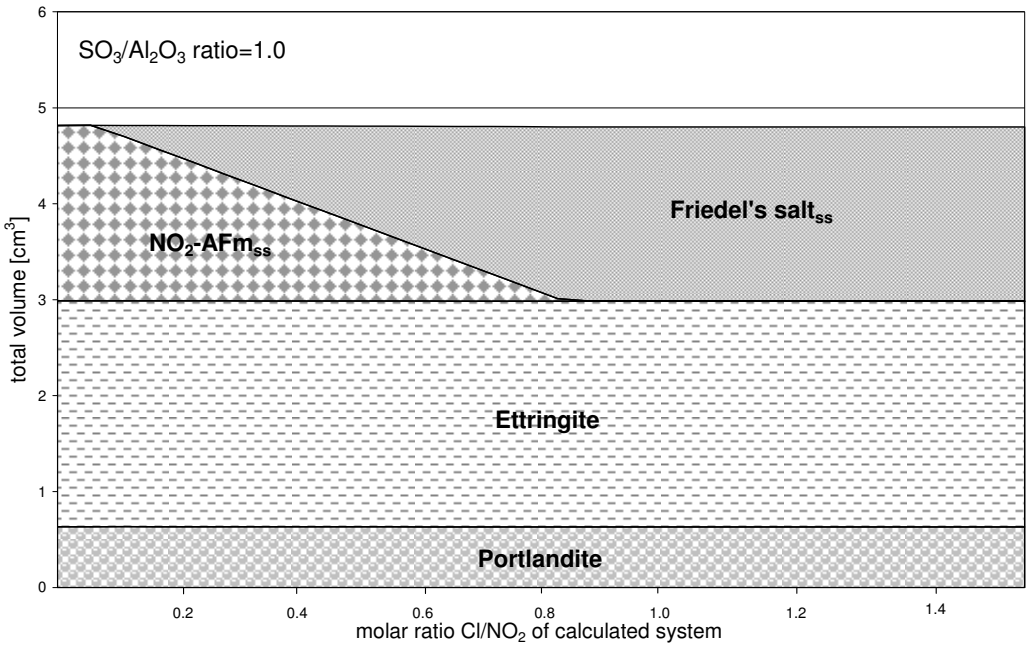

Figure 7.1(a): Calculated total volume of phases of a hydrated model mixture consisting of 0.01 moles C_3A, 0.015 moles portlandite, 0.01 moles $Ca(NO_2)_2$, 60 ml H_2O and with fixed initial sulfate ratio (SO_3/Al_2O_3=1) showing phase development and its dependence on changing chloride content at 25°C.

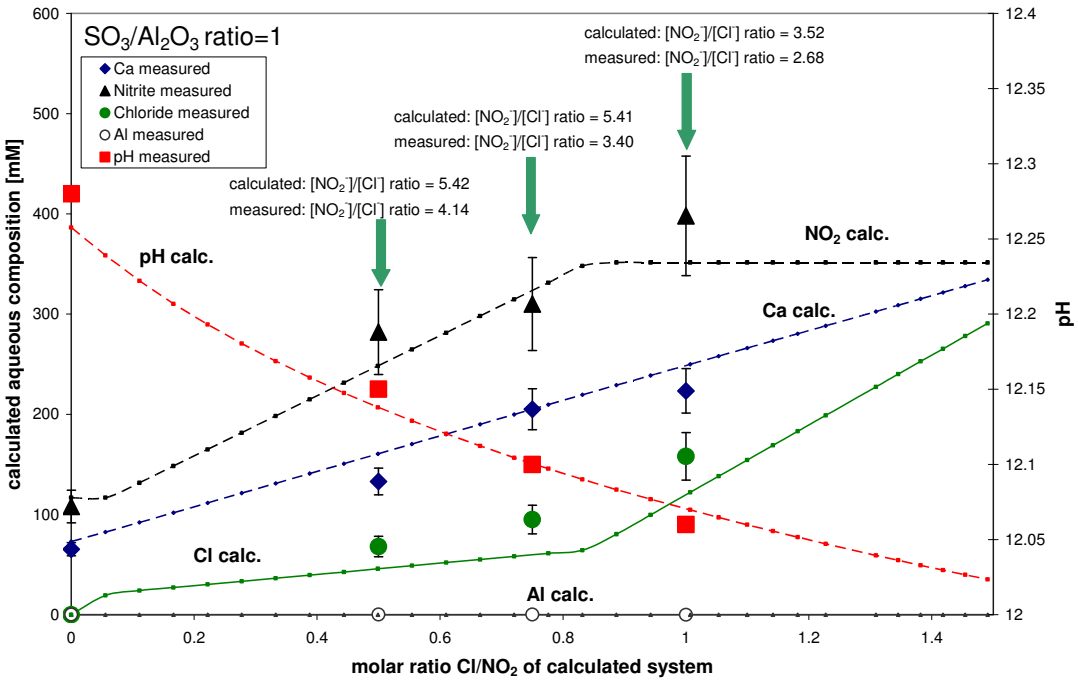

Figure 7.1(b): Calculated and experimental aqueous composition of hydrated model mixture consisting of 0.01 moles C_3A, 0.015 moles portlandite, 0.01 moles $Ca(NO_2)_2$, 60 ml H_2O and with fixed initial sulfate ratio (SO_3/Al_2O_3=1) showing its dependence on changing chloride content at 25°C. Error bars are shown where appropriate.

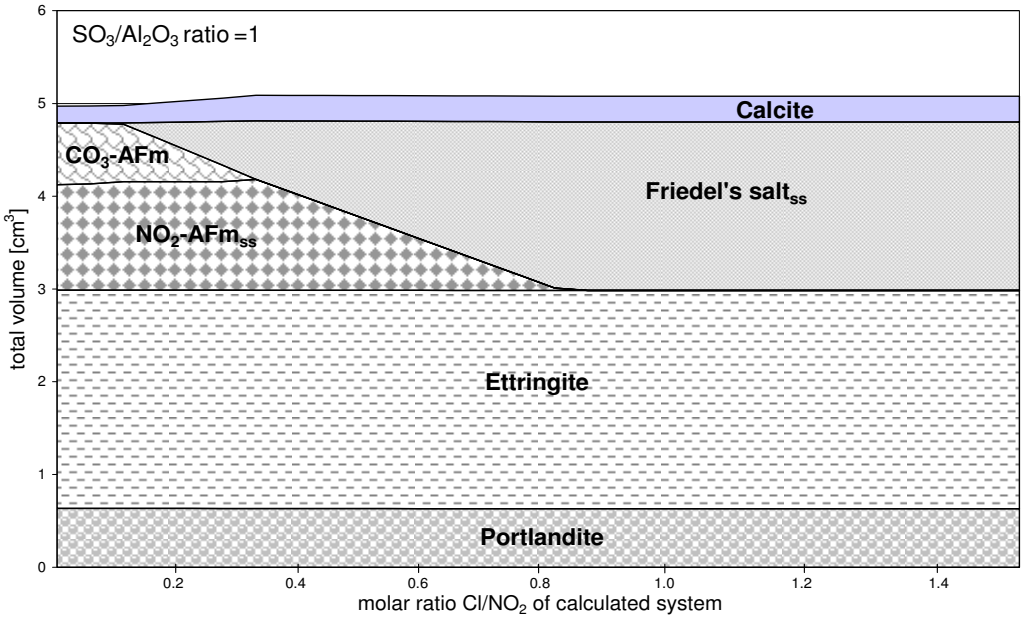

Figure 7.2(a): Calculated total volume of phases of a hydrated model mixture consisting of 0.01 moles C_3A, 0.015 moles portlandite, 0.0075 moles $CaCO_3$, 0.01 moles $Ca(NO_2)_2$ and 60 ml H_2O and with fixed initial sulfate ratio (SO_3/Al_2O_3=1) showing phase development and its dependence on changing chloride content at 25°C.

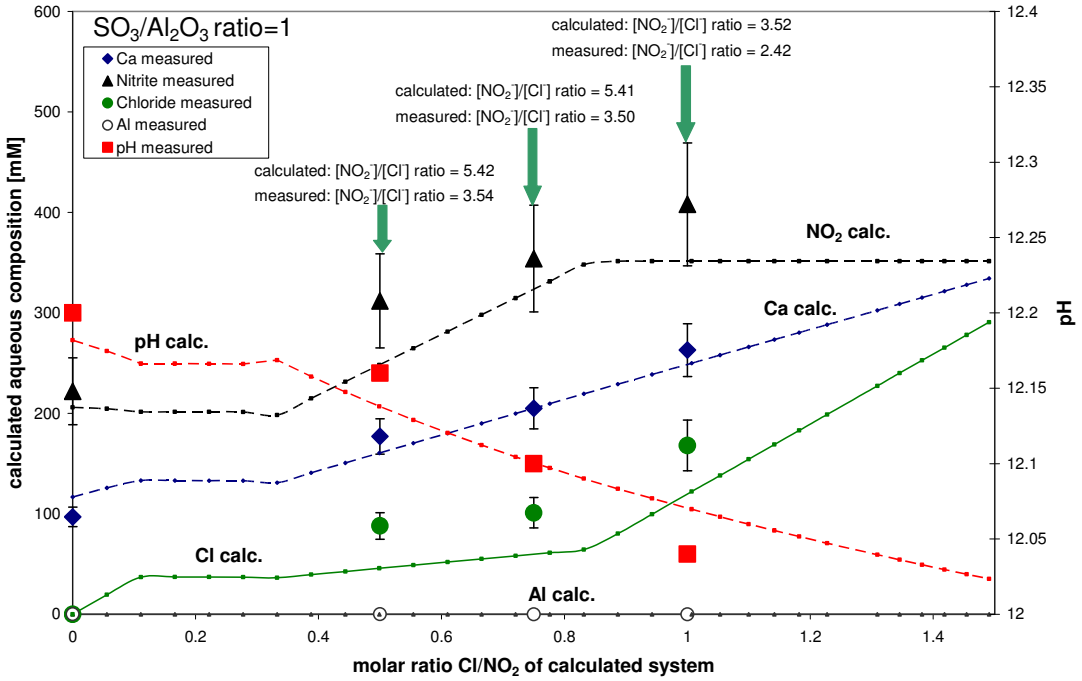

Figure 7.2(b): Calculated and experimental aqueous composition of hydrated model mixture consisting of 0.01 moles C_3A, 0.015 moles portlandite, 0.0075 moles $CaCO_3$, 0.01 moles $Ca(NO_2)_2$ and 60 ml H_2O and with fixed initial sulfate ratio (SO_3/Al_2O_3=1) showing its dependence on changing chloride content at 25°C. Error bars are shown where appropriate.

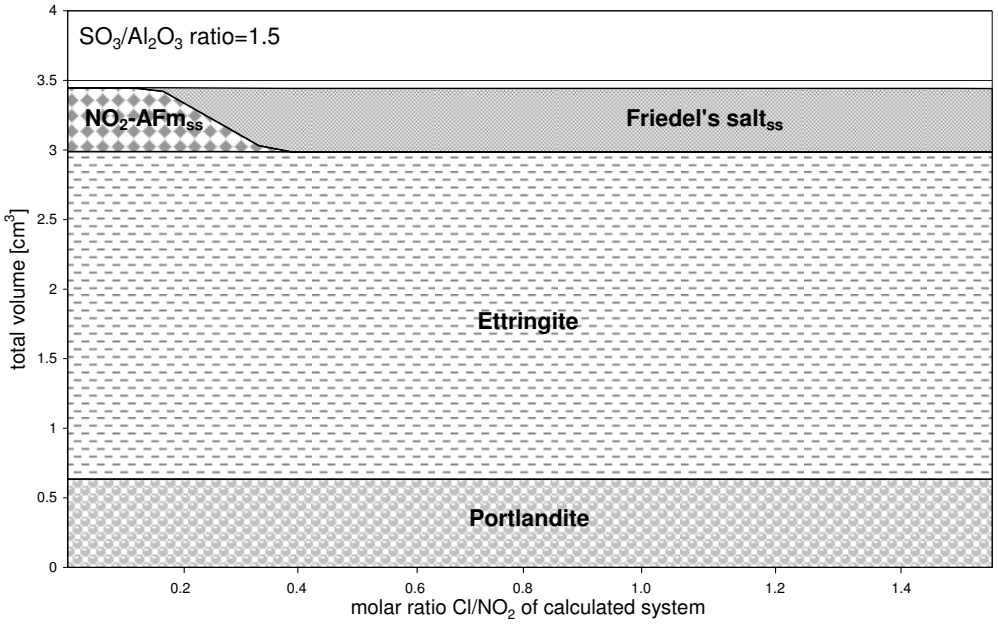

Figure 7.3(a): Calculated total volume of phases of a hydrated model mixture consisting of 0.005 moles C_3A, 0.015 moles portlandite, 0.01 moles $Ca(NO_2)_2$, 60 ml H_2O and with fixed initial sulfate ratio (SO_3/Al_2O_3=1.5) showing phase development and its dependence on changing chloride content at 25°C.

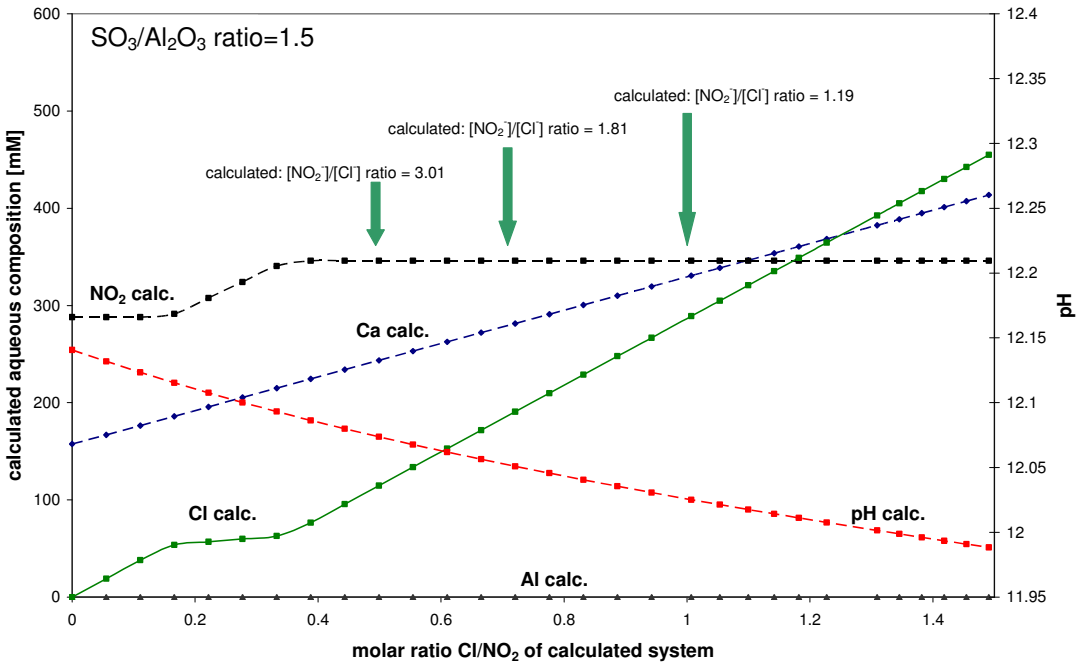

Figure 7.3(b): Calculated aqueous composition of hydrated model mixture consisting of 0.005 moles C_3A, 0.015 moles portlandite, 0.01 moles $Ca(NO_2)_2$, 60 ml H_2O and with fixed initial sulfate ratio (SO_3/Al_2O_3=1.5) showing its dependence on changing chloride content at 25°.

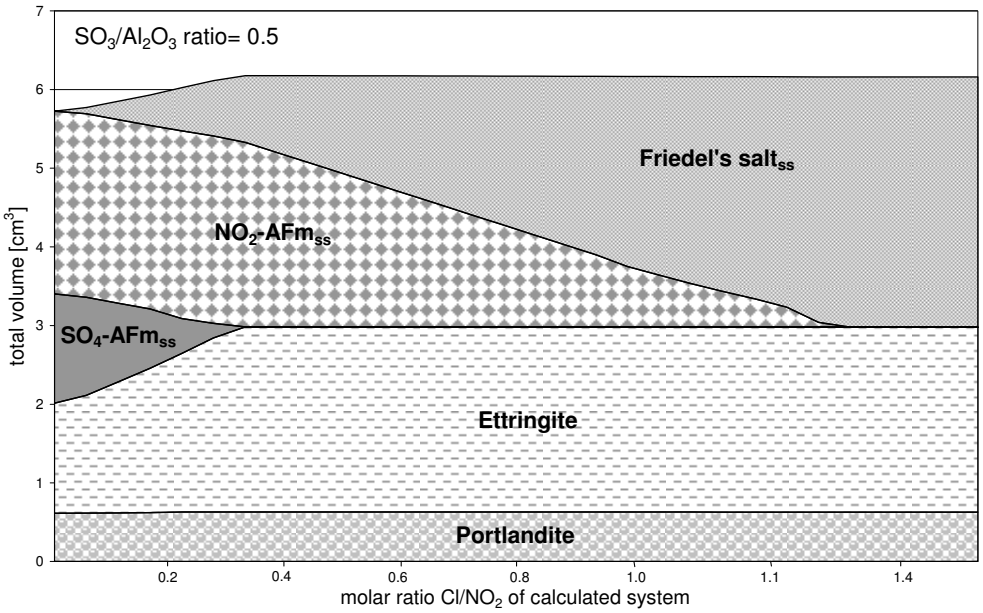

Figure 7.4(a): Calculated total volume of phases of a hydrated model mixture consisting of 0.015 moles C_3A, 0.015 moles portlandite, 0.01 moles $Ca(NO_2)_2$, 60 ml H_2O and with fixed initial sulfate ratio (SO_3/Al_2O_3=0.5) showing phase development and its dependence on changing chloride content at 25°C.

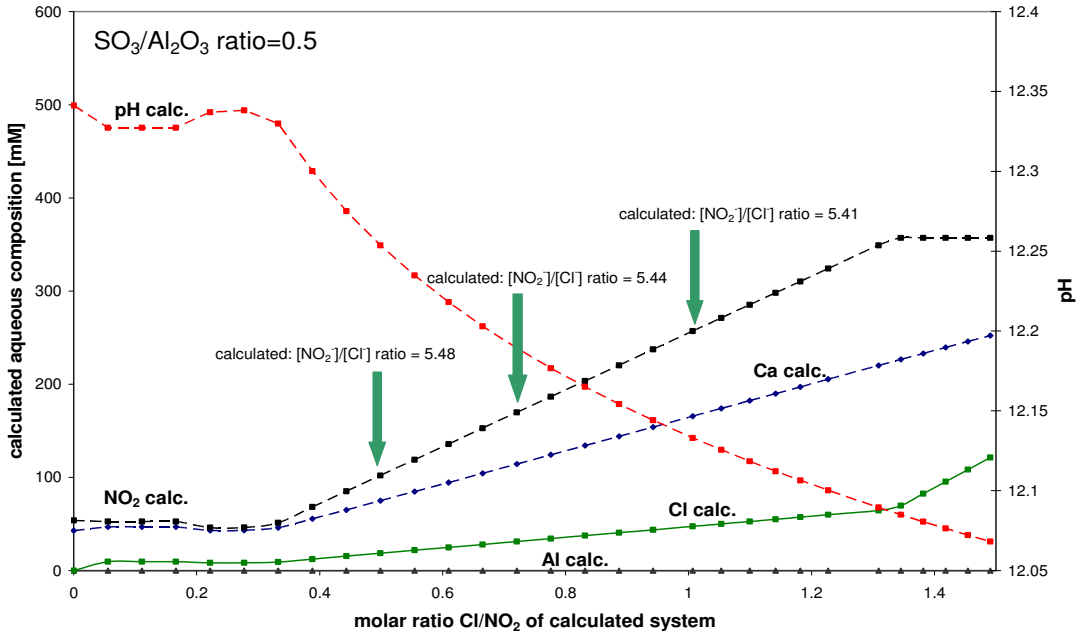

Figure 7.4(b): Calculated aqueous composition of hydrated model mixture consisting of 0.015 moles C_3A, 0.015 moles portlandite, 0.01 moles $Ca(NO_2)_2$, 60 ml H_2O and with fixed initial sulfate ratio (SO_3/Al_2O3=0.5) showing its dependence on changing chloride content at 25°C. The small fluctuations in pH at low Cl/NO_2 ratios are probably due to rounding errors in the computation.

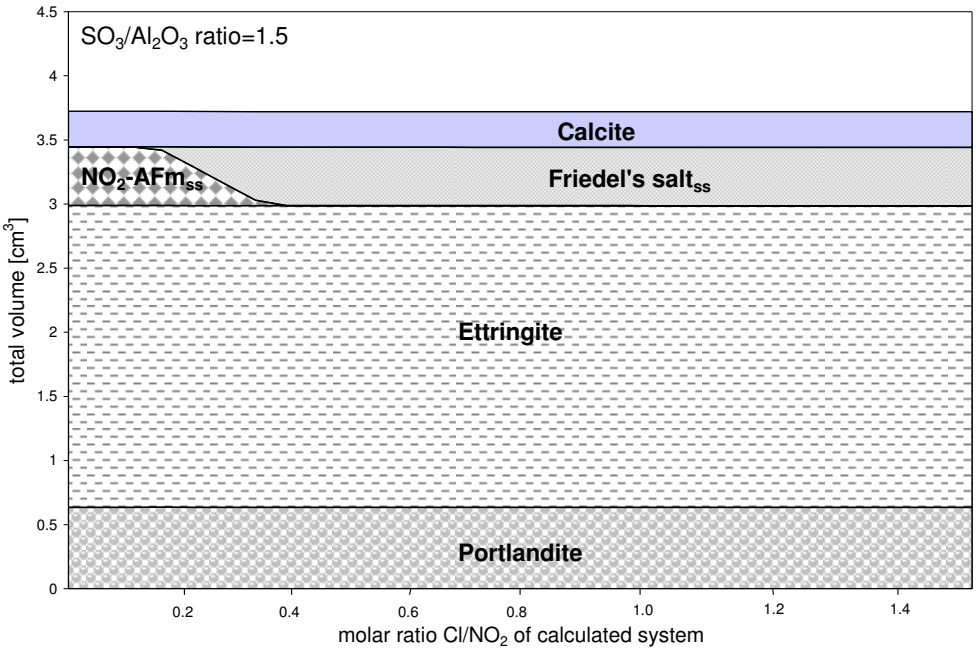

Figure 7.5(a): Calculated total volume of phases of a hydrated model mixture consisting of 0.005 moles C_3A, 0.015 moles portlandite, 0.01 moles $Ca(NO_2)_2$, 0.0075 moles $CaCO_3$, 60 ml H_2O and with fixed initial sulfate ratio (SO_3/Al_2O_3=1.5) showing phase development and its dependence on changing chloride content at 25°C.

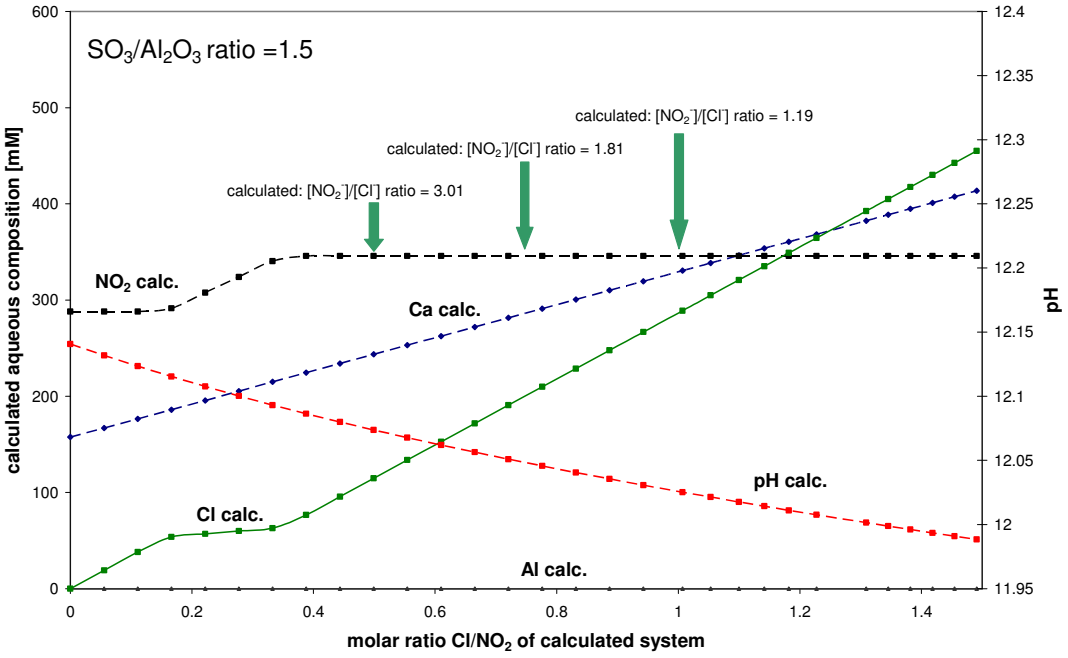

Figure 7.5(b): Calculated aqueous composition of hydrated model mixture consisting of 0.005 moles C_3A, 0.015 moles portlandite, 0.01 moles $Ca(NO_2)_2$, 0.0075 moles $CaCO_3$, 60 ml H_2O and with fixed initial sulfate ratio (SO_3/Al_2O_3=1.5) showing its dependence on changing chloride content at 25°C.

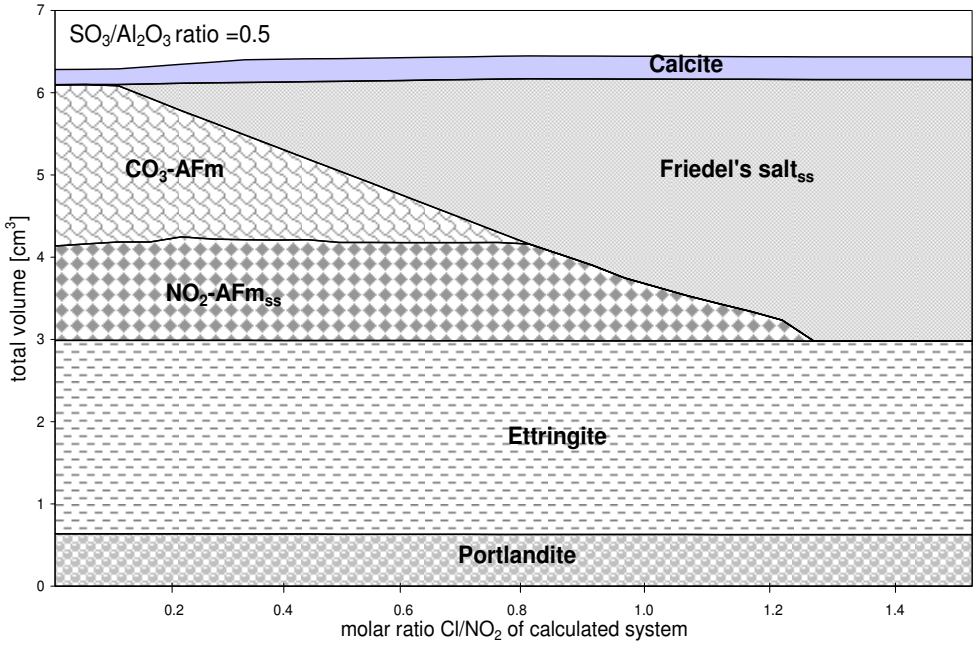

Figure 7.6(a): Calculated total volume of phases of a hydrated model mixture consisting of 0.015 moles C_3A, 0.015 moles portlandite, 0.01 moles $Ca(NO_2)_2$, 0.0075 moles $CaCO_3$, 60 ml H_2O and with fixed initial sulfate ratio (SO_3/Al_2O_3=0.5) showing phase development and its dependence on changing chloride content at 25°C.

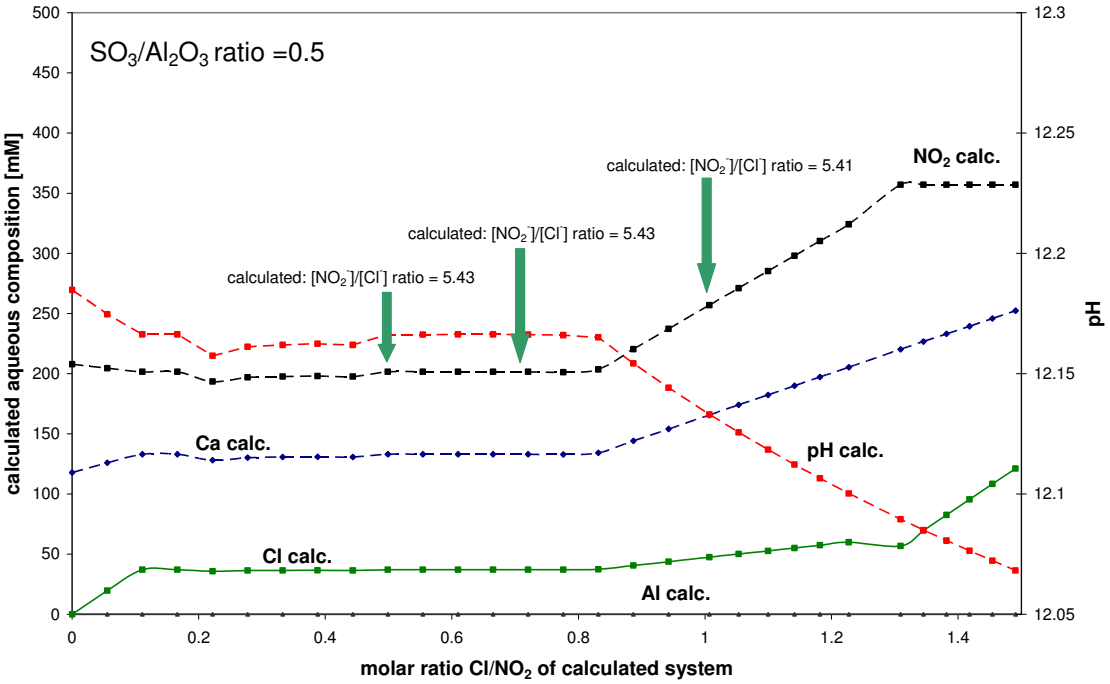

Figure 7.6(b): Calculated aqueous composition of hydrated model mixture consisting of 0.015 moles C_3A, 0.015 moles portlandite, 0.01 moles $Ca(NO_2)_2$, 0.0075 moles $CaCO_3$, 60 ml H_2O and with fixed initial sulfate ratio (SO_3/Al_2O_3=0.5) showing its dependence on changing chloride content at 25°C.

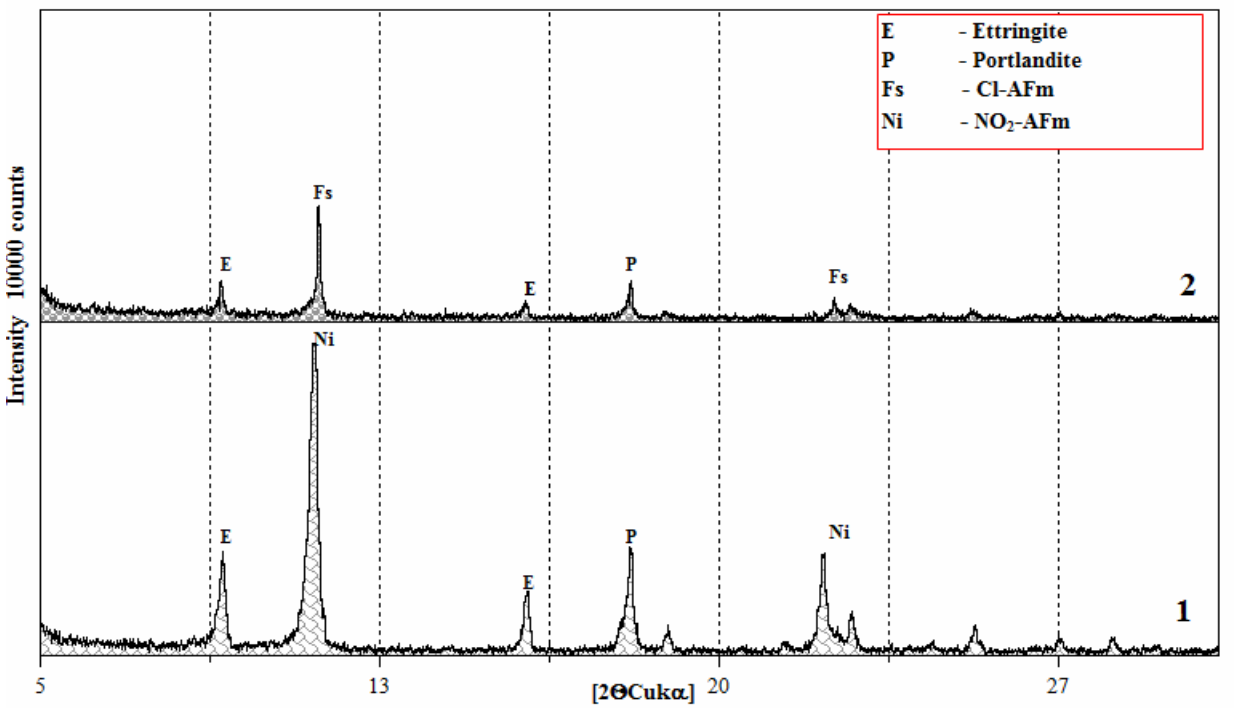

*Figure 7.7: XRD patterns showing mineralogical changes and influence of $CaCl_2$ addition for the system 0.01 moles C_3A-0.01 moles $Ca(NO_2)_2$-0.01 moles $CaSO_4$-0.015 moles $Ca(OH)_2$- 60 ml H_2O at 25±2˚C; **1**-no $CaCl_2$ present (Tab. 7.1, A_1); **2**-0.01 moles of $CaCl_2$ added (Tab. 7.1, D_1); high intensities of phases in pattern **1** are due to preferred orientation.*

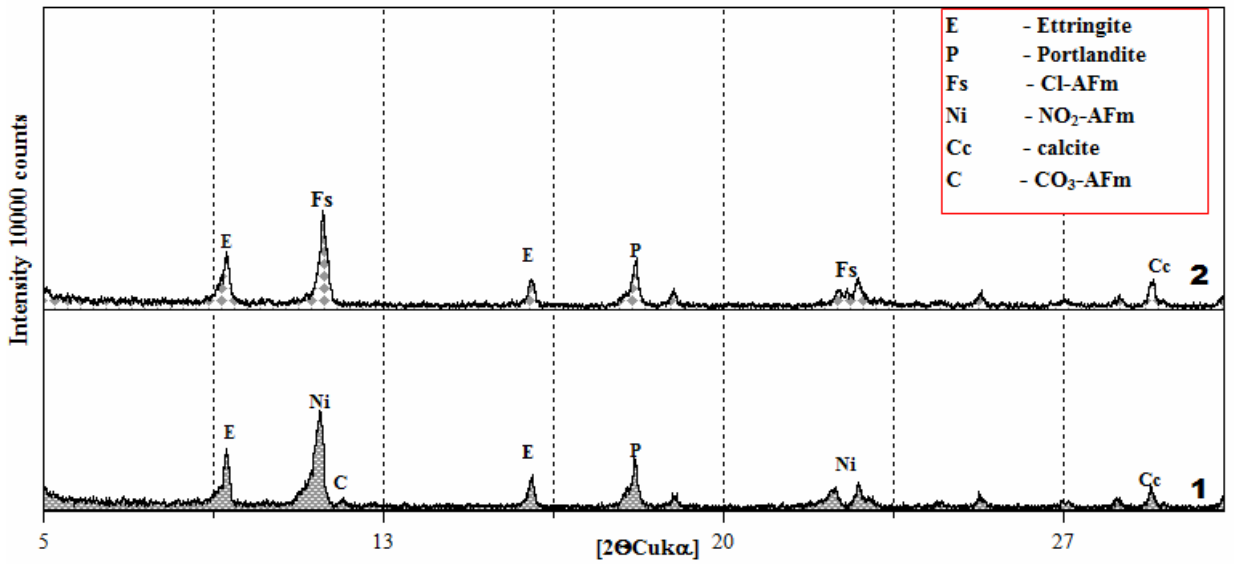

*Figure 7.8: XRD patterns showing mineralogical changes and influence of $CaCl_2$ addition for the system 0.01 moles C_3A-0.01 moles-0.01 moles $Ca(NO_2)_2$- $CaSO_4$-0.015 moles $Ca(OH)_2$-0.0075 moles $CaCO_3$- 60 ml H_2O at 25±2˚C; **1**-no $CaCl_2$ present (Tab. 7.2, A_2); **2**-0.01 moles of $CaCl_2$ added (Tab. 7.2, D_2).*

7.4 Discussion

7.4.1 Influence of chloride on nitrite binding in cement pastes

Steel embedded in well-made concrete is usually well- protected against corrosion although chloride ions are known to impair this protection. Typically, Portland cements are made and marketed essentially without chloride (typically < 0.10% by mass of cement) but in anticipation that (i) cement- bonded products will contain embedded steel and (ii) the service environment will contain mobile chloride, nitrites are often added with the mix water to inhibit chloride- induced corrosion in subsequent service. Adding nitrite to the mix water is known empirically to be a simple and effective way of mitigating the subsequent corrosive action of chloride. Although many excellent studies have been made showing its effectiveness and establishing a mechanistic basis for its action, actual demonstrations under controlled conditions are few and doubts remain about the influence of nitrite on cement properties, the long-term persistence of nitrite in cement and potential for loss by leaching, and the range of compositions over which nitrite affords protection: for example, does it afford protection in carbonate-filled cements? This chapter combines calculation and experiment to quantify factors related to the protective action of nitrite.

The first step, to make and determine the thermodynamic properties of nitrite AFm (NO_2-AFm), has been reported [67]. The finding that nitrite is strongly stabilised in AFm preferentially to other common anions in cement is perhaps surprising, as tetrahedral groups, *e.g.,* sulfate are generally regarded as being more strongly bonded into AFm than trigonal planar groups but, as the strong bonding of planar carbonate, nitrite and nitrate ions show, site preference depends on more than shape.

Of course the basis of comparison is influenced by concentration as well as binding and if we examine cement paste, the solubility limits of the relevant species differ markedly. For example, the highest carbonate concentration achievable in cement is limited by the solubility of $CaCO_3$ at the relevant temperature and pH. Thus in this study, aqueous carbonate concentrations were low, at or below carbonate analysis limits, *ca.* 1ppm. Other species have different controls. For example, sulfate concentrations in Portland cement pore fluids generally remain below the threshold

imposed by gypsum saturation at least until alteration is well advanced. Nevertheless this sulfate solubility, while low, is usually several orders of magnitude higher than carbonate. So, to establish relevance to the internal environment of Portland cement paste, author does not compare equal concentrations of the competing anions. For example, sulfate ion concentrations, typically a few millimolar, are controlled by the buffering pair (SO_4-AFm/AFt) [56]. These restrictions need to be carried in mind if attempting to explain anion partitioning. Actual concentrations are therefore shown in Figures and give a basis for comparison.

The presentation of results obtained on complex systems requires special treatment to preserve generic features. Data cannot be present for every permutation of each variable- but in any event, as noted above, not all permutations will be encountered. Diagrams contain only those phases which are required to balance reaction stoichiometry; others not involved in mass balances or not influencing pH are omitted. On this basis portlandite has to be retained, as explained subsequently.

Each isochemical group of calculations is grouped in Tab. 7.3. However in service, cement may gain sulfate by reaction with its environment; the sulfate ratio 0.5 is selected to represent fresh cement while higher ratios (1.0, 1.5) are calculated as representative of cements which have gained sulfate from the service environment.

Modern cements often contain up to 5% of calcium carbonate as permitted for example by EN-197-1, and even initially carbonate-free matrices may also gain carbonate in service conditions. Thus Fig. 7.2(a,b), in which carbonate is admitted to the calculation of chloride impacts on nitrite, depict the changing distribution of nitrite in commercial cements supplemented by calcite. Calcium carbonate is of course not completely inert in this application as it reacts with AFm in the course of hydration, displacing sulfate and hydroxide ions and forming hemi- and monocarboaluminate [20]. Thus carbonate-containing cements react differently towards nitrite than the equivalent but carbonate-free composition. The amount of carbonate included in specimen calculations has been chosen to be sufficient to convert all AFm to an equilibrium mixture of NO_2-AFm and monocarboaluminate, leaving an excess of calcite at 25˚C. It is worth to note that nitrite solubility, Fig. 7.2(b), is increased somewhat by the presence of carbonate, from ~100 to ~200 mmolar. In this respect, carbonate slightly reduces the effectiveness of nitrite

binding into the chloride free solid although the shift in equilibrium does not much decrease the continuing protection afforded by nitrite.

The solid solution of carbonate in AFt at 25ºC is low, ~9%, and is considered to have negligible effect on calculations. However carbonate solid solution in AFt increases rapidly with decreasing temperature [53, 56] and a task for the future is to determine if low temperatures, close to 0°C, much alter the 25°C distributions.

Fig. 7.1(a) shows the impact of chloride diffusing into a model plain Portland cement containing calcium nitrite such that all alumina is initially combined as equilibrium mixtures of AFt and NO_2-AFm [67]. Under these conditions, nitrite is relatively insoluble, ~100 mmolar, in the aqueous phase (Fig. 7.1(b)). Given these input assumptions, the initial phase proportions are shown at the left hand side of the diagram and the impact of increased chloride is assessed by constructing a vertical line and sweeping this line to the right, noting the length of line segments intercepted at field boundaries to determine phase proportions: aqueous functions are given in the appropriate matching Figure, as linked in Tab. 7.3. As explained, C-S-H does not need to be explicitly included in the model because it interacts only weakly with either chloride [205] or nitrite, although a caution should be noted that no data appear to have been reported in the literature showing nitrite sorption on C-S-H. Portlandite must however be included in the calculation because (i) it is required to ensure a mass balance amongst the other phases and does not occur in constant amount and (ii) it helps buffer pH in the range 12-12.5, thus controlling, or nearly so, one potential variable- the [OH] activity, and hence the aqueous pH. Thus an excess of portlandite is required to ensure that the calculation is valid, but those phases calculated to be stable do not depend on the amount of excess.

Calculated phase assemblages for example those in [Fig. 7.2(a)] were also verified experimentally, Fig. 7.8: calculations and experimental results were thus in agreement. Not every predicted point could be confirmed experimentally: calculation produces too great a volume of data. But the key points at which phase changes were predicted to occur and the coexisting aqueous phase compositions at these points were confirmed experimentally, as shown on Figs. 7.1(b), 7.2(b). The agreement also provides an indication of equilibration and hence kinetics: the experiments invariably showed that that when adding sufficient chloride to achieve a new phase distribution, the new and

different partition of Cl, NO_2 and OH, was attained rapidly, within a few days or weeks. It is not obvious that reaction need be rapid: inspection of the mass balances shows that reaction is not necessarily just a matter of ion exchange, for example of Cl for NO_2; the amounts of portlandite, the nature of the AFm polymorph(s) and the AFm/ AFt balances may also have to change as reaction to restore a new equilibrium proceeds. Comparing these kinetics with the time scale for spontaneous chloride diffusion into well-made concrete, the latter is generally a slow process, requiring months or even years; so on this time scale, the reactions between AFm and anionic species, as well as the changing mass balances with AFt and portlandite, are sufficiently rapid for a local equilibrium to be maintained. Thus points measured along chloride diffusion profiles in good quality concrete are probably also close to what would be expected if local equilibriums were maintained.

As chloride permeates the matrix, it will react sequentially displacing other anions in AFm. Under conditions depicted in Figures, reaction continues to a Cl/NO_2 mole ratio ~0.8 with eventual conversion of carbonate, sulfate and nitrite forms of AFm to Friedel's salt (Cl-AFm). The reaction is effectively a buffer for aqueous chloride concentration, with the result that chloride aqueous concentration remain low, around 30 mmolar in Figs. 7.1(b) and 7.2(b), until the buffering capacity is of the solids exhausted, which point is reached when ettringite, calcite and Friedel's salt coexist with other cement phases: portlandite and C-S-H (if present).

To link data obtained in this chapter to corrosion studies, where the literature is generally agreed that the boundary between passivation and active corrosion of embedded steel is defined by the aqueous $[NO_2^-]/[Cl^-]$ ratio, selected numerical values of the nitrite: chloride ratios are shown (arrowed) in Figures.

It is apparent from the data that AFm phase(s) containing nitrite cause the cement to behave as a 'smart' material in the course of chloride ingress. It initially stores nitrite in the AFm solid, providing some protection against leaching, but in response to chloride ingress, it exchanges chloride for nitrite, releasing nitrite in response to the rising local aqueous chloride concentrations, and thereby keeping the pore fluid chemistry within the envelope of passivating conditions until the buffering function is fully or almost fully utilised. This observation is fully in agreement with investigations reported by Brown [295].

In applying the data to commercial cements, it should be recalled that the reactive AFm solids are effectively diluted with much C-S-H; the paste may be only 5-15% of AFm, so the mass of nitrite requiring to optimise the "smart" behaviour is low, on the order of 1-2% by mass, which broadly accords with dosage recommendations given by suppliers.

Like all chemical mechanisms, corrosion protection is only achieved within chemical limits. In the presence of an infinite reservoir of chloride, passivation is limited by (i) its concentration in the reservoir, (ii) the amount of bound nitrite and its solubility in pore water, conveniently expressed as an aqueous ratio, $[NO_2^-]/[Cl^-]$, (arrowed on the relevant diagrams). As a consequence of nitrite binding, its solubility reaches but does not exceed an aqueous concentration ~ 350 mmolar. Once this plateau is attained, the numerical value of $[NO_2^-]/[Cl^-]$ ratio decreases as the absolute value of chloride continues to increase, with the result that the system progressively approaches the threshold for transition to a corrosion regime. In applying these data to concentrated solutions such as sea water, ~550 mmolar with respect to chloride, two problems arise. One is that the salinity is partly NaCl, whereas the calculations were made for $CaCl_2$. Fortunately sodium interacts only weakly with cement phases and up to ~0.5 molar, is believed not to affect the results. But by extension of trends established at lower chloride concentrations, the maximum practical concentration of nitrite from an AFm reservoir may no longer be sufficient for protection, especially as the pH is also diminished. But over wide ranges of lower chloride contents, as are often encountered in real exposures and in the course of intermediate stages of diffusion of sea water through cover concrete, nitrite from an AFm reservoir will give effective protection.
The total capacity of the cement solids for chloride binding is not shown because it depends primarily on cement composition, on the mass of AFm phase, as well as the activities of species which compete for anion sites in AFm. Thus alumina and sulfate contents, which affect the balance between AFm and AFt phases and accordingly, total AFm, are important variables with which to optimise in the first instance nitrite storage and subsequently, the 'smart' release mechanism triggered by chloride ion penetration. Although the composition of Friedel's salt is variable, and under some conditions up to 80% of the theoretical Cl content can be replaced by the OH [66], under conditions imposed on calculations, the Cl content of Friedel's salt will remain close to theoretical with the result that potential for chloride binding is high, close to theoretical. But pH

rising above the threshold conditioned by portlandite, as in very alkaline pH cements, could diminish the chloride binding in Friedel's salt by lowering its chloride content.

The role of alumina is shown more quantitatively by additional calculations for both higher SO_3/Al_2O_3 ratio of 1.5 in Figs. 7.3(a,b) and 7.5(a,b), without and with calcite as well as for lower SO_3/Al_2O_3 ratio 0.5 in Figs. 7.4(a,b) and 7,6(a,b) again without and with calcite. The basis for calculation is in each case the same as that previously described for Figs. 7.1(a,b) and 7.2(a,b).
Mass balances are probably temperature dependent and calculations have thus far been undertaken only for 25˚C so calculations at other temperatures remain a task for the future. However other reasons may exist why the amount of AFm cannot be optimised on the basis of chloride and nitrite uptake potential, as discussed below.

Sulfate may also enter the cement from its service environment and thereby increase the sulfate ratio in service conditions. Under these conditions AFm may convert to AFt with expansion so a high initial AFm content may not be desirable. If we consider the impact of changing sulfate ratio, comparison shows that under otherwise comparable conditions it becomes progressively more difficult to maintain high numerical values of the corrosion ratio $[NO_2^-]/[Cl^-]$ as the cement sulfate content increases. Likewise it is chemically more difficult to control chloride-induced corrosion in situations where sulfate will also diffuse into the cement and alter paste mineralogy so sulfate might be considered as making it more difficult to achieve corrosion resistance. However while straightforward ion exchange accounts for mass balances in AFm, the actual mechanism, as noted, may be more complex because of structural differences between different AFm phases and changing AFt/AFm balances. Calculation discloses that the specific volume of solids increases least in response to chloride penetration into carbonate-containing matrices Figs. 7.2(a), 7.6(a). The space filling effect is enhanced by initially low SO_3/Al_2O_3 ratios (Fig. 7.4(a)) and the absence or near absence of carbonate. Present evidence does not disclose if these volume changes are significant and no deleterious effects have been reported to author's knowledge but if concerns arise about possible physical expansion in low SO_3/Al_2O_3 ratio cements, the volume change attending chloride penetration could be reduced by adding calcite to cement.
Finally, it should be noted that although plain and carbonate- blended cements are not included in the scope of the study; additional data are required to treat blends high in

fly ash and slag [276]. The higher activities of alumina and silica in these cements result in formation of the aluminosilicate AFm (strätlingite) [255], whose exchange properties for nitrite and chloride are not known. Moreover, slag, with its content of reduced sulfur (S^{-2}), may affect the nature of corrosion process by initiating secondary reactions; for example, the content of chemically- reduced sulfur in slag, if not otherwise oxidised, could react with nitrite forming ammonia and effectively reduce or destroy the capacity of the system to overcome chloride-induced corrosion. But with these possible exceptions, the corrosion protection afforded by nitrite has a "smart" behaviour based on well- established physical chemistry.

7.4.2 Influence of nitrate on corrosion inhibition

Because nitrate is a common impurity in commercial grades of calcium nitrite, calcium nitrate is also included in discussion.

Some literature sources indicate that calcium nitrate may have some corrosion inhibiting properties of its own [280, 296, 297, 304]. Nitrate, like nitrite, acts as an electron acceptor and oxidises Fe(II) to Fe(III) at high pH. Part of the reasoning behind looking into calcium nitrate is that the electrochemical relation between nitrite and nitrate is energy-neutral (Eq. 7.2):

$$2NO_3^- + 2H_2O + 4e^- = 2NO_2^- + 4OH^- \qquad E_0 = +0.01\ V \qquad \textit{Eq. 7.2}$$

Nitrite ions in the NO_3-AFm and bound stronger than nitrite ions in the NO_2-AFm therefore nitrate ions will have priority over nitrite ions in occupying AFm sites. As mentioned in Section 6.6 chloride added to the system displaces nitrate from the NO_3-AFm forming Cl-AFm (Friedel's salt) (Fig. 6.34). NO_3-AFm is 'more resistant' than NO_2-AFm to chloride displacement so chloride needs to be use in an excess to fully displace nitrate from the NO_3-AFm. Ion exchange trend is suspected to be similar to the one observed in the case of NO_2-AFm and nitrate ions displaced from the NO_3-AFm are expected to be liberated into the aqueous phase.

8. Summary

Chapters 1, 2 and 3 compile introduction about: general history and chemistry of cement, cement hydration products, fundamentals of geochemical thermodynamic based equilibrium modelling and instrumental methods used during experimental work presented in this thesis.

A target of this thesis was to focus on calcium nitrate, nitrite and chloride which are used as set accelerating admixtures and by implementing thermodynamic modelling evaluate mineralogical changes which they cause within cement paste. The importance of nitrite to act as a corrosion inhibition of reinforcement in concrete which is a subject of chloride attack is described.

To evaluate volume changes accompanying mineralogical changes, collected densities of phases occurring in Portland cement are given in the chapter 4. Previous compilations were incomplete and the present dataset greatly extends the range of substances for which data are available. Chapter 4 contains calculated densities and a brief discussion of selected compounds and phases of interest in the chemistry of Portland and related cements. The thermodynamic database used for calculations has been updated with this new set of values for the densities. For crystalline substances, XRD data are deemed to be most reliable and provide a comparable basis. Basic measurement conditions are given, when known, to enable potential user to choose which values seem to be more reliable and useful [Appendix I]. If several values of density were given for the one phase give a recommended mean value was provided. Several examples of its use are given and the density database allowed volume changes caused by anion substitution in AFm phases with chloride, nitrate and nitrite and presented in the following chapters 5, 6 and 7.

In chapter 5 ,thermodynamic properties of chloride hydrates: Friedel's salt and Kuzel's salt were determined. Solid solutions have been investigated and compared with data reviewed in the literature. Data indicate solid solution formation between hydroxy AFm and Friedel's salt in the range of Cl/(Cl+OH) ratios: 0.2-1 and solid solution between monocarboaluminate and Friedel's salt for the $Cl/(Cl+1/2CO_3)$ ratios 0.1-1. No solid solution was found between Friedel's salt and monosulfoaluminate but an

ordered compound, Kuzel's salt, $Ca_4Al_2(SO_4)_{0.5}(Cl)(OH)_{12}\cdot 6H_2O$ was encountered. An equilibrium model of chloride binding by AFm and the influence of Cl on the AFm/AFt mineralogy has been proposed for the systems with and without calcium carbonate. At 25˚C chloride ions entering the system displace sulfate from monosulfoaluminate forming Kuzel's salt at lower chloride concentrations and Friedel's salt at higher concentrations. Liberated sulfate ions react with calcium and aluminium forming ettringite (AFt) which can cause volume expansion, or seal pores, or both. Chloride ions also have the ability to displace carbonate from the monocarboaluminate phase and form Friedel's salt but this reaction does not cause much change in the molar volume*:* the carbonate ions form calcite. If we compare plain and carbonate containing systems, a trade-off occurs. Carbonate suppresses potentially expansive reactions arising from chloride ingress but at the same time, reduces the total capacity to bind chloride and increases aqueous $[Cl^-]/[OH^-]$ ratios. Temperature can significantly influence phase distribution but was not explored in detail.

Chapter 6 reports experimental work to characterise the impact of nitrite and nitrate salts on cement mineralogy. Nitrite and nitrate interact strongly with AFm forming. $Ca_4Al_2(NO_3)_2(OH)_{12}\cdot 4H_2O$ and $Ca_4Al_2(NO_2)_2(OH)_{12}\cdot 4H_2O$ (nitrate and nitrite AFm). Both were synthesized and characterised. Data indicate solid solution formation between: nitrate AFm and hydroxy AFm in the range of $OH/(OH+NO_3)$ ratios around: 0-0.5, nitrate AFm and Friedel's salt in the range of $Cl/(Cl+NO_3)$ ratios around: 0-0.5, nitrite AFm and hydroxy AFm in the range of $OH/(OH+NO_2)$ ratios around: 0-0.5, nitrite AFm and nitrate AFm in the range of $NO_2/(NO_3+NO_2)$ ratios around: 0-0.4. No significant solid solutions were found between: nitrite AFm–monosulfoaluminate, nitrite AFm–monocarboaluminate, nitrate AFm–monosulfoaluminate, nitrate AFm-monocarboaluminate. It is possible that an ordered compond forms between monosulfoaluminate and nitrite AFm, $Ca_4Al_2(SO_4)_x(NO_2)_y(OH)_z\cdot aH_2O$, but it was never obtained in phse pure form hence its exact omposition is not known; it may be a subject for further research. Solid solution between nitrte AFm and Friedel's salt was also investigated but there is not enough information to define miscibility limits. Thermodynamic modelling, enabled by the newly derived thermodynamic data, was applied to predict phase changes in the course of admixing cement hydration accelerators: $Ca(NO_2)_2$ and $Ca(NO_3)_2$. At 25˚C nitrate/nitrite ions entering the system displace sulfate from

monosulfoaluminate forming nitrate AFm/nitrite AFm. Liberated sulfate ions react with calcium and aluminium forming ettringite which can result in volume expansion. Nitrate and nitrite ions also have the ability to displace carbonate from the monocarboaluminate phase and form nitrate AFm/nitrite AFm. Released carbonate ions form calcite. However in the presence of chloride nitrate/nitrite are displaced from the AFm structure. Chloride ions are strongly bound into the AFm and form Friedel's salt while nitrite/nitrate ions are released into the aqueous phase.

General preference for occupation of AFm sites at 25˚C under conditions encountered in cement paste can be described in a sequence:

$$OH^- < SO_4^{2-} < CO_3^{2-} < NO_2^- < NO_3^- < Cl^-$$

'Smart' behaviour of cements containing nitrite corrosion inhibitor has been described in chapter 7. Nitrite can be stored within the AFm phase. Sequestered nitrite is, however, released in response to chloride ingress. Entering chloride displaces nitrite from the AFm and is bound by forming Friedel's salt. Released nitrite ions are liberated to an aqueous phase and increase $[NO_2^-]/[Cl^-]$ ratios, which assure corrosion inhibition of embedded steel. The storage capacity of cement systems for nitrite is influenced by design of the cement system. Alumina and sulfate contents, which affect the balance between AFm and AFt phases and accordingly, total AFm, are important variables with which to optimise in the first instance, nitrite storage and subsequently, the 'smart' release mechanisms triggered by chloride ion penetration. Cements, with low SO_3/Al_2O_3 ratio, will have initially more AFm formed and therefore higher capacity for nitrite storage and, subsequently, for chloride binding into solids. That is, the capacity of the cement to behave as 'smart' material in respect to corrosion control is itself a function of cement composition. However, maximising sequestered nitrite is not the only factor for optimisation. In general, the, corrosion protection afforded by nitrite is not believed to be much affected by calcite additions or the presence of soluble alkalis at low concentrations and form the basis of a robust system for protection of embedded steel.

It is recommended for the future research to evaluate the role of C-S-H and C-A-S-H in sorbing chloride, nitrite and nitrate as well determining the influence of iron and alkalis; work presented in this thesis assumes alkali free conditions and no iron present.

Additional work is needed to establish existence of solid solution between nitrite AFm and Friedel's salt and exact composition of a potential new ordered compound, $Ca_4Al_2(SO_4)_x(NO_2)_y(OH)_z \cdot aH_2O$.

References

1. *Portland Cement Association: A History of Cement.* : p. http://www.rumford.com/articlemortar.html.

2. Taylor, H.F.W., *Cement Chemistry (2nd edition).* 1997, London: Thomas Telford Publishing.

3. Parrot, L.J., Killoh, D.C, *Prediction of cement hydration.* British Ceramic Proceedings, 1984. Vol. 35: p. 41-53.

4. Hong, S.Y., Glasser, F.P., *Alkali binding in cement pastes: Part I. The C-S-H phase* Cement and Concrete Research, 1999. 29: p. 1893-1903.

5. Hong, S.Y., Glasser, F.P., *Alkali sorption by C-S-H and C-A-S-H gels: Part II. Role of alumina* Cement and Concrete Research, 2002. 32(7): p. 1101-1111.

6. Brew, D.M.R., Glasser, F.P., *Synthesis and characterisation of magnesium silicate hydrate gels* Cement and Concrete Research, 2005. 35: p. 85-98

7. Brew, D.M.R., Glasser, F.P., *The magnesia–silica gel phase in slag cements: alkali (K, Cs) sorption potential of synthetic gels* Cement and Concrete Research 2005. 35: p. 77-83.

8. Pöllmann, H., *Incorporation of SO_4^{2-}, and CO_3^{2-} and OH^- in hydration products of tricalciumaluminate.* International Congress on the Chemistry of Cement, New Dehli, 1992. Vol.4: p. 361-369.

9. Matschei, T., Lothenbach, B., Glasser F.P., *The AFm phase in Portland cement* Cement and Concrete Research, 2007. 37(2): p. 118-130.

10. Nielsen, E., Herfort, D., Geiker, M., Hooton, D., *Effect of solid solution of AFm phases on chloride binding.* Proceedings, 11th Int. Congress on the Chemistry of Cement, South Africa, 2003.

11. Glasser, F.P., Kindness, A., Stronach, S.A., *Stability and solubility relationships in AFm phases Part I. Chloride, sulfate and hydroxide.* Cement and Concrete Research, 1999. 29: p. 861-866.

12. Pöllmann, H., *Solid solution of complex calcium aluminate hydrates containing Cl^-, OH^- and CO_3^{2-} - anions* Proc. 8th Int. Symp. On the Chem. Of Cement, Rio de Janeiro, 1986. 3: p. 300-306.

13. Kuzel, H.J., *Röntgenuntersuchung in System $3CaO•Al_2O_3•CaSO_4•nH_2O$-$3CaO•Al_2O_3•CaCl_2•nH_2O$-$H_2O$.* Neues Jahrbuch für Mineralogie Monatshefte, 1966: p. 193-200.

14. Gaines, R.V., Skinner, H.C.W., Foord, E.E., Mason, B., Rosenzweig, A., , *Dana's New Mineralogy, eighth edition.* John Wiley & Sons, New York, 1997: p. 1573-1586.

15. Sacerdoti, M., Passaglia, E., *Hydrocalumite from Latium, Italy: its crystal structure and relationship, with related synthetic phases, Locality: Montalto di Castro, Viterbo, Latium, Italy* Neues Jahrbuch fur Mineralogie Monatshefte 1988: p. 462-475.

16. Pöllmann, H., Witzke, T., Kohler, H., *Kuzelite.* American Mineralogist, 1998: p. 909 (abstract).

17. Pöllmann, H., *Characterization of Different Water Contents of Ettringite and Kuzelite.* Proc. XII International Congress on the Chemistry of Cement, Montreal, Canada, 2007. CD.

18. Birnin-Yauri, U.A., Glasser, F.P., *Friedel's salt, $Ca_2Al(OH)_6(Cl,OH).2H_2O$: its solid solutions and their role in chloride binding.* Cement and Concrete Research, 1998. 28(12): p. 1713-1723.

19. Rapin, J.P., Elkaim, E., Francois, M., Renaudin, G., *Structual transition of Friedel's salt $3CaO•Al_2O_3•CaCl_2•10H_2O$ studied by synchrotron powder diffraction.* Cement and Concrete Research 2002. 32: p. 513-519.

20. Matschei, T., Lothenbach B., Glasser F.P., *The role of calcium carbonate in cement hydration* Cement and Concrete Research, 2007. 37(4): p. 551-558.

21. Allmann, R., *Refinement of the hybrid layer structure $[Ca_2Al(OH)_6]+[1/2(SO_4)•3H_2O]$.* Neues Jahrbuch für Mineralogie Monatshefte 1977: p. 136-144.

22. Aruja, E., *The unit cell and space group of $4CaO.Al_2O_3.19H_2O$ polymorphs.* Acta Crystallographica, 1961. 14: p. 1213-1216.

23. Fischer, R., Kuzel, H.J., *Reinvestigation of the system $C_4A•nH_2O$-$C_4A•CO_2•nH_2O$.* Cement Concrete Research, 1982. 12: p. 517-526.

24. Balonis, M., Glasser, F.P., *The density of cement phases.* Cement and Concrete Research, 2009. 39: p. 733-739.

25. Struble, L.J., *Synthesis and characterisation of Ettringite and related phases.* 8th International Congress on the Chemistry of Cement, Rio de Janeiro, 1986. Vol. 6: p. 582-588.

26. Möschner, G., Lothenbach, B., Winnefeld, F., Ulrich, A., Figi, R., Kretzschmar, R., *Solid solution between Al-ettringite and Fe-ettringite ($Ca_6[Al_{1-x}Fe_x(OH)_6]_2(SO_4)_3·26H_2O$)* Cement and Concrete Research, 2009. 39(6): p. 482-489.

27. Pöllmann, H., Kuzel H.J., Wenda, R., *Compounds with ettringite structure.* Neues Jahrbuch für Mineralogie Abhandlungen, 1989. 160: p. 133-158.

28. Pöllmann, H., Kuzel, H.J., *Solid solutions of ettringites, part I: Incorporation of OH^- and CO_3^{2-} in $3CaO \cdot Al_2O_3 \cdot 3CaSO_4 \cdot 32H_2O$.* Cement and Concrete Research, 1990. 20: p. 941-947.

29. Paul, M., Glasser, F.P., *Impact of prolonged warm (85°C) moist cure on Portland cement paste.* Cement and Concrete Research 2000. 30: p. 1869 – 1877.

30. Eriksson, G., Hack, K., *ChemSage - A computer program for the calculation of complex chemical equilibria.* Metall. Trans.B, 1990. 21B: p. 1013-1023.

31. Davies, R.H., Dinsdale, A.T., Gisby, J.A., Hodson, S.M., Ball, R.G.J. , *in "Applications of Thermodynamics in the Synthesis and Processing of Materials", Eds. P. Nash and B. Sundman, TMS, Warrendale, PA.* 1995: p. 371-384.

32. Sundman, B., Jansson, B., Andersson, J.-O. , *The Thermo-Calc databank system* CALPHAD, 1985. 9: p. 153-190.

33. Kulik, D., Berner, U., Curti, E., *Modelling chemical equilibrium partitioning with the GEMS-PSI code.* PSI Scientific Report, http://gems.web.psi.ch., 2003. Vol. 4: p. 109-122.

34. Babushkin, V.I., Matveev, G.M., Mčedlov-Petrosjan, O.P., *Thermodinamika Silikatov.* Strojisdat, Moskau (in russian), 1965.

35. Reardon, E.J., *Problems and approaches to the prediction of the chemical composition in cement/water systems.* Waste Management, 1992. 12: p. 221-239.

36. Reardon, E.J., *An ion interaction model for the determination of chemical equilibria in cement/water systems.* Cement and Concrete Research, 1990. 20: p. 175-192.

37. Atkins, M., Glasser, F.P., Kindness, A . *Cement hydrate phases: Solubility at 25˚C.* Cement and Concrete Research, 1992. 22: p. 241-246.

38. Atkins, M., Bennett, D.G., Dawes, A.C., Glasser, F.P., Kindness, A ., Read, D., *A thermodynamic model for blended cements.* Cement and Concrete Research, 1992. 22(2-3): p. 497-502.

39. Stronach, S.A., *Thermodynamic Modelling and Phase Relations of Cementitious Systems.* Ph.D Thesis, University of Aberdeen, UK, 1996.

40. Damidot, D., Birnin-Yauri, U.A., Glasser, F.P., *Thermodynamic investigation of the $CaO-Al_2O_3-CaCl_2-H_2O$ system at 25°C and the influence of Na_2O.* IL Cemento, 1994. 91: p. 243-254.

41. Damidot, D., Glasser, F.P, *Thermodynamic investigation of the $CaO-Al_2O_3-SiO_2-H_2O$ system at 25°C by thermodynamic calculations.* Cement and Concrete Research, 1995. 25: p. 22-28.

42. Damidot, D., Barnett, S.J., Glasser, F.P., Macphee, D., *Investigation of the $CaO-Al_2O_3-SiO_2-CaSO_4-CaCO_3-H_2O$ system at 25°C by thermodynamic calculations.* Advances in Cement Research, 2004. 16: p. 69-76.

43. Damidot, D., Glasser, F.P., *Thermodynamic investigation of the $CaO-Al_2O_3-CaCO_3-H_2O$ system at 50°C and 85°C.* Cement and Concrete Research, 1992. 22(5): p. 1179-1191.

44. Damidot, D., Glasser, F.P., *Thermodynamic investigation of the $CaO-Al_2O_3-CaSO_4-H_2O$ system at 25°C and the influence of Na_2O.* Cement and Concrete Research 1993. 23: p. 221-238.

45. Damidot, D., Stronach S., Kindness, A., Atkins, M., Glasser F.P., *Thermodynamic investigation of the $CaO-Al_2O_3-CaCO_3-H_2O$ closed system at 25°C and the influence of Na_2O.* Cement and Concrete Research, 1994. 24(3): p. 563-572.

46. Lothenbach, B., Winnefeld, F., *Thermodynamic modelling of the hydration of Portland cement.* Cement and Concrete Research, 2006. 36: p. 209-226.

47. Lothenbach, B., Wieland, E., *A thermodynamic approach to the hydratation of sulphate-resisting Portland cement.* Waste Management, 2006. 26: p. 706 – 719.

48. Lothenbach, B., Matschei, T., Möschner, G., Glasser, F.P, *Thermodynamic modelling of the effect of temperature on the hydration and porosity of Portland cement.* Cement and Concrete Research, 2008. 38: p. 1-18.

49. Lothenbach, B., Le Saout, G., Gallucci, E., Scrivener, K., *Influence of limestone on the hydration of Portland cements.* Cement and Concrete Research, 2008. 38(6): p. 848-860.

50. Kulik, D.A., Kersten, M., *Aqueous solubility diagrams for cementitious waste stabilisation systems: II, End-member stoichiometries of ideal calcium silicate hydrate solid solutions.* Journal of the American Ceramic Society, 2001. 84: p. 3017-3026.

51. Matschei, T., Lothenbach, B., Glasser, F.P., *Thermodynamic properties of Portland cement hydrates in the system $CaO-Al_2O_3-SiO_2-CaSO_4-CaCO_3-H_2O$.* Cement and Concrete Research, 2007. 37: p. 1379- 1410.

52. Matschei, T., *Thermodynamics of Cement Hydration.* PhD thesis, University of Aberdeen, UK, 2007.

53. Matschei, T., Glasser, F.P., *Phase assemblages relevant to Portland cement hydration at low temperatures, 0-25°C.* Proceedings of the 17th Ibausil, Weimar, 2009. Vol. I: p. 01-219 – 01-233.

54. Matschei, T., Glasser, F.P., *Interactions between Portland cement and carbon dioxide.* Proceedings of the 12th Intern. Congress on the Chemistry of Cements, Montreal, 2007.

55. Matschei, T., Skapa, R., Lothenbach, B., Glasser, F.P., *The distribution of sulfate in hydrated Portland cement paste.* Proceedings of the 12th Intern. Congress on the Chemistry of Cements, Montreal, 2007.

56. Matschei, T., Glasser, F.P., *Temperature dependence, 0 to 40 °C, of the mineralogy of Portland cement paste in the presence of calcium carbonate.* Cement and Concrete Research, 2010. 40(5): p. 763-777.

57. Shock, E.L., Sassani, D.C., Willis, M., Sverjensky, D., *Inorganic species in geologic fluids: Correlations among standard molal thermodynamic properties of aqueous ions and hydroxide complexes.* Geochimica et Cosmochimica Acta, 1997. 61: p. 907-950.

58. Hummel, W., Berner; U., Curti, E., Pearson, F.J., Thönen, T., *Nagra/PSI Chemical Thermodynamic Data Base 01/01.* Universal Publishers, Parkland, Florida, USA, 2002.

59. Johnson, J.W., Ölkers, E.H., Helgeson, H.C., *SUPCRT92: A software package for calculating the standard molal thermodynamic properties of minerals, gases, aqueous species, and reactions from 1 to 5000 bar and 0 to 1000°C.* Computers & Geosciences, 1992. 18: p. 899-947.

60. Helgeson, H.C., Kirkham, D.H., Flowers, G.C., *Theoretical prediction of the thermodynamic behavior of aqueous electrolytes at high pressures and temperatures: IV. Calculation of activity coefficients, osmotic coefficients, and apparent molal and standard and relative partial molal properties to 600°C and 5 kb.* American Journal of Science, 1981. 281: p. 1249–1516.

61. Ederova, J., Satava, V., *Heat capacities of C_3AH_6, C_4AsH_{12} and $C_6As_3H_{32}$.* Thermochimica Acta 1979. 31: p. 126-128.

62. Helgeson, H.C., Delany, J.M., Nesbitt, H.W., Bird, D.K., *Summary and critique of the thermodynamic properties of rock forming minerals.* American Journal of Science, 1978. 278-A: p. 229.

63. Garvin, D., Parker, V.B., White, Jr., H. J., *Codata Thermodynamic Tables.* Hemisphere Publishing Corporation, Springer-Verlag, 1987.

64. Verdone, N., De Filippis, P., *Thermodynamic behaviour of sodium and calcium based sorbents in the emission control of waste incinerators.* Chemosphere, 2004. 54: p. 975-985.

65. Robie, R.A., Hemingway B.S., *Thermodynamic Properties of Minerals and Related Substances at 298.15 K and 1 Bar (105) Pressure and at Higher Temperatures.* United States Government Printing Office, Washington, 1995.

66. Balonis, M., Lothenbach, B., Le Saout, G., Glasser, F.P., *Impact of chloride on the mineralogy of hydrated Portland cement systems.* Cement and Concrete Research, 2010 40(7): p. 1009-1022.

67. Balonis, M., Mędala, M., Glasser, F.P., *Influence of calcium nitrate and nitrite on the constitution of the AFm and AFt cement hydrates - experiments and thermodynamic modelling.* Advances in Cement Research, submitted in 2009 (accepted for publication in 2010).

68. Kulik, D.A., *Dual-thermodynamic estimation of stoichiometry and stability of solid solution end members in aqueous–solid solution systems.* Geochemical Geology, 2006. 225: p. 189-212.

69. Kulik, D., *Thermodynamic properties of surface species at the mineral–water interface under hydrothermal conditions: A Gibbs energy minimisation single-site 2pKA triple-layer model of rutile in NaCl electrolyte to 250°C.* Geochimica et Cosmochimica Acta, 2000. 64: p. 3161-3169.

70. Kulik, D.A., *Minimising uncertainty induced by temperature extrapolations of thermodynamic data: a pragmatic view on the intergration of thermodynamic databases into geochemical computer codes.* Proceedings the use of thermodynamic databases in performance assessment, Barcelona, OECD, 2002: p. 125-137.

71. Macphee, D., Barnett, S., *Solution properties of solids in the ettringite—thaumasite solid solution series.* Cement and Concrete Research, 2004. 34: p. 1591-1598.

72. Möschner, G., Lothenbach, B., Winnefeld, F., Ulrich, A., Figi, R., Kretzschmar, R., *Solubility of Fe-ettringite and its solid solutions with Al-ettringite.* Proceedings of the 12th Intern. Congress on the Chemistry of Cements, Montreal, 2007.

73. Bruno, J., et al., *Chemical Thermodynamics Vol. 10. Chemical Thermodynamics of Solid Solutions of Interest in Nuclear Waste Management, ed. O.N.E.A.D,* Amsterdam, The Netherlands: North Holland Elsevier Science Publishers B.V., 2007.

74. Curti, E., *Coprecipitation of radionuclides with calcite: estimation of partition coefficients based on a review of laboratory investigations and geochemical data.* Applied Geochemistry, 1999. 14(4): p. 433-445.

75. Glynn, P.D., Reardon, E.J., Plummer, L.N., Busenberg, E., *Reaction paths and equilibrium end-points in solid-solution aqueous-solution systems.* Geochimica et Cosmochimica Acta, 1990. 54: p. 267-282.

76. Glynn, P.D., *Solid-solution solubilities and thermodynamics: sulfates, carbonates and halides. In: Sulfate Minerals: Crystallography, Geochemistry and Environmental Significance, Alpers C.N., Jambor J.L. and Nordstrom D.K. (eds.).* Mineralogical Society of America and Geochemical Society, Reviews in Mineralogy and Geochemistry, 2000. Vol. 40: p. 481-511.

77. Glynn, P.D., *MBSSAS: A code for the computing of margules parameters and equilibrium relations in binary solid-solutions aqueous-solution systems.* Computers & Geoscience, 1991. 17: p. 907-966.

78. Renaudin, G., Kubel, F., Rivera, J.P., Francois, M., *Structural phase transition and high temperature phase structure of Friedel's salt, $3CaO•Al_2O_3•CaCl_2•10H_2O$.* Cement and Concrete Research, 1999. 29: p. 1937-1942.

79. Rousselot, I., Taviot-Guého, C., Leroux, F., Léone, P., Palvadeau, P., Besse, J.P., *Insights on the structural chemistry of hydrocalumite and hydrotalcite-like materials: Investigation of the series $Ca_2M^{3+}(OH)_6Cl·2H_2O$ (M^{3+}: Al^{3+}, Ga^{3+}, Fe^{3+}, and Sc^{3+}) by X-ray powder diffraction.* Journal of Solid State Chemistry, 2002. 167(1): p. 137-144.

80. Terzis, A., Filippakis, S., Kuzel, H.J., Burzlaff, H. , *The crystal structure of $Ca_2Al(OH)_6Cl·2H_2O$.* Zeitschrift für Kristallographie 1981: p. 29-34.

81. Taylor, H.F.W., *Crystallographic Data for the Calcium Silicates* HMSO, London, UK, 1956.

82. Richardson, I.G., *The calcium silicate hydrates.* Cement and Concrete Research, 2008. 38: p. 137-158.

83. Feldman, R.F., *Helium flow and density measurement of the hydrated tricalcium silicate-water system.* Cement and Concrete Research 1972. 2: p. 123-136.

84. Costoya, M., *Kinetics and microstructural investigation on the hydration of tricalcium silicate.* Ph.D thesis, Ecole Polytechnique Fédérale de Lausanne, Switzerland, 2008.

85. Ramachandran, V.S., *Differential thermal method of estimating calcium hydroxide in calcium silicate and cement pastes* Cement and Concrete Research, 1979. 9: p. 677-684.

86. Chessin, H., Hamilton, W.C., Post, B. , *Position and thermal parameters of oxygen atoms in calcite.* Acta Crystallographica, 1965. 18 p. 689-693.

87. Flint, E.P., McMurdie, H. F., Wells, L. S. , *Hydrothermal and X-ray studies of the garnet-hydrogarnet series and the relationship of the series to hydration products of portland cement.* RP 1355, Journal of Research of the National Institute of Standards and Technology U.S., 1941. 26: p. 13-33.

88. Corazza, E., Sabelli, C., *The crystal structure of syngenite, $K_2Ca(SO_4)_2*(H_2O)$.* Zeitschrift fur Kristallographie, 1967. 124: p. 398-408.

89. Aruja, E., *On the Unit Cell of Calcium Potassium Sulphate Hydrate: Synthetic and Natural Syngenite.* Mineralogical Magazine, 1958. 31: p. 943-946.

90. Bokii, G.B., Pal'chik, N.A., Antipin, M.Y., *The crystal structure of syngenite.* Soviet Physics Crystallography, 1978. 23: p. 141-143.

91. Perkins, R., Palmer, C. D., *Solubility of ettringite $(Ca_6[Al(OH)_6]_2(SO_4)_3 .26H_2O)$ at 5-75°C.* Geochimica et Cosmochimica Acta, 1999. 63(13-14): p. 1969-1980.

92. Morris, M.C., McMurdie, H.F., Evans, E.H., Paretzkin, B., de Groot, J.H., Newberry, R. , Hubbard, C.R., Carmel, S.J., National Bureau of Standards Monograph, 1977. 25(14): p. 49.

93. Fiquet, G., Richet, P., Montagnac, G., *High-temperature thermal expansion of lime, periclase, corundum and spinel.* Physics and Chemistry of Minerals, 1999. 27: p. 103-111.

94. Hazen, R.M., *Effects of temperature and pressure on the cell dimensions and isotropic temperature factors of periclase.* American Mineralogist, 1976. 61 p. 266-271.

95. Maslen, E.N., Streltsov, V.A., Streltsova, N.R., Ishizawa, N., Satow, Y., *Synchrotron X-ray study of the electron density in α-Al_2O_3.* Acta Crystallographica, 1993. B49: p. 973-980.

96. Swanson, H.E., Tatge, E., National Bureau of Standards Circular, 1953. 539 (2): p. 20.

97. Glinnemann, J., King, H.E. Jr., Schulz, H. , Hahn, T., La Placa, S.J., Dacol, F. , *Crystal structures of the low-temperature quartz-type phases of SiO_2 and GeO_2 at elevated pressure.* Zeitschrift für Kristallographie, 1992. 198: p. 177-212.

98. Saalfeld, H., Wedde, M., *Refinement of the structure of gibbsite, $Al(OH)_3$.* Zeitschrift für Kristallographie 1974. 139: p. 129-135.

99. Balan, E., Lazzeri, M., Morin, G., Mauri, F., *First-principles study of the OH-stretching modes of gibbsite.* American Mineralogist 2006. 91: p. 115-119.

100. Swanson, H.E., Gilfrich, N.T., Cook, M. I., National Bureau of Standards Circular, 1956. 539(6): p. 62.

101. Desgranges, L., Calvarin, G., Chevrier, G., *Interlayer interactions in $M(OH)_2$: a neutron diffraction study of $Mg(OH)_2$.* Acta Crystallographica, 1996. B52: p. 82-86.

102. Desgranges, L., Grebille, D., Calvarin, G., Chevrier, G., Floquet, N., Niepce, J.C., *Hydrogen thermal motion in calcium hydroxide: $Ca(OH)_2$.* Acta Crystallographica, 1993. B49: p. 812-817.

103. Swanson, H.E., Tatge, E., National Bureau of Standards Circular, 1953. 539(1): p. 95.

104. Maslen, E.N., Streltsov, V.A., Streltsova, N.R., *X-ray study of the electron density in calcite, $CaCO_3$.* Acta Crystallographica, 1993. B49: p. 636-641.

105. Effenberger, H., Mereiter, K., Zemann, J., *Crystal structure refinements of magnesite, calcite, rhodochrosite, siderite, smithsonite, and dolomite, with discussion of some aspects of the stereochemistry of calcite type carbonates.* Zeitschrift für Kristallographie, 1981. 156: p. 233-243.

106. De Villiers, J.P.R., *Crystal structures of aragonite, strontianite, and witherite.* American Mineralogist, 1971. 56 p. 758-767

107. Morris, M.C., McMurdie, H.F., Evans, E.H, Paretzkin, B. , deGroot, J.H., Newberry, R., Hubbard, C.R., Carmel, S.J., National Bureau of Standards Monograph, 1977. 25(14): p. 44.

108. Kamhi, S.R., *On the structure of vaterite $CaCO_3$.* Acta Crystallographica, 1963. 16: p. 770-773.

109. Meyer, H.J., *Struktur and Fehlordnung des Vaterits.* Zeitschrift für Kristallographie, 1969. 128: p. 183-212.

110. Maslen, E.N., Streltsov, V.A., Streltsova, N.R., Ishizawa, N., *Electron density and optical anisotropy in rhombohedral carbonates. III. Synchrotron X-ray studies of $CaCO_3$, $MgCO_3$ and $MnCO_3$.* Acta Crystallographica 1995. B51: p. 929-939.

111. Reeder, R.J., Dollase, W.A., *Structural variation in the dolomite-ankerite solid-solution series: An X-ray, Mdssbauer, and TEM study.* American Mineralogist 1989. 74: p. 1159-1167.

112. Reeder, R.J., Markgraf, S.A., *High-temperature crystal chemistry of dolomite.* American Mineralogist, 1986. 71: p. 795-804.

113. Ross, N.L., Reeder, R.I., *High-pressure structural study of dolomite and ankerite.* American Mineralogist, 1992. 77: p. 412-421.

114. Kirfel, A., Will, G., *Charge density in anhydrite, $CaSO_4$, from X-ray and neutron diffraction measurements.* Acta Crystallographica, 1980. B36: p. 2881-2890.

115. Hawthorne, F.C., Ferguson, R.B., *Anhydrous sulphates; II, Refinement of the crystal structure of anhydrite* Canadian Mineralogist 1975. 13 p. 289-297.

116. Hartmann, R., *On the unit cell dimensions and bond lengths of anhydrite.* European Journal of Mineralogy, 1989. 1: p. 721-722.

117. Lager, G.A., Armbruster, T., Rotella, F.J., Jorgensen, J.D., Hinks, D.G., *A crystallographic study of the low-temperature dehydration products of gypsum, $CaSO_4.2H_2O$, hemihydrate $CaSO_4•0.5H_2O$, and 'γ'-$CaSO_4$.* American Mineralogist 1984. 69: p. 910-918.

118. Abriel, W., *Calcium sulfat subhydrat, $CaSO_4·0,8H_2O$.* Acta Crystallographica, 1983. C39 p. 956-958.

119. Pedersen, B.F., Semmingsen, D., *Neutron diffraction refinement of the structure of gypsum, $CaSO_4.2H_2O$.* Acta Crystallographica, 1982. B38: p. 1074-1077.

120. Schofield, P.F., Knight, K.S., Stretton, I.C., *Thermal expansion of gypsum investigated by neutron powder diffraction* American Mineralogist, 1996. 81: p. 847-851.

121. McGinnety, J.A., *Redetermination of the structures of potassium sulphate and potassium chromate: the effect of electrostatic crystal forces upon observed bond lengths* Acta Crystallographica, 1972. B28: p. 2845-2852.

122. Mehrotra, B.N., Hahn, Th., Eysel, W., Rtipke, H., Illguth, A., *Crystal chemistry of compounds with thenardite (Na_2SO_4V) structure.* Neues Jahrbuch für Mineralogie Monatshefte, 1978: p. 408-421.

123. Hawthorne, F.C., Ferguson, R.B., *Anhydrous sulphates; I, Refinement of the crystal structure of celestite with an appendix on the structure of thenardite* Canadian Mineralogist 1975. 13: p. 181-187.

124. Okada, K., Ossaka, J., *Structures of potassium sodium sulphate and tripotassium sodium disulphate.* Acta Crystallographica, 1980. B36: p. 919-921.

125. Halstead, P.E., Moore, A.E., *The composition and crystallography of an anhydrous calcium aluminosulphate occurring in expanding cement.* Journal of Applied Chemistry, 1962. 12: p. 413-417.

126. Brotherton, P.D., Epstein, J.M., Pryce, M.W., White, A.H., *Crystal structure of 'calcium sulphosilicate' $Ca_5(SiO_4)_2SO_4$.* Australian Journal of Chemistry, 1974. 27 p. 657-660.

127. Mondal, P., Jeffery, J.W., *The crystal structure of tricalcium aluminate, $Ca_3Al_2O_6$.* Acta Crystallographica, 1975. B31: p. 689-697.

128. Swanson, H.E., Fuyat, R.K., Ugrinic, G.M., National Bureau of Standards Circular 1955. 539(5): p. 20.

129. Cervantes Lee, F., Glasser, F.P., *Powder diffraction data for compounds in the series $Na_x(Ca_{3\pm x}Na_x)Al_2O_6$.* Journal of Applied Crystallography, 1979. 12 p. 407- 410.

130. Colville, A.A., Geller, S., *The crystal structure of brownmillerite, Ca_2FeAlO_5.* Acta Crystallographica, 1971. B27: p. 2311-2315.

131. Morris, M.C., McMurdie, H.F., Evans, E.H., Paretzkin, B., deGroot, J.H., Hubbard, C.R., Carmel, S.J. , National Bureau of Standards Monograph 1979. 25 (16): p. 186.

132. Nishi, F., Takeuchi, Y., *The rhombohedral structure of tricalcium silicate at 1200˚C.* Zeitschrift für Kristallographie 1984. 168 p. 197-212.

133. Ilyinets, A.M., Simonov, V.I., Bikbau., M.Ya., *New-data concerning atomic structures of Portland cement silicates.* 8th International Congress on the Chemistry of Cement, Rio de Janeiro, 1986. Vol. 6: p. 489- 491.

134. Nishi, F., Takeuchi, Y., Maki, I., *Tricalcium silicate $Ca_3O[SiO_4]$: The monoclinic superstructure.* Zeitschrift für Kristallographie, 1985. 172: p. 297-314.

135. Mumme, W.G., *Crystal structure of tricalcium silicate from a Portland cement clinker and its application toquantitative XRD analysis.* Neues Jahrbuch für Mineralogie Monatshefte, 1995: p. 145-160

136. Golovastikov, N.I., Matveeva, R.G., Belov, N.V., *Crystal structure of tricalcium silicate $CaO{\bullet}SiO_2$-C_3S* Soviet Physics Crystallography, 1975. 20: p. 441-445

137. Udagawa, S., Urabe, K., Iano, T., Review of the 34th General Meeting, Cement Association of Japan, Tokyo 1980: p. 37.

138. Saalfeld, H., *X-Ray Investigation of Single Crystals of β-Ca_2SiO_4 (Larnite) at High Temperatures.* American Mineralogist, 1975. 60: p. 824-827.

139. Jost, K.H., Ziemer, B., Seydel, R., *Redetermination of the structure of β-dicalcium silicate.* Acta Crystallographica, 1977. B33: p. 1696-1700.

140. Midgley, C.M., *The crystal structure of β-dicalcium silicate.* Acta Crystallographica, 1952. 5 p. 307-312.

141. Udagawa, S., Urabe, K., Natsume, M., Yano, T. , *Refinement of the crystal structure of gamma-Ca_2SiO_4* Cement Concrete Research, 1980. 10: p. 139-144.

142. Swanson, H.E., Gilfrich, N.T., Cook, M. I., Stinchfield, R., Parks, P.C., National Bureau of Standards Circular 1959. 539(8): p. 3.

143. Pöllmann, H., Auer, S., Kuzel, H.J., Wenda, R., *Solid solution of ettringites. II: Incorporation of $B(OH)_4^-$ and CrO_4^{2-} in $3CaO.Al_2O_3.3CaSO_4.32H_2O$.* Cement Concrete Research, 1993. 23: p. 422–430.

144. McMurdie, H.F., Morris, M.C., Evans, E.H., Paretzkin, E., Wong-Ng, W., Zhang, Y., *Standard X-ray diffraction powder patterns from the JCPDS research associateship.* Powder Diffraction, 1987. 2(1): p. 41-52.

145. Effenberger, H., Kirfel, A., Will, G., Zobetz, E., *A further refinement of the crystal structure of thaumasite, $Ca_3Si(OH)_6CO_3SO_4 \bullet 12H_2O$.* Neues Jahrbuch für Mineralogie Monatshefte, 1983: p. 60-68.

146. Jacobsen, S.D., Smyth, J.R., Swop, R.J., *Thermal expansion of hydrated six-coordinate silicon in thaumasite, $Ca_3Si(OH)_6(CO_3)(SO_4) \bullet 12H_2O$.* Physics and Chemistry of Minerals 2003. 30: p. 321-329.

147. Schwiete, H.E., Iwai, T., *Über das Verhalten der ferritischen Phase im Zement während der Hydratation.* Zement-Kalk-Gips, 1964. 17: p. 379-386.

148. Kuzel, H.J., *Erstaz von Al^{3+} durch Cr^{3+} und Fe^{3+} in $3CaO \bullet Al_2O_3 \bullet CaCl_2 \bullet nH_2O$ und $3CaO \bullet Al_2O_3 \bullet CaSO_4 \bullet nH_2O$.* Zement-Kalk-Gips, 1968. 21 p. 463-469.

149. Ecker, M., Pöllmann, H.J., PDF 42-1472, ICDD, Grant in Aid, 1991.

150. Kuzel, H.J., *Crystallographic data and thermal decomposition of synthetic gehlenite hydrate, $2CaO \bullet Al_2O_3 \bullet SiO_2 \bullet 8H_2O$.* Neues Jahrbuch für Mineralogie Abhandlungen, 1976. 148 p. 319-325

151. Hentschel, G., Kuzel, H.J., *Strätlingit, $2CaO\text{-}Al_2O_3\text{-}SiO_2 \cdot 8H_2O$, ein neues Mineral.* Neues Jahrbuch für Mineralogie Monatshefte, 1976: p. 326- 330.

152. Rinaldi, R., Sacerdoti, M., Passaglia, E., *Strätlingite: crystal structure, chemistry, and a reexamination of its polytype vertumnite.* European Journal of Mineralogy, 1990. 2: p. 841-849.

153. Renaudin, G., Francois, M., Evrard, O., *Order and disorder in the lamellar hydrated tetracalcium monocarboaluminate compound.* Cement Concrete Research, 1999. 29: p. 63-69.

154. Simon, G., Thesis, Erlangen, Germany, 1984.

155. Scheller, T., et al., 6th International Congress on the Chemistry of Cement, Moscow, 1976. Vol. 2, part 1: p. 217.

156. Kuzel, H.J., *Röntgenuntersuchung in System $3CaO \bullet Al_2O_3 \bullet CaSO_4 \bullet nH_2O\text{-}3CaO \bullet Al_2O_3 \bullet CaCl_2 \bullet nH_2O\text{-}\ nH_2O$* Neues Jahrbuch für Mineralogie Monatshefte, 1966: p. 193-200.

157. Rapin, J.P., Renaudin,G., Elkaim, E., Francois, M., *Structual transition of Friedel's salt $3CaO \bullet Al_2O_3 \bullet CaCl_2 \bullet 10H_2O$ studied by synchrotron powder diffraction.* Cement and Concrete Research, 2002. 32: p. 513-519.

158. Götz Neunhoeffer, F., PhD thesis (in german), University of Erlangen-Nürnberg, Germany 1996: p. 124-135.

159. Kuzel, H.J., *Uber die orientierte entwässerung von tricalciumaluminathydrat* $3CaO{\cdot}Al_2O_3{\cdot}6H_2O$. Neues Jahrbuch für Mineralogie Monatshefte, 1969: p. 397-404.

160. Brandenberger, E., *Kristallstrukturelle Untersuchungen an Ca-Aluminathydraten.* Schweizerische Mineralogische und Petrographische Mitteilungen 1933. 13: p. 569 (abstract).

161. Lager, G.A., Armbruster, T., Faber, J., *Neutron and X-ray diffraction study of hydrogarnet* $Ca_3Al_2(O_4H_4)_3$. American Mineralogist, 1987. 72: p. 756-765.

162. Rinaldi, R., Passaglia, E., *Katoite, a new nember of the* $Ca_3Al_2(SiO_4)_3$-$Ca_3Al_2(OH)_{12}$ *series and a new nomenclature for the hydrogrossular group of minerals.* Bulletin de Mineralogie 1984. 107: p. 606-618.

163. Gard, J.A., Taylor, H.F.W., Cliff, G., Lorimer, G.W., *A re-examination of jennite.* American Mineralogist 1977. 62: p. 365-368.

164. Bonaccorsi, E., Merlino, S., Taylor, H.F.W., *The crystal structure of jennite* $Ca_9Si_6O_{18}(OH)_6{\bullet}8H_2O$. Cement and Concrete Research 2004. 34 p. 1481-1488.

165. Bonaccorsi, E., Merlino, S., Kampf, A.R., *The crystal structure of Tobermorite 14Å (Plombierite), a C-S-H phase.* Journal of the American Ceramic Society, 2005. 88(3): p. 505-512.

166. Malik, K.M.A., Jeffery, J.W., *A re-investigation of the structure of afwillite.* Acta Crystallographica, 1976. B32: p. 475-480.

167. Megaw, H.D., *The structure of afwillite,* $Ca_3(SiO_3OH)_2.2H_2O$. Acta Crystallographica, 1952. 5: p. 477-491.

168. Bellotto, M., Rebours, B., Clause, O., Lynch, J., Bazin, D. , *A Reexamination of Hydrotalcite Crystal Chemistry.* Journal of Physical Chemistry, 1996. 100: p. 8527-8534.

169. Allmann, R., Jepsen, H.P., *Die struktur des hydrotalkits.* Jahrbuch für Mineralogie Monatshefte, 1969: p. 544-551.

170. Sato, T., Fujita, H., Endo, T., Shimada, M., Tsunashima, A. , *Synthesis of hydrotalcite-like compounds and their physico-chemical properties.* Reactivity of Solids, 1988. 5 p. 219-228.

171. Koritnig, S., Süsse, P., *Meixnerite.* American Mineralogist, 1976. 61: p. 176 (abstract).

172. Mascolo, G., Marino, O., *A new synthesis and characterization of magnesium-aluminium hydroxides.* Mineralogical Magazine, 1980. 43: p. 619-621.

173. Renaudin, G., PhD thesis (in french), University of Henri Poincaré, Nancy, France, 1998: p. 150.

174. Chatterjee, S., *Mechanism of the $CaCl_2$ attack on portland cement concrete.* Cement and Concrete Research, 1978. 8: p. 461-468.

175. Conjeaud, M., *Mecanisme d'attaque des Ciments Portland par $CaCl_2$.* Semin. Intern., Torino, Italy, 1982.

176. Ramachandran, V.S., *Concrete Admixtures Handbook: Properties, Science and Technology.* Noyes Publications, 1984.

177. Abdelrazig, B.E.I., Bonner, D.G., Nowell, D.V., Dransfield, J.M., Egan P.J., *The solution chemistry and early hydration of ordinary portland cement pastes with and without admixtures.* Thermochimica Acta, 1999. 340-341: p. 41-430.

178. Andrade, C., *Calculation of chloride diffusion coefficients in concrete from ionic migration measurements* Cement and Concrete Research, 1993. 23(3): p. 724-742.

179. Brown, P., Bothe Jr., J., *The system CaO-Al_2O_3-$CaCl_2$-H_2O at 23±2˚C and the mechanisms of chloride binding in concrete.* Cement and Concrete Research, 2004. 34: p. 1549-1553.

180. Csizmadia, J., Balazs, G., Tamas, F.D., *Chloride ion binding capacity of aluminoferrites.* Cement and Concrete Research, 2001. 31(4): p. 577-588.

181. Delagrave, A., Marchand, J., Ollivier, J.P., Julien, S., Hazrati, K., *Chloride binding capacity of various hydrated cement paste systems.* Advanced Cement Based Materials, 1997. 6(1): p. 28-35.

182. Dhir, R.K., El-Mohr, M.A.K., Dyer, T.D., *Chloride Binding in GGBS concrete.* Cement and Concrete Research, 1996. 26(12): p. 1767-1773.

183. Geiker, M., Nielsen, E.P., Herfort, D., *Prediction of chloride ingress and binding in cement paste.* Materials and Structures, 2007. 40: p. 405-417.

184. Hirao, H., Yamada, K., Takahashi, H., Zibara, H., *Chloride Binding of Cement Estimated by Binding Isotherms of Hydrates.* Journal of Advanced Concrete Technology, 2005. 3(1): p. 77-84.

185. Kopecskó, K., Balázs, Gy., *Chloride ion binding of steam cured aluminates and cements.* Symposium Dubrovnik, Croatia, 20–23 May 2007. Concrete Structures - Stimulators of Development, Dubrovnik, 2007.

186. Kurdowski, W., Taczuk, L., Trybalska, B., *Behaviour of high alumina cement in chloride solutions.* In: R.J. Mangabhai, Editor, Calcium Aluminate Cements, E & FN Spon, London 1990: p. 222-229.

187. Luping, T., Nilsson, L.O., *Chloride binding capacity and binding isotherms of OPC pastes and mortars.* Cement and Concrete Research, 1993. 23(2): p. 247-253.

188. Nielsen, E.P., Herfort, D., Geiker, M. R., *Binding of chloride and alkalis in Portland cement systems.* Cement and Concrete Research, 2005. 35: p. 117-123.

189. Schwiete, H.E., Ludwig, U., *Combining of Calcium Chloride and Calcium Sulphate in Hydration of Aluminate-Ferrite Clinker Constituents.* Zement Kalk Gips, 1969. 22: p. 225-234.

190. Sumranwanich, T., Tangtermsirikul, S., *A model for predicting time-dependent chloride binding capacity of cement-fly ash cementitious system.* Materias and Structures, 2004. 37: p. 387-396.

191. Suryavanshi, A.K., Scantlebury, J.D., Lyon, S.B., *The binding of chloride ions by sulphate resistant Portland cement.* Cement and Concrete Research, 1995. 25(3): p. 581-592.

192. Tritthart, J., *Chloride binding in Cement, II the influence of the hydroxide concentration in the pore solution of hardened cement paste on chloride binding.* Cement and Concrete Research, 1989. 19: p. 683-691.

193. Xu, Y., *The influence of sulphates on chloride binding and pore solution chemistry.* Cement and Concrete Research, 1997. 27(12): p. 1841-1850.

194. Yuan, Q., Shi, C., De Schutter, G., Audenaert, K., Deng, D., *Chloride binding of cement-based materials subjected to external chloride environment – A review.* Construction and Building Materials, 2009. 23: p. 1-13.

195. Zibara, H., *Binding of external chlorides by cement pastes.* PhD-Thesis, University of Toronto, Canada, 2001.

196. Zibara, H., Hooton, D., Yamada, K., Thomas, M.D.A., *Roles of cement mineral phases in chloride binding.* Cement Science and Concrete Technology, 2002. 56: p. 384-391.

197. Gégout, P., Revertégat, E., Moine, G., *Action of chloride ions on hydrated cement pastes : Influence of the cement type and long time effect of the concentration of chlorides.* Cement and Concrete Research, 1992. 22: p. 451-457.

198. Richartz, W., *Die Bindung von Chlorid bei Zementerhärtung.* Zement Kalk Gips, 1969. 10: p. 447-456.

199. Fischer, R., Kuzel, H.J., Schellhorn, H., *Hydrocalumit, Mischkristalle von 'Friedelschem Salz' $3CaO•Al_2O_3•CaCl_2•10H_2O$' und Tetrecalciuminathydrat?* . Neues Jahrbuch für Mineralogie Monatshefte 1982. 7: p. 322-334.

200. Pöllmann, H., *Mischkristallbildung in den Systemen $3CaO•Al_2O_3•CaCl_2•10H_2O$-$3CaO•Al_2O_3•CaCO_3•11H_2O$ und $3CaO•Al_2O_3•CaCl_2•10H_2O$-$3CaO•Al_2O_3•Ca(OH)_2•12H_2O$* Diploma Thesis, 1980.

201. Hobbs, M., *Solubilities and ion exchange properties of solid solutions between the OH, Cl and CO_3 end members of the monocalcium aluminate hydrates.* PhD Thesis, University of Waterloo, Canada, 2001.

202. Hirao, H., Yokoyama, S., *Behavior of chloride ions in hardened ecocement: a new type Portland cement made from municipal waste incinerator ash.* 11 th International Congress on the Chemistry of Cement, Durban, South Africa, 2003: p. 1271-1273.

203. Theissing, E.M., Mebius-Van De Laar, T., De Wind, G., *The combining of sodium chloride and calcium chloride by the hardened Portland cement compounds C_3S, C_2S, C_3A and C_4AF.* Proceedings of 8th International Symposium on Chemistry of Cement, Rio de Janeiro, 1986: p. 823-828.

204. Vialis Terrisse, H., *Interaction des Silicates de Calcium Hydratés, principaux constituants du ciment, avec les chlorures d'alcalins. Analogie avec les argiles.* Ph.D Thesis (in french), Université de Bourgogne, France, 2000.

205. Beaudoin, J.J., Ramachandran, V.S., Feldman, R.F, *Interaction of chloride and C-S-H.* Cement and Concrete Research, 1990. 20: p. 875-883.

206. Page, C.L., Short, N.R., El Tarras, A., *Diffusion of chloride ions in hardened cement pastes* Cement and Concrete Research, 1981. 11(3): p. 395-406.

207. Page, C.L., Short N.R., Holden, W.R., Materials Research Group, *The Influence of Different Cements on Chloride-Induced Corrosion of Reinforcing Steel.* Cement and Concrete Research, 1986. 16: p. 79-86.

208. Diamond, S., *Chloride concentrations in concrete pore solutions resulting from calcium and sodium chloride admixtures.* Cement, Concrete and Aggregates, 1986. 8(2): p. 97-102.

209. Kayyali, O.A., Haque, M.N., *Chloride penetration and the ratio of Cl^-/OH^- in the pores of cement paste.* Cement and Concrete Research, 1988. 18: p. 895-900.

210. Sagoe Crentsil, K.K., Glasser, F.P., *Steel in Concrete: Part 1 A Review of Electrochemical and Thermodynamic aspects.* Magazine of Concrete Research, 1989. 41: p. 205-212.

211. Bentur, A., Diamond, S., Berke, N.S., Steven, B.N., *Steel corrosion in concrete: fundamentals and civil engineering practise*. 1997, London: E&FN Spon.

212. Birnin-Yauri, U.A., *Chloride in cement: Study of the system CaO-Al_2O_3-$CaCl_2$-H_2O.* PhD Thesis, University of Aberdeen, UK, 1993.

213. Sagoe Crentsil, K.K., Glasser, F.P., *"Green rust", iron solubility and the role of chloride in the corrosion of steel at high pH.* Cement and Concrete Research, 1993. 23(4): p. 785-791.

214. Monosi, S., Alvera, I., Collepardi, M., *Chemical Attack of Calcium Chloride on the Portland Cement Paste.* Il Cemento, 1989. 2: p. 97-104.

215. Monosi, S., Collepardi, M., *Research on $3CaO \cdot CaCl_2 \cdot 15H_2O$ Identified in Concrete Damaged by $CaCl_2$ attack.* Il Cemento, 1990. 1: p. 3-8.

216. Tanoutasse, N., *The Hydration Mechanism of C_3A and C_3S in the presence of Calcium chloride and calcium sulphate.* Proc. 5th Int. Symp. On the Chem. Of Cement, Tokyo, 1968. Part 2: p. 372-378

217. Ramachandran, V.S., *Possible State of Chloride in the Hydration of Tricalcium Silicate in the Presence of Calcium Chloride.* Mater. et Constr., 1971. 4(19): p. 3-12.

218. Ramachandran, V.S., *Kinetics of Hydration of Tricalcium Silicate in Presence of Calcium Chloride by Thermal Methods* Thermochimica Acta, 1971. 2: p. 41-55.

219. Odler, I., Skalny, J., *Influence of Calcium Chloride on Paste Hydration of Tricalcium Silicate.* American Ceramic Society, 1971. 54: p. 362-363.

220. Skalny, J., Odler, I., *The Effect of Chlorides upon the Hydration of Portland Cement and Upon Some Clinker Minerals.* Mag. Concr. Res. , 1967. 19: p. 203-210.

221. Pruckner, F., Gjørv, O.E., *Effect of $CaCl_2$ and NaCl additions on concrete corrosivity.* Cement and Concrete Research, 2004. 34: p. 1209-1217.

222. Reddy, B., Glass, G.K., Lim, P.J., Buenfeld, N.R., *On the corrosion risk presented by chloride bound in concrete.* Cement & Concrete Composites, 2002. 24: p. 1-5.

223. Friedel, P.M., *Sur un chloro-aluminate de calcium hydrate se maclant par compression.* Bull. Soc. Fran. Min. Crist., 1897. 20: p. 122-136.

224. Renaudin, G., Kubel, F., Rivera, J.P., Francois, M., *Structural phase transition and high temperature structure of Friedel's salt $3CaO \cdot Al_2O_3 \cdot CaCl_2 \cdot 10H_2O$.* Cement and Concrete Research, 1999. 29(1937-1942).

225. Andersen, M.D., Jakobsen, H.J., Skibsted, J., *Characterization of the $\alpha-\beta$ Phase Transition in Friedels Salt ($Ca_2Al(OH)_6Cl \cdot 2H_2O$) by Variable-Temperature 27Al MAS NMR Spectroscopy.* The Journal of Physical Chemistry, 2002. 106(28): p. 6676–6682.

226. Reardon, E.J., Dewaele, P., *Chemical model for the carbonation of grout/water slurry.* Journal of American Ceramic Society, 1990. 73: p. 1681-1690.

227. Ben Yair, M., *Studies on the stability of calcium chloroaluminate.* Israel Journal of Chemistry, 1971. 9: p. 529-536.

228. Lea, F.M., *The Chemistry of Cement and Concrete (third edition).* Edward Arnold (Publishers) Ltd, 1970.

229. Bensted, J., *Chloroaluminates and the role of calcium chloride in accelerated hardening of Portland cement.* World Cement Technology, 1977. Sept.-Oct.: p. 171-175.

230. Schwiete, H.E., Ludwig, U., *Crystal Structures and properties of Cement Hydration Products (Hydrated Calcium Aliuminates and Ferrites).* Fifth Int. Symp. On the Chem. Of Cement, Tokyo, Japan, 1968: p. 37-67.

231. Schwiete, H.E., Ludwig, U., Albreck, J., *Bindung von Calciumchlorid bei Hydratation der aluminatisch-ferritischen Bestandteile des Portlandzementes.* Die Naturwissenschaften, 1968. 55(4): p. 179.

232. Hussain, E.S., Rasheeduzzafar, Al-Gahtani, A.S., *Influence of sulfates on chloride binding in cements'.* Cement and Concrete Research, 1994. 24(1): p. 8-24.

233. Arya, C., Buenfeld, N.R., Newman, J.B., *Factors influencing chloride-binding in concrete.* Cement and Concrete Research, 1990. 20(2): p. 291-300.

234. Kurdowski, W., *The protective layer and decalcification of C-S-H in the mechanism of chloride corrosion of cement paste.* Cement and Concrete Research, 2004. 34: p. 1555-1559.

235. Kurdowski, W., Duszak, S., *Changes of C-S-H gel in strong chloride solutions.* Advances in Cement Research 1995. 28(7): p. 143-149.

236. Allan, I., Herfort, D., *The mineralogy of chloride attack on concrete with limestone filler.* unpublished paper, Aalborg Portland, 2009.

237. Rasheeduzzafar Hussain, E.S., Al-Saadoun, S.S., *Effect of cement composition on chloride binding and corrosion of reinforcing steel in concrete.* Cement and Concrete Research, 1991. 21(5): p. 777-794.

238. Jensen, O.M., Korzen, M.S.H., Jakobsen, H.J., Skibsted, J., *Influence of cement constitution and temperature on chloride binding in cement paste.* Advances in Cement Research, 2000. 12: p. 57-64.

239. Justnes, H., *A review of chloride binding in cementitious systems.* Nordic Concr. Res., 1998. 21: p. 1-6.

240. Lothenbach, B., Balonis, M., Geiker, M., Glasser, F.P., Thomas, M.D.A., Hooton, D., *Chloride binding in cements.* Under development for submission, 2010.

241. Suryavanshi, A.K., Scantlebury, J.D., Lyon, S.B., *Mechanisms of Friedel's Salt Formation in Cements Rich in Tri-calcium Aluminate.* Cement and Concrete Research, 1996. 26(5): p. 717-727.

242. Rasheeduzzafar , H., E.S., Al-Saadoun, S.S., *Effect of Tricalcium Aluminate Content of Cement on Chloride Binding and Corrosion of Reinforcing Steel in Concrete.* ACI Materials Journal, 1992. 89: p. 3-12.

243. Al-Amoudi, O.S.B., Rasheeduzzafar, Maslehuddin, M., Abduljauwad, S.N., *Influence of chloride ions on sulphate deterioration in plain and blended cements.* Magazine of Concrete Research, 1994. 46(167): p. 113-123.

244. Kuzel, H.J., *X-ray investigations of some complex calcium aluminate hydrates and related compounds.* Proc. Fifth Int. Symp. On the Chem. of Cement, Tokyo, Japan, Supplementary Paper II-19, 1968: p. 92-97.

245. Nielsen, E.P., *The durability of white Portland cement to chemical attack.* Ph.D Thesis, DTU, Denmark, 2004.

246. Page, C.L., Vennesland, Ø, *Pore solution composition and chloride binding capacity of silica-fume cement pastes.* Materials and Structures, 1983. 16: p. 19-25.

247. Sumranwanich, T., Tangtermsirikul, S., *A model for predicting time-dependent chloride binding capacity of cement-fly ash cementitious system* Materials and Structures, 2006: p. 387-396.

248. Jensen, H.U., Pratt, P.L., *The binding of chloride ions by pozzolanic product in fly ash cement blends.* Advances in Cement Research, 1989. 2(7): p. 121-129.

249. Dhir, R.K., Jones, M.R., *Development of chloride-resisting concrete using fly ash.* Fuel, 1999. 78: p. 137–142

250. Fajardo, G., Valdez, P., Pacheco, J., *Corrosion of steel rebar embedded in natural pozzolan based mortars exposed to chlorides.* Constr. Build. Mater., 2009. 23: p. 768–774.

251. Arya, C., Xu, Y., *Effect of cement type on chloride binding and corrosion of steel in concrete.* Cement and Concrete Research, 1995. 25: p. 893–902.

252. Luo, R., Cai, Y., Wang, C., Huang, X., *Study of chloride binding and diffusion in GGBS concrete.* Cement and Concrete Research, 2003. 33(1): p. 1-7.

253. Mohammed, T.U., Hamada H., *Relationship between free chloride and total chloride contents in concrete* Cement and Concrete Research, 2003. 33(9): p. 1487-1490.

254. Song, S., Jennings, H.M., *Pore solution chemistry of alkali-activated ground granulated blast-furnace slag.* Cement and Concrete Research, 1999. 29(2): p. 159-170.

255. Lothenbach, B., Gruskovnjak, A., *Hydration of alkali-activated slag: thermodynamic modelling.* Advances in Cement Research 2007. 19: p. 81-92.

256. Wang, S.D., Scrivener, K.L., *Hydration products of alkali activated slag cement* Cement and Concrete Research, 1995. 25(3): p. 561-571.

257. Andersen, M.D., Jakobsen, H.J., Skibsted, J., *Characterization of the α−β Phase Transition in Friedels Salt ($Ca_2Al(OH)_6Cl{\cdot}2H_2O$) by Variable-Temperature 27Al MAS NMR Spectroscopy.* The Journal of Physical Chemistry A, 2002. 106(28): p. 6676–6682.

258. Bothe Jr, J.V., Brown, P.W., *PhreeqC modeling of Friedel's salt equilibria at 23±1˚C.* Cement and Concrete Research, 2004. 34: p. 1057-1063.

259. Ahmed, S.J., Dent-Glasser, L.S., Taylor, H.F.W., *Crystal structures and reactions of C_4AH_{12} and derived basic salts.* Proceedings 5th International Symposium on the Chemistry of Cement Suppl.-Paper II-77, Tokyo, Japan, 1968: p. 118-127.

260. Vieille, L., Rousselot, I., Leroux, F., Besse, J.P., Taviot-Guého, C., *Hydrocalumite and its polymer derivatives. 1. Reversible thermal behavior of Friedel's salt: a direct observation by means of high-temperature in situ powder X-ray diffraction.* Chemistry of Materials 2003. 15: p. 4361-4368.

261. Trezza, M.A., Lavat, A.E., *Analysis of the system $3CaO{\cdot}Al_2O_3$–$CaSO_4{\cdot}2H_2O$–$CaCO_3$–H_2O by FT-IR spectroscopy.* Cement and Concrete Research, 2001. 31(6): p. 869-872.

262. Pöllmann, H., Kuzel, H. J., *Synthesis and polymorphic transformations of solid solutions in the system $3CaO{\bullet}Al_2O_3{\bullet}CaCl_2{\bullet}nH_2O$-$3CaO{\bullet}Al_2O_3{\bullet}Ca(OH)_2{\bullet}nH_2O$-$H_2O$.* Neues Jahrbuch für Mineralogie Monatshefte 1988: p. 193-202.

263. Roberts, M.H., *Calcium Aluminate Hydrates and Related Basic Salt Solid Solutions.* Proc. Fifth Int. Symp. On the Chem. Of Cement, Tokyo, Japan, Supplementary Paper II, 1968: p. 104-117.

264. Turriziani, R., Schippa, G., *Contribution to the knowledge of hydrated calcium chloro-aluminates.* Ric. Scient. , 1955. 25: p. 3102-3106.

265. Hirao, H., *Current state of the studies on chloride binding by cement (draft).* Committee of literature survey, Material Div., 2003.

266. Loser, R., Lothenbach, B., Leemann, A., Tuchschmid, M., *Chloride resistance of concrete and its binding capacity – Comparison between experimental results and thermodynamic modeling* Cement & Concrete Composites, 2010. 32(1): p. 34-42.

267. Hall, C., Barnes, P., Billimore, A.D., Jupe, A.C., Turrillas, X., *Thermal decomposition of ettringite $Ca_6[Al(OH)_6]_2(SO_4)_3{\cdot}26H_2O$.* Journal of the Chemical Society, Faraday Transactions 1996. 92(12): p. 2125–2129.

268. Zhou, Q., Glasser, F.P., *Thermal stability and decomposition mechanisms of ettringite at <120°C.* Cement and Concrete Research, 2001. 31(9): p. 1333-1339.

269. Alonso, C., Andrade, C., Castellote, M., Castro, P., *Chloride threshold values to depassivate reinforcing bars embedded in a standardized OPC mortar.* Cement and Concrete Research, 2000. 30(7): p. 1047– 1055.

270. Ann, K.Y., Jung, H.S., Kim, H.S., Kim, S.S., Moon, H.Y., *Effect of calcium nitrite-based corrosion inhibitor in preventing corrosion of embedded steel in concrete.* Cement and Concrete Research, 2006. 36: p. 530-535.

271. Ann, K.Y., Buenfeld, N.R., *The effect of calcium nitrite on the chloride-induced of steel in concrete.* Magazine of Concrete Research, 2007. 59(9): p. 689-697.

272. Berke, N.S., Hicks, M.C, *Predicting long-term durability of steel reinforced concrete with calcium nitrite corrosion inhibitor.* Cement & Concrete Composites, 2004. 26: p. 191-198.

273. Gonzalez, J.A., Ramirez, E., Bautista, A., *Protection of steel embedded in chloride-containing concrete by means of inhibitors.* Cement and Concrete Research, 1998. 28(4): p. 577-589.

274. Mammoliti, L., Hansson, C.M. , Hope, B.B., *Corrosion inhibitors in concrete Part II: Effect on chloride threshold values for corrosion of steel in synthetic pore solutions.* Cement and Concrete Research, 1999. 29: p. 1583-1589.

275. Ormellese, M., Berra, M., Bolzoni, F., Pastore, T., *Corrosion inhibitors for chlorides induced corrosion in reinforced concrete structures.* Cement and Concrete Research, 2006. 36: p. 536-547.

276. Reou, J.S., Ann, K.Y., *The electrochemical assessment of corrosion inhibition effect of calcium nitrite in blended concretes.* Materials Chemistry and Physics, 2008. 109: p. 526-533.

277. Sideris, K.K., Savva, A.E., *Durability of mixtures containing calcium nitrite based corrosion inhibitor.* Cement & Concrete Composites, 2005. 27: p. 277-287.

278. Andrade, C., *Some laboratory experiments on the Inhibitor Effect of Sodium Nitrite on Reinforcement Corrosion.* Cement, Concrete & Aggregates, 1986. 8(2): p. 110-116.

279. Rosenberg, A.M., Gaidis, J.M., Kossivas, T.G., Previte, R.W., *A corrosion inhibitor formulated with calcium nitrite for use in concrete. In: Chloride corrosion of steel in concrete.* Tonini DE, Dean Jr SW, editors. ASTM STP 629. American Society for Testing and Materials, 1977: p. 89-99.

280. Justnes, H., Nygaard, E.C., *Technical calcium nitrate as set accelerator for cement at low temperatures.* Cement and Concrete Research, 1995. 25(8): p. 1766-1774.

281. Dodson, V.H., *Set Accelerating Admixtures.* Concrete Admixtures, Structual Engineering Series, Van Norstrand Reinhold, Chapter 4, 1990: p. 73-102.

282. Aggoun, S., Cheikh-Zouaoui, M., Chikh, N., Duval, R., *Effect of some admixtures on the setting time and strength evolution of cement pastes at early ages* Construction and Building Materials, 2008. 22: p. 106-110.

283. Wiltbank, K., Schwartz, S., Schindler W., *Effect of Selected Accelerants on the Physical Properties of Mineral Trioxide Aggregate and Portland Cement.* Journal of Endodontics, 2007. 33(10): p. 1235-1238.

284. Kuzel, H.J., *Über die Hydratstufen der Hydroxisalze $3CaO•Me_2O_3•CaCl_2•nH_2O$ und $3CaO•Me_2O_3•Ca(NO_3)_2•nH_2O$.* Neues Jahrbuch für Mineralogie Monatshefte, 1970: p. 363-374.

285. Dumm, J.Q., Brown, P.W., *Phase assemblages in the system $Ca(OH)_2$-Al_2O_3-$Ca(NO_3)_2$-H_2O.* Advances in Cement Research, 1996. 32: p. 143-153.

286. Kuzel, H.J., *X-ray investigations of some complex calcium aluminate hydrates and related compounds.* Supplementary Paper II-19, Proceeding of the 5th International Symposium on the Chemistry of Cement, Part 2, Vol.2, Tokyo, Japan, 1968: p. 92-97.

287. Goske, J., Stober, S., Pölmann, H., Martin-Luther Univ., Halle Germany, ICDD Grant-in-Aid, 2000.

288. Asaga, K., Tsuchiya, Y., Shimada, N., Torii, H., *Reaction between NO_3^- Ion and $3CaO•Al_2O_3$ in Aqueous Solutions with or without SO_4^{2-} and Cl^- Ions* AIP Conference Proceedings, 2006. 833: p. 190-195.

289. Renaudin, G., Rapin, J.P., Humbert, B., François, M., *Thermal behaviour of the nitrated AFm phase $Ca_4Al_2(OH)_{12}(NO_3)_2•4H_2O$ and structure determination of the intermediate hydrate $Ca_4Al_2(OH)_{12}(NO_3)_2•2H_2O$* Cement and Concrete Research, 2000. 30(2): p. 307-314.

290. Renaudin, G., François, M., *The lamellar double-hydroxide (LDH) compound with composition $3CaO•Al_2O_3•Ca(NO_3)_2•10H_2O$.* Acta Crystallographica, 1999. C55: p. 835–838

291. Foret, J., *Calcium nitroaluminate.* Compt. rend. , 1930. 191: p. 52-54.

292. Rozenberg, T.I., Breitman, E.D., Gracheva, O.I., *Investigation of Products of Interaction between Calcium Nitrate and Tricalcium Aluminate.* Doklady Akademii Nauk SSSR-Doklady Chemistry, 1971. 199-201: p. 780-782.

293. Mędala, M., *Etudes des interactions entre les phases minérales constituant le ciment portland et des solutions salines concentrées.* AGH (Cracow, Poland), Université de Bourgogne (Dijon, France), Ph.D thesis (in french), 2005.

294. Feitknecht, W., Buser, H. W., *Über den Bau der plättchenförmigen Calcium-Aluminiumhydroxysalze.* Helvetica Chimica Acta, 1951. 34: p. 128-142.

295. Brown, P.W., *Method of resisting corrosion in metal reinforcing elements contained in concrete and related compounds and structures.* US Patent 6755925 (2004).

296. Justnes, H., Nygaard, E.C., *The influence of technical calcium nitrate additions on the chloride binding capacity of cement and the rate of chloride induced corrosion of steel embedded in mortars.* In: Swamy RN, editor. Proceedings of international conference on corrosion and corrosion protection of steel in concrete. UK: Sheffield, 1994: p. 491-502.

297. Gaidis, J.M., *Chemistry of corrosion inhibitors.* Cement & Concrete Composites, 2004. 26: p. 181-189.

298. Park, J.Y., Byun, H.J., Choi, W.H., Kang, W.H., *Cement paste column for simultaneous removal of fluoride, phosphate, and nitrate in acidic wastewater* Chemosphere, 2007. 70: p. 1429-1437.

299. Amadelli, R., Samiolo, L., *Concrete Containing TiO_2: An Overview Of Photocatalytic NO_x Abatement.* International RILEM Symposium on Photocatalysis, Environment and Construction Materials, Florence, Italy, 8-9 October 2007.

300. Guerrini, G.L., Peccati, E., *Photocatalytic Cementitious Roads for Depollution.* International RILEM Symposium on Photocatalysis, Environment and Construction Materials, Florence, Italy, 8-9 October 2007.

301. Andrade, C., PhD. Thesis, Universidad Complutense de Madrid, Spain, 1973.

302. Gaidis, J.M., Rosemberg, A.M., *The Inhibition of Chloride-Induced Corrosion in Reinforced Concrete by Calcium Nitrite.* Journal of Cement, Concrete and Aggregates, 1987. 9(1): p. 30.

303. Tritthart, J., Banfill, P.F.G., *Nitrite binding in cement.* Cement and Concrete Research, 2001. 31: p. 1093-1100.

304. Justnes, H., *Calcium nitrate as corrosion inhibitor for reinforced concrete.* Innovations and Development in Concrete Materials and Construction, Thomas Telford Publishing, 2002: p. 391-401.

305. Sverjensky, D., Shock E.L., Helgeson, H.C., *Prediction of the thermodynamic properties of aqueous metal complexes to 1000°C and 5 kbar.* Geochimica et Cosmochimica Acta, 1997. 61: p. 1359-1412

306. Sà, J., Anderson, J.A., *FTIR study of aqueous nitrate reduction over Pd/TiO_2.* Applied Catalysis B: Environmental, 2008. 77: p. 409-417

307. Garcia Lodeiro, I., Fernández-Jimenez, A. Palomo, A., Macphee D.E**,** *Effect on fresh C-S-H gels of the simultaneous addition of alkali and aluminium.* Cement and Concrete Research, 2010. 4: p. 27-32

Figures and Tables

Figures

Figure 4.1: Density trends in the (OH, CO_3) AFm phases. 47

Figure 4.2: Relation between water content and density of: OH-AFm (a ,top), SO_4-AFm (b, middle) and SO_4-AFt (c, bottom). 50

Figure 5.1: Powder pattern of Friedel's salt containing a mixture of monoclinic and rhombohedral polymorphs. 59

Figure 5.2: Powder patterns of Friedel's salt after 3 months of equilibration with water at different temperatures. HG peaks are attributed to hydrogarnet. 61

Figure 5.3: Powder patterns of Kuzel's salt after 3 months of equilibration with water at different temperature; Ms-monosulfoaluminate, Ks-Kuzel's salt, Fs-Friedel's salt.64

Figure 5.6(a): Partial XRD patterns of the solid solution formation at 25˚C between Friedel's salt and hydroxy AFm: wet samples.. 69

Figure 5.6(b): Partial XRD patterns of the solid solution formation at 25˚C between Friedel's salt and hydroxy AFm: wet samples. 69

Figure 5.7(a): Partial XRD patterns of the solid solution formation at 25±2˚C between Friedel's salt and hydroxy AFm: samples dried at 35% RH. 70

Figure 5.7(b): Partial XRD patterns of the solid solution formation at 25±2˚C between Friedel's salt and hydroxy AFm: samples dried at 35% RH..... 70

Figure 5.8(a): Equilibrium calcium and aluminium aqueous concentrations commencing from undersaturation for samples between hydroxy AFm (Cl/Al=0) - Friedel's salt (Cl/Al=1) and with an excess of calcium chloride (values > 1); at 25±2ºC and after 180 days of equilibration.. 72

Figure 5.8(b): Equilibrium chloride aqueous concentrations commencing from undersaturation for samples between hydroxy AFm (Cl/Al=0) and Friedel's salt (Cl/Al=1) and with an excess of calcium chloride (values > 1); at 25±2ºC and after 180 days of equilibration. 72

Figure 5.9.: Gibbs energy of ideal mixing, ΔGid, excess Gibbs energy of mixing, ΔGex, and resulting molar Gibbs energy of mixing, ΔGM, calculated from Eq. for the Friedel's salt (Cl-AFm)-hydroxy AFm (OH-AFm) solid solution series assuming incomplete solid solution and Guggenheim parameters a_0=0.669 and a_1=2.59 for miscibility gap fractions $0.03 \leq x \leq 0.2$. 73

Figure 5.10(a): Partial XRD patterns of mixtures between Friedel's salt and monosulfoaluminate at 25±2˚C; note formation of Kuzel's salt at SO4/(SO4+2Cl) ratio 0.5. 74

Figure 5.10(b): Partial XRD patterns of mixtures between Friedel's salt and monosulfoaluminate at 25±2˚C; note formation of Kuzel's salt at $SO_4/(SO_4+2Cl)$ ratio 0.5. 74

Figure 5.11(a): Equilibrium calcium and aluminium aqueous concentrations commencing from undersaturation for samples between monosulfoaluminate (Cl/Al=0) - Friedel's salt (Cl/Al=1) at 25±2ºC and after 180 days of equilibration. .. 76

Figure 5.11(b): Equilibrium chloride aqueous concentrations commencing from undersaturation for samples between monosulfoaluminate (Cl/Al=0) and Friedel's salt (Cl/Al=1) at 25±2ºC and after 180 days of equilibration.. 76

Figure 5.12(a): Partial XRD patterns of the solid solution formation at 25±2˚C between Friedel's salt and monocarboaluminate. Drying at 35% RH does not introduce phase changes. 78

Figure 5.12(b): Partial XRD patterns of the solid solution formation at 25±2˚C between Friedel's salt and monocarboaluminate. Drying at 35% RH does not introduce phase changes. 78

Figure 5.13(a): Equilibrium calcium and aluminium aqueous concentrations, commencing from undersaturation, for solids between monocarboaluminate (Cl/Al=0) - Friedel's salt (Cl/Al=1) and with an excess of calcium chloride (values > 1) at 25±2ºC and 180 days of equilibration. 80

Figure 5.13(b): Equilibrium chloride aqueous concentrations, commencing from undersaturation for solids between monocarboaluminate (Cl/Al=0) - Friedel's salt (Cl/Al=1) and with an excess of calcium chloride (values > 1) at 25±2ºC and after 180 days of equilibration. 80

Figure 5.14: XRD patterns showing mineralogical phase assemblage of the mixture containing 0.01 moles Friedel's salt and 0.01 moles $Ca(OH)_2$ which was kept with continuous stirring in 60 ml H_2O at 25±2˚C for 180 days. 81

Figure 5.15: XRD patterns showing mineralogical phase assemblage of the mixture containing 0.01 moles Friedel's salt, 0.01 moles $Ca(OH)_2$ and 0.01 moles $CaCO_3$ which was kept with continuous stirring in 60 ml H_2O at 25±2˚C for 180 days. 81

Figure 5.16: XRD patterns showing mineralogical phase assemblage of the mixture containing 0.01 moles Friedel's salt, 0.01 moles $Ca(OH)_2$ and 0.005 moles $CaSO_4$ which was kept with continuous stirring in 60 ml H_2O at 25±2˚C for 180 days. 82

Figure 5.17: XRD patterns showing mineralogical phase assemblage of the mixture containing 0.01 moles Friedel's salt, 0.01 moles $Ca(OH)_2$ and 0.02 moles $CaSO_4$ which was kept with continuous stirring in 60 ml H_2O at 25±2˚C for 180 days. 82

Figure 5.18: Relative amount of solid hydrate phases of a hydrated model mixture consisting of initially 1 mol C_3A, excess of portlandite and with fixed initial sulfate ratio (SO_3/Al_2O_3=1) showing phase development and its dependence on changing chloride ratio ($2Cl/Al_2O_3$) at 25°C. 84

Figure 5.19(a): Calculated total volume of solid phases of a hydrated model mixture initially consisting of 0.01 moles C_3A, 60 ml H_2O, 0.015 moles portlandite and with fixed initial sulfate ratio (SO_3/Al_2O_3=1) showing phase development and its dependence on changing chloride ratios ($2Cl/Al_2O_3$) at 25°C.. 86

Figure 5.19(b): Calculated and experimental aqueous composition of hydrated model mixture initially consisting of 0.01 moles C_3A, 0.015 moles portlandite, 60 ml H_2O and with fixed initial sulfate ratio (SO_3/Al_2O_3=1) showing its dependence on changing chloride ratio ($2Cl/Al_2O_3$) at 25±2°C. 86

Figure 5.20: XRD patterns showing mineralogical changes and influence of $CaCl_2$ addition for the system: 0.01 moles C_3A-0.01 moles $CaSO_4$-0.015 moles $Ca(OH)_2$- 60 ml H_2O at 25±2˚C; respectively plots: **1**-no $CaCl_2$ present; **2**-0.003 moles of $CaCl_2$ added; **3**-0.005 moles $CaCl_2$ added; **4**-0.01 moles $CaCl_2$ added. 87

Figure 5.21(a): Total volume of solid phases of a hydrated model mixture initially consisting of 0.01 moles C_3A, 60 ml H_2O, 0.015 moles portlandite, 0.0075 moles $CaCO_3$ and with fixed initial sulfate ratio (SO_3/Al_2O_3=1) showing phase development and its dependence on changing chloride ratios ($2Cl/Al_2O_3$) at 25°C..... 89

Figure 5.21(b): Calculated and experimental aqueous composition of hydrated model mixture initially consisting of 0.01 moles C_3A, 0.015 moles portlandite, 0.0075 mol $CaCO_3$, 60 ml H_2O and with fixed initial sulfate ratio (SO_3/Al_2O_3=1) showing its dependence on changing chloride ratios ($2Cl/Al_2O_3$) at 25±2°C. 89

Figure 5.22: XRD patterns showing mineralogical changes and influence of $CaCl_2$ addition for the system 0.01 moles C_3A-0.01 moles $CaSO_4$-0.015 moles $Ca(OH)_2$-0.0075 moles $CaCO_3$- 60 ml H_2O at 25±2˚C; 1-no $CaCl_2$ present; 2-0.01 moles of $CaCl_2$ added. 90

Figure 5.23: Schematic phase relations at 25˚C, between Friedel's salt, monosulfoaluminate and monocarboaluminate..... 91

Figure 5.24: Schematic phase relations at 25˚C, between Friedel's salt, hydroxy AFm and monocarboaluminate. 92

Figure 5.25: Calculated total volume of solid phases of a hydrated model mixture initially consisting of 0.01 moles C_3A, 60 ml H_2O, 0.015 moles portlandite and with fixed initial sulfate ratio (SO_3/Al_2O_3=1) showing phase development and its dependence on changing chloride ratios ($2Cl/Al_2O_3$) at 5°C. 93

Figure 5.26: Calculated total volume of solid phases of a hydrated model mixture initially consisting of 0.01 moles C_3A, 60 ml H_2O, 0.015 moles portlandite and with fixed initial sulfate ratio (SO_3/Al_2O_3=1) showing phase development and its dependence on changing chloride ratios ($2Cl/Al_2O_3$) at 55°C. 94

Figure 5.27: Calculated total volume of solid phases of a hydrated model mixture initially consisting of 0.01 moles C_3A, 60 ml H_2O, 0.015 moles portlandite and with fixed initial sulfate ratio (SO_3/Al_2O_3=1) showing phase development and its dependence on changing chloride ratios ($2Cl/Al_2O_3$) at 85°C. 95

Figure 5.28: Calculated total volume of solid phases of a hydrated model mixture initially consisting of 0.01 moles C_3A, 60 ml H_2O, 0.015 moles portlandite and with fixed initial sulfate ratio (SO_3/Al_2O_3=1) and chloride ratio ($2Cl/Al_2O_3$=0.5) showing phase development and its dependence on changing temperature. 96

Figure 5.29: Calculated total volume of solid phases of a hydrated model mixture initially consisting of 0.01 moles C_3A, 60 ml H_2O, 0.015 moles portlandite and with fixed initial sulfate ratio (SO_3/Al_2O_3=1) and chloride ratio ($2Cl/Al_2O_3$=1) showing phase development and its dependence on changing temperature. 97

Figure 5.30: Total volume of solid phases of a hydrated model mixture initially consisting of 0.01 moles C_3A, 60 ml H_2O, 0.015 moles portlandite, 0.0075 moles $CaCO_3$ and with fixed initial sulfate ratio (SO_3/Al_2O_3=1) showing phase development and its dependence on changing chloride ratios ($2Cl/Al_2O_3$) at 5°C..... 98

Figure 5.31: Total volume of solid phases of a hydrated model mixture initially consisting of 0.01 moles C_3A, 60 ml H_2O, 0.015 moles portlandite, 0.0075 moles $CaCO_3$ and with fixed initial sulfate ratio (SO_3/Al_2O_3=1) showing phase development and its dependence on changing chloride ratios ($2Cl/Al_2O_3$) at 55°C..... 99

Figure 5.32: Total volume of solid phases of a hydrated model mixture initially consisting of 0.01 moles C_3A, 60 ml H_2O, 0.015 moles portlandite, 0.0075 moles $CaCO_3$ and with fixed initial sulfate ratio (SO_3/Al_2O_3=1) showing phase development and its dependence on changing chloride ratios ($2Cl/Al_2O_3$) at 85°C..... 100

Figure 5.33: Total volume of solid phases of a hydrated model mixture initially consisting of 0.01 moles C_3A, 60 ml H_2O, 0.015 moles portlandite, 0.0075 moles $CaCO_3$ and with fixed initial sulfate ratio (SO_3/Al_2O_3=1) and chloride ratio ($2Cl/Al_2O_3$=0.5) showing phase development and its dependence on changing temperature. 101

Figure 5.34: Total volume of solid phases of a hydrated model mixture initially consisting of 0.01 moles C_3A, 60 ml H_2O, 0.015 moles portlandite, 0.0075 moles $CaCO_3$ and with fixed initial sulfate ratio (SO_3/Al_2O_3=1) and chloride ratio ($2Cl/Al_2O_3$=1) showing phase development and its dependence on changing temperature. 102

Figure 6.1: XRD powder patterns of nitrate AFm phases at different moisture conditions. 111

Figure 6.2: TG/DTG characteristics of nitrate AFm. Values of the mass losses were determined from the TG curve by the points of deviation for the tangent lines of weight loss slope versus temperature. The initial sample had been dried at room temperature and 35% RH 111

Figure 6.3: FTIR pattern of nitrate AFm dried at 35% RH. 112

Figure 6.4: XRD powder patterns of nitrite AFm phases at different moisture conditions; note NO_3-AFm impurity for the sample prepared from commercial $Ca(NO_2)_2$. 116

Figure 6.5: TG/DTG characteristics of nitrite AFm. Values of the mass losses were determined from the TG curve by the points of deviation for the tangent lines of weight loss slope versus temperature. The initial sample was dried at 35% RH. 116

Figure 6.6: FTIR pattern of nitrite AFm dried at 35% RH..... 117

Figure 6.7: SEM micrographs of the nitrate (a) and nitrite (b) AFm phases. 121

Figure 6.8(a): Partial XRD patterns of the solid solution formation at 25˚C between nitrate AFm and hydroxy AFm. 123

Figure 6.8(b): Partial XRD patterns of the solid solution formation at 25˚C between nitrate AFm and hydroxy AFm. 123

Figure 6.9(a): Equilibrium calcium and aluminium aqueous concentrations commencing from undersaturation for samples between hydroxy AFm (NO_3/Al=0)– nitrate AFm (NO_3/Al=1) at 25±2ºC after 180 days of equilibration. 125

Figure 6.9(b): Equilibrium nitrate aqueous concentrations commencing from undersaturation for samples between hydroxy AFm (NO_3/Al=0) – nitrate AFm (NO_3/Al=1) at 25±2ºC and after 180 days of equilibration..... 125

Figure 6.10: Gibbs energy of ideal mixing, ΔGid, excess Gibbs energy of mixing, ΔGex, and resulting molar Gibbs energy of mixing, ΔGM, calculated for the nitrate AFm (NO_3-AFm)-hydroxy AFm (OH-AFm) solid solution series assuming Guggenheim parameters a_0=0.188 and a_1=2.49 for miscibility gap fractions $0.03 \leq x \leq 0.5$. 126

Figure 6.11(a): Partial XRD patterns of mixtures between nitrate AFm and monosulfoaluminate at 25±2˚C 127

Figure 6.11(b): Partial XRD patterns of mixtures between nitrate AFm and monosulfoaluminate at 25±2˚C 127

Figure 6.12(a): Equilibrium calcium and aluminium aqueous concentrations commencing from undersaturation for samples between monosulfoaluminate (NO_3/Al=0) – nitrate AFm (NO_3/Al=1) at 25±2ºC and after 180 days of equilibration..... 129

Figure 6.12(b): Equilibrium nitrate aqueous concentrations commencing from undersaturation for samples between monosulfoaluminate (NO_3/Al=0) and nitrate AFm (NO_3/Al=1) at 25±2ºC and after 180 days of equilibration.. 129

Figure 6.13(a): Partial XRD patterns of mixtures between nitrate AFm and monocarboaluminate at 25±2˚C 130

Figure 6.13(b): Partial XRD patterns of mixtures between nitrate AFm and monocarboaluminate at 25±2˚C 130

Figure 6.14(a): Equilibrium calcium and aluminium aqueous concentrations commencing from undersaturation for samples between monocarboaluminate (NO_3/Al=0) – nitrate AFm (NO_3/Al=1) at 25±2ºC and after 180 days of equilibration. 132

Figure 6.14(b): Equilibrium nitrate aqueous concentrations commencing from undersaturation for samples between monocarboaluminate (NO_3/Al=0) and nitrate AFm (NO_3/Al=1) at 25±2ºC and after 180 days of equilibration.. 132

Figure 6.15(a): Partial XRD patterns of the solid solution formation at 25˚C between nitrate AFm and Friedel's salt. 134

Figure 6.15(b): Partial XRD patterns of the solid solution formation at 25˚C between nitrate AFm and Friedel's salt. 134

Figure 6.16(a): Equilibrium calcium and aluminium aqueous concentrations commencing from undersaturation for samples between Friedel's salt (NO_3/Al=0)– nitrate AFm (NO_3/Al=1) at 25±2ºC and after 180 days of equilibration. 136

Figure 6.16(b): Equilibrium nitrate and chloride aqueous concentrations commencing from undersaturation for samples between Friedel's salt (NO_3/Al=0) – nitrate AFm (NO_3/Al=1) at 25±2ºC and after 180 days of equilibration..... 136

Figure 6.17(a): Partial XRD patterns of the solid solution formation at 25˚C between nitrite AFm and hydroxy AFm: wet samples. 138

Figure 6.17(b): Partial XRD patterns of the solid solution formation at 25˚C between nitrite AFm and hydroxy AFm: wet samples. 138

Figure 6.18(a): Partial XRD patterns of the solid solution formation at 25±2˚C between nitrite AFm and hydroxy AFm: samples dried at 35% RH..... 139

Figure 6.18(b): Partial XRD patterns of the solid solution formation at 25±2˚C between nitrite AFm and hydroxy AFm: samples dried at 35% RH..... 139

Figure 6.19(a): Equilibrium calcium and aluminium aqueous concentrations commencing from undersaturation for samples between hydroxy AFm (NO_2/Al=0)– nitrite AFm (NO_2/Al=1) at 25±2ºC and after 180 days of equilibration. 141

Figure 6.19(b): Equilibrium nitrite aqueous concentrations commencing from undersaturation for samples between hydroxy AFm (NO_2/Al=0) – nitrite AFm (NO_2/Al=1) at 25±2ºC and after 180 days of equilibration..... 141

Figure 6.20(a): Partial XRD patterns of mixtures between nitrite AFm and monosulfoaluminate at 25±2˚C 143

Figure 6.20(b): Partial XRD patterns of mixtures between nitrite AFm and monosulfoaluminate at 25±2˚C 143

Figure 6.20(c): Partial XRD patterns of selected mixtures between nitrite AFm and monosulfoaluminate measured after 180 days of equilibration in distilled water at 25±2˚C; note unidentified 'X' phase (unknown phase of basal d spacing 8.42 Å which appears after dissolution of samples containing monosulfoaluminate and nitrite AFm). 145

Figure 6.21: XRD pattern showing formation of potential ordered compound ('X' phase) after mixing monosulfoaluminate and nitrite AFm in 1:1 molar ratios in distilled water with continuous agitation for 6 months at 25˚C. 145

Figure 6.22(a): Equilibrium calcium and aluminium aqueous concentrations commencing from undersaturation for samples between monosulfoaluminate (NO_2/Al=0)–nitrite AFm (NO_2/Al=1) at 25±2ºC and after 180 days of equilibration. 146

Figure 6.22(b): Equilibrium nitrite aqueous concentrations commencing from undersaturation for samples between monosulfoaluminate (NO2/Al=0) and nitrite AFm (NO2/Al=1) at 25±2ºC and after 180 days of equilibration. 146

Figure 6.23(a): Partial XRD patterns of mixtures between nitrite AFm and monocarboaluminate at 25±2˚C 147

Figure 6.23(b): Partial XRD patterns of mixtures between nitrite AFm and monocarboaluminate at 25±2˚C 147

Figure 6.24(a): Equilibrium calcium and aluminium aqueous concentrations commencing from undersaturation for samples between monocarboaluminate (NO_2/Al=0)–nitrite AFm (NO_2/Al=1) at 25±2ºC and after 180 days of equilibration. 149

Figure 6.24(b): Equilibrium nitrite aqueous concentrations commencing from undersaturation for samples between monocarboaluminate (NO_2/Al=0)–nitrite AFm (NO_2/Al=1) at 25±2ºC and after 180 days of equilibration..... 149

Figure 6.25(a): Partial XRD patterns investigating potential solid solution formation at 25˚C between nitrite AFm and Friedel's salt 151

Figure 5.25(b): Partial XRD patterns investigating potential solid solution formation at 25˚C between nitrite AFm and Friedel's salt. 151

Figure 6.26: FTIR patterns of the NO_2-AFm and Friedel's salt mixtures..... 152

Figure 6.27(a): Equilibrium calcium and aluminium aqueous concentrations commencing from undersaturation for samples between Friedel's salt (NO_2/Al=0)–nitrite AFm (NO_2/Al=1) at 25±2ºC and after 180 days of equilibration. 154

Figure 6.27(b): Equilibrium nitrite and chloride aqueous concentrations commencing from undersaturation for samples between Friedel's salt (NO_2/Al=0) – nitrite AFm (NO_2/Al=1) at 25±2ºC and after 180 days of equilibration..... 154

Figure 6.28(a): Partial XRD patterns showing solid solution formation at 25˚C between nitrate AFm and nitrite AFm. 155

Figure 6.28(b): Partial XRD patterns showing solid solution formation at 25˚C between nitrate AFm and nitrite AFm. 155

Figure 6.29(a): Equilibrium calcium and aluminium aqueous concentrations commencing from undersaturation for samples between nitrite AFm (NO_3/Al=0)– nitrate AFm (NO_3/Al=1) at 25±2ºC and after 180 days of equilibration. 157

Figure 6.29(b): Equilibrium nitrate and nitrite aqueous concentrations commencing from undersaturation for samples between nitrite AFm (NO_3/Al=0) – nitrate AFm (NO_3/Al=1) at 25±2ºC and after 180 days of equilibration. 157

Figure 6.30: XRD patterns showing mineralogical phase assemblage of the mixture containing 0.01 moles nitrate AFm and 0.01 moles $Ca(OH)_2$ which was kept with continuous stirring in 60 ml H_2O at 25±2˚C for 180 days. 160

Figure 6.31: XRD patterns showing mineralogical phase assemblage of the mixture containing 0.01 moles nitrate AFm, 0.01 moles $Ca(OH)_2$ and 0.01 moles $CaCO_3$ which was kept with continuous stirring in 60 ml H_2O at 25±2˚C for 180 days. 160

Figure 6.32: XRD patterns showing mineralogical phase assemblage of the mixture containing 0.01 moles nitrate AFm, 0.01 moles $Ca(OH)_2$ and 0.005 moles $CaSO_4$ which was kept with continuous stirring in 60 ml H_2O at 25±2˚C for 180 days. 161

Figure 6.33: XRD patterns showing mineralogical phase assemblage of the mixture containing 0.01 moles nitrate AFm, 0.01 moles $Ca(OH)_2$ and 0.02 moles $CaSO_4$ which was kept with continuous stirring in 60 ml H_2O at 25±2˚C for 180 days. 161

Figure 6.34: XRD patterns showing mineralogical phase assemblage of the mixture containing 0.01 moles nitrate AFm, 0.01 moles $Ca(OH)_2$ and 0.01 moles $CaCl_2$ which was kept with continuous stirring in 60 ml H_2O at 25±2˚C for 180 days. 162

Figure 6.35: XRD patterns showing mineralogical phase assemblage of the mixture containing 0.01 moles nitrate AFm, 0.01 moles $Ca(OH)_2$ and 0.01 moles $Ca(NO_2)_2$ which was kept with continuous stirring in 60 ml H_2O at 25±2˚C for 180 days. 162

Figure 6.36: XRD patterns showing mineralogical phase assemblage of the mixture containing 0.01 moles nitrite AFm and 0.01 moles $Ca(OH)_2$ which was kept with continuous stirring in 60 ml H_2O at 25±2˚C for 180 days. 163

Figure 6.37: XRD patterns showing mineralogical phase assemblage of the mixture containing 0.01 moles nitrite AFm, 0.01 moles $Ca(OH)_2$ and 0.01 moles $CaCO_3$ which was kept with continuous stirring in 60 ml H_2O at 25±2˚C for 180 days. 163

Figure 6.38: XRD patterns showing mineralogical phase assemblage of the mixture containing 0.01 moles nitrite AFm, 0.01 moles $Ca(OH)_2$ and 0.005 moles $CaSO_4$ which was kept with continuous stirring in 60 ml H_2O at 25±2˚C for 180 days. 164

Figure 6.39: XRD patterns showing mineralogical phase assemblage of the mixture containing 0.01 moles nitrite AFm, 0.01 moles $Ca(OH)_2$ and 0.02 moles $CaSO_4$ which was kept with continuous stirring in 60 ml H_2O at 25±2˚C for 180 days. 164

Figure 6.40: XRD patterns showing mineralogical phase assemblage of the mixture containing 0.01 moles nitrite AFm, 0.01 moles $Ca(OH)_2$ and 0.01 moles $CaCl_2$ which was kept with continuous stirring in 60 ml H_2O at 25±2˚C for 180 days. 165

Figure 6.41: XRD patterns showing mineralogical phase assemblage of the mixture containing 0.01 moles nitrite AFm, 0.01 moles $Ca(OH)_2$ and 0.01 moles $Ca(NO_3)_2$ which was kept with continuous stirring in 60 ml H_2O at 25±2˚C for 180 days. 165

Figure 6.42(a): Calculated total volume of phases of a hydrated model mixture consisting of 0.01 moles C_3A, 60 ml H_2O, 0.015 moles portlandite and with fixed initial sulfate ratio (SO_3/Al_2O_3=1) showing phase development and its dependence on changing nitrate ratios ($2NO_3/Al_2O_3$) at 25°C..... 167

Figure 6.42(b): Calculated and experimental aqueous composition of hydrated model mixture consisting of 0.01 moles C_3A, 0.015 moles portlandite, 60 ml H_2O and with fixed initial sulfate ratio (SO_3/Al_2O_3=1) showing its dependence on changing nitrate ratios ($2NO_3/Al_2O_3$) at 25±2°C. 167

Figure 6.43(a): Calculated total volume of phases of a hydrated model mixture consisting of 0.01 moles C_3A, 60 ml H_2O, 0.015 moles portlandite and with fixed initial sulfate ratio (SO_3/Al_2O_3=1) showing phase development and its dependence on changing nitrite ratios ($2NO_2/Al_2O_3$) at 25°C. 168

Figure 6.43(b): Calculated and experimental aqueous composition of hydrated model mixture consisting of 0.01 moles C_3A, 0.015 moles portlandite, 60 ml H_2O and with fixed initial sulfate ratio (SO_3/Al_2O_3=1) showing its dependence on changing nitrite ratios ($2NO_2/Al_2O_3$) at 25±2°C.. 168

Figure 6.44: XRD patterns showing mineralogical changes and influence of $Ca(NO_3)_2/Ca(NO_2)_2$ addition for the system: 0.01 moles C_3A-0.01 moles $CaSO_4$-0.015 moles $Ca(OH)_2$- 60 ml H_2O at 25±2˚C; respectively plots: **1**-no $Ca(NO_3)_2/Ca(NO_2)_2$ present; **2**-0.01 moles of $Ca(NO_3)_2$ added; **3**-0.01 moles $Ca(NO_2)_2$ added..... 169

Figure 6.45(a): Total volume of phases of a hydrated model mixture consisting of 0.01 moles C_3A, 60 ml H_2O, 0.015 moles portlandite, 0.0075 moles $CaCO_3$ and with fixed initial sulfate ratio (SO_3/Al_2O_3=1) showing phase development and its dependence on changing nitrate ratios ($2NO_3/Al_2O_3$) at 25°C..... 171

Figure 6.45(b): Calculated and experimental aqueous composition of hydrated model mixture consisting of 0.01 moles C_3A, 0.015 moles portlandite, 0.0075 mol $CaCO_3$, 60 ml H_2O and with fixed initial sulfate ratio (SO_3/Al_2O_3=1) showing its dependence on changing nitrate ratios ($2NO_3/Al_2O_3$) at 25±2°C. 171

Figure 6.46(a): Total volume of phases of a hydrated model mixture consisting of 0.01 moles C_3A, 60 ml H_2O, 0.015 moles portlandite, 0.0075 moles $CaCO_3$ and with

fixed initial sulfate ratio (SO_3/Al_2O_3=1) showing phase development and its dependence on changing nitrite ratios ($2NO_2/Al_2O_3$) at 25°C. 172

Figure 6.46(b): Calculated and experimental aqueous composition of hydrated model mixture consisting of 0.01 moles C_3A, 0.015 moles portlandite, 0.0075 mol $CaCO_3$, 60 ml H_2O and with fixed initial sulfate ratio (SO_3/Al_2O_3=1) showing its dependence on changing nitrite ratios ($2NO_2/Al_2O_3$) at 25±2°C.. 172

Figure 6.47: XRD patterns showing mineralogical changes and influence of $Ca(NO_3)_2/Ca(NO_2)_2$ addition for the system 0.01 moles C_3A-0.01 moles $CaSO_4$-0.015 moles $Ca(OH)_2$-0.0075 moles $CaCO_3$- 60 ml H_2O at 25±2˚C; **1**-no $Ca(NO_3)_2/Ca(NO_2)_2$ present; **2**-0.01 moles of $Ca(NO_3)_2$ added; **3**-0.01 moles of $Ca(NO_2)_2$ added..... 173

Figure 6.48: Calculated total volume of solid phases of a hydrated model mixture initially consisting of 0.01 moles C_3A, 60 ml H_2O, 0.015 moles portlandite and with fixed initial sulfate ratio (SO_3/Al_2O_3=1) and nitrate ratio ($2NO_3/Al_2O_3$=0.5) showing phase development and its dependence on changing temperature. 174

Figure 6.49: Calculated total volume of solid phases of a hydrated model mixture initially consisting of 0.01 moles C_3A, 60 ml H_2O, 0.015 moles portlandite and with fixed initial sulfate ratio (SO_3/Al_2O_3=1) and nitrate ratio ($2NO_3/Al_2O_3$=1) showing phase development and its dependence on changing temperature. 174

Figure 6.50: Calculated total volume of solid phases of a hydrated model mixture initially consisting of 0.01 moles C_3A, 60 ml H_2O, 0.015 moles portlandite and with fixed initial sulfate ratio (SO_3/Al_2O_3=1) and nitrite ratio ($2NO_2/Al_2O_3$=0.5) showing phase development and its dependence on changing temperature. 175

Figure 6.51: Calculated total volume of solid phases of a hydrated model mixture initially consisting of 0.01 moles C_3A, 60 ml H_2O, 0.015 moles portlandite and with fixed initial sulfate ratio (SO_3/Al_2O_3=1) and nitrite ratio ($2NO_2/Al_2O_3$=1) showing phase development and its dependence on changing temperature. 175

Figure 7.1(a): Calculated total volume of phases of a hydrated model mixture consisting of 0.01 moles C_3A, 0.015 moles portlandite, 0.01 moles $Ca(NO_2)_2$, 60 ml H_2O and with fixed initial sulfate ratio (SO_3/Al_2O_3=1) showing phase development and its dependence on changing chloride content at 25°C. 187

Figure 7.1(b): Calculated and experimental aqueous composition of hydrated model mixture consisting of 0.01 moles C_3A, 0.015 moles portlandite, 0.01 moles $Ca(NO_2)_2$, 60 ml H_2O and with fixed initial sulfate ratio (SO_3/Al_2O_3=1) showing its dependence on changing chloride content at 25°C. 187

Figure 7.2(a): Calculated total volume of phases of a hydrated model mixture consisting of 0.01 moles C_3A, 0.015 moles portlandite, 0.0075 moles $CaCO_3$, 0.01 moles $Ca(NO_2)_2$ and 60 ml H_2O and with fixed initial sulfate ratio (SO_3/Al_2O_3=1) showing phase development and its dependence on changing chloride content at 25°C..... 188

Figure 7.2(b): Calculated and experimental aqueous composition of hydrated model mixture consisting of 0.01 moles C_3A, 0.015 moles portlandite, 0.0075 moles $CaCO_3$, 0.01 moles $Ca(NO_2)_2$ and 60 ml H_2O and with fixed initial sulfate ratio (SO_3/Al_2O_3=1) showing its dependence on changing chloride content at 25°C. 188

Figure 7.3(a): Calculated total volume of phases of a hydrated model mixture consisting of 0.005 moles C_3A, 0.015 moles portlandite, 0.01 moles $Ca(NO_2)_2$, 60 ml H_2O and with fixed initial sulfate ratio (SO_3/Al_2O_3=1.5) showing phase development and its dependence on changing chloride content at 25°C. 189

Figure 7.3(b): Calculated aqueous composition of hydrated model mixture consisting of 0.005 moles C_3A, 0.015 moles portlandite, 0.01 moles $Ca(NO_2)_2$, 60 ml H_2O and with fixed initial sulfate ratio (SO_3/Al_2O_3=1.5) showing its dependence on changing chloride content at 25°..... 189

Figure 7.4(a): Calculated total volume of phases of a hydrated model mixture consisting of 0.015 moles C_3A, 0.015 moles portlandite, 0.01 moles $Ca(NO_2)_2$, 60 ml H_2O and with fixed initial sulfate ratio (SO_3/Al_2O_3=0.5) showing phase development and its dependence on changing chloride content at 25°C. 190

Figure 7.4(b): Calculated aqueous composition of hydrated model mixture consisting of 0.015 moles C_3A, 0.015 moles portlandite, 0.01 moles $Ca(NO_2)_2$, 60 ml H_2O and with fixed initial sulfate ratio (SO_3/Al_2O_3=0.5) showing its dependence on changing chloride content at 25°C. 190

Figure 7.5(a): Calculated total volume of phases of a hydrated model mixture consisting of 0.005 moles C_3A, 0.015 moles portlandite, 0.01 moles $Ca(NO_2)_2$, 0.0075 moles $CaCO_3$, 60 ml H_2O and with fixed initial sulfate ratio (SO_3/Al_2O_3=1.5) showing phase development and its dependence on changing chloride content at 25°C..... 191

Figure 7.5(b): Calculated aqueous composition of hydrated model mixture consisting of 0.005 moles C_3A, 0.015 moles portlandite, 0.01 moles $Ca(NO_2)_2$, 0.0075 moles $CaCO_3$, 60 ml H_2O and with fixed initial sulfate ratio (SO_3/Al_2O_3=1.5) showing its dependence on changing chloride content at 25°C. 191

Figure 7.6(a): Calculated total volume of phases of a hydrated model mixture consisting of 0.015 moles C_3A, 0.015 moles portlandite, 0.01 moles $Ca(NO_2)_2$, 0.0075 moles $CaCO_3$, 60 ml H_2O and with fixed initial sulfate ratio (SO_3/Al_2O_3=0.5) showing phase development and its dependence on changing chloride content at 25°C..... 192

Figure 7.6(b): Calculated aqueous composition of hydrated model mixture consisting of 0.015 moles C_3A, 0.015 moles portlandite, 0.01 moles $Ca(NO_2)_2$, 0.0075 moles $CaCO_3$, 60 ml H_2O and with fixed initial sulfate ratio (SO_3/Al_2O_3=0.5) showing its dependence on changing chloride content at 25°C. 192

Figure 7.7: XRD patterns showing mineralogical changes and influence of $CaCl_2$ addition for the system 0.01 moles C_3A-0.01 moles $Ca(NO_2)_2$-0.01 moles $CaSO_4$-0.015 moles $Ca(OH)_2$- 60 ml H_2O at 25±2˚C; **1**-no $CaCl_2$ present (Tab. 7.1, A_1); **2**-

0.01 moles of $CaCl_2$ added (Tab.1, D_1); high intensities of phases in pattern **1** are due to preferred orientation. 193

Figure 7.8: XRD patterns showing mineralogical changes and influence of $CaCl_2$ addition for the system 0.01 moles C_3A-0.01 moles-0.01 moles $Ca(NO_2)_2$- $CaSO_4$-0.015 moles $Ca(OH)_2$-0.0075 moles $CaCO_3$- 60 ml H_2O at 25±2˚C; **1**-no $CaCl_2$ present (Tab. 7.2, A_2); **2**-0.01 moles of $CaCl_2$ added (Tab. 7.2, D_2). 193

Tables

Table 2.1: Standard molar thermodynamic properties of cement hydrates at 25 ℃, 1 bar. 23

Table 2.2: Reference reactions used to calculate heat capacities of relevant AFm phases. 24

Table 2.3: Equations used to calculate heat capacities of relevant AFm phases..... 24

Table 2.4: Dissolution reactions used to calculate solubility products. 25

Table 4.1: Density of Selected Cement Phases at 20-25ºC 41

Table 4.2: Density of Selected Cement Phases given by some authors, where recalculation of density does not agree with the author's own calculation. 49

Table 5.1: Solubility data for Friedel's salt - $Ca_4Al_2(OH)_{12.05}(Cl)_{1.95}\cdot 4H_2O$. 62

Table 5.3: FTIR identification of the Kuzel's salt..... 65

Table 5.2: Solubility data for Kuzel's salt - $Ca_4Al_2(SO_4)_{0.5}(Cl)(OH)_{12}\cdot 6H_2O$. 66

Table 5.4: Aqueous solution compositions measured from undersaturation for samples between the hydroxy AFm (Cl/Al=0) and the Friedel's salt (Cl/Al=1) and with an excess of $CaCl_2$ (values >1); at 25±2ºC and after 180 days of equilibration.. 71

Table 5.5: Aqueous solution compositions measured from undersaturation for samples between monosulfoaluminate (Cl/Al=0) and Friedel's salt (Cl/Al=1) at 25±2ºC and after 180 days of equilibration..... 75

Table 5.6: Aqueous solution compositions measured from undersaturation for samples between monocarboaluminate (Cl/Al=0) and Friedel's salt (Cl/Al=1), and with an excess of $CaCl_2$ (values >1); at 25±2ºC and after 180 days of equilibration. 79

Table 5.7: Standard molar thermodynamic properties of Friedel's salt and Kuzel's salt at 25˚C. 83

Table 5.8: Fraction of chloride bound per g of phase. 106

Table 6.1: FTIR identification of the nitrate AFm. 112

Table 6.2: Solubility data for nitrate AFm-$Ca_4Al_2(OH)_{12}(NO_3)_2 \cdot 4H_2O$ 114

Table 6.3: FTIR identification of the nitrite AFm. 117

Table 6.4: Solubility data for nitrite AFm-$Ca_4Al_2(OH)_{12}(NO_2)_2 \cdot 4H_2O$, prepared from commercial $Ca(NO_2)_2$. 119

Table 6.5: Solubility data for nitrite AFm-$Ca_4Al_2(OH)_{12}(NO_2)_2 \cdot 4H_2O$, prepared from the analytical purity $NaNO_2$. 120

Table 6.6: Aqueous solution compositions measured from undersaturation for samples between the hydroxy AFm (NO_3/Al=0) and the nitrate AFm (NO_3/Al=1) at 25±2ºC and after 180 days of equilibration. 124

Table 6.7: Aqueous solution compositions measured from undersaturation for samples between the monosulfoaluminate (NO_3/Al=0) and the nitrate AFm (NO_3/Al=1) at 25±2ºC and after 180 days of equilibration. 128

Table 6.8: Aqueous solution compositions measured from undersaturation for samples between the monocarboaluminate (NO_3/Al=0) and the nitrate AFm (NO_3/Al=1) at 25±2ºC and after 180 days of equilibration. 131

Table 6.9: Aqueous solution compositions measured from undersaturation for samples between the Friedel's salt (NO_3/Al=0) and the nitrate AFm (NO_3/Al=1) at 25±2ºC and after 180 days of equilibration. 135

Table 6.10: Aqueous solution compositions measured from undersaturation for samples between the hydroxy AFm (NO_2/Al=0) and the nitrite AFm (NO_2/Al=1) at 25±2ºC and after 180 days of equilibration. 140

Table 6.11: Aqueous solution compositions measured from undersaturation for samples between the monosulfoaluminate (NO_2/Al=0) and the nitrite AFm (NO_2/Al=1) at 25±2ºC and after 180 days of equilibration. 144

Table 6.12: Aqueous solution compositions measured from undersaturation for samples between the monocarboaluminate (NO_2/Al=0) and the nitrite AFm (NO_2/Al=1) at 25±2ºC and after 180 days of equilibration. 148

Table 6.13: Aqueous solution compositions measured from undersaturation for samples between the Friedel's salt (NO_2/Al=0) and the nitrite AFm (NO_2/Al=1) at 25±2ºC and after 180 days of equilibration. 153

Table 6.14: Aqueous solution compositions measured from undersaturation for samples between the nitrite AFm (NO_3/Al=0) and the nitrate AFm (NO_3/Al=1) at 25±2ºC and after 180 days of equilibration. 156

Table 6.15: Summary of the solid solution investigations amongst nitrate/nitrite AFm and other AFm phases. 158

Table 6.16: Standard molar thermodynamic properties of nitrate AFm and nitrite AFm at 25˚C. 166

Table 6.17: Example of conversion factors for cements with various Al_2O_3 content, constant of SO_3=3.15 wt%, plus added $Ca(NO_3)_2$ or $Ca(NO_3)_2$ at 1 wt%. 176

Table 7.1: Molar ratios of mixtures: carbonate-free compositions. 181

Table 7.2: Molar ratios of mixtures: carbonate-containing compositions..... 181

Table 7.3: Guide to data presentation: Cl/NO_2 mole ratio is the system variable..... 184

Appendix

Appendix I : The density of cement phases: worksheets

Appendix II: Standard (partial molar) thermodynamic properties of aqueous species used in GEMS calculations at 25˚C, 1 bar

Appendix I

SIMPLE OXIDES AND HYDRATED OXIDES

1 Lime

Formula: CaO
Formula Weight: 56.08 g/mol
Space group: Fm3m
Conventional cement shorthand notation: C

1.1 Cell Dimensions: a = 4.8105 Å
Number of formula units in the unit cell: Z = 4
Density (calculated for cubic crystal system): 3345 kg/m^3
Reference: Morris M.C. et al., National Bureau of Standards Monograph 25 (1977), Vol. 14, 49

Cell parameters were determined at 298 K from X-ray powder patterns. The type of diffractometer and origin of the sample are not specified. The diffractometer was equipped with a focusing graphite monochromator; an internal standard (high purity 99.99% Si standard) and CuKα radiation (1.5405 Å) were used.

Density calculated by Morris, et al.: **3345 kg/m^3**

1.2 Cell Dimensions: a = 4.815 Å
Number of formula units in the unit cell: Z = 4
Density (calculated for cubic crystal system): 3338 kg/m^3
Reference: Fiquet G. et al., Physics and Chemistry of Minerals (1999), Vol. 27, 103-111

Cell parameters were determined at 298 K from X-ray diffraction experiments with synchrotron radiation; type of diffractometer and origin of the sample are not given..

1.3 Mean density of lime: Dx = 3341 kg/m^3

1.4 <u>Comment:</u>
Free lime is a minor constituent of most Portland cement clinkers. Large quantities (e.g,. greater than a few percent) possibly indicate poor control in manufacture. Lime hydrolyzes in water to $Ca(OH)_2$ and to mixtures of $CaCO_3$ and $Ca(OH)_2$ in moist air.

2 Periclase

Formula: MgO
Formula Weight: 40.30 g/mol
Space group: Fm3m
Conventional cement shorthand notation: M

2.1 Cell Dimensions: a = 4.211 Å
Number of formula units in the unit cell: Z = 4
Density (calculated for cubic crystal system): 3581 kg/m^3
Reference: Hazen R.M., American Mineralogist (1976), Vol. 61, 266-271

Cell parameters were determined at 296 K, from single crystal X-ray structure refinements of synthetic periclase, using a Picker four circle diffractometer and Mo Kα radiation.

2.2 **Cell Dimensions:** a = 4.210 Å
Number of formula units in the unit cell: Z = 4
Density (calculated for cubic crystal system): 3587 kg/m^3
Reference: Fiquet G. et al., Physics and Chemistry of Minerals (1999), Vol. 27, 103-111

Cell parameters were determined at 298 K, from X-ray diffraction experiments with synchrotron radiation. The type of diffractometer and origin of the sample are not given.

2.3 **Mean density of periclase: Dx = 3584 kg/m^3**

2.4 **Comment:**
Occurs in some Portland cement clinkers. Hydrolyzes in water to $Mg(OH)_2$ and in air, to mixtures of hydroxide, carbonate and hydroxycarbonates.

3 Corundum

Formula: Al_2O_3
Formula Weight: 101.96 g/mol
Space group: R $\bar{3}$c
Conventional cement shorthand notation: A

3.1 **Cell Dimensions:** a = 4.758 Å, c = 12.991 Å
Number of formula units in the unit cell: Z = 6
Density (calculated for hexagonal/trigonal system): 3988 kg/m^3
Reference: Swanson H.E. et al., National Bureau of Standards Circular 539 (1953), Vol. 2, 20

Cell parameters of a synthetic sample were determined at 300K, from X-ray powder patterns; X-ray intensities were collected with a Guiner-type camera using an internal standard and CuKα radiation (1.5405 Å).

Density calculated by Swanson, et al.: **3987 kg/m^3**

3.2 **Cell Dimensions:** a = 4.758 Å, c = 12.996 Å
Number of formula units in the unit cell: Z = 6
Density (calculated for hexagonal/trigonal system): 3987 kg/m^3
Reference: Fiquet G. et al., Physics and Chemistry of Minerals (1999), Vol. 27, 103-111

Cell parameters were determined at 298 K, from X-ray diffraction using synchrotron radiation; the origin of the sample is not specified.

3.3 **Cell Dimensions:** a = 4.7540 Å, c = 12.9820 Å
Number of formula units in the unit cell: Z = 6
Density (calculated for hexagonal/trigonal system): 3997 kg/m^3
Reference: Maslen E.N. et al., Acta Crystallographica (1993), Vol. B49, 973-80

Cell parameters were determined at 293 K, from single crystal X-ray structure refinements of α-Al_2O_3 crystals (origin: not specified), using a Syntex $P2_1$ four circle diffractometer (with graphite monochromator) and MoKα radiation (0.7106 Å).

Density calculated by Maslen, et al.: **3997 kg/m^3**

3.4 Mean density of corundum: Dx = 3990 kg/m^3

3.5 <u>Comment:</u>
Alumina, Al_2O_3, occurs in various polymorphs. Alpha (corundum) is probably the only stable polymorph at 1 bar. Some of the 'polymorphs' are chemically stabilized: for example 'β Al_2O_3' is actually close in composition to $Na_2O \cdot 11Al_2O_3$. Corundum is not normally present in Portland cement clinkers but has sometimes been reported in special cement made using bauxite, for example in high-alumina or sulfoaluminate clinkers.

4 Quartz

Formula: SiO_2
Formula Weight: 60.08 g/mol
Space group: $P3_121$
Conventional cement shorthand notation: S

4.1 Cell Dimensions: *a* = 4.9133 Å, *c* = 5.4053 Å
Number of formula units in the unit cell: Z = 3
Density (calculated for hexagonal/trigonal system): 2648 kg/m^3
Reference: Gaines V.R. et al., *Dana's New Mineralogy*, eighth edition (1997), 1573-1586

Phase: synthesized α - quartz ('low' temperature form)
Details of the measurement are not given

The density given in *Dana's New Mineralogy*: **2660 kg/m^3**

4.2 Cell Dimensions: *a* = 4.92 Å, *c* = 5.42 Å
Number of formula units in the unit cell: Z = 3
Density (calculated for hexagonal/trigonal system): 2634 kg/m^3
Reference: Glinnemann J. et al., Zeitschrift für Kristallographie (1992), Vol. 198, 177-212

Cell parameters were determined at 'room temperature', from X-ray structure refinements of a synthetic phase, using a Philips PW 1100 four circle diffractometer (with graphite monochromator) and MoKα radiation (0.7106 Å).

4.3 Mean density of α - quartz: Dx = 2641 kg/m^3

4.4 <u>Comment:</u>
Two forms of quartz exist, alpha-quartz which is stable up to 573°C and beta -quartz, the high temperature form, stable between 573°C and 867°C. High quartz cannot usually be quenched to ambient so "quartz" usually refers to the alpha phase. However some schemes use the reverse assignment, in which 'low' (temperature) form is designated beta.
Quartz is not nominally a phase found in Portland cement but is used in its manufacture, and is often added to autoclaved cements and oil well cements intended for high

temperature service. On account of the sensitivity of X-ray diffraction to quartz and its almost universal presence in nature, it is frequently encountered as a trace impurity of Portland cement.

5 Gibbsite

Formula: $Al(OH)_3$
Formula Weight: 78.00 g/mol
Space group: $P2_1/c$
Conventional cement shorthand notation: AH_3

5.1 **Cell Dimensions:** a = 8.684 Å, b = 5.078 Å, c = 9.736 Å, β = 94.54°
Number of formula units in the unit cell: Z = 8
Density (calculated for monoclinic crystal system): 2421 kg/m^3
Reference: Saalfeld H. et al., Zeitschrift für Kristallographie (1974), Vol. 139, 129-135

Cell parameters were determined at 'room temperature', from X-ray structure refinements of a natural mineral from Langesunjfjord, Norway, using an automated Siemens diffractometer and CuKα radiation.

Identical values of the unit cell parameters were given by Balan E. et al, American Mineralogist (2006); Vol. 91, 115-119

5.3 **Recommended density of gibbsite: Dx = 2421 kg/m^3**

5.4 **Comment:**
Gibbsite may be considered as the hexagonally-packed AX_3 layer structure but also has a cubic polymorph, bayerite. Many types of mixed stacking, some disordered and some ordered, are known as intermediates between gibbsite and bayerite.

6 Brucite

Formula: $Mg(OH)_2$
Formula Weight: 58.32 g/mol
Space group: $P\bar{3}m1$
Conventional cement shorthand notation: MH

6.1 **Cell Dimensions:** a = 3.147 Å, c = 4.769 Å
Number of formula units in the unit cell: Z = 1
Density (calculated for hexagonal/trigonal crystal system): 2368 kg/m^3
Reference: Swanson H.E. et al., National Bureau of Standards Circular 539 (1956), Vol.6, 62

Cell parameters were determined at room temperature, 300 K, from X- ray powder patterns of a synthetic sample (from MgO and water held at 600ºC and 1333 bars water vapour pressure for 3 days), using: a Guiner-type camera (with Ni filter), Cu Kα radiation (1.5405 Å) and an internal standard.

Density calculated by Swanson et al.**: 2368 kg/m^3**

6.2 **Cell Dimensions:** a = 3.148 Å, c= 4.779 Å
Number of formula units in the unit cell: Z = 1
Density (calculated for hexagonal/trigonal crystal system): 2368 kg/m^3
Reference: Desgranges L. et al., Acta Crystallographica (1996), Vol. B52, 82-86

Cell parameters were determined at 'room temperature', from single crystal X-ray structure refinements of a natural sample (origin-not specified), using a four circle P110 neutron diffractometer at the Orphee Reactor (CEN-Saclay).

Density calculated by Desgranges et al.**: 2360 kg/m^3**

6.3 **Mean density of brucite: Dx = 2368 kg/m^3**

6.4 **Comment:**
Brucite has been reported to occur as a hydration product of slag-cement blends and as an alteration product of Portland cement in sea water, brines, etc. A number of basic carbonates of general formula $xMg(OH)_2 \cdot yMgCO_3 \cdot H_2O$ also exist but differ in structure from brucite. The basic carbonates have not been reported to occur as Portland cement hydration products.

7 Portlandite

Formula: $Ca(OH)_2$
Formula Weight: 74.09 g/mol
Space group: P $\bar{3}$m1
Conventional cement shorthand notation: CH

7.1 **Cell Dimensions:** a = 3.589 Å, c= 4.911 Å
Number of formula units in the unit cell: Z = 1
Density (calculated for hexagonal/trigonal crystal system): 2260 kg/m^3
Reference: Desgranges L. et al., Acta Crystallographica (1993), Vol. B49, 812-817

Cell parameters were determined at 'room temperature', from single crystal X-ray structure refinements of a synthetic sample (crystals were prepared by slow diffusion of calcium chloride into a sodium hydroxide solution), using a four circle P110 diffractometer (with Cu(220) monochromator) and MoKα radiation (0.8330 Å).

Density calculated by Desgranges et al.**: 2260 kg/m^3**

7.2 **Cell Dimensions:** a = 3.593 Å, c = 4.909 Å
Number of formula units in the unit cell: Z = 1
Density (calculated for hexagonal/trigonal crystal system): 2242 kg/m^3
Reference: Swanson H.E. et al., National Bureau of Standards Circular 539 (1953), Vol.1, 95

Cell parameters were determined at room temperature, 300 K, from X-ray powder patterns; X-ray intensities were collected with a Guiner type camera (with Ni filter) using CuKα radiation (1.5405 Å) and an internal standard; the origin of the sample is not specified.

Density calculated by Swanson et al.**: 2241 kg/m^3**

7.3 Mean density of portlandite: Dx = 2251 kg/m^3

7.4 Comment:
A major constituent of hydrated Portland cement. The structure consists of layers formed from rows of linked $Ca(OH)_6$ octahedra. Calcium hydroxide dehydrates to calcium oxide at about 400°C. It carbonates readily in humid air.

CARBONATES

8 Calcite

Formula: $CaCO_3$
Formula Weight: 100.09 g/mol
Space group: R $\bar{3}$c
Conventional cement shorthand notation: C$\bar{C}$

8.1 Cell Dimensions: *a* = 4.991 Å, *c* = 17.062 Å
Number of formula units in the unit cell: Z = 6
Density (calculated for hexagonal/trigonal crystal system): 2710 kg/m^3
Reference: Maslen E.N. et al., Acta Crystallographica (1993), Vol. B49, 636-641

Cell parameters were determined at 293 K, from single crystal X-ray structure refinements of $CaCO_3$ samples (crystals were grown from aqueous solution by slow diffusion), using a Syntex P3 four circle diffractometer with graphite monochromator and MoKα radiation (0.7107 Å).

Density calculated by Maslen et al.**: 2709 kg/m^3**

8.2 Cell Dimensions: *a* = 4.9896 Å, *c* = 17.0610 Å
Number of formula units in the unit cell: Z = 6
Density (calculated for hexagonal/trigonal crystal system): 2710 kg/m^3
Reference: Effenberger H. et al., Zeitschrift für Kristallographie (1981), Vol. 156, 233-243

Cell parameters were determined at 'room temperature' from single crystal X-ray structure refinements of a natural sample (locality: Iceland), using a Philips PW 1100 four circle diffractometer with graphite monochromator and MoKα radiation.

8.3 Cell Dimensions: *a* = 4.990 Å, *c* = 17.002 Å
Number of formula units in the unit cell: Z = 6
Density (calculated for hexagonal/trigonal crystal system): 2722 kg/m^3
Reference: Chessin H. et al., Acta Crystallographica (1965), Vol. 18, 689-693

Cell parameters were determined at 300K, from X-ray structure refinements of single crystals (origin: not specified); data were collected on an integrating Weissenberg camera using MoKα radiation.

8.4 Recommended density of calcite: Dx = 2710 kg/m^3

8.5 **Comment**:
On account of the lower accuracy of the Weissenberg method of determining cell parameters, the value in 8.3 is not preferred.
Calcite is the chief constituent of limestone, a basic raw material used in cement manufacture. It decomposes at about 900°C. In nature considerable substitution of Mg for Ca may occur. This random substitution gives rise to 'magnesian calcite', in which some Mg substitutes randomly on nominally Ca positions: it is not to be confused with dolomite, in which Ca-Mg ordering occurs.

9 Aragonite

Formula: $CaCO_3$
Formula Weight: 100.09 g/mol
Space group: Pmcn
Conventional cement shorthand notation: $C\bar{C}$

9.1 **Cell Dimensions:** a = 4.96 Å, *b* = 7.97 Å, *c* = 5.74 Å
Number of formula units in the unit cell: Z = 4
Density (calculated for orthorhombic crystal system): 2929 kg/m^3
Reference: De Villiers J.P.R, American Mineralogist (1971), Vol. 56, 758-767

Cell parameters were determined at 294 K, from single crystal X-ray structure refinements of a natural sample (locality: Grapevine Mountains, Nevada), using: a Super-Pace automated single crystal diffractometer and CuKα radiation (1.5405 Å).

9.2 **Cell Dimensions:** *a* = 4.9614 Å, *b* = 7.966 Å, *c* = 5.740 Å
Number of formula units in the unit cell: Z = 4
Density (calculated for orthorhombic crystal system): 2931 kg/m^3
Reference: Morris M.C. et al., National Bureau of Standards Monograph 25 (1977), Vol. 14, 44

Cell parameters were determined at 298 K, from X-ray powder patterns using: diffractometer with a focusing graphite monochromator, CuKα radiation, and an internal standard (high purity 99.99% Si); origin of the sample is not specified.

9.3 **Mean density of aragonite: Dx = 2930 kg/m^3**

9.4 **Comment:**
Aragonite is a stable high-pressure polymorph. It occurs in certain metamorphic rocks but is also formed metastably at low pressure. Thus it is frequently encountered as a product of rapid carbonation of cements. It is also commonly encountered in biological composites such as shells of marine organisms, where it is apparently stabilized by intercalation with protein-like substances. Upon heating in the air at 1 bar total pressure, aragonite converts to calcite prior to decomposition.

10 Vaterite

Formula: μ -$CaCO_3$
Formula Weight: 100.09 g/mol
Space group: $P6_3/mmc$

Conventional cement shorthand notation: $C\bar{C}$

10.1 Cell Dimensions: a =7.16 Å, c = 16.98 Å
Number of formula units in the unit cell: Z = 12
Density (calculated for hexagonal/trigonal crystal system): 2664 kg/m^3
Reference: Kamhi S.R., Acta Crystallographica (1963), Vol. 16, 770-773

Cell parameters were determined from single crystal X-ray structure refinements of synthetic crystals (grown by ionic diffusion in aqueous solution), using a Picker diffractometer equipped with a General Electric single crystal orienter. Crystal sizes and habits were dependent upon the temperature at which experiment was performed (temperatures in the region 45°C to 60°C were found to give the best yields).

10.2 Cell Dimensions: a = 7.15 Å, c = 16.94 Å
Number of formula units in the unit cell: Z = 12
Density (calculated for hexagonal/trigonal crystal system): 2659 kg/m^3
Reference: Meyer H.J., Zeitschrift für Kristallographie (1969), Vol. 128, 183-212

Cell parameters were determined from single crystal X-ray structure refinements of crystals (origin: not specified), using a Hilger & Watts microfocus diffractometer and CuKα radiation; temperature of the measurement is not specified.

10.3 Mean density of vaterite: Dx = 2661 kg/m^3

10.4 Comment:
Vaterite is a low density polymorph of $CaCO_3$. It is believed to be metastable under all conditions. It may occur as a product of rapid precipitation often in mixtures with calcite, etc., as a product of cement carbonation. Upon heating in air, vaterite converts to calcite prior to decomposition.

11 Magnesite

Formula: $MgCO_3$
Formula Weight: 84.31 g/mol
Space group: $R\bar{3}c$
Conventional cement shorthand notation: $M\bar{C}$

11.1 Cell Dimensions: a = 4.632 Å, c = 15.007 Å
Number of formula units in the unit cell: Z = 6
Density (calculated for hexagonal/trigonal crystal system): 3013 kg/m^3
Reference: Maslen E.N. et al., Acta Crystallographica (1995), Vol. B51, 929-939

Cell parameters were determined at 295 K, from single crystal X-ray structure refinements of a synthetic sample (prepared hydrothermally), using a four circle diffractometer and MoKα radiation (0.7073 Å).

Density calculated by Maslen et al**: 3013 kg/m^3**

11.2 Cell Dimensions: a = 4.632 Å, c = 15.013 Å
Number of formula units in the unit cell: Z = 6

Density (calculated for hexagonal/trigonal crystal system): 3009 kg/m^3
Reference: Effenberger H. et al., Zeitschrift für Kristallographie (1981), Vol. 156, 233-243

Cell parameters were determined at 'room temperature' from single crystal X-ray structure refinements of a natural sample (locality: Oberdorf, Austria), using a Philips PW 1100 four circle diffractometer with graphite monochromator and MoKα radiation.

11.3 Mean density of magnesite: Dx = 3011 kg/m^3

11.4 <u>Comment:</u>
See also brucite, for mention of 'hydroxycarbonates'.

12 Dolomite

Formula: $CaMg(CO_3)_2$
Formula Weight: 184.40 g/mol
Space group: $R\bar{3}$
Conventional cement shorthand notation: $CM\bar{C}_2$

12.1 Cell Dimensions: *a* = 4.8312 Å, *c* = 16.166 Å
Number of formula units in the unit cell: Z = 3
Density (calculated for hexagonal/trigonal crystal system): 2811 kg/m^3
Reference: Reeder R.J. et al., American Mineralogist (1989), Vol. 74, 1159-1167

Cell parameters were determined at 'room temperature', from single crystal X-ray structure refinements of a natural sample (locality: Erzberg, Austria), using a Picker four circle diffractometer equipped with a graphite monochromator and MoKα radiation (0.7107 Å).

12.2 Cell Dimensions: *a* = 4.8069 Å, *c* = 16.002 Å
Number of formula units in the unit cell: Z = 3
Density (calculated for hexagonal/trigonal crystal system): 2868 kg/m^3
Reference: Reeder R.J. et al., American Mineralogist (1986), Vol. 71, 795-804

Cell parameters were determined at 297 K, from single crystal X-ray structure refinements of a natural sample (locality: Eugui, Spain), using a Picker four circle diffractometer equipped with graphite monochromator and MoKα radiation (0.7107 Å).

12.3 Cell Dimensions: *a* = 4.8064 Å, *c* = 16.006 Å
Number of formula units in the unit cell: Z = 3
Density (calculated for hexagonal/trigonal crystal system): 2868 kg/m^3
Reference: Ross N.L. et al., American Mineralogist (1992), Vol. 77, 412-421

Cell parameters were determined at 'room temperature', from single crystal X-ray structure refinements of a natural sample (locality: Eugui, Spain), using a Picker four circle diffractometer equipped with graphite monochromator and MoKα radiation (0.7107 Å).

12.4 Cell Dimensions: *a* = 4.812 Å, *c* = 16.020 Å
Number of formula units in the unit cell: Z = 3
Density (calculated for hexagonal/trigonal crystal system): 2859 kg/m^3
Reference: Effenberger H. et al., Zeitschrift für Kristallographie (1981), Vol. 156, 233-243

Cell parameters were determined at 'room temperature', from single crystal X-ray structure refinements of a natural sample (locality: Oberdorf, Austria), using a Philips PW 1100 four circle diffractometer equipped with graphite monochromator and MoKα radiation.

12.5 Mean density of dolomite: Dx = 2852 kg/m^3

12.6 Comment:

Date are given for ideal dolomite, having Ca/Mg = 1. However natural dolomite exhibits a range of Ca/Mg ratios. Its synthesis has been reported but insufficient data are given to calculate a density [1,2].

[1] Usdowski E., Naturwissenschaften (1989), Vol. 76, 374-375
[2] Babcan J. et al., Geologica Carpathica (2001), Vol. 52, 139-146

SULFATES AND HYDRATED SULFATES

13 Anhydrite

Formula: $CaSO_4$
Formula Weight: 136.14 g/mol
Space group: Amma, Bbmm
Conventional cement shorthand notation: C$\bar{S}$

13.1 Cell Dimensions: *a* = 7.006 Å, *b* = 6.998 Å, *c* = 6.245 Å
Number of formula units in the unit cell: Z = 4
Density (calculated for orthorhombic crystal system): 2952 kg/m^3
Reference: Kirfel A. et al., Acta Crystallographica (1980), Vol. B36, 2881-2890

Cell parameters were determined at 'room temperature', from single crystal X-ray structure refinements of natural crystals (locality: Strassfurt, Germany), using a Syntex four circle diffractometer equipped with a graphite monochromator and MoKα radiation (0,7106 Å).

Density calculated by Kirfel et al.: **2952 kg/m^3**

13.2 Cell Dimensions: *a* = 7.6993 Å, *b* = 6.995 Å, *c* = 6.245 Å
Number of formula units in the unit cell: Z = 4
Density (calculated for orthorhombic crystal system): 2988 kg/m^3
Reference: Hawthorne F.C. et al., Canadian Mineralogist (1975), Vol. 13, 289-297

Cell parameters were determined at 'room temperature', from single crystal X-ray structure refinements of natural crystals (locality: Leopoldshall, Germany), using a Syntex four circle diffractometer equipped with a graphite monochromator and MoKα radiation (0,7106 Å).

13.3 Cell Dimensions: *a* = 6.992 Å, *b* = 6.998 Å, *c* = 6.238 Å
Number of formula units in the unit cell: Z = 4
Density (calculated for orthorhombic crystal system): 2963 kg/m^3
Reference: Hartmann R et al., European Journal of Mineralogy (1989), Vol. 1, 721-722

13.4 Mean density of anhydrite: Dx = 2968 kg/m^3

13.5 Comment:
Active, or gamma, anhydrite is often added to Portland cement to regulate its set time in which application its readily-soluble properties are desirable. 'Active anhydrite' is characterized by having a high specific surface often with poor crystallinity: see 'soluble anhydrite' and is structurally different than anhydrite.

14 'Soluble Anhydrite'

Formula: γ - $CaSO_4$, $Ca(SO_4)\cdot<0.05\ H_2O$
Formula Weight: 136.14 g/mol
Space group: $P6_222$
Conventional cement shorthand notation: γ -$C\bar{S}$

14.1 Cell Dimensions: a = 6.9695 Å, c = 6.3033 Å
Number of formula units in the unit cell: Z = 3
N.B The formula used for calculation assumes 0.00 H_2O
Density (calculated for hexagonal/trigonal crystal system): 2958 kg/m^3
Reference: Lager G.A. et al., American Mineralogist (1984), Vol. 69, 910-918

Cell parameters were determined at 295 K, from single crystal X-ray photography of synthetic crystals using a Guiner-type focusing camera.

14.2 Recommended density of 'soluble anhydrite': Dx = 2958 kg/m^3

14.3 Comment:
Considerable controversy exists in the literature concerning existence of the γ phase or 'active anhydrite', as distinct from normal anhydrite. However, it would appear to be established as a distinct compound. It rehydrates readily to mixtures of hemihydrate and gypsum in the presence of water.

15a Hemihydrate

Formula: $Ca(SO_4)\cdot 0.5\ H_2O$
Formula Weight: 145.14 g/mol
Space group: I2
Conventional cement shorthand notation: $C\bar{S}H_{0.5}$

15a.1 Cell Dimensions: a = 6.930 Å, b = 12.062 Å, c = 12.66 Å, α =90.0°
Number of formula units in the unit cell: Z = 12
Density (calculated for monoclinic crystal system): 2733 kg/m^3
Reference: Lager G.A. et al., American Mineralogist (1984), Vol. 69, 910-918

Cell parameters were determined at 295 K, from single crystal X-ray photography of synthetic crystals (grown from aqueous NaCl, and chemically analyzed with an electron microprobe), using a Guiner-type focusing camera.

15a.2 Recommended density of hemihydrate: Dx = 2733 kg/m^3

15a.3 Comment:

Also known as 'plaster of Paris'. It is made by partial dehydration of gypsum and is often produced in Portland cement during intergrinding of clinker to which gypsum has been added: the heat generated by grinding leads to its partial dehydration. The structure of hemihydrate is closely related to that of its precursor, gypsum, and in the presence of liquid water, it readily re-hydrates to gypsum.

There is uncertainty as to the maximum H_2O water content of hemihydrate. Kuzel [1] found that variation was continuous from 0.53-0.62 H_2O, but that a miscibility gap existed at 0.03-0.53 H_2O. Abriel [2] reported a crystal structure refinement for a preparation with 0.8 H_2O: see subsequent sheet and comment. The water content used in density calculations is stated in the formula.

[1] Kuzel H.J., Neues Jahrbuch für Mineralogie Abhandl. (1987), Vol. 156, 155
[2] Abriel W., Acta Crystallographica (1983), Vol. C39, 956-958

15b Hemihydrate

Formula: $Ca(SO_4)\cdot 0.8\ H2O$
Formula Weight: 150.54 g/mol
Space group: $P3_121$
Conventional cement shorthand notation: $C\bar{S}H_{0.8}$

15b.1 Cell Dimensions: a = 6.968 Å, c = 6.410 Å
Number of formula units in the unit cell: Z = 3
Density (calculated for hexagonal/trigonal crystal system): 2783 kg/m^3
Reference: Abriel W., Acta Crystallographica (1983), Vol. C39, 956-958

Cell parameters were determined at 'room temperature', from single crystal X-ray structure refinements (origin of the crystals: not specified), using a Huber RHD-402 diffractometer equipped with graphite monochromator) and MoKα radiation (0,7107 Å).

Density calculated by Abriel: **2630 kg/m^3**
Note: even assuming the high water content, the reported density seems low.

15b.2 Recommended density of hemihydrate: Dx = 2783 kg/m^3

16 Gypsum

Formula: $CaSO_4\cdot 2H_2O$
Formula Weight: 172.17 g/mol
Space group: I2/a
Conventional cement shorthand notation: $C\bar{S}H_2$

16.1 Cell Dimensions: a = 5.679 Å, b = 15.202 Å, c = 6.522 Å, β= 118.43°
Number of formula units in the unit cell: Z = 4
Density (calculated for monoclinic crystal system): 2310 kg/m^3
Reference: Pedersen B.F., Acta Crystallographica (1982), Vol. B38, 1074-1077

Cell parameters were determined at 294 K, from single crystal X-ray structure refinements of a natural sample (locality: Hampshire, England), using a Siemens CIRCUS four circle diffractometer.

Density calculated by Pedersen**: 2300 kg/m^3**

16.2 Cell Dimensions: *a* = 5.6765 Å, *b* = 15.1952 Å, *c* = 6.5243 Å, β= 118.49°
Number of formula units in the unit cell: Z = 4
Density (calculated for monoclinic crystal system): 2312 kg/m^3
Reference: Schofield P.F. et al., American Mineralogist (1996), 847-851

Cell parameters were determined at 300 K, from X-ray structure refinements of a natural sample (locality: Tuscany, Italy), using a neutron powder diffraction data, which were collected on a medium resolution Polaris diffractometer.

16.3 Mean density of gypsum: Dx = 2311 kg/m^3

16.4 Comment:
Interground with Portland cement clinker to retard set. Its dehydration in air at 70-200°C gives hemihydrate ($CaSO_4 \sim 0.5H_2O$), or γ - $CaSO_4$ ('soluble anhydrite'), or mixtures.

17 Arcanite

Formula: K_2SO_4
Formula Weight: 174.26 g/mol
Space group: Pnam
Conventional cement shorthand notation: K$\bar{S}$

17.1 Cell Dimensions: *a* = 7.476Å, *b* = 10.071 Å, *c* = 5.763 Å
Number of formula units in the unit cell: Z = 4
Density (calculated for orthorhombic crystal system): 2668 kg/m^3
Reference: McGinnety J.A., Acta Crystallographica (1972), Vol. B28, 2845-2852

Cell parameters were determined at 291 K, from single crystal X-ray structure refinements (origin of crystals: not specified), using a Picker (Hilger & Watts) four circle diffractometer and MoKα radiation (0,7093 Å).

17.2 Recommended density of arcanite: Dx = 2668 kg/m^3

17.3 Comment:
"K_2SO_4" is often reported as vapor- phase condensates on clinker or as having crystallised from sulfate-rich interstitial sulfate-rich melts trapped within clinker. It is likely that the formulation is approximate because at elevated temperature, extensive solid solution occurs with substitution of sulfate by carbonate. K_2SO_4 is also polymorphous. Data reported here are for the low-temperature phase although the high temperature phase is frequently reported to occur in clinker. Since this composition is not quenchable to ambient as the "high temperature" polymorph, its frequent occurrence in clinker is probably stabilized by solid solution. Solid solution will of course affect the density so the value given here may require appropriate adjustment.

18 Thenardite

Formula: Na_2SO_4
Formula Weight: 142.04 g/mol
Space group: Fddd
Conventional cement shorthand notation: N$\bar{S}$

18.1 Cell Dimensions: *a* = 5.861 Å, *b* = 9.815 Å, *c* = 12.307 Å
Number of formula units in the unit cell: Z = 8
Density (calculated for orthorhombic crystal system): 2665 kg/m^3
Reference: Mehrotra B.N. et al., Neues Jahrbuch für Mineralogie Monatshefte (1978), 408-421

Cell parameters were determined at 'room temperature', from single crystal X-ray structure refinements of synthetic crystals, grown from aqueous solution, using a Siemens automatic diffractometer and MoKα radiation.

18.2 Cell Dimensions: *a* = 5.868 Å, *b* = 9.829 Å, *c* = 12.302 Å
Number of formula units in the unit cell: Z = 8
Density (calculated for orthorhombic crystal system): 2659 kg/m^3
Reference: Hawthorne F.C., Canadian Mineralogist (1975), Vol. 13, 181-187

Cell parameters were determined at 'room temperature', from single crystal X-ray structure refinements of natural crystals (locality: Borax Lake, California); the type of diffractometer is not given.

18.3 Mean density of thenardite: Dx = 2662 kg/m^3

19 Aphthitalite

Formula: $K_3Na(SO_4)_2$
Formula Weight: 332.27 g/mol
Space group: P $\bar{3}$m1
Conventional cement shorthand notation: K_3 N $\bar{S}_2$

19.1 Cell Dimensions: *a* = 5.680 Å, *c* = 7.309 Å
Number of formula units in the unit cell: Z = 1
Density (calculated for hexagonal/trigonal crystal system): 2703 kg/m^3
Reference: Okada K. et al., Acta Crystallographica (1980), Vol. B36, 919-921

Cell parameters were determined at 'room temperature', from single crystal X-ray structure refinements of synthetic crystals, using a Philips PW 1100 automated four-circle diffractometer equipped with graphite monochromator.

Density calculated by Okada et al.**: 2690 kg/m^3**

19.2 Recommended density of aphthitalite: Dx = 2703 kg/m^3

19.3 Comment:

Density is calculated for the ideal formula. Some variation in Na/K ratio occurs as result of solid solution**,** cell parameters decreasing with increasing Na/K ratio.

20 Syngenite

Formula: $K_2Ca(SO_4)_2 \cdot H_2O$
Formula Weight: 328.42 g/mol
Space group: $P2_1/m$
Conventional cement shorthand notation: $KC\bar{S}_2H$

20.1 Cell Dimensions: a = 6.225 Å, b = 7.127 Å, c = 9.727 Å, β = 104.153°
Number of formula units in the unit cell: Z = 2
Density (calculated for monoclinic crystal system): 2607 kg/m^3
Reference: Bokii G.B. et al., Soviet Physics Crystallography (1978), Vol. 23, 141-143

Cell parameters were determined at 153 K, from single crystal X-ray structure refinements of natural crystals (locality: not specified), using a Syntex $P2_1$ four circle diffractometer equipped with graphite monochromator.

Density calculated by Bokii G.B. et al.**: 2607 kg/m^3**

20.2 Cell Dimensions: a = 6.25 Å, b = 7.15 Å, c = 9.77 Å, β = 104°
Number of formula units in the unit cell: Z = 2
Density (calculated for monoclinic crystal system): 2575 kg/m^3
Reference: Corazza E. et al., Zeitschrift fur Kristallographie (1967), Vol. 124, 398-408

Cell parameters were determined at 'room temperature', from single crystal X-ray structure refinements of natural crystals (locality: Kalusz, Galicia); intensity data were collected using an integrating Buerger precession camera.

Density calculated by Corazza E. et al.**: 2575 kg/m^3**

20.3 Cell Dimensions: a = 6.251 Å, b = 7.156 Å, c = 9.775 Å, β = 104°
Number of formula units in the unit cell: Z = 2
Density (calculated for monoclinic crystal system): 2575 kg/m^3
Reference: Aruja E., Mineralogical Magazine (1958), Vol. 31, 943-946

Powder photographs were taken in at 18-cm diameter Debeye–Scherrer camera as well as on a focusing camera (Cu radiation) at 'room temperature'; a synthetic sample was prepared by immersing gypsum plaster in shallow dish of aqueous K_2SO_4 for 2 weeks.

20.4 Recommended density of syngenite: Dx = 2575 kg/m^3

20.5 Comment:

Syngenite may form in cement during storage by reaction of potassium sulfate with gypsum. It has also been found in secondary deposits in deteriorating concrete.
The values by Corazza E. et al. and Aruja et al. value are preferred because the coefficients of thermal dilation, necessary to correct data (obtained at 154 K) to ambient are not available.

21 'Aluminosulfate' (calcium sulfoaluminate)

Formula: $Ca_4(Al_6O_{12})(SO_4)$
Formula Weight: 610.26 g/mol
Space group: $I4_132$; I23 also proposed
Conventional cement shorthand notation: $C_4A_3\bar{S}$

21.1 Cell Dimensions: a = 18.39 Å
Number of formula units in the unit cell: Z = 16
Density (calculated for cubic crystal system): 2607 kg/m^3
Reference: Halstead P.E. et al., Journal of Applied Chemistry (1962), Vol. 12, 413-417

Cell parameters were determined from X-ray powder data of a synthetic sample (mixtures of CaO, Al_2O_3 and $CaSO_4$ in appropriate proportions were heated in platinum containers), X-ray powder data were obtained using a diffractometer equipped with a Geiger counter detector and CuKα radiation; temperature of measurement was not specified.

Density calculated by Halstead et al.**: 2607 kg/m^3**

21.2 Recommended density of calcium sulfoaluminate: Dx = 2607 kg/m^3

21.3 Comment:
The phase occurs in commercial calcium sulfoaluminate cement clinkers as a principal clinker mineral, probably with some Fe(III) substituting for Al(III). It has also been manufactured as an expansive admixture intended to produce shrinkage-compensated or expansive formulations in mixtures with Portland or calcium aluminate cements.

22 'Silicosulfate' (calcium sulfosilicate)

Formula: $Ca_5(SiO_4)_2(SO_4)$
Formula Weight: 480.58 g/mol
Space group: Pcmn
Conventional cement shorthand notation: $C_5S_2\bar{S}$

22.1 Cell Dimensions: a = 10.182 Å, b = 15.398 Å, c = 6.850 Å
Number of formula units in the unit cell: Z = 4
Density (calculated for orthorhombic crystal system): 2972 kg/m^3
Reference: Brotherton P.D. et al., Australian Journal of Chemistry (1974), Vol. 27, 657-660

Cell parameters were determined at 'room temperature', from X-ray structure refinements of a synthetic phase (found coating from a lime kiln), using a Syntex four circle diffractometer equipped with Ni filter and CuKα radiation.

Density calculated by Brotherton et al.**: 2973 kg/m^3**

22.2 Recommended density of calcium sulfosilicate: Dx = 2972 kg/m^3

22.3 Comment:

It is obtained on heating mixtures of appropriate composition in air of ordinary humidity, and in this environment, it is stable up to 1298°C at which point it decomposes with loss of sulfur. The phase is also known as "sulfospurrite" on account of its similarity with spurrite, calcium silicocarbonate, with which it may form solid solution.

23 Tricalcium aluminate (cubic)

Formula: $Ca_3Al_2O_6$, $3CaO \cdot Al_2O_3$**,**
Formula Weight: 270.19 g/mol
Space group: Pa3
Conventional cement shorthand notation: C_3A (cubic)

23.1 Cell Dimensions: *a* = 15.263 Å
Number of formula units in the unit cell: Z **=** 24
Density (calculated for cubic crystal system): 3028 kg/m^3
Reference: Mondal P. et al., Acta Crystallographica (1975), Vol. B31, 689-697

Cell parameters were determined from single crystal data, which were collected on a Nonius integrating camera using CuKα radiation (1.5405 Å); temperature of the measurement is not given.

Density calculated by Mondal et al.**: 3027 kg/m^3**

23.2 Cell Dimensions: *a* = 15.262 Å
Number of formula units in the unit cell: Z **=** 24
Density (calculated for cubic crystal system): 3030 kg/m^3
Reference: Swanson H.E. et al., National Bureau of Standards Circular 539 (1955), Vol. 5

Cell parameters of a synthetic sample were determined at 298 K, from X-ray powder patterns, using: a Guiner-type camera with Ni filter, an internal standard and CuKα radiation (1.5405 Å).

23.3 Cell Dimensions: *a* = 15.268 Å
Number of formula units in the unit cell: Z **=** 24
Density (calculated for cubic crystal system): 3030 kg/m^3
Reference: Lee, F. et.al, Journal of Applied Crystallography (1979), Vol. 12, 407- 410

X-ray examinations of the synthetic samples were done at 'room temperature'. Three graduated exposures were taken on a Guinier camera (Incentive Research and Development, Model XDC 700) with Cu Kα radiation. The films were read with a scanning microdensitometer specially developed at Aberdeen for reading powder films; it had a relative accuracy of ±3 parts in 10^5.

23.4 Mean density of cubic tricalcium aluminate: Dx = 3030 kg/m^3

23.5 Comment:

Tricalcium aluminate reacts strongly with water, and it is the most reactive of all the Portland clinker phases. Its rapid hydration to form phases of the type $Ca_2AlO_3(OH) \cdot nH_2O$

leads to the phenomenon of "flash set", and a large amount of heat is generated in the course of hydration.

24 Tricalcium aluminate (orthorombic)

Formula: $Ca_3Al_2O_6$, $3CaO \cdot Al_2O_3$**,**
Formula Weight: 270.19 g/mol
Space group: Pcaa
Conventional cement shorthand notation: C_3A (orthorombic)

24.1 Cell Dimensions: a = 10.873 Å, b = 10.851 Å, c = 15.115 Å
Number of formula units in the unit cell: Z = 12
Density (calculated for orthorombic crystal system): 3023 kg/m^3
Reference: Lee, F. et.al, Journal of Applied Crystallography (1979), Vol. 12, 407- 410

X-ray examinations of the synthetic samples were done at 'room temperature'. Three graduated exposures were taken on a Guinier camera (Incentive Research and Development, Model XDC 700) with CuKα radiation. The films were read with a scanning microdensitometer specially developed at Aberdeen for reading powder films; it had a relative accuracy of ±3 parts in 10^5.

24.2 Mean density of orthorhombic tricalcium aluminate: Dx = 3023 kg/m^3

24.3 <u>Comment:</u>
The orthorhombic polymorph is stabilized by Na_2O. Cubic $Ca_3Al_2O_6$ is stable with contents of up to 2% by weight of Na_2O and the orthorhombic phase is stable between 3.5 and 4.5% Na_2O in the temperature range 293 to 1810 K Thus the exact composition of the orthorhombic phase is not known but probably contained about 4 wt% sodium oxide (above 7.85 wt% Na_2O monoclinic form reported). The sodium substitution mechanism is believed to involve replacement of 1 calcium by 2 sodium, one of which occupies an otherwise vacant site. The mass change is however slight Ca = 40, 2 Na = 46, so the partial substitution does not much affect the density.

25 Tetracalcium aluminoferrite (brownmillerite)

Formula: $Ca_2(Al,Fe)_2O_5$, $4CaO \cdot Al_2O_3 \cdot Fe_2O_3$
Formula Weight: 242.97 g/mol
Space group: Ibm2
Conventional cement shorthand notation: C_4AF

25.1 Cell Dimensions: a = 5.584 Å, b = 14.60 Å, c = 5.374 Å
Number of formula units in the unit cell: Z = 4
Density (calculated for orthorhombic crystal system): 3684 kg/m^3
Reference: Colville A.A. et al., Acta Crystallographica (1971), Vol. B27, 2311-2315

Cell parameters were determined from single crystal data, which were collected on a Buerger-Supper-Pace-Picker automatic diffractometer using CuKα radiation (1.5405 Å); temperature of the measurement and origin of the sample were not specified.

Density calculated by Colville et al.**: 3684 kg/m^3**

25.2 Cell Dimensions: a = 5.5672 Å, b = 14.521 Å, c = 5.349 Å
Number of formula units in the unit cell: Z = 4
Density (calculated for orthorhombic crystal system): 3732 kg/m^3
Reference: Morris M.C. et al., National Bureau of Standards Monograph 25 (1979), Vol.16, 186

Cell parameters were determined at 298 K, from X-ray powder patterns of the sample (origin -not specified), using: diffractometer equipped with a focusing graphite monochromator, CuKα radiation (1.540598 Å) and an internal standard (high purity 99.99% Si standard).

25.3 Mean density of tetracalcium aluminoferrite: Dx = 3708 kg/m^3

25.4 Comment:
C_4AF is a member of a solid solution series based on C_2F ($Ca_2Fe_2O_5$). At 1 bar pressure, solid solution extends continuously from C_2F to ~70 mol % C_2A. The C_4AF composition is thus an arbitrary composition in this series and is not a discrete compound, as is often claimed. However a gradual symmetry change occurs in the solid solutions, from Pcmm at C_2F to Ibm2 at the C_4AF composition and higher Al substitutions. Data are only given for C_4AF composition free from other substituents: the ferrite in Portland cement is often a complex solid solution, containing significant Mg, Ti and Si. These substituents affect the crystallography; polytypism is also common. In general, substitution of Mg and Ti increase the resemblance of the overall structure to a perovskite-like arrangement.

TRICALCIUM SILICATE

Tricalcium silicate is the major, and characteristic, mineral constituent in Portland cement, responsible for setting and development of "early" strength.
At high temperatures, Ca_3SiO_5 is rhombohedral (R). However, in the course of cooling, a series of phase changes occurs spontaneously. This sequence is sensitive to solid solution. The lower temperature phases are distorted rhombohedral with actual monoclinic (M) or triclinic (T) symmetry. Several variants of M and T are known. It is agreed that impurity stabilizes the M and R phases to ambient, but that relatively high levels of doping, several wt%, may be required to obtain R at ambient. Therefore data given here for R are for the pure phase, but obtained at high temperature, while data for the other polymorphs and polymorphic variants are at ambient.

A summary of the polymorphs of tricalcium silicate, Ca_3SiO_5, is as follows:

>1070°C : R, Rhombohedral
1060-1070°C : M3, Monoclinic
990-1060°C : M2, Monoclinic
980-990°C : M1, Monoclinic
920-980°C : T3, Triclinic
620-920°C : T2, Triclinic
<620°C T1: Triclinic

26 R-Tricalcium silicate (at 1200°C)

Formula: Ca_3SiO_5, $3CaO \cdot SiO_2$
Formula Weight: 228.32 g/mol
Space group: R3m
Conventional cement shorthand notation: R-C_3S

26.1 Cell Dimensions: *a* = 7.135 Å, *c* = 25.586 Å
Number of formula units in the unit cell: Z = 9
Density (calculated for hexagonal/trigonal crystal system): 3025 kg/m^3
Reference: Nishi F. et al., Zeitschrift für Kristallographie (1984), Vol. 168, 197-212

Cell parameters were determined at temperature 1473 K from X-ray structure refinements of a synthetic phase, using a Syntex four circle diffractometer (equipped with graphite monochromator) and MoKα radiation (0.7106 Å).

26.2 Recommended density of R-tricalcium silicate at 1200˚C: Dx = 3025 kg/m

27 R-Tricalcium silicate (stabilized with Sr)

Formula: Ca_3SiO_5, $3CaO \cdot SiO_2$**,**
Formula Weight: 228.32 g/mol
Space group: R3m
Conventional cement shorthand notation: R-C_3S

27.1 Cell Dimensions: *a* = 7.0767 Å, *c* = 24.974 Å
Number of formula units in the unit cell: Z = 9
Density (calculated for hexagonal/trigonal crystal system): 3168 kg/m^3
Reference: Ilyinets A.M. et al., 8th International Congress on the Chemistry of Cement, Vol. 6, (1986), 489- 491

Cell parameters were determined from single-crystal X-ray structure refinements of synthetic crystals stabilized with Sr (Sr content was not given, hence the formula is shown without Sr); details of the measurement are not specified, but are believed to have been obtained at ambient temperature.

27.2 Recommended density of R-tricalcium silicate stabilized with Sr: Dx = 3168 kg/m^3

28 M3-tricalcium silicate (stabilized with Mg)

Formula: Ca_3SiO_5, $3CaO \cdot SiO_2$
Formula Weight: 228.32 g/mol
Space group: Cm
Conventional cement shorthand notation: M3-C_3S

28.1 Cell Dimensions: *a* =33.083 Å, *b* =7.027 Å, c = 18.499Å, β = 94.12
Number of formula units in the unit cell: Z = 36
Density (calculated for monoclinic crystal system): 3182 kg/m^3
Reference: Nishi F. et al., Zeitschrift für Kristallographie (1985), Vol. 172, 297-314

Cell parameters were determined from X-ray structure refinements of a synthetic phase (mixture of C_3S, MgO and $CaCl_2$ -flux component), using a Rigaku AFC-5 diffractometer equipped with a graphite monochromator and MoKα radiation; temperature of the measurement is not specified but is believed to be at ambient temperature. The Mg content is not known and is therefore not shown in the formula.

28.2 Recommended density of M3-tricalcium silicate stabilized with Mg: Dx = 3182 kg/m^3

29 M3-tricalcium silicate (less well ordered)

Formula: Ca_3SiO_5, $3CaO{\cdot}SiO_2$,
Formula Weight: 228.32 g/mol
Space group: Cm
Conventional cement shorthand notation: M3-C_3S

29.1 Cell Dimensions: a = 12.235 Å, b = 7.073 Å, c = 9.298 Å, β = 116.31°
Number of formula units in the unit cell: Z = 6
Density (calculated for monoclinic crystal system): 3153 kg/m^3
Reference: Mumme W.G., Neues Jahrbuch für Mineralogie Monatshefte (1995), 145-160

Cell parameters were determined from single crystal X-ray structure refinements of a synthetic C_3S crystals (extracted from a sample of cement clinker provided by British Cement Association), using a Siemens AED diffractometer and MoKα radiation (0.710687 Å); temperature of the measurement is not specified but is believed to be at ambient

29.2 Recommended density of M3-tricalcium silicate (less well ordered): Dx = 3153 kg/m^3

29.3 <u>Comment:</u>
At high temperatures tricalcium silicate is rhombohedral. However, in the course of cooling to ambient, several minor phase transformations occur. These lower the symmetry of C_3S. But the nature, sequence and temperature at which transformations occur are variable depending on amount and chemical nature of impurity. As a consequence, the phase obtained at ambient typically has a large unit cell although of course retaining a simple rhombohedral pseudocell. Moreover, quenched in disorder may persist. But while doubts may persist over the symmetry unit cell and order- disorder state of the product, it is likely that the density is not significantly affected and it is appropriate to use densities in the range **3168±15 kg/m^3**.
See also data for the triclinic (T1) phase.

30 T1-tricalcium silicate

Formula: Ca_3SiO_5, $3CaO{\cdot}SiO_2$
Formula Weight: 228.32 g/mol
Space group: $P\bar{1}$
Conventional cement shorthand notation: T1-C_3S

30.1 Cell Dimensions: a = 11.67 Å, b = 14.24Å, c = 13.72 Å, α = 105.5°, β = 94.3°, γ = 90.0°
Number of formula units in the unit cell: Z = 18
Density (calculated for triclinic crystal system): 3120 kg/m^3

Reference: Golovastikov N.I. et al., Soviet Physics Crystallography (1975), Vol. 20, 441-445

Cell parameters were determined from X-ray structure refinements of a synthetic phase (C_3S containing traces of MgO, Al_2O_3, Cr_2O_3, Ge), using an integrating Weissenberg camera and Mo Kα radiation; temperature of the measurement is not specified but probably ambient.

30.2 Recommended density of T1-tricalcium silicate: Dx = 3120 kg/m^3

30.3 <u>Comment:</u>

The reported density of T1, 3120 kg/m^3 is close to that reported for less well ordered C_3S (sheet - 29), density of 3153 kg/m³ also to that of M3 (3182 kg/m^3). The preparations differ slightly in chemistry and it is not possible to deconvolute differences in density arising from composition and structure. Also, many cements contain mixtures of C_3S variants.

DICALCIUM SILICATE

Dicalcium silicate is a major component of Portland cement and is believed to be responsible for the development of strength at later ages.
As bar pressure and as e temperature changes, dicalcium silicate passes through several polymorphic states. The higher temperature polymorphs cannot normally be preserved by cooling to room temperature unless stabilized by substituent ions. Thus several of the polymorphs are normally encountered at ambient as impurity - stabilized phases. For pure dicalcium silicate, the sequence of phase transformations and stability range of polymorphs is shown below. Rapidly reversible phase transitions are marked *:

* >1425 °C: α Ca_2SiO_4
* 1160-1425°C: α'_H Ca_2SiO_4
* 680-1160°C: α'_L Ca_2SiO_4
500-680°C: β Ca_2SiO_4
<500°C: γ Ca_2SiO_4

31 α-dicalcium silicate (stabilized to ambient with Ba)

Formula: Ca_2SiO_4, $2CaO \cdot SiO_2$,
Formula Weight: 172.24 g/mol
Space group: $P6_3/mmc$
Conventional cement shorthand notation: α-C_2S

31.1 Cell Dimensions: *a* = 5.579 Å, *c* = 7.150 Å
Number of formula units in the unit cell: Z = 2
Density (calculated for hexagonal/trigonal crystal system): 2968 kg/m^3
Reference: Udagawa S. et al., Review of the 34th General Meeting, Cement Association of Japan, Tokyo (1980), 37

The original reference has not been consulted. These data are taken from: Taylor H.F.W., "Cement Chemistry" 2nd edition 1997, Thomas Telford Publishing, London, UK.

31.2 Recommended density of α-dicalcium silicate: Dx = 2968 kg/m^3

32 α'$_H$-dicalcium silicate (1200°C, stabilized with P_2O_5)

Formula: Ca_2SiO_4, $2CaO \cdot SiO_2$,
Formula Weight: 172.24 g/mol
Space group: Pcmn
Conventional cement shorthand notation: α'_H-C_2S

32.1 Cell Dimensions: *a* = 9.49 Å, *b* = 5.59 Å, *c* = 6.85 Å
Number of formula units in the unit cell: Z = 4
Density (calculated for orthorhombic crystal system): 3148 kg/m^3
Reference: Saalfeld H. et al., American Mineralogist (1975), Vol. 60, 824-827

Cell parameters were determined at 1723 K, from single crystal X-ray structure refinements of a synthetic phase, using an integrating Weissenberg camera and MoKα radiation.

32.2 Recommended density of α'$_H$ - dicalcium silicate at 1723K : Dx = 3148 kg/m^3

33 α'$_L$-dicalcium silicate (stabilized with Sr)

Formula: Ca_2SiO_4, $2CaO \cdot SiO_2$,
Formula Weight: 172.24 g/mol
Space group: $Pcna2_1$
Conventional cement shorthand notation: α'_L-C_2S

33.1 Cell Dimensions: *a* = 20.871 Å, *b* = 9.496 Å, *c* = 5.6 Å
Number of formula units in the unit cell: Z = 12
Density (calculated for orthorhombic crystal system): 3092 kg/ m^3
Reference: Ilyinets A.M. et al., 8th International Congress on the Chemistry of Cement, Vol. 6, (1986), 489- 491

Cell parameters were determined from single-crystal X-ray structure refinements of synthetic crystals stabilized with Sr. The Sr content is not given and details of the measurement are not specified.

33.2 Recommended density of α'$_L$ -dicalcium silicate : Dx = 3092 kg/m^3

34 β-dicalcium silicate

Formula: Ca_2SiO_4, $2CaO \cdot SiO_2$,
Formula Weight: 172.24 g/mol
Space group: $P2_1/n$
Conventional cement shorthand notation: β-C_2S

34.1 Cell Dimensions: *a* = 5.502 Å, *b* = 6.745 Å, *c* = 9.297 Å
Number of formula units in the unit cell: Z = 4
Density (calculated for orthorhombic crystal system): 3326 kg/m^3

Reference: Jost K.H. et al., Acta Crystallographica (1977), Vol. B33, 1696-1700

Cell parameters were determined at 293 K, from single crystal X-ray structure refinements of synthetic crystals (grown from a $CaCl_2$ flux without other stabilizing reagents, at 1300°C), using a Hilger four circle diffractometer equipped with graphite monochromator and MoKα radiation.

Density calculated by Jost et al**: 3326 kg/m^3**

34.2 Cell Dimensions: a = 5.48 Å, b = 6.76 Å, c = 9.28 Å, β= 94.33°
Number of formula units in the unit cell: Z = 4
Density (calculated for monoclinic crystal system): 3326 kg/m^3
Reference: Midgley C.M., Acta Crystallographica (1952), Vol. 5, 307-312

Cell parameters were determined from single crystal X-ray structure refinements of a synthetic phase, using an integrating Weissenberg camera; temperature of the measurement is not specified but probably ambient.

34.3 Mean density of β-dicalcium silicate: Dx = 3326 kg/m^3

34.4 <u>Comment:</u>
See discussion on γ - dicalcium silicate, entry No. 35

35 γ-dicalcium silicate

Formula: Ca_2SiO_4, $2CaO \cdot SiO_2$,
Formula Weight: 172.24 g/mol
Space group: Pbnm
Conventional cement shorthand notation: γ-C_2S

35.1 Cell Dimensions: a = 5.081 Å, b = 11.224 Å, c = 6.778 Å
Number of formula units in the unit cell: Z = 4
Density (calculated for orthorhombic crystal system): 2960 kg/m^3
Reference: Udagawa S. et al., Cement Concrete Research (1980), Vol. 10, 139-144

Cell parameters were determined from powder diffraction X -ray structure refinements of a synthetic phase, using a Rigaku four circle diffractometer equipped with a graphite monochromator) and using MoKα radiation; temperature of the measurement is not specified.

35.2 Recommended density of γ -dicalcium silicate : Dx = 2960 kg/m^3

35.2 <u>Comment:</u>
α, α'_H and α'_L polymorphs of Ca_2SiO_4 are only stable at elevated temperatures. These polymorphs can only be obtained at ambient if stabilized by solid solution and consequently, uncertainty about the unit cell contents. The normal sequence of cooling results in a reconstructive transformation to the γ polymorph. Its structure is markedly less dense than those of the other polymorphs. However, formation of the γ polymorph during cooling is often slow; γ persists metastably to ~650°C at which temperature, a metastable

transformation to β occurs. The beta phase has a slightly collapsed version of the α' type structure and its density, 3326 kg/m^3, is markedly higher than for the γ polymorph . Preservation of α'_L below its normal stability limit, allowing β to form, is assisted by ions in solid solution: Mg, Al, Fe, etc. The resulting complex series of transformations are partially manifesting by a complex internal structure of beta marked by several types of twinning and also by exsolution of other phases as the belite host composition approaches the ideal Ca_2SiO_4 formula. Crystals are frequently strained as a result. Densities given are therefore approximate on account of the presence of exsolution lammelae in the β phase.

ALUMINATE - FERRITE -TRISUBSTITUENT PHASE (AFt)

36 Ettringite

Formula: $[Ca_3Al(OH)_6]_2(SO_4)_3\cdot(24+2)H_2O$, $3CaO\cdot Al_2O_3\cdot 3CaSO_4\cdot 32H_2O$
Formula Weight: 1255,11 g/mol
Space group: P31c
Conventional cement shorthand notation: $C_6A\bar{S}_3H_{32}$

36.1 **Cell Dimensions:** *a* = 11.23 Å, *c* = 21.50 Å
Number of formula units in the unit cell: Z = 2
Density (calculated for hexagonal/trigonal crystal system): 1775 kg/m^3
Reference: Struble L.J., 8th International Congress on the Chemistry of Cement, Vol. 6, (1986), 582-588

Cell parameters were determined at 'room temperature', from X-ray powder patterns of a synthetic ettringite, using an internal standard (high purity 99.99% Si standard); other details of the measurement are not specified.

36.2 **Formula:** $[Ca_3Al(OH)_6]_2(SO_4)_3\cdot(24+2)H_2O$, $3CaO\cdot Al_2O_3\cdot 3CaSO_4\cdot 32H_2O$
Formula Weight: 1255,11 g/mol
Space group: P31c
Conventional cement shorthand notation: $C_6A\bar{S}_3H_{32}$

Cell Dimensions: *a* = 11.23 Å, *c* = 21.44 Å
Number of formula units in the unit cell: Z = 2
Density (calculated for hexagonal/trigonal crystal system): 1780 kg/m^3
Reference: Swanson H.E. et al., National Bureau of Standards Circular 539 (1959), Vol. 8, 3

Cell parameters were determined at 300 K, from X-ray powder patterns of a sample (origin-not specified), using: a Guiner-type camera with Ni filter, an internal standard and CuKα radiation (1.5405 Å).

Density calculated by Swanson et al.: **1754 kg/m^3**

36.3 **Formula:** $[Ca_3Al(OH)_6]_2(SO_4)_3\cdot(24+2)H_2O$, $3CaO\cdot Al_2O_3\cdot 3CaSO_4\cdot 32H_2O$
Formula Weight: 1255,11 g/mol
Space group: P31c
Conventional cement shorthand notation: $C_6A\bar{S}_3H_{32}$

Cell Dimensions: *a* = 11.22 Å, *c* = 21.48 Å
Number of formula units in the unit cell: Z = 2
Density (calculated for hexagonal/trigonal crystal system): 1780 kg/m^3
Reference: Pöllmann H., 'Characterization of Different Water Contents of Ettringite and Kuzelite', proc. XII International Congress on the Chemistry of Cement, 8-13 July 2007, Montreal, Canada

Cell parameters were determined by X-ray diffraction of a synthetic phase at 35% relative humidity (CO_2 free conditions) at room temperature, using analytical X-Pert and Bruker D5000 diffractometers.

36.4 **Formula:** $[Ca_3Al(OH)_6]_2(SO_4)_3\cdot(24+2)H_2O$, $3CaO\cdot Al_2O_3\cdot 3CaSO_4\cdot 32H_2O$
Formula Weight: 1255,11 g/mol
Space group: P31c
Conventional cement shorthand notation: $C_6A\bar{S}_3H_{32}$

Cell Dimensions: *a* = 11.23 Å, *c* = 21.52 Å
Number of formula units in the unit cell: Z = 2
Density (calculated for hexagonal/trigonal crystal system): 1774 kg/m^3
Reference: Pöllmann H., Cement Concrete Research (1993), Vol. 23, 422 - 430

Cell parameters were determined from X-ray powder patterns of a synthetic sample made by the 'sucrose method'(using sugar to enhance solubilities) and measured at relative humidity 35%; an internal Si standard (a_o= 5.4308 Å) and CuKα radiation were used; measurements made at 297 K.

36.5 **Cell Dimensions:** *a* = 11.23 Å, *c* = 21.49 Å
Number of formula units in the unit cell: Z = 2
Density (calculated for hexagonal/trigonal crystal system): 1776 kg/m^3
Reference: this study

Cell parameters were determined at ambient pressure and 303 K, from X-ray powder diffraction diagrams of a synthetic sample. Data were collected using a Bruker D8 advance powder diffractometer, CuKα radiation (1.54060 Å). The angular range was set between 5-55° 2θ. Unit cell parameters were refined from the powder diffraction patterns (71 selected reflections) using CELREF 2 software; mean square deviation: M_D = 0.00816

36.6 **Mean density of ettringite: Dx = 1778 kg/m^3**

36.7 **<u>Comment:</u>**
Ettringite (shorthand: AFt (aluminate-ferrite-trisubstituted) type compound) typically grows in needle-shaped morphologies, hexagonal prisms, ect. Its water content ranges between 30 and 32 H_2O and water within this range is zeolitic: it can be gained or lost without significant change in structure or cell dimensions. Consequently, there is always slight uncertainty about the water contents, and hence the density. The calculations assume 32 H_2O.
Water contents below 30 H_2O are also reported but Zhou and Glasser showed that the structure degraded and 'metaettringite' was obtained [1]. Pöllmann describes a 36 H_2O variant at 100% relative humidity [2]
See also the carbonate and iron analogues included in this compilation.

[1] Zhou Q., Glasser F.P, Lachowski E.E., Cement and Concrete Research (2004), Vol. 34, 703- 710
[2] Pöllmann H, Proc. XII International Congress on the Chemistry of Cement, 8-13 July 2007, Montreal, Canada

36.8a Ettringite low water content

Formula: $[Ca_3Al(OH)_6]_2(SO_4)_3 \cdot 24\ H_2O$, $3CaO \cdot Al_2O_3 \cdot 3CaSO_4 \cdot 30H_2O$
Formula Weight: 1219,11 g/mol
Space group: P31c
Conventional cement shorthand notation: $C_6A\bar{S}_3H_{30}$

36.8a$_1$ Cell Dimensions: a = 11.14 Å, c = 21.30 Å
Number of formula units in the unit cell: Z = 2
Density (calculated for hexagonal/trigonal crystal system): 1768 kg/m^3
Reference: Pöllmann H, 'Characterization of Different Water Contents of Ettringite and Kuzelite', proc. XII International Congress on the Chemistry of Cement, 8-13 July 2007, Montreal, Canada

Cell parameters were determined by X-ray diffraction of synthetic, acetone-dried sample (CO_2 free conditions) at room temperature, using analytical X-Pert and Bruker D5000 diffractometers.

36.8a$_2$ Recommended density of ettringite with 30 H_2O: Dx = 1768 kg/m^3

36.8b Ettringite with high water content

Formula: $[Ca_3Al(OH)_6]_2(SO_4)_3 \cdot (24+6)\ H_2O$, $3CaO \cdot Al_2O_3 \cdot 3CaSO_4 \cdot 36H_2O$
Formula Weight: 1327,11 g/mol
Space group: P31c
Conventional cement shorthand notation: $C_6A\bar{S}_3H_{36}$

36.8b$_1$ Cell Dimensions: a = 11.26 Å, c = 21.56 Å
Number of formula units in the unit cell: Z = 2
Density (calculated for hexagonal/trigonal crystal system): 1861 kg/m^3
Reference: Pöllmann H, 'Characterization of Different Water Contents of Ettringite and Kuzelite', proc. XII International Congress on the Chemistry of Cement, 8-13 July 2007, Montreal, Canada

Cell parameters were determined by X-ray diffraction of synthetic, (100% relative humidity, CO_2 free conditions) at room temperature, using analytical X-Pert and Bruker D5000 diffractometers.

36.8b$_2$ Cell Dimensions: a = 11.255 Å, c = 21.54 Å
Number of formula units in the unit cell: Z = 2
Density (calculated for hexagonal/trigonal crystal system): 1865 kg/m^3
Reference: this study

Cell parameters were determined at ambient pressure, 303 K, from X-ray powder diffraction diagrams of a synthetic wet sample (100% relative humidity) covered with

Mylar foil to prevent water loss and carbonation. Data were collected by a Bruker D8 advance powder diffractometer, using CuKα radiation (1.54060 Å). The angular range was set between 5-55º 2θ. Unit cell parameters were refined from the powder diffraction patterns (38 selected reflections) using CELREF 2 software, mean square deviation: M_D = 0.00918

36.8b$_3$ Mean density of ettringite with 36 H_2O: Dx = 1863 kg/m^3

37 'Carbonate Ettringite', 'CO$_3$-AFt'

Formula: $[Ca_3Al(OH)_6]_2(CO_3)_3\cdot(24+2)H_2O$, $3CaO\cdot Al_2O_3\cdot 3CaCO_3\cdot 32H_2O$
Formula Weight: 1146.94 g/mol
Space group: P31c (determined using X- ray powder pattern)
Conventional cement shorthand notation: $C_6A\bar{C}_3H_{32}$

37.1 Cell Dimensions: *a* = 10.834 Å, *c* = 21.25 Å
Number of formula units in the unit cell: Z = 2
Density (calculated for hexagonal/trigonal crystal system): 1763 kg/m^3
Reference: Struble L.J., 8th International Congress on the Chemistry of Cement, Vol. 6, (1986), 582- 588

Cell parameters were determined at 'room temperature', from X-ray powder patterns of a synthetic ettringite, using an internal standard (high purity 99.99% Si standard); other details of the measurement are not specified.

37.2 Cell Dimensions: *a* = 10.851 Å, *c* = 21.257 Å
Number of formula units in the unit cell: Z = 2
Density (calculated for hexagonal/trigonal crystal system): 1757 kg/m^3
Reference: this study

Cell parameters were determined at ambient pressure, 303 K, from X-ray powder diffraction diagrams of a synthetic sample. Data were collected by a Bruker D8 advance powder diffractometer, using CuKα radiation (1.54060 Å). The angular range was set between 5-55º 2θ. Unit cell parameters were refined from the powder diffraction patterns (35 selected reflections), using CELREF 2 software, mean square deviation: M_D = 0.00818

37.3 Mean density of carbonate ettringite: Dx = 1760 kg/m^3

37.4 <u>Comment:</u>
Carbonate ettringite appears to be stabilized by low temperatures, close to 0°C. It accommodates limited sulfate in solid solution. However sulfate ettringite can accommodate up to ~ 50 mol% of "carbonate ettringite" at 20°-25°C.

38 'Iron Ettringite'

Formula: $[Ca_3Fe(OH)_6]_2(SO_4)_3\cdot(24+2)H_2O$, $3CaO\cdot Fe_2O_3\cdot 3CaSO_4\cdot 32H_2O$
Formula Weight: 1312.84 g/mol
Space group: P31c (determined using X- ray powder pattern)
Conventional cement shorthand notation: $C_6F\bar{S}_3H_{32}$

38.1 Cell Dimensions: *a* = 11.182 Å, *c* = 22.008 Å

Number of formula units in the unit cell: Z = 2
Density (calculated for hexagonal/trigonal crystal system): 1830 kg/m^3
Reference: Struble L.J., 8th International Congress on the Chemistry of Cement, Vol. 6, (1986), 582- 588

Cell parameters were determined at 'room temperature', from X-ray powder patterns of a synthetic ettringite, using an internal standard (high purity 99.99% Si standard); other details of the measurement-not specified.

38.2 Cell Dimensions: *a* = 11.1817 Å, *c* = 22.007 Å
Number of formula units in the unit cell: Z = 2
Density (calculated for hexagonal/trigonal crystal system): 1830 kg/m^3
Reference: McMurdie et.al, Powder Diffraction, Vol. 2 (1), (1987), 41- 52

Cell parameters were determined at 'room temperature', from X-ray powder patterns of a synthetic ettringite.

38.3 Mean density of iron ettringite: Dx = 1830 kg/m^3

38.4 <u>Comment:</u>
The extent of iron substitution in the ettringite of Portland cement is believed to be small. The extent of solid solution between Al/OH- ettringite and Fe/OH- ettringite is reported in [1].
[1] Möschner G., et al., Cement and Concrete Research (2009), Vol. 39, 482-489

39 Thaumasite

Formula: $Ca_3(SO_4)(CO_3)[Si(OH)_6]\cdot 12H_2O$
Formula Weight: 622.62 g/mol
Space group: $P6_3$
Conventional cement shorthand notation: $C_3S\bar{C}\bar{S}H_{15}$

39.1 Cell Dimensions: *a* = 11.030 Å, *c* = 10.396 Å
Number of formula units in the unit cell: Z = 2
Density (calculated for hexagonal/trigonal crystal system): 1888 kg/m^3
Reference: Effenberger H. et al., Neues Jahrbuch für Mineralogie Monatshefte (1983), 60-68

Cell parameters were determined at 293 K, from single-crystal X-ray structure refinements of natural crystals (locality: Langban, Sweden), using a Syntex four circle diffractometer equipped with a graphite monochromator and MoKα radiation (0.7107 Å).

Density calculated by Effenberger H. et al.: **1876 kg/m^3**

39.2 Cell Dimensions: *a* = 11.0538 Å, *c* = 10.4111 Å
Number of formula units in the unit cell: Z = 2
Density (calculated for hexagonal/trigonal crystal system): 1876 kg/m^3
Reference: Jacobsen S.D. et al., Physics and Chemistry of Minerals, (2003), Vol. 30, 321-329

Cell parameters were determined at 298 K, from single-crystal X-ray structure refinements of natural thaumasite (locality: not specified), using a Siemens P4 four circle diffractometer equipped with a graphite monochromator and MoKα radiation (0.7109 Å)

Density calculated by Jacobsen S.D. et al: **1876 kg/m^3**

A discrepancy exists between data presented in Gaines V.R. et al., *Dana's New Mineralogy*, Eighth edition (1997); the density data for thaumasite on page 671 differ from those on page 568 although both appear to rest on the same dataset.

39.3 Mean density of thaumasite: Dx = 1882 kg/m^3

39.4 Comment.

Thaumasite is a naturally occurring mineral, usually found in hydrothermally -altered rocks, as a late stage, low temperature mineral. It is very similar to ettringite: limited solid solutions occur between the two minerals[1]. Thaumasite is also well known as a product of sulfate and carbonate attack on concrete. Thaumasite is noteworthy because it contains $Si(OH)_6$ groups yet does not require high pressure for its formation. The phase relations and extent of solid solution between thaumasite, carbonate ettringite and sulfate ettringite are not known in detail.

[1] Macphee D.E. et al., Cement and Concrete Research (2004), Vol. 34, Issue 9, 1591-1598

ALUMINATE-FERRITE-MONOSUBSTITUENT PHASE (AFm)

Phases in this family are comprised of a layer structure containing the basic unit $Ca_2(Al,Fe^{III})(OH)_6^+$. The positive charge is balanced in interlayer positions by either monovalent (OH^-,Cl^-) or divalent (SO_4^{2-}, etc.) ions. Additional water is present in the interlayer. The phases listed here are those the most relevant to cement hydration but others occur in nature, for example with Fe and Cr(III) in the layer. Solid solution between different AFm phases is always incomplete when the substituent anion differs in charge and may be incomplete even when the charge is the same, as with (OH, Cl). The water content much affects the *c* axis spacing, for example, C_4AH_{19} and C_4AH_{13}. However the preservation for analysis is often difficulty: C_4AH_{19} readily looses water and often appears in XRD as C_4AH_{13} having lost water in the course of specimen preparation and handling. The stacking of layers can differ leading to polytypism. The polytypes have not been classified but it is believed that while the existence of different stackings may affect the true symmetry and intensity of X- ray reflections, its effect on density is not significant.

40 Tetracalcium aluminate-13-hydrate (hydroxy AFm)

Formula: $Ca_4Al_2(OH)_{14}\cdot 6H_2O$, $4CaO\cdot Al_2O_3\cdot 13H_2O$
Formula Weight: 560.47 g/mol
Space group: R--
Conventional cement shorthand notation: C_4AH_{13}

40.1 Cell Dimensions: *a* = 5.752 Å, *c* = 95.27 Å
Number of formula units in the unit cell: Z = 6
Density (calculated for hexagonal/trigonal crystal system): 2046 kg/m^3

Reference: Fischer R. et al., Cement Concrete Research (1982), Vol. 12, 517-526

Cell parameters were determined at 295 K, from X-ray powder diffraction diagrams of a synthetic phase (all chemicals used were of reagent quality), using an internal standard (high purity 99.99% Si standard); when single crystals were available, lattice constants were determined using a Weissenberg camera. Precise determination of space group was not possible.

40.2 **Cell Dimensions:** a = 5.758 Å, c = 95.226 Å
Number of formula units in the unit cell: Z = 6
Density (calculated for hexagonal/trigonal crystal system): 2042 kg/m^3
Reference: this study

Cell parameters were determined at ambient pressure, 303 K, from X-ray powder diffraction diagrams of a synthetic sample. Data were collected by a Bruker D8 advance powder diffractometer, using CuKα radiation (1.54060 Å). The angular range was set between 5-55º 2θ. Unit cell parameters were refined from the powder diffraction patterns (22 selected reflections) using CELREF 2 software. Refinement was made for the space group R $\bar{3}$, mean square deviation: M_D = 0.02030

40.3 **Mean density of hydroxy-AFm: Dx = 2044 kg/m^3**

41 Tetracalcium ferrite-13-hydrate (Fe-hydroxy AFm)

Formula: $Ca_4Fe_2(OH)_{14}\cdot 6H_2O$, $4CaO\cdot Fe_2O_3\cdot 13H_2O$
Formula Weight: 618.19 g/mol
Space group: R--
Conventional cement shorthand notation: C_4FH_{13}

41.1 **Cell Dimensions:** a = 5.89 Å, c = 7.902 Å
Number of formula units in the unit cell: Z = 1/2
Density (calculated for hexagonal/trigonal crystal system): 2162 kg/m^3
Reference: Schwiete H.E. et al., Zement-Kalk-Gips (1964), Vol. 17, 379-386
Cell parameters were determined at 'room temperature', from X-ray powder pattern of a synthetic phase.

41.2 **Recommended density of Fe-hydroxy AFm: Dx = 2162 kg/m^3**

41.3 **Comment:**
Believed to form a continuous series of solid solutions with $Ca_4Al_2(OH)_{14}\cdot 6H_2O$. As in the corresponding system with Al_2O_3, the phase was coexisting in solution with the 19- hydrate phase.

42 α_1-Tetracalcium aluminate-19-hydrate

Formula: $Ca_4Al_2(OH)_{14}\cdot 12H_2O$, $4CaO\cdot Al_2O_3\cdot 19H_2O$
Formula Weight: 668.48 g/mol
Space group: R $\bar{3}$c or R3c
Conventional cement shorthand notation: α1 - C_4AH_{19}

42.1 Cell Dimensions: a = 5.77 Å, c = 64.08 Å
Number of formula units in the unit cell: Z =3
Density (calculated for hexagonal/trigonal crystal system): 1804 kg/m^3
Reference: Aruja E., Acta Crystallographica (1961), Vol. 14, 1213-1216

Cell parameters were determined at 'room temperature', from X-ray powder diffraction diagrams of a synthetic phase, using a Guiner-type focusing camera; specimens were made in a glove box under controlled atmospheric conditions and exposed to X-rays in a sealed envelope to avoid carbonation.

Density calculated by Aruja**: 1804 kg/m^3**

42.2 Recommended density of α_1-Tetracalcium aluminate-19-hydrate: Dx = 1804 kg/m^3

43 α_2-Tetracalcium aluminate-19-hydrate

Formula: $Ca_4Al_2(OH)_{14}\cdot 12H_2O$, $4CaO\cdot Al_2O_3\cdot 19H_2O$
Formula Weight: 668.48 g/mol
Space group: $P6_3/m$ or $P6_322$
Conventional cement shorthand notation: $\alpha 2$ - C_4AH_{19}

43.1 Cell Dimensions: a = 5.77 Å, c = 21.37 Å
Number of formula units in the unit cell: Z = 1
Density (calculated for hexagonal/trigonal crystal system): 1802 kg/m^3
Reference: Aruja E., Acta Crystallographica (1961), Vol. 14, 1213-1216

Cell parameters were determined at 'room temperature', from X-ray powder diffraction diagrams of a synthetic phase, using a Guiner-type focusing camera; specimens were made in a glove box under controlled atmospheric conditions and exposed to X-rays in a sealed capsule to avoid carbonation.

Density calculated by Aruja**: 1802 kg/m^3**

43.2 Recommended density of α_2-Tetracalcium aluminate-19-hydrate: Dx = 1802 kg/m^3

43.3 <u>Comment:</u>
C_4AH_{19} is structurally derived from C_4AH_{13} by the addition of an extra H_2O molecules. Two polytypes (α_1 and α_2) are distinguished.

44 Tetracalcium aluminate monosulfate-12-hydrate (monosulfoaluminate)

Formula: $Ca_4Al_2(SO_4)(OH)_{12}\cdot 6H_2O$, $3CaO\cdot Al_2O_3\cdot CaSO_4\cdot 12H_2O$
Formula Weight: 622.52 g/mol
Space group: $R\bar{3}$
Conventional cement shorthand notation: $C_4A\bar{S}H_{12}$

44.1 Cell Dimensions: a = 5.758 Å, c = 26.794 Å
Number of formula units in the unit cell: Z = 3/2
Density (calculated for hexagonal/trigonal crystal system): 2020 kg/m^3

Reference: Allmann R., Neues Jahrbuch für Mineralogie Monatshefte (1977), 136-144

Cell parameters were determined at 'room temperature', from single-crystal X-ray structure refinements of a synthetic phase, using a Philips PW 1100 four circle diffractometer (equipped with graphite monochromator) and Mo Kα radiation.

Density calculated by Allmann R**: 2020 kg/m^3**

44.2 Cell Dimensions: *a* = 5.76 Å, *c* = 53.66 Å
Number of formula units in the unit cell: Z = 3
Density (calculated for hexagonal/trigonal crystal system): 2014 kg/m^3
Reference: Pöllman H. et al., American Mineralogist (1998), 909 (abstract only)

Cell parameters were determined at room temperature, from X-ray powder pattern of a synthetic phase, using Cu Kα radiation.

44.3 Cell Dimensions: *a* = 5.76 Å, *c* = 26.79 Å
Number of formula units in the unit cell: Z = 3/2
Density (calculated for hexagonal/trigonal crystal system): 2014 kg/m^3
Reference: Pöllmann H, 'Characterization of Different Water Contents of Ettringite and Kuzelite', proc. XII International Congress on the Chemistry of Cement, 8-13 July 2007, Montreal, Canada

Cell parameters were determined by X-ray diffraction of synthetic, sample at 25˚C (CO_2 free conditions), using analytical X-Pert and Bruker D5000 diffractometers.

44.4 Cell Dimensions: *a* = 5.763 Å, *c* = 53.661 Å
Number of formula units in the unit cell: Z = 3
Density (calculated for hexagonal/trigonal crystal system): 2014 kg/m^3
Reference: this study

Cell parameters were determined at ambient pressure, 303 K, from X-ray powder diffraction diagrams of a synthetic sample. Data were collected by a Bruker D8 advance powder diffractometer, using CuKα radiation (1.54060 Å). The angular range was set between 5-55º 2θ. Unit cell parameters were refined from the powder diffraction patterns (23 selected reflections) using CELREF 2; software gave a mean square deviation: M_D = 0.01361

44.5 Mean density of monosulfoaluminate (12 H_2O): Dx = 2015 kg/m^3

44.6 Monosulfoaluminate with high water content (14 H_2O)

Formula: $Ca_4Al_2(SO_4)(OH)_{12}\cdot 8H_2O$, $3CaO\cdot Al_2O_3\cdot CaSO_4\cdot 14H_2O$
Formula Weight: 658.52 g/mol
Space group: R $\bar{3}$
Conventional cement shorthand notation: $C_4A\bar{S}H_{14}$

Cell Dimensions: *a* = 5.748 Å, *c* = 28.69 Å
Number of formula units in the unit cell: Z = 3/2
Density (calculated for hexagonal/trigonal crystal system): 1998 kg/m^3

Reference: Pöllmann H, 'Characterization of Different Water Contents of Ettringite and Kuzelite', proc. XII International Congress on the Chemistry of Cement, 8-13 July 2007, Montreal, Canada

Cell parameters were determined by X-ray diffraction of synthetic phase at 25˚C (below 100% relative humidity, CO_2-free conditions), using analytical X-Pert and Bruker D5000 diffractometers.

44.7 Recommended density of monosulfoaluminate (14 H_2O): Dx = 1998 kg/m^3

44.8 Monosulfoaluminate with high water content (16 H_2O)

Formula: $Ca_4Al_2(SO_4)(OH)_{12}\cdot 10H_2O$, $3CaO\cdot Al_2O_3\cdot CaSO_4\cdot 16H_2O$
Formula Weight: 694.52 g/mol
Space group: R $\bar{3}$
Conventional cement shorthand notation: $C_4A\bar{S}H_{16}$

Cell Dimensions: *a* = 5.73 Å, *c* = 30.67 Å
Number of formula units in the unit cell: Z = 3/2
Density (calculated for hexagonal/trigonal crystal system): 1983 kg/m^3
Reference: Pöllmann H, 'Characterization of Different Water Contents of Ettringite and Kuzelite', proc. XII International Congress on the Chemistry of Cement, 8-13 July 2007, Montreal, Canada

Cell parameters were determined by X-ray diffraction of synthetic phase at 25˚C (100% relative humidity, CO_2-free conditions), using analytical X-Pert and Bruker D5000 diffractometers.

44.9 Recommended density of monosulfoaluminate (16 H_2O): Dx = 1983 kg/m^3

44.10 <u>Comment:</u>
Monosulfoaluminate forms solid solutions in which the SO_4^{2-} is partly replaced by OH^- at ~ 25°C; solid solution extends to ~ 50 mole % replacement.

45 Tetracalcium ferrite monosulfate-12-hydrate (Fe-monosulfoaluminate)

Formula: $Ca_4Fe_2(SO_4)(OH)_{12}\cdot 6H_2O$, $3CaO\cdot Fe_2O_3\cdot CaSO_4\cdot 12H_2O$
Formula Weight: 680.24 g/mol
Space group: R $\bar{3}$
Conventional cement shorthand notation: $C_4F\bar{S}H_{12}$

45.1 Cell Dimensions: *a* = 5.888 Å, *c* = 26.625 Å
Number of formula units in the unit cell: Z = 3/2
Density (calculated for hexagonal/trigonal crystal system): 2119 kg/m^3
Reference: Kuzel H.J., Zement-Kalk-Gips (1968), Vol. 21, 463-469

Cell parameters were determined at 298 K, from X-ray powder pattern of a synthetic phase (prepared under CO_2-free conditions) and using an internal standard (high purity 99.99% Si).

45.2 Cell Dimensions: a = 5.889 Å, c = 26.669 Å
Number of formula units in the unit cell: Z = 3/2
Density (calculated for hexagonal/trigonal crystal system): 2115 kg/m^3
Reference: Ecker M. et al., Mineralogical Institute of University, Erlagen, Germany, PDF 41-1472, ICDD, Grant in Aid (1991)

Cell parameters were determined at 'room temperature', from X-ray powder pattern of a synthetic phase using diffractometer with Ni filter and CuKα radiation (1.5405 Å).

45.3 Mean density of Fe-monosulfoauminate: Dx = 2117 kg/m^3

45.4 Comment:
$C_4F\bar{S}H_{12}$ forms solid solutions with $C_4A\bar{S}H_{12}$. Solid solution is continuous at 100˚C but at 25 and 50˚C, a miscibility gap exists; at~25°C, solid solution extends to~50 mole %.

46 Dicalcium aluminate monosilicate-8-hydrate (strätlingite)

Formula: $Ca_2Al_2SiO_7 \cdot 8H_2O$, $2CaO \cdot Al_2O_3 \cdot SiO_2 \cdot 8H_2O$
Formula Weight: 418.21 g/mol
Space group: R $\bar{3}$ or R 3
Conventional cement shorthand notation: C_2ASH_8

46.1 Cell Dimensions: a = 5.747 Å, c = 37.64 Å
Number of formula units in the unit cell: Z = 3
Density (calculated for hexagonal/trigonal crystal system): 1936 kg/m^3
Reference: Kuzel H.J., Neues Jahrbuch für Mineralogie Monatshefte (1976), 319-325

Cell parameters were determined at 'room temperature' from single -crystal X-ray structure refinements of a synthetic phase (crystals were prepared by hydration of a glass of the gehlenite composition), using: X-ray rotation and precession cameras, CuKα radiation and an internal standard (high purity 99.99% Si standard).

Density calculated by Kuzel: **1940 kg/m^3**

46.2 Cell Dimensions: a = 5.737 Å, c = 37.59 Å
Number of formula units in the unit cell: Z = 3
Density (calculated for hexagonal/trigonal crystal system): 1948 kg/m^3
Reference: Hentschel G. et al., Neues Jahrbuch für Mineralogie Monatshefte (1976), 326-330

Cell parameters were determined at room temperature, from single-crystal X-ray structure refinements of a natural mineral (limestone inclusion of a basalt from the Bellerberg /Mayen region (Germany)), using X-ray rotation and precession cameras and CuKα radiation.
Density calculated by Kuzel et al**: 1950 kg/m^3**

46.3 Cell Dimensions: a = 5.745 Å, c = 37.77 Å
Number of formula units in the unit cell: Z = 3
Density (calculated for hexagonal/trigonal crystal system): 1930 kg/m^3
Reference: Rinaldi R. et al., European Journal of Mineralogy (1990), Vol. 2, 841-849

Cell parameters were determined at 'room temperature', from single-crystal X-ray structure refinements of natural crystals (locality: Montalto di Castro, Italy), using a Philips PW 1100 four circle diffractometer equipped with a graphite monochromator and MoKα radiation.

Density calculated by Rinaldi R. et al.**: 1960 kg/m^3**

46.4 **Cell Dimensions:** a = 5.747 Å, c = 37.638 Å
Number of formula units in the unit cell: Z = 2
Density (calculated for hexagonal/trigonal crystal system): 1936 kg/m^3
Reference: this study

Cell parameters were determined at ambient pressure, 303 K, from X-ray powder diffraction diagrams of a synthetic sample. Data were collected using a Bruker D8 advance powder diffractometer, CuKα radiation (1.54060 Å). The angular range was set between 5-55° 2θ. Unit cell parameters were refined from the powder diffraction patterns (29 selected reflections) using CELREF 2 software; mean square deviation: M_D = 0.01183.

46.5 **Mean density of strätlingite: Dx = 1937 kg/m^3**

46.6 **Comment:**
Has been called "gehlenite" hydrate. It is an AFm phase including silicate anions in interlayer positions. The identity of natural phases including strätlingite and vertumnite, with the synthetic is not proven. Gehlenite hydrate is a commonly- occurring constituent of lime-pozzolan, cement-pozzolan and slag-blended cements. Its low physical density suggests that it is partly responsible for the good space filling and low permeability characteristic of well- cured blends.

47 Tetracalcium aluminate carbonate-11-hydrate (monocarboaluminate)

Formula: $Ca_4Al_2(CO_3)(OH)_{12}\cdot 5H_2O$, $3CaO\cdot Al_2O_3\cdot CaCO_3\cdot 11H_2O$
Formula Weight: 568.29 g/mol
Space group: $P\bar{1}$ or P1
Conventional cement shorthand notation: $C_4A\bar{C}H_{11}$

47.1 **Cell Dimensions:** a = 5.781 Å, b = 5.744 Å, c = 7.855 Å, α = 92.61°, β = 101.96°, γ = 120.09°
Number of formula units in the unit cell: Z = 1/2
Density (calculated for triclinic crystal system): 2170 kg/m^3
Reference: Fischer R. et al., Cement Concrete Research (1982), Vol. 12, 517-525

Cell parameters were determined at 295 K, from X-ray powder diffraction diagrams of a synthetic phase (all chemicals used were of reagent quality), using an internal standard (high purity 99.99% Si standard); when single crystals were available, lattice constants were determined using rotation and Weissenberg methods.

47.2 **Cell Dimensions:** a = 5.742 Å, b = 5.744 Å, c = 15.09 Å, α = 92.29°, β = 87.45°, γ = 119.54°
Number of formula units in the unit cell: Z = 1
Density (calculated for triclinic crystal system): 2182 kg/m^3
Reference: Renaudin G. et al., Cement Concrete Research (1999), Vol. 29, 63-69

Cell parameters were determined at 293 K, from a single crystal (prepared by hydrothermal synthesis), mounted in an automatic Nonius diffractometer.

47.3 Cell Dimensions: a = 5.768 Å, b = 5.742 Å, c = 7.862 Å, α = 92.68°, β = 101.89°, γ = 120.01°
Number of formula units in the unit cell: Z = 1/2
Density (calculated for triclinic crystal system): 2174 kg/m^3
Reference: this study

Cell parameters were determined at ambient pressure, 303 K, from X-ray powder diffraction diagrams of a synthetic phase. Data were collected by a Bruker D8 advance powder diffractometer, using CuKα radiation (1.54060 Å). The angular range was set between 5-55º 2θ. Unit cell parameters were refined from the powder diffraction patterns (27 selected reflections) using CELREF 2 software; mean square deviation: M_D = 0.01253.

47.4 Mean density of monocarboaluminate: Dx = 2175 kg/m^3

48 Tetracalcium ferrite carbonate-12-hydrate (Fe-monocarboaluminate)

Formula: $Ca_4Fe_2(CO_3)(OH)_{12}\cdot 6H_2O$, $3CaO\cdot Al_2O_3\cdot CaCO_3\cdot 12H_2O$
Formula Weight: 644.11 g/mol
Space group: R3c
Conventional cement shorthand notation: $C_4F\bar{C}H_{12}$

48.1 Cell Dimensions: a = 5.917 Å, c = 47.679 Å
Number of formula units in the unit cell: Z = 3
Density (calculated for hexagonal/trigonal crystal system): 2219 kg/m^3
Reference: Simon G. , Erlagen, Germany, Thesis, (1984)

Cell parameters were determined at room temperature, from X- ray powder patterns of a synthetic sample; using a diffractometer equipped CuKα radiation (1.5405 Å)

48.2 Recommended density of Fe- monocarboaluminate: Dx = 2219 kg/m^3

49 Tetracalcium aluminate hemicarbonate-12-hydrate (hemicarboaluminate)

Formula: $Ca_4Al_2(CO_3)_{0.5}(OH)_{13}\cdot 5.5H_2O$
Formula Weight: 564.45 g/mol
Space group: R $\bar{3}$c or R3c
Conventional cement shorthand notation: $C_4A\bar{C}_{0.5}H_{12}$

49.1 Cell Dimensions: a = 5.77 Å, c = 49.159 Å
Number of formula units in the unit cell: Z = 3
Density (calculated for hexagonal/trigonal crystal system): 1984 kg/m^3
Reference: Fischer R. et al., Cement Concrete Research (1982), Vol. 12, 517-526

Cell parameters were determined at 295 K, from X-ray powder diffraction diagrams of a synthetic phase (all chemicals used were of reagent quality), using an internal standard

(high purity 99.99% Si); when single crystals were available, lattice constants were determined using rotation and Weissenberg cameras.

49.2 Cell Dimensions: a = 5.761 Å, c = 49.252 Å
Number of formula units in the unit cell: Z = 3
Density (calculated for triclinic crystal system): 1986 kg/m^3
Reference: this study

Cell parameters were determined at ambient pressure, 303 K, from X-ray powder diffraction diagrams of a synthetic phase. Data were collected by a Bruker D8 advance powder diffractometer, using CuKα radiation (1.54060 Å). The angular range was set between 5-55º 2θ. Unit cell parameters were refined from the powder diffraction patterns (22 selected reflections) using CELREF 2 software mean square deviation: M_D = 0.01904.

49.3 Mean density of hemicarboaluminate: Dx = 1985 kg/m^3

49.4 Comment:
Most commercial Portland cements contain sufficient carbonate to form hemicarboaluminate. However, cements blended with calcium carbonate normally contain monocarboaluminate, which is more stable than AFm phases with (OH^-, SO_4^{2-}).

50 Dicalcium aluminate-8-hydrate

Formula: $Ca_2Al_2(OH)_{10}\cdot 3H_2O$, $2CaO\cdot Al_2O_3\cdot 8H_2O$
Formula Weight: 358.23 g/mol
Space group: R $\bar{3}$c
Conventional cement shorthand notation: C_2AH_8

50.1 Cell Dimensions: a = 5.74 Å, c = 10.7 Å
Number of formula units in the unit cell: Z = 1
Density (calculated for hexagonal/trigonal crystal system): 1950 kg/m^3
Reference: Scheller T. et al., 6th International Congress on the Chemistry of Cement (Moscow) (1976), Vol. 2, part 1, 217

Reference cannot be traced.

50.2 Recommended density of dicalcium aluminate-8-hydrate: Dx = 1950 kg/m^3

51 α-Tetracalcium aluminate dichloride-10-hydrate (Friedel's salt)

Formula: $Ca_4Al_2(Cl)_2(OH)_{12}\cdot 4H_2O$, $3CaO\cdot Al_2O_3\cdot CaCl_2\cdot 10H_2O$
Formula Weight: 561.34 g/mol
Space group: C2/c or Cc
Conventional cement shorthand notation: α-C_3A $CaCl_2$ H_{10}

51.1 Cell Dimensions: a = 9.98 Å, b = 5.74 Å, c = 16.79 Å, β=110.2°
Number of formula units in the unit cell: Z = 2
Density (calculated for monoclinic crystal system): 2065 kg/m^3
Reference: Kuzel H.J., Neues Jahrbuch für Mineralogie Monatshefte (1966), 193-200

Cell parameters were determined at 298 K, from single-crystal X-ray structure refinements of synthetic crystals (prepared hydrothermally), using a Philips Norelco diffractometer.

51.2 **Cell Dimensions:** a = 9.979 Å, b = 5.751 Å, c = 16.320 Å, β=104.53°
Number of formula units in the unit cell: Z = 2
Density (calculated for monoclinic crystal system): 2056 kg/m^3
Reference: Terzis A. et al., Zeitschrift für Kristallographie (1981), 29-34

Cell parameters were determined at room temperature, from single-crystal X-ray structure refinements of synthetic crystals.

51.3 **Cell Dimensions:** a = 9.960 Å, b = 5.744 Å, c = 16.268 Å, β=104.471°
Number of formula units in the unit cell: Z = 2
Density (calculated for monoclinic crystal system): 2068 kg/m^3
Reference: Rapin J.P. et al., Cement and Concrete Research (2002), Vol. 32, 513-519

Cell parameters were determined at 20°C, from crystalline samples prepared by hydrothermal synthesis. Compound was studied by synchrotron radiation using the WDIF4C powder diffractometer on the DW22 beamline of LURE.

51.4 **Cell Dimensions:** a = 9.955 Å, b = 5.748 Å, c = 16.754 Å, β = 110.02°
Number of formula units in the unit cell: Z = 2
Density (calculated for monoclinic crystal system): 2070 kg/m^3
Reference: this study

Cell parameters were determined at ambient pressure, 300 K, from X-ray powder diffraction diagrams of a synthetic phase. Data were collected using a Bruker D8 advance powder diffractometer, CuKα radiation (1.54060 Å). The angular range was set between 5-55° 2θ. Unit cell parameters were refined from the powder diffraction patterns (23 selected reflections) using CELREF 2 software.

51.5 Mean density of Friedel's salt: Dx = 2064 kg/m^3

51.6 **Comment:**
The monoclinic low temperature phase is transforms to a trigonal phase at 33 ± 2°C, therefore two phases (α and β) are distinguished. Friedel's salt - $Ca_4Al_2(Cl)_2(OH)_{12}\cdot 4H_2O$ ($C_3A\ CaCl_2\ H_{10}$) is a product of chloride interaction with a cement paste [1-2].
[1] Nielsen E., Denmark, DTU, PhD thesis (2004)
[2] Glasser F.P, Kindness A., Stronach A., Cement and Concrete Research (1999),Vol. 29, 861-866

52 β-Tetracalcium aluminate dichloride-10-hydrate (Friedel's salt)

Formula: $Ca_4Al_2(Cl)_2(OH)_{12}\cdot 4H_2O$, $3CaO\cdot Al_2O_3\cdot CaCl_2\cdot 10H_2O$
Formula Weight: 561.34 g/mol
Space group: R $\bar{3}$c or R3c
Conventional cement shorthand notation: β-$C_3A\ CaCl_2\ H_{10}$

52.1 **Cell Dimensions:** a = 5.74 Å, c = 46.88 Å

Number of formula units in the unit cell: Z = 3
Density (calculated for hexagonal/trigonal crystal system): 2090 kg/m^3
Reference: Kuzel H.J., Neues Jahrbuch für Mineralogie Monatshefte (1966), 193-200

Cell parameters were determined at 308 K, from single-crystal X-ray structure refinements of synthetic crystals, prepared hydrothermally, using a Philips Norelco diffractometer.

52.2 Cell Dimensions: a = 5.739 Å, c = 46.87 Å
Number of formula units in the unit cell: Z = 3
Density (calculated for hexagonal/trigonal crystal system): 2092 kg/m^3
Reference: Kuzel H.J., Zement-Kalk-Gips (1968), Vol.21, 463-469

Cell parameters were determined at 298 K, from X-ray powder pattern of a synthetic phase (prepared hydrothermally under CO_2-free conditions) and using an internal standard (high purity 99.99% Si).

52.3 Cell Dimensions: a = 5.724 Å, c = 46.689 Å
Number of formula units in the unit cell: Z = 3
Density (calculated for hexagonal/trigonal crystal system): 2111 kg/m^3
Reference: Renaudin G., Cement and Concrete Research (1999), Vol.29, 1937-1942

Cell parameters were determined at 310 K, from a single crystal (prepared by hydrothermal synthesis), using INEL CPS 120 diffractometer equipped with a high temperature system.

52.4 Cell Dimensions: a = 5.75 Å, c = 46.89 Å
Number of formula units in the unit cell: Z = 3
Density (calculated for monoclinic crystal system): 2083 kg/m^3
Reference: Rapin J.P. et al., Cement and Concrete Research (2002), Vol. 32, 513-519

Cell parameters were determined at 40˚C, from crystalline samples prepared by hydrothermal synthesis. Compound was studied by synchrotron radiation using the WDIF4C powder diffractometer on the DW22 beamline of LURE.

52.5 Mean density of β-Friedel's salt: Dx = 2094 kg/m^3

53 Tetracalcium ferrite dichloride-10-hydrate (Fe-Friedel's salt)

Formula: $Ca_4Fe_2(Cl)_2(OH)_{12}\cdot 4H_2O$, $3CaO\cdot Fe_2O_3\cdot CaCl_2\cdot 10H_2O$
Formula Weight: 619.07 g/mol
Space group: R $\bar{3}$, R3, R $\bar{3}$m, R3m or R32
Conventional cement shorthand notation: $C_3F\ CaCl_2\ H_{10}$

53.1 Cell Dimensions: a = 5.858 Å, c = 23.267 Å
Number of formula units in the unit cell: Z = 3/2
Density (calculated for hexagonal/trigonal crystal system): 2230 kg/m^3
Reference: Kuzel H.J., Zement-Kalk-Gips (1968), Vol.21, 463-469

Cell parameters were determined at 298 K, from X-ray powder pattern of a synthetic phase (prepared under CO_2-free conditions) and using an internal standard (high purity 99.99% Si).

53.2 Cell Dimensions: a = 5.861 Å, c = 23.279 Å
Number of formula units in the unit cell: Z = 3/2
Density (calculated for hexagonal/trigonal crystal system): 2226 kg/m^3
Reference: F. Götz Neunhoeffer, Ph.D thesis (in german) (1996), University of Erlagen Nürnberg, Germany, 124-135

Cell parameters were determined at room temperature (relative humidity 35%), from X-ray powder pattern of a synthetic phase.

53.3 Mean density of Fe- Friedel's salt: Dx = 2228 kg/m^3

54 Tetracalcium aluminate sulfate chloride-12-hydrate (Kuzel's salt)

Formula: $Ca_4Al_2\ (SO_4)_{1/2}\ (Cl)(OH)_{12}\cdot 6H_2O$
Formula Weight: 610.07 g/mol
Space group: R3c or R $\bar{3}$c
Conventional cement shorthand notation: C_3A ½ $C\bar{S}$ ½ $CaCl_2$ H_{12}

54.1 Cell Dimensions: a = 5.750 Å, c = 100.62 Å
Number of formula units in the unit cell: Z = 6
Density (calculated for hexagonal/trigonal crystal system): 2110 kg/m^3
Reference: Kuzel H.J., Zement-Kalk-Gips (1968), Vol.21, 463-469

Cell parameters were determined at 298 K, from X-ray powder pattern of a synthetic phase (prepared under CO_2-free conditions) and using an internal standard (high purity 99.99% Si).

54.2 Cell Dimensions: a = 5.74 Å, c = 100.6 Å
Number of formula units in the unit cell: Z = 6
Density (calculated for hexagonal/trigonal crystal system): 2118 kg/m^3
Reference: Kuzel H.J., Neues Jahrbuch für Mineralogie Monatshefte (1966), 193-200

Cell parameters were determined at 298 K, from single-crystal X-ray structure refinements of synthetic crystals (prepared hydrothermally), using a Philips Norelco diffractometer.

54.3 Mean density of Kuzel's salt: Dx = 2114 kg/m^3

54.4 <u>Comment:</u>
Kuzel's salt - $Ca_4Al_2\ (SO_4)_{1/2}\ (Cl)(OH)_{12}\cdot 6H_2O$ (C_3A ½ $C\bar{S}$ ½ $CaCl_2$ H_{12}) is an ordered compound containing both mono and divalent anions, with molar ratio 1:0.5 Cl^- and SO_4^{2-} [1]. It was reported as a product of chloride attack at lower $CaCl_2$ concentrations [2].
[1] Glasser F.P, Kindness A., Stronach A, Cement and Concrete Research (1999),Vol. 29, 861-866
[2] Hirao H. et. al, Journal of Advanced Concrete Technology (2005), Vol. 3, 77-84

55 Tetracalcium ferrite sulfate chloride-12-hydrate (Fe-Kuzel's salt)

Formula: $Ca_4Fe_2\ (SO_4)_{1/2}\ (Cl)(OH)_{12}\cdot 6H_2O$, $3CaO\cdot Fe_2O_3\cdot ½\ CaSO_4\cdot ½\ CaCl_2\cdot 12H_2O$
Formula Weight: 667.71 g/mol
Space group: R*c
Conventional cement shorthand notation: $C_3F\ ½\ C\bar{S}\ ½\ CaCl_2\ H_{12}$

55.1 Cell Dimensions: a = 5.876 Å, c = 50.08 Å
Number of formula units in the unit cell: Z = 3
Density (calculated for hexagonal/trigonal crystal system): 2222 kg/m^3
Reference: Kuzel H.J., Zement-Kalk-Gips (1968), Vol.21, 463-469

Cell parameters were determined at 298 K, from X-ray powder pattern of a synthetic phase (prepared under CO_2-free conditions) and using an internal standard (high purity 99.99% Si).

55.2 Recommended density of Fe-Kuzel's salt: Dx = 2222 kg/m^3

HYDROGARNET PHASES

56 Tricalcium aluminate-6-hydrate (hydrogarnet)

Formula: $Ca_3Al_2(OH)_{12,}\ 3CaO\cdot Al_2O_3\cdot 6H_2O$
Formula Weight: 378.28 g/mol
Space group: Ia3d
Conventional cement shorthand notation: C_3AH_6

56.1 Cell Dimensions: a = 12.5755 Å
Number of formula units in the unit cell: Z = 8
Density (calculated for cubic crystal system): 2527 kg/m^3
Reference: Kuzel H.J., Neues Jahrbuch für Mineralogie Monatshefte (1969), 397-404

Cell parameters were determined at 300 K, from single -crystal X-ray structure refinements of synthetic crystals, prepared hydrothermally, using a Philips powder diffractometer and a Si internal standard.

56.2 Cell Dimensions: a = 12.56 Å
Number of formula units in the unit cell: Z = 8
Density (calculated for cubic crystal system): 2535 kg/m^3
Reference: Brandenberger E., Schweitzeriche Mineralogische und Pertographische Mitteilungen (1933), 569 (abstract)

Details of the measurement - not given

56.3 Cell Dimensions: a = 12.5695 Å
Number of formula units in the unit cell: Z = 8
Density (calculated for cubic crystal system): 2529 kg/m^3
Reference: Lager G.A. et al., American Mineralogist (1987), Vol. 72, 756-765

Cell parameters were determined at 300 K, from single-crystal X-ray structure refinements of synthetic crystals, using an Enraf Nonius diffractometer equipped with a graphite monochromator and MoKα radiation.

56.4 Mean density of hydrogarnet: Dx = 2530 kg/m^3

56.5 Comment:

An end -member of the hydrogrossular solid-solution series, having the general formula $Ca_3Al_2(SiO_4)_{3-x}(OH)_{4x}$; x = 1.5-3.0 for katoite. Hydrogarnet is not normally a product of modern OPC hydration, although reported to occur in older Portland cements, in calcium aluminate cements (CAC) and in heat cured Portland cements. See also section 58.

57 Tricalcium ferrite-6-hydrate

Formula: $Ca_3Fe_2(OH)_{12}$, $3CaO{\cdot}Fe_2O_3{\cdot}6H_2O$,
Formula Weight: 436.02 g/mol
Space group: Ia3d
Conventional cement shorthand notation: C_3FH_6

57.1 Cell Dimensions: *a* = 12.73 Å
Number of formula units in the unit cell: Z = 8
Density (calculated for cubic crystal system): 2809 kg/m^3
Reference: Taylor, H.F.W. (1989), "Cement Chemistry" 2nd edition 1997, Thomas Telford Publishing, London, UK, 171

Details of the measurement are not given

57.2 Cell Dimensions: *a* = 12.74 Å
Number of formula units in the unit cell: Z = 8
Density (calculated for cubic crystal system): 2801 kg/m^3
Reference: Flint E.P et al., Journal of Research of the National Institute of Standards and Technology U.S., (1941), Vol. 26, 13-33

Cell parameters were determined at room temperature, from X-ray powder patterns of the synthetic phase (hydrothermal preparations). The samples were mounted on fine glass rods in the center of cylindrical cameras having radii of about 5.7 cm, and were rotated during exposure; CuKα radiation was used. The absolute accuracy of this method is however relatively low.

57.3 Recommended density of Fe-hydrogarnet: Dx = 2809 kg/m^3

58 'Siliceous' hydrogarnet

Formula: $Ca_3Al_2\,SiO_4(OH)_8$
Formula Weight: 402.37 g/mol
Space group: Ia3d
Conventional cement shorthand notation: C_3ASH_4

58.1 Cell Dimensions: *a* = 12.358 Å
Number of formula units in the unit cell: Z = 8
Density (calculated for cubic crystal system): 2832 kg/m^3
Reference: Rinaldi E. et al., Bulletin de Mineralogie (1984), Vol. 107, 606-618

Cell parameters were determined at 298 K, from single-crystal X-ray structure refinements of natural crystals from Lazio, Italy, using: a Philips diffractometer, CuKα radiation (1.54051 Å) and an internal standard. Natural crystal contained various inclusions (Mg, S) but these are not believed to affect measurements. Formula determined in above reference nearly corresponded to the idealized formula, $Ca_3Al_2\ SiO_4(OH)$, therefore minor elements were not included in the calculation.

Density calculated by Rinaldi et al.**: 2760 kg/m^3**

58.2 Cell Dimensions: *a* = 12.32 Å
Number of formula units in the unit cell: Z = 8
Density (calculated for cubic crystal system): 2858 kg/m^3
Reference: Flint E.P et al., Journal of Research of the National Institute of Standards and Technology U.S., (1941), Vol. 26, 13-33

Cell parameters were determined at room temperature, from X-ray powder patterns of the synthetic phase (hydrothermal preparations). The samples were mounted on fine glass rods in the center of cylindrical cameras having radii of about 5.7 cm, and were rotated during exposure; CuKα radiation was used. This method has relatively poor absolute accuracy.

58.3 Recommended density of siliceous hydrogarnet: Dx = 2832 kg/m^3

58.4 <u>Comment:</u>
Jappy et.al reported that at 1 bar pressure $Ca_3Al_2\ SiO_4(OH)_8$ forms only limited solid solution with $Ca_3Al_2(OH)_{12}$ Numerous minseralogical investigations of siliceous hydrogarnets report weak optical birefringence and the cubic symmetry may be only a pseudo- symmetry
[1] Jappy T.G. et. al, Advances in Cement Research, (1991/1992), Vol. 4, 1-8

CRYSTALLINE CALCIUM SILICATE HYDRATES RELATED TO C-S-H GEL

Although crystalline calcium silicate hydrates do not occur in constructional concretes, our knowledge of the structure of the semi amorphous C-S-H is in part modelled on the known structures of several crystalline calcium silicate hydrates. These phases also occur in autoclaved or heat treated cements and on that account, three hydrates, tobermorite, jennite and afwillite have been selected for inclusion in this compilation. The three structures can be considered as layer structures with Ca-OH layers resembling those in portlandite ($Ca(OH)_2$)and the silicate layer being more or less complete, to achieve the Ca/Si ratios characteristic of each phase.
Afwillite has an essentially fixed stoichiometry, while tobermorite has a defect structure which can tolerate some variation in Ca/ Si ratio. Jennite is believed to be close to stoichiometric, although the evidence is as yet inconclusive.

59 Jennite

Formula: $9CaO{\cdot}6SiO_2{\cdot}11H_2O$

Formula Weight: 1063.44 g/mol
Space group: P1 or P $\bar{1}$
Conventional cement shorthand notation: $C_9S_6H_{11}$

59.1 **Cell Dimensions:** *a* = 9.96 Å, *b* = 3.64 Å, *c* = 21.36 Å, α = 91.8°, β = 101.8°, γ = 89.6°
Number of formula units in the unit cell: Z = 1
Density (calculated for triclinic crystal system): 2332 kg/m^3
Reference: Taylor H.F.W. (1989), Data published in Cement Chemistry 2nd edition 1997, Thomas Telford Publishing, London, UK, 130

Details of the measurement-not given

Density given by Taylor**: 2332 kg/m^3**

59.2 **Cell Dimensions:** *a* = 10.593 Å, *b* = 7.284 Å, *c* = 10.839 Å, α = 99.67°, β = 97.65°, γ = 110.11°
Number of formula units in the unit cell: Z = 1
Density (calculated for triclinic crystal system): 2336 kg/m^3
Reference: Gard J.A. et al., American Mineralogist (1977), Vol. 62, 365-368

Cell parameters were determined from X-ray powder patterns of a natural (Crestmore) sample, using a Guiner - type camera, an internal standard (high purity 99.99 % Si standard) and CuKα radiation; temperature of the measurement is not specified.

Density calculated by Gard et al: **2330 kg/m^3**

59.3 **Cell Dimensions:** *a* = 10.576 Å, *b* = 7.265 Å, *c* = 10.931 Å, α = 101.30°, β = 96.98°, γ = 109.65°
Number of formula units in the unit cell: Z = 1
Density (calculated for triclinic crystal system): 2325 kg/m^3
Reference: Bonaccorsi E. et al., Cement and Concrete Research (2004), Vol. 34, 1481-1488

Cell parameters were determined from single crystal X-ray diffraction of a natural (Fuka, Japan) sample, using synchrotron radiation at the Elettra facility (Trieste, Italy).

59.4 **Mean density of jennite: Dx = 2331 kg/m^3**

60 Tobermorite (14 Å)

Formula: $5CaO \cdot 6SiO_2 \cdot 8H_2O$
Formula Weight: 785.03 g/mol
Space group: B11b
Conventional cement shorthand notation: $C_5S_6H_8$

60.1 **Cell Dimensions:** *a* = 56.735 Å, *b* = 7.425 Å, *c* = 27.987 Å, β = 123.25
Number of formula units in the unit cell: Z = 2
Density (calculated for monoclinic crystal system): 2228 kg/m^3
Reference: Bonaccorsi E. et. al, Journal of the American Ceramic Society (2005), Vol. 88, 505-512

Cell parameters were determined at room temperature, from single-crystal X-ray structure refinements of natural crystals (Crestmore). Two polytypes were detected but reflections of

the other polytype were too weak to be used in a structure refinement and only approximate cell parameters of second polytype are given (space group: F2dd, *a*~11.2 Å, *b*~7.3 Å, *c* ~56 Å)

60.2 Cell Dimensions: *a* = 5.624 Å, *b* = 3.670 Å, *c* = 27.97 Å
Number of formula units in the unit cell: Z = 1
Density (calculated for orthorhombic crystal system): 2224 kg/m^3
Reference: Taylor H.F.W. (1989), Data published in Cement Chemistry 2nd edition 1997, Thomas Telford Publishing, London, UK, 130

Details of the measurement are not given. Idealized formula postulated: $5CaO{\cdot}6SiO_2{\cdot}9H_2O$ but the actual formula given in the reference is near $5CaO{\cdot}5.5SiO_2{\cdot}9H_2O$. Calculation of density was performed for $5CaO{\cdot}5.5SiO_2{\cdot}9H_2O$.

Density given by Taylor**: 2224 kg/m^3**
Uncertainty regarding composition therefore value given by Bonaccorsi et al. preferred.

60.3 Recommended density of tobermorite 14 Å: Dx = 2228 kg/m^3

61 Afwillite

Formula: $3CaO{\cdot}2SiO_2{\cdot}3H_2O$, $Ca_3Si_2O_4(OH)_6$
Formula Weight: 342.45 g/mol
Space group: Cc
Conventional cement shorthand notation: $C_3S_2H_3$

61.1 Cell Dimensions: *a* = 16.278 Å, *b* = 5.6321 Å, *c* = 13.236 Å, β = 134.898°
Number of formula units in the unit cell: Z = 4
Density (calculated for monoclinic crystal system): 2646 kg/m^3
Reference: Malik K.M.A .et al., Acta Crystallographica (1976), Vol. B32, 475-480

Cell parameters were determined at room temperature, from single-crystal X-ray structure refinements of natural crystals (Kimberly, South Africa), using a Hilger and Watts Y290 four-circle automatic diffractometer and MoKα radiation (0.70926 Å).

61.2 Cell Dimensions: *a* = 16.27 Å, *b* = 5.632 Å, *c* = 13.23 Å, β = 134.80°
Number of formula units in the unit cell: Z = 4
Density (calculated for monoclinic crystal system): 2644 kg/m^3
Reference: Megaw H.D., Acta Crystallographica (1952), Vol. 5, 477-491

Unit cell dimensions were determined at room temperature, from oscillation photographs with CuKα radiation (1.5405 Å). Natural crystals from the Scawt Hill (Northern Ireland) were generally used but later compared with crystals from Kimberley (South Africa), which had identical unit cell dimensions. However unit cell dimensions determined by this method have low absolute accuracy.
Density calculated by Megaw**: 2634 kg/m^3**

61.3 Mean density of afwillite: Dx = 2645 kg/m^3

HYDROTALCITE TYPE AND RELATED PHASES

"Hydrotalcite" refers both to a single mineral and a family of minerals with related structures. Structural relations are not completely known for all members of the group and therefore we should strictly regard phases other than hydrotalcite itself as "hydrotalcite- like".

The hydrotalcite structure is derived form that of brucite, $Mg(OH)_2$. The brucite structure is consists of electrically neutral sheets of net composition $Mg(OH)_2$; the Mg is in octahedral coordination. In derivative structures such as hydrotalcite, part of the Mg is replaced by a trivalent ion, typically Al, on an ordered basis. The unbalance of charge is accommodated by introducing anions in interlayer positions: sufficient space also exists for water molecules The ratio Mg/(Mg + Al) varies from 0.67 to 0.75. While both natural and synthetic products exhibit variable ratios, natural specimens tend to have ratios close to 0.75 (Taylor H.F.W) while the synthetics tend to have lower ratios, close to 0.67. The stacking plan of constituent layers can also vary, giving rise to polytypes.

Analysis of the synthetic is handicapped by the fine -grained nature of hydrotalcite crystals. Electron microprobe methods do not enable distinction and quantification of OH/CO_3 ratios and furthermore, are frequently not reliable for Mg/Al ratios. Therefore a degree of uncertainty exists about the number of phases in this family and their properties. We have included a number of examples relevant to cement and where composition, crystallography and hence unit cell contents seem to be well established.

62 Hydrotalcite

Formula: $Mg_4Al_2(OH)_{12}CO_3 \cdot 3H_2O$
Formula Weight: 469.32 g/mol
Space group: R $\bar{3}$m or R3m
Conventional cement shorthand notation: $M_4A\bar{C}H_9$

62.1 **Cell Dimensions:** *a* = 3.054 Å, *c* = 22.81 Å
Number of formula units in the unit cell: Z = 1/2
Density (calculated for hexagonal/trigonal crystal system): 2117 kg/m^3
Reference: Allmann R.et al., Jahrbuch für Mineralogie Monatshefte (1969), 544-551

Cell parameters were determined from X-ray structure refinements of natural crystals (Vezna, Western Moravia), using CuKα radiation; other details of the measurement are not specified.

Density calculated by Allmann R. et al.**: 2117 kg/m^3**

62.2 **Cell Dimensions:** *a* = 3.051 Å, *c* = 22.81 Å
Number of formula units in the unit cell: Z = 1/2
Density (calculated for hexagonal/trigonal crystal system): 2119 kg/m^3
Reference: Sato T. et al., Reactivity of Solids (1988), Vol. 5, 219-228

Cell parameters were determined by X-ray powder diffractometry of synthetic phases; Ni-filtered CuKα radiation was used. Lattice constants were calculated using silicon as an internal standard.

62.3 Cell Dimensions: a = 3.046 Å, c = 22.772 Å
Number of formula units in the unit cell: Z = 1/2
Density (calculated for hexagonal/trigonal crystal system): 2129 kg/m^3
Reference: Bellotto M. et al., Journal of Physical Chemistry (1996), Vol. 100, 8527-8534

Cell parameters were determined for synthetic phases (composition checked by XRF); X-ray diffraction powder patterns were measured using a Siemens D501 diffractometer with CuKα radiation and a graphite diffracted monochromator.

62.4 Mean density of hydrotalcite : Dx = 2122 kg/m^3

63 Fe-Hydrotalcite

Formula: $Mg_4Fe_2(OH)_{12}CO_3 \cdot 3H_2O$
Formula Weight: 527.06 g/mol
Space group: R $\bar{3}$m or R3m
Conventional cement shorthand notation: $M_4F\bar{C}H_9$

63.1 Cell Dimensions: a = 3.104 Å, c = 23.12 Å
Number of formula units in the unit cell: Z = 1/2
Density (calculated for hexagonal/trigonal crystal system): 2269 kg/m^3
Reference: Sato T. et al., Reactivity of Solids (1988), Vol. 5, 219-228

Cell parameters were determined by X-ray powder diffractometry of synthetic phases; Ni-filtered CuKα radiation was used. Lattice constants were calculated using silicon as an internal standard.

63.2 Recommended density of Fe-hydrotalcite: Dx = 2269 kg/m^3

64 Meixnerite

Formula: $Mg_6Al_2(OH)_{18} \cdot 4H_2O$
Formula Weight: 577.99 g/mol
Space group: R $\bar{3}$m
Conventional cement shorthand notation: M_6AH_{13}

64.1 Cell Dimensions: a = 3.046 Å, c = 22.93 Å
Number of formula units in the unit cell: Z = 3/8
Density (calculated for hexagonal/trigonal crystal system): 1953 kg/m^3
Reference: Koritnig S. et al., American Mineralogist (1976), Vol. 61, 176 (abstract)

Cell parameters were determined from X-ray structure refinements of natural crystals (Ybbs-Presenberg, Austria); other details of the measurement are not specified.

64.2 Formula: $Mg_6Al_2(OH)_{18} \cdot 4.5H_2O$
Formula Weight: 586.99 g/mol

Space group: R $\bar{3}$m

Cell Dimensions: *a* = 3.054 Å, *c* = 23.40 Å
Number of formula units in the unit cell: Z = 3/8
Density (calculated for hexagonal/trigonal crystal system): 1934 kg/m^3
Reference: Mascolo G. et al., Mineralogical Magazine (1980), Vol. 43, 619-621

Cell parameters were determined from the X-ray powder patterns obtained by using Guiner de Wolff camera with CuKα radiation; $Pb(NO_3)_2$ was used as a reference material. Synthetic samples were prepared under CO_2-free conditions.

64.3 Mean density of meixnerite: Dx = 1945 kg/m^3

64.4 <u>Comment:</u>
The density seems to decrease as the ratio Mg/(Mg+Al) increases.

65 OH-Hydrotalcite

Formula: $Mg_4Al_2(OH)_{14}\cdot 3H_2O$
Formula Weight: 443.33 g/mol
Space group: R $\bar{3}$m or R3m
Conventional cement shorthand notation: M_4AH_{10}

65.1 Cell Dimensions: *a* = 3.038 Å, *c* = 22.62 Å
Number of formula units in the unit cell: Z = 1/2
Density (calculated for hexagonal/trigonal crystal system): 2036 kg/m^3
Reference: Mascolo G. et al., Mineralogical Magazine (1980), Vol. 43, 619-621

Cell parameters were determined from the X-ray powder patterns obtained by using Guiner de Wollf camera with CuKα radiation; $Pb(NO_3)_2$ was used as a reference material. Synthetic samples were prepared under CO_2-free conditions.

65.2 Recommended density of OH- hydrotalcite: Dx = 2036 kg/m^3

Appendix II

Standard (partial molar) thermodynamic properties of aqueous species used in GEMS calculations at 25˚C, 1 bar [52, 57, 59, 305].

species	ΔG^0	ΔH^0	S^0	C_p^0	V^0	a_1	a_2	a_3	a_4
	[kJ/mol]	*[kJ/mol]*	*[J/(K·mol)]*	*[J/(K·mol)]*	*[cm³/mol]*	*[cal/(bar·mol)]*	*[cal/mol]*	*[calK/(bar·mol)]*	*[calK/mol]*
Al^{3+}	-483.71	-530.63	-325.10	-128.70	-45.24	-0.33802	-1700.71	14.5185	-20758
AlO^+ (+ H_2O = $Al(OH)_2^+$)	-660.42	-713.64	-112.97	-125.11	0.31	0.21705	-248.11	6.7241	-26763
AlO_2^- (+ $2H_2O$ = $Al(OH)_4^-$)	-827.48	-925.57	-30.21	-49.04	9.47	0.37221	399.54	-1.5879	-29441
AlO_2H (*aq*) (+$2H_2O$ = $Al(OH)_3$ *(aq)*	-864.28	-947.13	20.92	-209.21	13.01	0.35338	84.85	5.4132	-28140
$AlOH^{2+}$	-692.60	-767.27	-184.93	55.97	-2.73	0.20469	-278.13	6.8376	-26639
$AlSO_4^+$	-1250.43	-1422.67	-172.38	-204.01	-6.02	0.13869	-439.2	7.4693	-25974
$Al(SO_4)_2^-$	-2006.30	-2338.40	-135.50	-268.37	31.11	0.68275	889.25	2.2479	-31466
Ca^{2+}	-552.79	-543.07	-56.48	-30.92	-18.44	-0.01947	-725.2	5.2966	-24792
$CaOH^+$	-717.02	-751.65	28.03	6.05	5.76	0.27243	-113.03	6.1958	-27322
$CaCO_3$ *(aq)*	-1099.18	-1201.92	10.46	-123.86	-15.65	-0.03907	-873.25	9.1753	-24179
$CaHCO_3^+$	-1146.04	-1231.94	66.94	233.70	13.33	0.3706	126.7	5.252	-28310
$CaSO_4$ *(aq)*	-1310.38	-1448.43	20.92	-104.60	4.70	0.24079	-189.92	6.4895	-27004
CO_2 *(aq)*	-386.02	-413.84	117.57	243.08	32.81	0.62466	747.11	2.8136	-30879
CO_3^{2-}	-527.98	-675.31	-50.00	-289.33	-6.06	0.28524	-398.44	6.4142	-26143
HCO_3^-	-586.94	-690.01	98.45	-34.85	24.21	0.75621	115.05	1.2346	-28266
SO_4^{2-}	-744.46	-909.70	18.83	-266.09	12.92	0.83014	-198.46	-6.2122	-26970
HSO_4^-	-755.81	-889.23	125.52	22.68	34.84	0.69788	925.9	2.1108	-31618
OH^-	-157.27	-230.01	-10.71	-136.34	-4.71	0.12527	7.38	1.8423	-27821
Cl^-	-131.29	-167.11	56.73	-122.49	1.73	0.4032	480.1	5.563	-28470
NO_3^-	-110.90	-206.88	146.94	-66.80	2.86	0.73161	678.24	-4.6838	-30594
NO_2^-	-552.79	-543.06	-56.484	-30.92	-1.84	-0.01947	-725.2	5.2966	-24792